

**The Development of Bio-Analytical Techniques for the Treatment of Psoriasis and
Related Skin Disorders.**

A thesis submitted to the University of Manchester for the degree of Doctor of Philosophy in
the Faculty of Engineering and Physical Sciences

2010

Katherine Anne Hollywood

School of Chemistry

Table of Contents

LIST OF FIGURES	9
LIST OF TABLES	16
ABSTRACT	19
DECLARATION	20
ABBREVIATIONS	21
ACKNOWLEDGEMENTS	22
CHAPTER 1: INTRODUCTION	26
1.1 SIGNIFICANCE	26
1.2 AIMS AND OBJECTIVES	26
1.3 PSORIASIS.....	28
1.3.1 <i>Introduction to Psoriasis</i>	28
1.3.1.1 Clinical Appearance.....	28
1.3.1.2 Associated Co-morbidities	29
1.3.2 <i>Histological Features of Psoriasis.</i>	30
1.3.3 <i>Pathogenesis of Psoriasis: Current Thoughts</i>	33
1.3.4 <i>Current treatment methods for Psoriasis</i>	34
1.3.4.1 Topical Treatments	35
1.3.4.1.1 Dithranol	35
1.3.4.2 Systemic Treatments.....	36
1.3.4.2.1 Methotrexate	37
1.3.4.2.2 Ciclosporin.....	39
1.3.4.3 Biologic Treatments	40
1.4 METABOLOMICS	42
1.4.1 <i>Introduction to Metabolomics.</i>	42
1.4.2 <i>Analytical Platforms for Metabolomics</i>	43
1.4.2.1 FT-IR spectroscopy	44

1.4.2.1.1	General FT-IR Introduction	44
1.4.2.1.2	FT-IR Microspectroscopy	46
1.4.2.1.3	FT-IR applications in Clinical Metabolomics	46
1.4.2.2	Mass Spectrometry	48
1.4.2.2.1	General Overview	48
1.4.2.2.2	GC-MS	49
1.4.2.2.3	Quadrupole	51
1.4.2.2.4	Time of Flight (TOF) Analyser	52
1.4.2.2.5	Tandem Mass Spectrometry (MS/MS)	52
1.4.2.2.6	GC-MS Applications in Clinical Metabolomics	53
1.5	PROTEOMICS.....	55
1.5.1	<i>Introduction to Proteomics</i>	55
1.5.2	<i>Analytical Platforms for Proteomics</i>	55
1.5.2.1	2D Gel Electrophoresis	55
1.5.2.2	MALDI-MS	56
1.5.2.3	LC-MS	57
1.5.2.3.1	Orbitrap	58
1.5.3	<i>Proteomics for Dermatological Research</i>	59
CHAPTER 2: MALDI-MS BASED SPATIAL PROTEOMIC ANALYSIS TO INVESTIGATE VARIANCES BETWEEN NORMAL AND PSORIATIC SKIN.		60
2.1	INTRODUCTION	60
2.2	MATERIAL AND METHODS	60
2.2.1	<i>Sample Collection</i>	60
2.2.2	<i>Sample Preparation</i>	61
2.2.3	<i>MALDI-MS</i>	63
2.2.4	<i>Data Analysis</i>	63
2.3	RESULTS AND DISCUSSION	63
CHAPTER 3: PHENOTYPIC PROFILING OF EXTRALESIONAL KELOID SCAR TISSUE CROSS SECTIONS USING FT-IR MICROSPECTROSCOPY REVEALS UNIQUE SPECTRAL SIGNATURE FOR KELOID SCARS...66		

3.1	INTRODUCTION	66
3.2	MATERIALS AND METHODS.....	69
3.2.1	<i>Patients & Samples</i>	69
3.2.2	<i>Fourier Transform infrared (FT-IR) microspectroscopy</i>	71
3.2.3	<i>Sample Preparation</i>	72
3.2.4	<i>FT-IR Data Collection and Chemometric Analyses</i>	73
3.2.4.1	MCT Infrared Analysis	73
3.2.4.2	FPA Image Analysis.....	74
3.3	RESULTS & DISCUSSION	75
3.3.1	<i>Histological Findings</i>	75
3.3.2	<i>FT-IR microspectroscopy</i>	76
3.3.3	<i>Chemometric analyses</i>	76
3.3.4	<i>FT-IR microspectroscopic imaging</i>	78
3.4	DISCUSSION	83
3.5	CONCLUSION.....	86
CHAPTER 4: A METABOLOMIC BASED APPROACH TO INVESTIGATE THE RESPONSE OF HACAT CELLS UPON EXPOSURE TO THREE WELL ESTABLISHED ANTI-PSORIATIC DRUGS.		87
4.1	INTRODUCTION	87
4.2	MATERIALS AND METHODS.....	88
4.2.1	<i>Materials</i>	88
4.2.2	<i>Methods</i>	88
4.2.2.1	Cell Culture.....	88
4.2.2.1.1	Resurrection of Frozen Cell Lines	88
4.2.2.1.2	Replacement of Used Media	88
4.2.2.1.3	Sub-Culturing Monolayer Cell Cultures	90
4.2.2.1.4	Cryogenic Preservation of Cell Lines	90
4.2.2.2	Drug Exposures	91
4.2.2.3	Sample Preparation.....	91
4.2.2.3.1	Metabolomic Footprint Sample Collection.....	94

4.2.2.3.2	Metabolomic Fingerprint Sample Collection	94
4.2.2.4	Metabolomic GC-MS Analysis	94
4.2.2.5	GC-MS Data Processing	95
4.3	RESULTS AND DISCUSSION	96
4.3.1	<i>Metabolite Detection</i>	96
4.3.2	<i>ANOVA Analysis</i>	96
4.3.2.1	Dithranol Fingerprint	97
4.3.2.2	Dithranol Footprint	97
4.3.2.3	Methotrexate Fingerprint	98
4.3.2.4	Methotrexate Footprint	99
4.3.2.5	Ciclosporin Fingerprint	100
4.3.2.6	Ciclosporin Footprint	101
4.3.3	<i>Identification of Metabolites</i>	102
4.3.3.1	Dithranol Identification	102
4.3.3.2	Methotrexate & Ciclosporin Identification	103
4.3.4	<i>Spring embedded correlation analysis</i>	107
4.3.4.1	Dithranol Fingerprint	107
4.3.4.2	Dithranol Footprint	111
4.3.4.3	Methotrexate Fingerprint	112
4.3.4.4	Methotrexate Footprint	115
4.3.4.5	Ciclosporin Fingerprint	118
4.3.4.6	Ciclosporin Footprint	119
4.3.5	<i>Dithranol Interpretation</i>	121
4.3.6	<i>Methotrexate and Ciclosporin Interpretation</i>	128
4.4	CONCLUSION AND FURTHER WORK	129
CHAPTER 5: A PROTEOMIC-BASED APPROACH TO INVESTIGATE THE RESPONSE OF HACAT CELLS		
UPON EXPOSURE TO THREE WELL ESTABLISHED ANTI-PSORIATIC DRUGS		131
5.1	INTRODUCTION	131
5.2	MATERIALS AND METHODS	131
5.2.1	<i>Materials</i>	131

5.2.2	<i>Methods</i>	131
5.2.2.1	Cell Culture and Drug Exposure.....	131
5.2.2.2	Sample Collection.....	132
5.2.2.3	Sample Clean Up	132
5.2.2.4	Protein Quantification.....	133
5.2.2.5	1D Gel Electrophoresis	134
5.2.2.5.1	Separating Buffer	134
5.2.2.5.2	Separating Gel	134
5.2.2.5.3	Stacking Gel.....	134
5.2.2.5.4	Pouring of Gel.....	134
5.2.2.5.5	Sample Cracking	134
5.2.2.5.6	Running Buffer	135
5.2.2.5.7	Gel Running	135
5.2.2.6	2D Gel Electrophoresis.....	135
5.2.2.6.1	Rehydration of Immobilised pH Gradient (IPG) Strip and isoelectric focussing.....	135
5.2.2.6.2	Equilibration Buffer I	136
5.2.2.6.3	Equilibration Buffer II	136
5.2.2.6.4	Gel Preparation and Running Procedure.....	137
5.2.2.7	Coomassie Stain	137
5.2.2.8	Staining Procedure	137
5.2.2.9	Visualisation of Gels	138
5.2.2.10	LC-MS	138
5.2.2.10.1	Sample Preparation	138
5.2.2.10.2	Nano-LC-MS/MS	138
5.2.2.10.3	Mass Spectrometry.....	139
5.2.2.10.4	Data analysis	139
5.3	RESULTS & DISCUSSION	140
5.3.1	<i>Protein Quantification</i>	140
5.3.2	<i>Gel Electrophoresis</i>	144
5.3.3	<i>LC-MS Results</i>	146
5.3.3.1	Dithranol	147

5.3.3.2	Methotrexate	155
5.3.3.3	Ciclosporin.....	161
5.4	CONCLUSIONS	166
CHAPTER 6: METABOLOMIC ANALYSIS OF PLASMA SAMPLES COLLECTED FROM PSORIASIS PATIENTS DURING METHOTREXATE TREATMENT: A SHORT STUDY.		169
6.1	INTRODUCTION	169
6.2	MATERIAL AND METHODS	171
6.2.1	<i>Materials</i>	171
6.2.2	<i>Methods</i>	171
6.2.2.1	Patient Selection	171
6.2.2.2	GC-MS Sample Preparation.....	171
6.2.2.3	Quality Control Samples.....	172
6.2.2.4	GC-MS Data Analysis	173
6.3	RESULTS AND DISCUSSION	174
6.3.1	<i>Post treatment metadata</i>	174
6.3.2	<i>Principal Components Analysis</i>	175
6.3.3	<i>Kruskal-Wallis Analysis</i>	176
6.3.4	<i>Multivariate Predictive Analysis</i>	180
6.4	CONCLUSIONS & FUTURE WORK.....	180
CHAPTER 7: MONITORING THE SUCCINATE DEHYDROGENASE ACTIVITY ISOLATED FROM MITOCHONDRIA BY SURFACE ENHANCED RAMAN SCATTERING.....		182
7.1	INTRODUCTION	182
7.2	MATERIALS & METHODS.....	186
7.2.1	<i>Chemical and reagents</i>	186
7.2.2	<i>Extraction of mitochondria</i>	186
7.2.3	<i>Monitoring enzyme activity</i>	187
7.2.4	<i>Surface enhanced Raman scattering</i>	188
7.2.4.1	Colloid preparation	188

7.2.4.2	Aggregation.....	189
7.2.4.3	Instrumentation	189
7.3	RESULTS AND DISCUSSION.....	190
7.3.1	<i>Validation of the enzyme systems under study</i>	190
7.3.2	<i>SERS optimisation</i>	192
7.3.3	<i>Monitoring succinate dehydrogenase activity using SERS</i>	193
7.4	CONCLUDING REMARKS.....	197
CHAPTER 8:	OVERALL SUMMARY AND CONCLUSIONS	198
CHAPTER 9:	REFERENCES.....	202
APPENDIX A	ADDITIONAL METABOLITE BOX PLOTS FOR METHOTREXATE TREATMENT: FINGERPRINT	214
APPENDIX B	ADDITIONAL METABOLITE BOX PLOTS FOR METHOTREXATE TREATMENT: FOOTPRINT	218
APPENDIX C	ADDITIONAL METABOLITE BOX PLOTS FOR CICLOSPORIN TREATMENT: FINGERPRINT	220
APPENDIX D	ADDITIONAL METABOLITE BOX PLOTS FOR CICLOSPORIN TREATMENT: FOOTPRINT	220
APPENDIX E	PROTEOME RESULTS FOR DITHRANOL TREATMENT.....	221
APPENDIX F	PROTEOME RESULTS FOR METHOTREXATE TREATMENT.....	224
APPENDIX G	PROTEOME RESULTS FOR CICLOSPORIN TREATMENT.....	229

Word Count: 52,537

List of Figures

Figure 1-1: An example of plaque psoriasis exhibited in the elbow region of a psoriasis patient (Provided by Prof. CEM. Griffiths, University of Manchester).....	29
Figure 1-2: Haematoxylin & Eosin stained sections for a) normal skin section, b) Involved psoriasis section, c) Uninvolved psoriasis section. All images collected using a Zeiss Imager A1 microscope at 400X magnification. Images captured using a Canon Powershot G6 camera.	31
Figure 1-3: Schematic diagram illustrating the structure and composition of skin.	32
Figure 1-4: The chemical structure of dithranol.....	36
Figure 1-5: The chemical structure of methotrexate.	37
Figure 1-6: The chemical structure of ciclosporin.	40
Figure 1-7: A schematic representation of an FT-IR instrument.	46
Figure 1-8: Schematic diagram of a mass spectrometer. A sample is introduced into an ion source where positive or negatively charged ions are created, separation of ions according to their mass to charge (m/z) ratio occurs within the mass analyser followed by detection within the detector element. Instrumental components and experimental parameters are controlled computationally and in addition all data is collected and stored on the connected PC. Adapted from (Dunn, 2008).	48
Figure 1-9: Schematic diagram of a quadrupole mass analyser.....	51
Figure 1-10: Schematic representation of a TOF mass analyser.	52
Figure 1-11: Schematic illustration of the MALDI process.	56
Figure 2-1: Diagram illustrating the experimental set-up for MALDI-MS profiling. Three replicate tissue sections are thaw mounted onto a MALDI target plate. A matrix array is	

applied through CHIP application proving an array of XxY spots. In the example shown complete matrix coverage requires 9x12 spots equating to 108 individual profiles. 62

Figure 2-2: Schematic diagram demonstrating the spot size and associated pitch to allow approximation of sample area to be profiled. 63

Figure 2-3: A visible image captured by the CHIP scanner illustrating the matrix deposition applied to a normal skin section in a 16x22 array. The example spectrum illustrates a number of peaks which have arisen from the surface of the skin. 64

Figure 3-1: Diagrammatic and histological cross section of an extralesional keloid scar including: A: The Grenz zone in a keloid; the histological area corresponding to papillary dermis of normal dermis located between the epidermal basement membrane and the upper edge of the reticular dermis. B: View of thick hyalinized collagen bundles typically found in middle of keloid scars. C: Keloid with circumscribed borders (marked in blue) which are well-demarcated demonstrating the periphery or margin of the keloid scars. 67

Figure 3-2: This cross section of a typical keloid scar (sample number 3) excised from the chest wall demonstrates anatomical locations within the keloid scar. Lines in green show where line mapping using FT-IR spectroscopy was taken; this resulted in 38 spectra in total: 3 epidermal, 21 normal and 14 from the reticular dermis of the keloid scar. The cyan area shows where FT-IR chemical maps were collected from: this included 14 individual maps containing 64x64 pixels and covered an area of approximately 3.5 x 0.25 mm. 70

Figure 3-3: A) Typical FT-IR absorbance spectra collected from normal skin tissue, and keloid epidermal and dermal regions. B) Expansion of lipid region C) Expansion of amide region, and D) Offset graph demonstrates a spectrum of collagen. 77

Figure 3-4: (A) PCA scores plot from one of sample no 4 with lines (2nd horizontal line) showing clear differentiation between normal tissue and keloid scar. (B) Corresponding PC1 loadings plots showing features that are discriminatory. 78

Figure 3-5: Results from PLS-DA bootstrap analysis from 100 spectra selected from six samples. (A) Average receiver operating characteristic plots from the test data only from the 10,000 models and (B) Box whisker plots showing the data from all training and test data from the 10,000 PLS-DA models that were constructed. Boxes represent the lower median and upper quartiles. Whiskers represent the range or 1.5 x the length of the box, whichever is shorter. Outliers (+) are the values out of the whisker range. 79

Figure 3-6: Chemical image plots from sample number 3 of chest wall generated from IR microspectroscopy. The light image is shown from the unstained tissue and corresponds to the area detailed in Figure 3-2. The first four false colour coded maps are from the sum of the total IR signal, area under lipid, amide and phosphate bands respectively. The next nine image maps represent the first 9 PC scores. 80

Figure 3-7: Typical FT-IR absorbance spectra collected from normal and keloid skin tissue. The spectra are annotated to illustrate the wavenumber regions of interest highlighted in Table 3-3. 81

Figure 3-8: Corresponding PC loadings plots from the PCA of IR microspectroscopy in Figure 3-6. 82

Figure 4-1: A summary diagram to illustrate the successive stages in the collection of fingerprint and footprint samples. 93

Figure 4-2: A scatter plot of metabolite feature index vs. p value for all metabolite peaks identified for the dithranol fingerprint analysis. Peaks that were identified as significant from ANOVA analysis with a p value < 0.05 are labelled with a number corresponding to feature index to allow identification of the peak. 97

Figure 4-3: A scatter plot of metabolite feature index vs. p value for all metabolite peaks identified for the dithranol footprint analysis. Peaks that were identified as significant from

ANOVA analysis with a p value < 0.05 are labelled with a number corresponding to feature index to allow identification of the peak..... 98

Figure 4-4: A scatter plot of metabolite feature index vs. p value for all metabolite peaks identified for the methotrexate fingerprint analysis. Peaks that were identified as significant from ANOVA analysis with a p value < 0.05 are labelled with a number corresponding to feature index to allow identification of the peak..... 99

Figure 4-5: A scatter plot of metabolite feature index vs. p value for all metabolite peaks identified for the methotrexate footprint analysis. Peaks that were identified as significant from ANOVA analysis with a p value < 0.05 are labelled with a number corresponding to feature index to allow identification of the peak..... 100

Figure 4-6: A scatter plot of metabolite feature index vs. p value for all metabolite peaks identified for the ciclosporin fingerprint analysis. Peaks that were identified as significant from ANOVA analysis with a p value < 0.05 are labelled with a number corresponding to feature index to allow identification of the peak..... 101

Figure 4-7: A scatter plot of metabolite feature index vs. p value for all metabolite peaks identified for the ciclosporin footprint analysis. Peaks that were identified as significant from ANOVA analysis with a p value < 0.05 are labelled with a number corresponding to feature index to allow identification of the peak..... 102

Figure 4-8: Spring embedded correlation plot for the analysis of the internal metabolome of dithranol treated HaCaT cells. The metabolite peaks are represented by the circles and the number within the circle is the metabolite ID. The larger the circle the more significant the metabolite was determined to be by ANOVA analysis. The links shown between metabolites illustrate the correlations present, the magnitude of which is shown by the number. The nearer the number is to 1 the greater the degree of correlation..... 109

Figure 4-9: Box and whisker plots of dithranol concentration ($\mu\text{g}/\text{mL}$) vs. % peak area to illustrate the general trends observed from the correlation analysis for groups A, B and C.110

Figure 4-10: Spring embedded correlation plot for the analysis of the external metabolome of dithranol treated HaCaT cells. The metabolite peaks are represented by the circles and the number within the circle is the metabolite ID. The larger the circle the more significant the metabolite was determined to be by ANOVA analysis. The links shown between metabolites illustrate the correlations present, the magnitude of which is shown by the number. The nearer the number is to 1 the greater the degree of correlation. 111

Figure 4-11: Box and whisker diagrams correlating to metabolites 113, 62, 100 and 109 showing dithranol exposure concentration ($\mu\text{g}/\text{mL}$) vs. % peak area for the external metabolome. 112

Figure 4-12: Spring embedded correlation plot for the analysis of the internal metabolome of methotrexate treated HaCaT cells. The metabolite peaks are represented by the circles and the number within the circle is the metabolite ID. The larger the circle the more significant the metabolite was determined to be by ANOVA analysis. The links shown between metabolites illustrate the correlations present, the magnitude of which is shown by the number. The nearer the number is to 1 the greater the degree of correlation. 113

Figure 4-13: Box and whisker plots to illustrate the effect of methotrexate exposure within the internal metabolome of HaCaT cells. Metabolites 62, 70, 134 were selected from within the right hand side of the correlation plot while metabolites 57, 113, 150 and 105 were selected from the left hand side. 114

Figure 4-14: Spring embedded correlation plot for the analysis of the metabolic footprint of methotrexate treated HaCaT cells. The metabolite peaks are represented by the circles and the number within the circle is the metabolite ID. The larger the circle the more significant the metabolite was determined to be by ANOVA analysis. The links shown between

metabolites illustrate the correlations present, the magnitude of which is shown by the number. The nearer the number is to 1 the greater the degree of correlation. 116

Figure 4-15: Box and whisker plots to illustrate the effect of methotrexate exposure within the metabolic footprint of HaCaT cells..... 117

Figure 4-16: Spring embedded correlation plot for the analysis of the internal metabolome of ciclosporin treated HaCaT cells. The metabolite peaks are represented by the circles and the number within the circle is the metabolite ID. The larger the circle the more significant the metabolite was determined to be by ANOVA analysis. The links shown between metabolites illustrate the correlations present, the magnitude of which is shown by the number. The nearer the number is to 1 the greater the degree of correlation..... 118

Figure 4-17: Box and whisker plots to illustrate the affect of ciclosporin exposure within the internal metabolome of HaCaT cells. Metabolites 7, 83, 100 and 134 were chosen as example metabolites. The metabolites exhibit varying responses to the drug. Metabolites 7 and 134 increase steadily in concentration until $2 \times 10^{-7} \text{M}$, and follow by a notable decrease in concentration at $2.5 \times 10^{-7} \text{M}$. In comparison metabolite 83 increases slightly and plateaus over the drug exposure range. Metabolite 100 reaches the highest concentration at $1.5 \times 10^{-7} \text{M}$ and decreases slightly thereafter. 119

Figure 4-18: Spring embedded correlation plot for the analysis of the metabolic footprint of ciclosporin treated HaCaT cells. The metabolite peaks are represented by the circles and the number within the circle is the metabolite ID. The larger the circle the more significant the metabolite was determined to be by ANOVA analysis. The links shown between metabolites illustrate the correlations present, the magnitude of which is shown by the number. The nearer the number is to 1 the greater the degree of correlation..... 120

Figure 4-19: Box and Whisker plots for metabolites 28, 32, 120 and 135 to illustrate a degree of metabolic response to ciclosporin exposure within the metabolic footprint. All

metabolites show a positive response to initial treatment through an increase in concentration between $0-1 \times 10^{-7}$ M followed by a decrease in concentration between $1-2.5 \times 10^{-7}$ M..... 121

Figure 4-20: Constructed metabolite map to illustrate the affect of dithranol treatment of HaCaT cells..... 123

Figure 5-1: Protein quantification standard curve for dithranol treated HaCaT cells..... 140

Figure 5-2: An example result for 1D gel electrophoresis analysis of the proteome of control HaCaT cells..... 144

Figure 5-3: 2D gel electrophoresis results illustrating the protein presence and localisation within a control, dithranol treated, methotrexate treated and a ciclosporin treated sample. 145

Figure 5-4: Schematic representation indicating the proportion of proteins which were up-regulated, down-regulated, deemed equivalent or non significant within the proteome of dithranol treated HaCaT cells. 147

Figure 5-5: Reconstructed metabolite map depicting the proteins (*red italics*) successfully identified within dithranol treated HaCaT cells and the corresponding linked metabolites (black normal font). Adjacent metabolites are linked with block lines while pathways with some metabolites omitted are linked with dashed lines. The presence of proteins over the concentration range is summarised within the box diagrams whereby green implies that the protein was present within all three replicate samples, blue indicates that the protein was detected within two replicates and red indicates that the protein was not detected. The control sample is the left hand box and the highest concentration the right hand box. 149

Figure 5-6: Schematic representation indicating the proportion of proteins which were up-regulated, down-regulated, deemed equivalent or not significant within the proteome of methotrexate treated HaCaT cells. 155

Figure 5-7: Reconstructed metabolite map depicting the proteins (*purple italics*) successfully identified within methotrexate treated HaCaT cells and the corresponding linked metabolites (black). Adjacent metabolites are linked with block lines while pathways with some metabolites omitted are linked with dashed lines. The presence of proteins over the concentration range is summarised within the box diagrams whereby green implies that the protein was present within all three replicate samples, blue indicates that the protein was detected within two replicates and red indicates that the protein was not detected. The control sample is the left hand box and the highest concentration the right hand box. 158

Figure 5-8: Schematic representation indicating the proportion of proteins which were up-regulated, down-regulated, deemed equivalent or non significant within the proteome of ciclosporin treated HaCaT cells. 162

Figure 5-9: Reconstructed metabolite map depicting the proteins (*orange*) successfully identified within ciclosporin treated HaCaT cells and the corresponding linked metabolites (black). Adjacent metabolites are linked with block lines while pathways with some metabolites omitted are linked with dashed lines. The presence of proteins over the concentration range is summarised within the box diagrams whereby green implies that the protein was present within all three replicate samples, blue indicates that the protein was detected within two replicates and red indicates that the protein was not detected. The control sample is the left hand box and the highest concentration the right hand box. 164

Figure 6-1: PCA plots of PC1 vs PC2 accounting for 76.82% total explained variance from the complete data set. Plot A illustrates the variance within the data in terms of response;

responder (R), intermediate responder (I), non-responder (N) and QC sample (Q). Plot B illustrates the variance using the sample order as the naming structure..... 176

Figure 7-1: Detection of enzyme activity and reactions involved. (A) Schematic drawing of DCPIP (the final electron acceptor) in its oxidised and reduced form. (B) Representation of the reduction of DCPIP by FADH_2 from its oxidised blue form of the dye to the reduced colourless form. (C) The reaction catalysed by the enzyme succinate dehydrogenase (EC 1.3.5.1)..... 184

Figure 7-2: Schematic representations of (A) the citric acid cycle showing where succinate is converted into fumarate, and (B) the electron transport chain detailing where sodium azide inhibits cytochrome oxidase. (C) SERS spectra of the artificial electron acceptor DCPIP in its oxidised and reduced forms which occurs due to the redirection of electrons from the electron transport chain..... 185

Figure 7-3: Transmission electron micrograph of citrate reduced Au colloids showing good homogeneity. The scale bar is 50nm..... 189

Figure 7-4: Graph representing the kinetic experiments ($\text{DCPIP}_{\text{ox}} \rightarrow \text{DCPIP}_{\text{red}}$) monitored spectrophotometrically. The wavelength used for analysis is 600 nm. From the top to bottom are the controls employed to assay the enzyme activity; see text for full details. Correlations coefficients (R^2) are also shown in the inset. 191

Figure 7-5: Representative raw Raman and SERS spectra, from top to bottom: Raman spectra of DCPIP in the solid state; followed by SERS spectra collected after 5 min aggregation at pH 7.2, pH 5.5 and pH 2.2 respectively. The three vibrational bands from SERS that were used for kinetic analysis are indicated by arrows and these are at 243, 404 and 498 cm^{-1} 192

Figure 7-6: SERS spectra of the succinate dehydrogenase enzyme reaction. Aggregation was performed without poly L-lysine at (A) pH 5.5, (C) pH 2.2 and (E) pH 7.2 - from top to bottom

the spectra shown were collected after 5, 10, 15, 20, 25 and 30 min of enzyme reaction. Plots of \log_{10} peak area *versus* time for the vibrational bands at (B) 238 cm^{-1} for measurements conducted at pH 5.5, (D) 257 cm^{-1} ($R^2 = 0.983$) for SERS at pH 2.2, and (F) for readings at pH 7.2 for bands 243 , 404 and 498 cm^{-1} ($R^2 = 0.952$, 0.976 and 0.939 , respectively); error bars show standard deviations from the three replicate measurements.

..... 195

List of Tables

Table 1-1: A summary table illustrating three biological pathways which have been highlighted as possible targets during methotrexate treatment. Adapted from Bangert & Costner, 2007.	39
Table 1-2: Summary table of biological treatments, their target, year of approval and biological composition. Summarised from (Sauder and Mamelak, 2004)	41
Table 2-1: Metadata for samples collected for image analysis. Colour coding indicates the pairing of control and diseased samples. Samples are age and sex matched as closely as possible. *day of birth unavailable.....	61
Table 3-1: Demographic details of keloid cases involved in the study.....	71
Table 3-2: Clinical details (patient history and examination findings) of keloid scars analysed in the study, * represents variation to the surrounding skin.....	71
Table 3-3: Tentative infrared vibrational band assignments for regions of interest.	81
Table 4-1: DMEM culture media composition.	89
Table 4-2: A summary of the results gained from the internal and external metabolome of HaCaT cells exposed to dithranol, methotrexate and ciclosporin. The table highlights the overall number of metabolite peaks identified, the number of metabolite peaks declared significant and the number of significant metabolite peaks which were identified.....	96
Table 4-3: Identified metabolites from the internal and external metabolome of dithranol treated HaCaT cells. The majority of metabolites were identified solely within the internal metabolome (indicated in black) while five metabolites were recorded in the external metabolome. A reference number corresponding to the human metabolome database and the chemical formula is given. The correlation group number is supplied for internal metabolites as discussed in Section 4.3.4.1. Metabolite ID's labelled with a * highlight multiple derivatisation products.	104
Table 4-4: Identified metabolites from the internal and external metabolome of dithranol treated HaCaT cells. The majority of metabolites were identified solely within the internal metabolome (indicated in black) while five metabolites were recorded in the external metabolome. A reference number corresponding to the human metabolome database and the chemical formula is given. The correlation group number is supplied for internal	

metabolites as discussed in Section 4.3.4.1. Metabolite ID's labelled with a * highlight multiple derivatisation products. 105

Table 4-5: Identified metabolites from the internal and external metabolome of methotrexate and ciclosporin treated HaCaT cells. A reference number corresponding to the human metabolome database, the chemical formula and corresponding *p* values supplied for all metabolites. Metabolite ID's labelled with a * highlight multiple derivatisation products..... 106

Table 5-1: A table to illustrate the protein content of HaCaT cells exposed to dithranol. The sample name prefix corresponds to the concentration of dithranol ($\mu\text{g}/\text{mL}$) or control (c). The sample name suffix corresponds to the replicate number. 141

Table 5-2: A table to illustrate the protein content of HaCaT cells exposed to methotrexate. The sample name prefix corresponds to the concentration of methotrexate ($\times 10^{-7}\text{M}$) or control (c). The sample name suffix corresponds to the replicate number..... 142

Table 5-3: A table to illustrate the protein content of HaCaT cells exposed to ciclosporin. The sample name prefix corresponds to the concentration of ciclosporin ($\times 10^{-7}\text{M}$) or control (c). The sample name suffix corresponds to the replicate number. 143

Table 5-4: Summary table illustrating the proteins identified within the proteome of dithranol treated HaCaT cells. The protein name, associated EC number and the metabolism location is provided. The colour scheme dictates the presence or omission of a protein at the given drug treatment concentration. Green implies that the protein was present within all three replicate samples, blue indicates that the protein was detected within two replicates and red indicates that the protein was not detected. 148

Table 5-5: Summary table illustrating additional identified proteins within the proteome of dithranol treated HaCaT cells. The colour scheme dictates the presence or omission of a protein at the given drug treatment concentration. Green implies that the protein was present within all three replicate samples, blue indicates that the protein was detected within two replicates and red indicates that the protein was not detected. 151

Table 5-6: Summary table illustrating the proteins identified within the proteome of methotrexate treated HaCaT cells. The protein name, associated EC number and the metabolism location is provided. The colour scheme dictates the presence or omission of a protein at the given drug treatment concentration. Green implies that the protein was

present within all three replicate samples, blue indicates that the protein was detected within two replicates and red indicates that the protein was not detected. 156

Table 5-7: Summary table illustrating additional identified proteins within the proteome of methotrexate treated HaCaT cells. The colour scheme dictates the presence or omission of a protein at the given drug treatment concentration. Green implies that the protein was present within all three replicate samples, blue indicates that the protein was detected within two replicates and red indicates that the protein was not detected. 159

Table 5-8: Summary table illustrating the proteins identified within the proteome of ciclosporin treated HaCaT cells. The protein name, associated EC number and the metabolism location is provided. The colour scheme dictates the presence or omission of a protein at the given drug treatment concentration. Green implies that the protein was present within all three replicate samples, blue indicates that the protein was detected within two replicates and red indicates that the protein was not detected. 163

Table 5-9: Summary table illustrating additional identified proteins within the proteome of ciclosporin treated HaCaT cells. The colour scheme dictates the presence or omission of a protein at the given drug treatment concentration. Green implies that the protein was present within all three replicate samples, blue indicates that the protein was detected within two replicates and red indicates that the protein was not detected. 165

Table 6-1: Patient metadata collected prior to treatment with methotrexate. The table illustrates the patient identification code, sex, age and baseline PASI score. 173

Table 6-2: Patient information illustrating the dose of methotrexate administered, the starting PASI score, the PASI score post treatment and the corresponding response rate and status. 174

Table 6-3: Kruskal-Wallis results table identifying metabolites significantly related to response to treatment. The metabolite identification and subsequent *p* value is shown. The box & whisker plot illustrates the metabolite level in responders (left), intermediate responders (middle) and non-responders (right)..... 177

Table 6-4: Kruskal-Wallis results table identifying metabolites significantly related to sex of patient. The metabolite identification and subsequent *p* value is shown. The box & whisker plot illustrates the metabolite level in male patients (left) and female patients (right). 179

Abstract

The University of Manchester

Katherine Anne Hollywood: June 2010

Degree of Doctor of Philosophy in the Faculty of Engineering and Physical Sciences

The Development of Bio-Analytical Techniques for the Treatment of Psoriasis and Related Skin Disorders.

In this investigation a number of post-genomic technologies have been applied to study the dermatological disorders of psoriasis and keloid disease. In spite of considerable research focus on these diseases the pathogenesis remains unclear and currently no cure is available however, both diseases are manageable by drug intervention. It is common place that patients who are suffering from skin disorders are diagnosed and the extent of the disease assessed by a dermatologist which may be subjective due to human error. The availability and application of methods to screen patients and quantify the level of disease or response to treatment has obvious benefits in disease management.

The work has incorporated a two-pronged approach combining the spectroscopic analysis of excised tissue samples and the phenotypic profiling of a rapidly proliferating cell line in response to drug intervention. The initial analysis of psoriatic skin samples by MALDI-MS provided poor results which remain relatively unexplained; however similar problems have been observed by other research groups. In a complementary approach the HaCaT cell line was exposed to increasing concentrations of three anti-psoriatic drugs namely dithranol, methotrexate and ciclosporin and the cells profiled using both metabolomic and proteomic methods. A number of metabolic pathways were highlighted including glycolysis and the TCA cycle. This has resulted in a selection of potential biomarkers which could be investigated in further work. In a small follow on study a collection of plasma samples from patients undergoing methotrexate treatment were analysed. The level of patient metadata and the number of samples was relatively limiting however, a subset of metabolites were significantly altered between responders and non-responders and with further validation could be potential biomarkers of successful treatment. The analysis of excised keloid samples was conducted using FT-IR microspectroscopy where it was possible to successfully discriminate between keloid and normal tissue. The use of imaging FTIR illustrated the complex cellular composition within a keloid scar, with increased lipid, amide and phosphate levels being observed. These measurable variations could, in the future, be incorporated into surgical procedures to allow targeted excision ensuring all keloid areas are removed. Finally a SERS-based analysis was conducted to investigate the possibility of probing dynamic enzymatic processes. This was successful and with the use of varying reporter molecules could be a beneficial tool for the analysis of metabolic processes.

This project has successfully used a number of bio-analytical techniques to investigate dermatological problems. While the ultimate goal would be the application of a single analytical technique to provide answers to biological questions, it has been found that a number of complimentary techniques and statistical data handling approaches can provide a valuable insight into the problems posed.

Declaration

No portion of the work referred to in the thesis has been submitted in support of an application for another degree or qualification of this or any other university or other institute of learning.

Notes on Copyright:

- i. The author of this thesis (including any appendices and/or schedules to this thesis) owns certain copyright or related rights in it (the "Copyright") and s/he has given The University of Manchester certain rights to use such Copyright, including for administrative purposes.
- ii. Copies of this thesis, either in full or in extracts and whether in hard or electronic copy, may be made **only** in accordance with the Copyright, Designs and Patents Act 1988 (as amended) and regulations issued under it or, where appropriate, in accordance with licensing agreements which the University has from time to time. This page must form part of any such copies made.
- iii. The ownership of certain Copyright, patents, designs, trademarks and other intellectual property (the "Intellectual Property") and any reproductions of copyright works in the thesis, for example graphs and tables ("Reproductions"), which may be described in this thesis, may not be owned by the author and may be owned by third parties. Such Intellectual Property and Reproductions cannot and must not be made available for use without the prior written permission of the owner(s) of the relevant Intellectual Property and/or Reproductions.
- iv. Further information on the conditions under which disclosure, publication and commercialisation of this thesis, the Copyright and any Intellectual Property and/or Reproductions described in it may take place is available in the University IP Policy (see <http://www.campus.manchester.ac.uk/medialibrary/policies/intellectual-property.pdf>), in any relevant Thesis restriction declarations deposited in the University Library, The University Library's regulations (see <http://www.manchester.ac.uk/library/aboutus/regulations>) and in The University's policy on presentation of Theses.

Abbreviations

2D	2 dimensional
APCI	atmospheric pressure chemical ionisation
APPI	atmospheric pressure photo ionisation
ATP	adenosine triphosphate
ATR	attenuated total reflectance
ChIP	chemical inkjet printer
CI	chemical ionisation
DA	discriminant analysis
DC	direct current
DHB	2,5-dihydroxybenzoic acid
DTGS	deuterated triglycine sulphate
EI	electron impact
ESI	electospray ionisation
FDA	United States food and drug administration
FPA	focal plane array
FPGS	folypolyglutamyl synthase
FTICR	Fourier transform ion cyclotron resonance
FT-IR	Fourier transform infrared
GC-MS	gas chromatography mass spectrometry
IEF	isoelectric focussing
KD	keloid disease
LC-MS	liquid chromatography mass spectrometry
LD	laser desorption
MALDI	matrix assisted laser desorption ionisation
MCT	HgCdTe
MS	mass spectrometry
OCT	optimal cutting temperature
PASI	psoriasis area severity index
PC	principal component
PCA	principal components analysis
PLS	partial least squares
PLS-DA	partial least square-discriminant analysis
Q	linear quadrupole
QQQ	triple quadrupole
Q-TOF	quadrupole-time of flight
RF	radio frequency
ROC	receiver operator curve
RT	retention time
SDS	sodium dodecyl sulphate
TMS	trimethylsilyl
TNF	tumor necrosis factor
TOF	time of flight
UV	ultraviolet

Acknowledgements

I am deeply thankful to my PhD supervisor Prof Roy Goodacre for his encouragement, support and guidance throughout my time within his group and for giving me the opportunity undertake my PhD. A huge amount of my gratitude is extended to Dr Catherine Winder and Dr Rick Dunn for their friendship and support and who have both assisted my work in countless ways and to Dr David Broadhurst for his encouragement and belief in my work. I am also sincerely grateful to Dr Iqbal Shadi and Dr Kathleen Carroll for sharing their knowledge and expertise and for inviting me to participate in their area of research. Aside from my research group, I have been fortunate to collaborate with a number of people. Great thanks have to be extended to Prof Christopher Griffiths, Dr Richard Warren and Dr Rachel Watson whose discussion and thoughts on psoriasis have been greatly beneficial and who have permitted my access to clinical samples. In addition my gratitude is given to Dr Ardeshir Bayat for sharing his expertise on keloid disease and the provision of samples.

Along the way I have been assisted by a number of extremely kind and helpful people who have gone above and beyond to help; Ms Susan Slack (for not running away when my required cell growth escalated at rapid rates) and Sr. June Bowden for recruiting volunteers and for collecting the required biopsy samples (when I was too squeamish to watch!).

I also need to express my gratitude to my Mum for the initial encouragement and support to undertake a university education and for believing in the completion of my PhD! Not forgetting the Meehan/Kane clan for their support and encouragement and especially Sarah and Jim (*aka 009*) for providing my Manchester base during the concluding stages. David, thank you for being part of our team and for helping to get me through this, I'm very excited about our future together.

Ultimately the work presented within this thesis was made possible due to the financial sponsorship granted from Stiefel Laboratories, Inc.

Chapter 1: Introduction

1.1 Significance

In modern biological research a number of common diseases such as an array of cancers, diabetes, Crohn's disease and psoriasis remain at the forefront of focus. The precise etiology of these diseases is often unknown and complex. The onset of the 'omic era has provided novel routes for high-throughput analysis and subsequent interpretation of biological questions. These include investigations at the level of gene expression (transcriptomics), protein translation (proteomics) and more recently the metabolite network (metabolomics). The implementation of such approaches is often accompanied with the use of systems biology techniques. Systems biology is a broad term to describe the use of informatics to explore and interpret complex data sets which are generated during 'omic procedures. It is often possible to identify potential biomarkers for disease by utilising these types of approaches. It is envisaged that by incorporating a range of bio-analytical platforms and 'omic approaches into the area of psoriasis research it could be possible to uncover underlying information regarding the onset and pathogenesis of the disease, and ultimately treatment.

1.2 Aims and Objectives

The aim of the work presented within this thesis is to incorporate the use of a variety of bio-analytical platforms in the field of dermatological research. There are vast arrays of analytical platforms commercially available for biological research which could provide novel routes for the detection, diagnosis or for investigating the pathogenesis of disease. These techniques could provide an automated standardised approach, independent of personal assessment by dermatologists.

In a two-pronged approach analysis will be performed on both biopsy tissue samples and cultured cells. The analysis of psoriasis tissue samples will be analysed *via* matrix assisted laser desorption ionisation (MALDI) mass spectrometry (MS) and keloid tissue samples analysed by Fourier transform infrared (FT-IR) microspectroscopy. Through the spatial imaging of diseased and non-diseased skin it will be possible to identify variations in biological composition between samples and also through varying regions within single tissue samples. As cell culture is more controllable this will be used in a metabolomic and proteomic-based analysis of psoriasis. The HaCaT cell type was chosen to mimic the cellular level of a psoriatic outbreak. In an attempt to probe the metabolite and protein variation in psoriasis, the cells will be exposed to a selection of well established anti-psoriatic drugs. It is hoped that variations in certain metabolite/protein concentrations will be determined; which could provide additional information regarding the drug mode of action and identify potential biomarkers for disease. In a small follow on study a metabolomics approach will be applied to a selection of plasma samples provided from a psoriasis drop in clinic. Although this study is limited in terms of sample numbers it could provide additional information regarding metabolite variation during onset of disease. In a final study we aim to investigate the possibility of using Raman spectroscopy to monitor the enzyme kinetics of a biological pathway. This is an area that with further research could be extremely beneficial for metabolomic and proteomic experiments and consequently could be transferable to dermatological research in the future.

1.3 Psoriasis

1.3.1 Introduction to Psoriasis

Psoriasis is a chronic immune inflammatory mediated disease which affects approximately 2-3% of the world population. The disease primarily manifests itself in the skin; however an additional effect is regularly exhibited in nails and joints. Psoriasis can begin at any age, although the approximate mean age of onset has been estimated to be 33 years, with 75% of cases occurring before 46 years of age (Nevitt and Hutchinson, 1996). The occurrence of skin lesions however, varies throughout life and there may be periods of remissions and exacerbations which are often prompted by environmental or emotional triggers. The severity of the disease can greatly differ from patient to patient, and beyond the physical cutaneous symptoms are physiological and social effects on the patient's life. Psoriasis had a great impact on the sufferer and has a well known association with depression and low quality of life (Rapp et al., 1999), (Krueger et al., 2001).

1.3.1.1 Clinical Appearance

The most prevalent form of psoriasis, psoriasis vulgaris, accounts for 90% of all cases (Bhalerao and Bowcock, 1998). Psoriasis vulgaris is characterized by the appearance of reddened scaly plaques (Figure 1.1) which vary in density and size and can occupy any location on the body. A symmetrical distribution is common with the most prominent areas to be affected being the scalp, knees, elbows and lower back, (Altman and Kamino, 1999).



Figure 1-1: An example of plaque psoriasis exhibited in the elbow region of a psoriasis patient (Provided by Prof. CEM. Griffiths, University of Manchester).

The remaining 10% of psoriasis cases comprise of guttate psoriasis, inverse psoriasis, pustular psoriasis, palmoplantar psoriasis and erythroderma.

1.3.1.2 Associated Co-morbidities

A factor that greatly increases the significance of psoriasis is its association with other disorders. Psoriasis patients are often at risk of suffering from concurring debilitating and life threatening morbidities. Psoriasis and other associated diseases are thought to share common inflammatory pathways. The most prominent non-cutaneous disease associated with psoriasis is psoriatic arthritis (FitzGerald and Winchester, 2009), a potentially disabling inflammatory condition that affects 5-30% of patients with psoriasis (Kaltwasser et al., 2004). Irritable bowel syndrome also known as Crohn's disease is a chronic inflammatory disease of the digestive system and whose prevalence was shown to be significantly higher in psoriasis patients compared to a control group (0.5% and 0.2% respectively) (Cohen et al., 2009). However in recent years the link between psoriasis and cardiometabolic conditions such as cardiovascular disease, diabetes as well as the metabolic syndrome has received greater attention (Gottlieb et al., 2008). An increased mortality from cardiovascular diseases have been documented in patients with severe psoriasis, (Mallbris et al., 2004), confirmed by a cohort study indicating a twofold more prevalent occurrence for psoriasis patients in comparison to age matched control patients (Henseler and Christophers, 1995). Several

studies have indicated a possible correlation between psoriasis and diabetes including noticeable variations in glucose levels and insulin resistance (Boehncke et al., 2007), (Brenelli et al., 1995),(Henseler and Christophers, 1995). Patients with psoriasis are additionally at a greater risk of suffering from metabolic syndrome (Girolomoni and Gisondi, 2008). The metabolic syndrome is a cluster of risk factors and in general is defined as the presence of 3 or more of the following components: abdominal obesity, increased insulin resistance/elevated fasting glucose level, elevated blood levels of triglycerides and/or cholesterol and hypertension (Gottlieb and Dann, 2009). It is common that symptoms of the metabolic syndrome go concomitantly with an increased risk of diabetes and cardiovascular disease. These additional co-morbidities could provide increased levels of variation in metabolites and proteins during a psoriatic outbreak.

1.3.2 Histological Features of Psoriasis.

The fundamental variations between psoriatic and normal skin is visible through the interpretation of haematoxylin and eosin (H&E) stained histological skin sections. Figure 1.2 illustrates normal skin (A), involved psoriatic skin (B) and non-involved psoriatic skin (C). In terms of psoriatic skin, an involved section is taken from an area where a psoriatic plaque is visible on the surface while a non-involved section is representative of an area which on the surface appears unaffected.

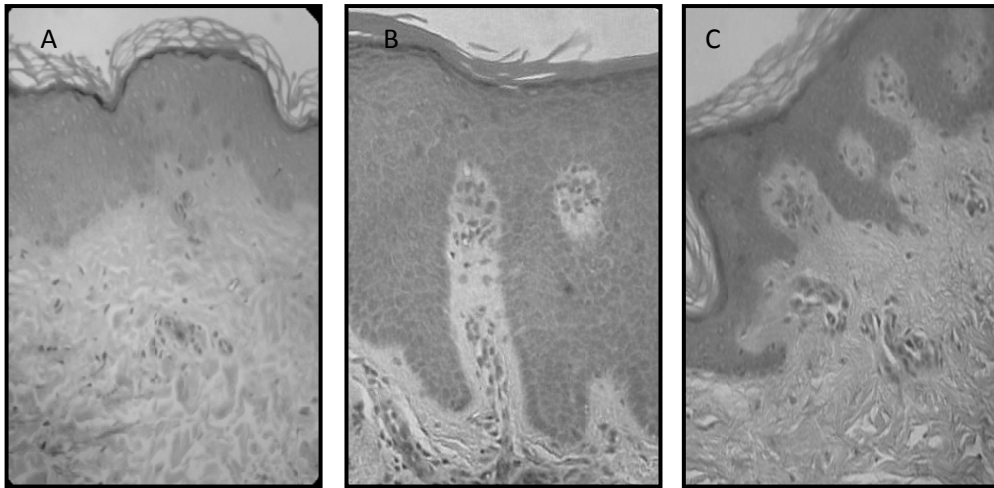


Figure 1-2: Haematoxylin & Eosin stained sections for a) normal skin section, b) Involved psoriasis section, c) Uninvolved psoriasis section. All images collected using a Zeiss Imager A1 microscope at 400X magnification. Images captured using a Canon Powershot G6 camera.

Normal skin is constructed of two fundamental layers, the epidermis and the dermis. A schematic diagram is illustrated in Figure 1.3. The epidermis is the upper most layer of the skin whose objective is to provide a waterproof protection. The epidermis itself can be divided into five areas; the outermost area is termed the stratum corneum which is visible as a “basket weave” type structure, the stratum lucidum a layer only found in thick areas of skin *i.e.* palms of hands or soles of feet, the stratum granulosum, the stratum spinosum and finally the deepest layer the stratum basale. Keratinocytes are the principal cell type found in the epidermis and are produced by cell division occurring through the stratum basale. The keratinocytes move progressively through the epidermis to the upper layers of the skin while undergoing a process termed terminal differentiation, to resultantly form the stratum corneum. The average epidermal transit is 8-10 weeks; the loss of cells from the surface is co-ordinated with production in order to maintain a constant epidermal thickness. Within the stratum granulosum the migrating keratinocytes continue to differentiate, synthesise keratin and begin to flatten in structure. The presence of keratin is important in water barrier formation and as a source of energy and flexibility for the cells. The epidermis also contains melanocytes and Langerhan cells. Melanocytes are responsible for the production

of melanin, the pigment accountable for the colour of human skin and for the provision of protection from UV radiation. Langerhans cells are present to provide immunological protection.

The dermis, the pale pink area beneath the epidermis, forms a significant part of the structure of skin. The dermis is a much thicker component in size than the epidermis and is constructed of a network of connective tissue. The dermis contains a variety of important structures including blood and lymphatic vessels, sweat glands, nerve endings and hair follicles. The dermis is responsible for the regulation of body temperature through the release of sweat and the erection and detracting of hairs on the skin surface and provides routes of transport through a complex capillary network.

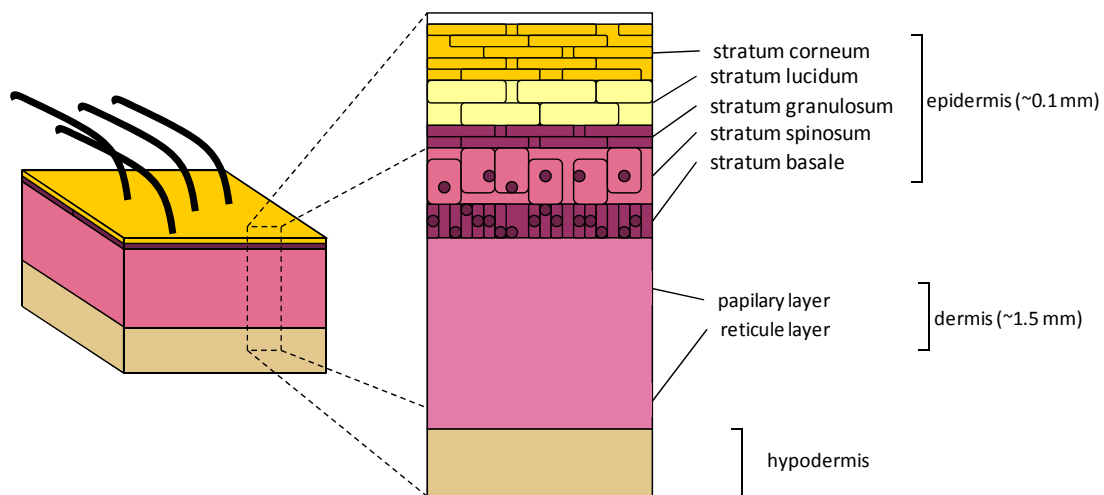


Figure 1-3: Schematic diagram illustrating the structure and composition of skin.

Psoriatic skin is characterised by a greatly thickened epidermal layer or epidermal hyperplasia (Figure 1-2). The hyperplastic epidermal changes are associated with an under expression of markers of keratinocyte differentiation, including keratin K1 and K10 (Griffiths and Barker, 2007). The thickened epidermis configuration shows elongated retes that protrude into the dermis. The amount of epidermal hyperplasia visible is correlated to the severity of the disease in the patient. An additional feature of psoriatic skin is the presence

of prominent blood vessels in the dermis and the collection of neutrophils in the epidermis and stratum corneum. The histology of non-involved skin is deemed to be normal.

1.3.3 Pathogenesis of Psoriasis: Current Thoughts.

The pathogenesis of psoriasis has been subject to evolving theories over the last couple of decades. Environmental and genetic factors are important in the etiology of psoriasis. The complex interplay amongst epidermal keratinocytes, mononuclear leukocytes, neutrophils, dendritic cells, and activated T cells, together with growth factors, chemokines, and cytokines, is now recognised as playing a major role in the pathogenesis of psoriasis (Lowe et al., 2007).

Dysfunctional keratinocyte apoptosis occurs in psoriatic skin (Laporte et al., 2000). Apoptotic cell death is critical for balancing keratinocyte proliferation as well as for the formation of the stratum corneum and hence without sufficient regulation the presence of overgrown psoriatic plaques is observed. The paradigm of activators, inhibitors, adapters and effectors is reiterated in multiple apoptotic pathways in mammalian cells, (Raj et al., 2006). Biochemical studies have illustrated specific changes in the expression of many cellular markers in psoriasis. The markers of epidermal proliferation; the keratins (namely K6, K10, K16 and K17), epidermal growth factor (EGF) receptor and ornithine decarboxylase are usually up-regulated in psoriasis, (Duvic et al., 1997).

Most current models of pathogenesis are focused on the actions of activated leucocytes and secreted cytokines that, in turn, produce reactive changes in skin cells according to pre-programmed pathways (Krueger and Bowcock, 2005). Nickoloff *et al.* provides a comprehensive review on the involvement of cytokines and chemokines in psoriasis, (Nickoloff et al., 2007). Cytokines are responsible for cellular communication required for the mediation of reactions between cells. Cytokines are generally recognised for their ability to influence the proliferation, differentiation, or secretion of proinflammatory or anti-

inflammatory factors by resident and recruited cell types. Chemokines are similar in function but are readily associated with the modulation of migratory cell movement. Types of cytokines which have been indicated as significant during a psoriasis outbreak include tumour necrosis factor (TNF), interleukins (ILs) and interferons (IFNs).

Three types of dendritic cells are found in involved skin but absent in normal skin; dermal factor dendritic cells, a subset of dendritic cells known as plasmacytoid dendritic cells, and Langerhans cells in the epidermis (Griffiths and Barker, 2007). Dendritic cells (DCs) are a unique population of leukocytes that regulate immune responses and have the ability to interact with and activate T cells. Langerhans cells (LCs) are members of this wider family of DCs. LCs reside in the epidermis, where they serve as guards of the immune system, their responsibility being to sample the external environment for changes and challenges and to deliver information (antigen) to T cells within skin-draining lymph nodes. The ability of LCs to migrate from epidermis to regional lymph nodes is thus of pivotal importance to the induction of cutaneous immune responses (Cumberbatch et al., 2006).

This immunological response is often triggered by an external factor, *i.e.* a physical injury, infections or stress and external factors such as drugs, smoking and alcohol is known to increase the likelihood of a psoriatic outbreak in individuals whom have a genetic predisposition. The concordance of psoriasis in monozygotic twins has been shown to be significantly greater than in dizygotic twins; data which is consistent to there being a strong genetic component to the disease (Bowcock and Krueger, 2005).

1.3.4 Current treatment methods for Psoriasis

There are a number of varying methods available for the treatment of psoriasis. The treatments can be classified into three arrays; topical, systemic and the more recently developed biologics. The selection of a treatment method is often dependent of individual patient needs, cost and geographical location. It is additionally common that multiple

treatment methods are used in a multi-targeted approach. A brief introduction will be given into each type of treatment and greater emphasis placed on the specific drugs which will be investigated within the work to be presented.

1.3.4.1 Topical Treatments

Topical treatments are those which are applied directly to the area of inflammation on the surface of the skin. They are usually the first stage of treatment for mild to moderate cases of psoriasis. Topical therapies are also advised to patients with more severe disease, mostly in combinations such as with photo(chemo)therapy (UVB, PUVA), oral systemic agents, or biological methods (Bos and Spuls, 2008). Several topical treatments are available for psoriasis sufferers; however the effectiveness varies between cases. The most frequently used and prevalent forms of topical psoriasis agents are vitamin A and D analogues, tar preparations and dithranol. The advantage with topical treatments is their availability for home application and at day centres. There are however, as with most types of treatments, problems with attributed side-effects and a particular limitation is patient compliance (van de Kerkhof et al., 2008).

1.3.4.1.1 Dithranol

Dithranol also known as anthralin has been a mainstay in psoriasis treatment for more than eight decades and is a natural derivative of chrysarobin, prepared from the araroba tree. Dithranol's IUPAC name is 1,8-dihydroxy-9-anthrone whose chemical structure is shown in Figure 1-4.

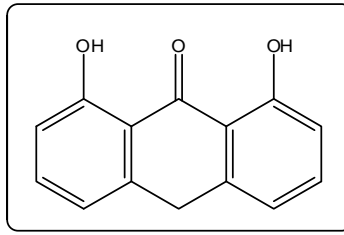


Figure 1-4: The chemical structure of dithranol.

The primary cellular target for dithranol treatment is the mitochondria of cells where it has been shown to accumulate by using fluorescence and confocal microscopy (McGill et al., 2005). Dithranol has been shown to act as an electron donor to membrane-associated redox components and to inhibit adenosine triphosphate (ATP) synthesis. It is proposed that ATP depletion will limit energy dependent metabolism and thus could provide a mechanism for inhibition of cell proliferation (Fuchs et al., 1990).

It has been shown through retrospective studies that dithranol can induce the clearance of psoriasis outbreaks in 72-95% of patients whom were treated for 24h (van de Kerkhof et al., 2008). It can be found in varying formulations including pastes, creams or ointments. Nevertheless, the use of dithranol is deemed inconvenient and troublesome due to its irritation and discolouration of normal as well as diseased skin.

1.3.4.2 Systemic Treatments

Systemic treatments are used in moderate to severe cases where topical treatments have failed to show a significant effect. These forms of treatment are administered orally or intravenously and therefore the effect of the drug is less localised and witnessed within the entire body. This approach is advantageous as the underlying biological triggers (as discussed in Section 1.3.3) are targeted in addition to the presented plaques on the surface of the skin. The most common and readily administered systemic treatments are methotrexate, ciclosporin and retanoids. These treatments are sometimes prescribed in varying combinations depending on the patient's response rates. However, with systemic

treatments there are greater risks of the onset of physical and mental side effects and hence treatment selection is greatly influenced by a number of factors including, age, sex, general health, ability to comply with the treatment, previous treatments, as well as the type, extent and duration of the disease (Spuls et al., 1997). A major advantage of systemic treatments, especially in respect to newer biological approaches, is the cost; for example the cost of methotrexate treatment is approximately £55 compared to £10,000 for biological treatment per annum (Warren et al., 2008).

1.3.4.2.1 Methotrexate

Methotrexate, a folic acid derivative, was approved for use in the treatment of psoriasis in 1972 by the United States food and drug administration (FDA) for the treatment of severe, recalcitrant, disabling psoriasis (Kalb et al., 2009). The structure of methotrexate is shown in Figure 1-5. Methotrexate has been known as the gold standard within the field of systemic treatments (Saporito and Menter, 2004), however this award is currently being challenged by the increasing use of new biological treatments. Methotrexate has a number of adverse side effects associated with its use including severe liver toxicity and bone marrow suppression. Patients prescribed with methotrexate must be monitored closely and long term use is not recommended.

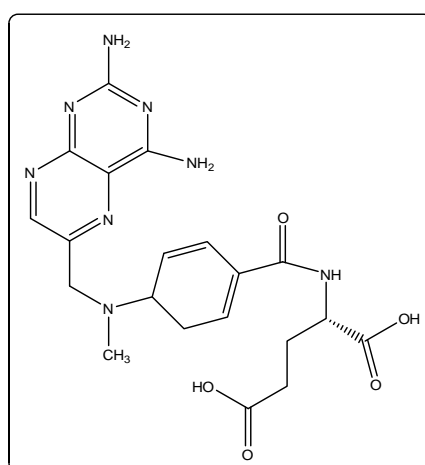


Figure 1-5: The chemical structure of methotrexate.

Methotrexate is a drug used to treat many diseases. The general mode of action of methotrexate is well established; however, the exact action of methotrexate in the anti-psoriatic process is somewhat unknown. Methotrexate as a folic acid antagonist functions as an immunosuppressive agent. Methotrexate competitively inhibits the reduction of folate co-factors by binding intra-cellularly to dihydrofolate reductase thus preventing the conversion of dihydrofolate to tetrahydrofolate (Strober and Menon, 2005). Tetrahydrofolate is a co-factor for a number of enzymes and is linked to amino acid and nucleic acid synthesis. A number of reactions which are subject to alteration are described in Table 1.1. This illustrates that *via* affecting purine and pyrimidine nucleotide synthesis, DNA and RNA synthesis is impaired hence cellular reproduction capabilities are reduced. A postulated mechanism of action in psoriasis treatment has also been proposed by Warren et al., 2008. This mechanism focuses attention on the importance of adenosine and glutamate. The mechanism involves methotrexate entering the cells through transport *via* a solute carrier. Within the cell methotrexate undergoes polyglutamation under the enzymatic regulation of folypolyglutamyl synthase (FPGS). In the polyglutamated form methotrexate inhibits aminoimidazole-4-carboxamide ribonucleotide transformylase, which is suggested as a possible route for some of the anti-inflammatory effects observed. This is proposed to be a result of an intracellular rise in adenosine which is reported to interact with a number of adenosine receptors. This theory could surmise that folate inhibition may not be as important as first thought.

Pathway	Enzyme inhibited	Step involved
De novo pyrimidine synthesis	Thymidylate synthetase	dUMP → dTMP (cofactor THF)
	Dihydrofolate reductase	DHF → THF (cofactor for above rxn)
De novo purine synthesis	GAR transformylase (early)	GAR → FGAR (cofactor THF)
	AICAR transformylase (late)	AICAR → FAICAR (cofactor THF)
DNA methylation	Methionine synthase	Homocysteine → Methionine (cofactor THF, B12)

Table 1-1: A summary table illustrating three biological pathways which have been highlighted as possible targets during methotrexate treatment. Adapted from Bangert & Costner, 2007.

1.3.4.2.2 Ciclosporin

Ciclosporin, whose structure is shown in Figure 1-6 was isolated originally from a soil fungus, *Tolypocladium inflatum Gams*, and was initially used as an anti-fungal agent. However in 1979 ciclosporin was reported to be beneficial in the treatment of psoriasis (Mueller and Herrmann, 1979) and since then the immuno-suppressive effect of ciclosporin has been readily utilised. Ciclosporin is a prodrug which activates upon forming a complex with cytoplasmic proteins called immunophilins (Madan and Griffiths, 2007). The primary effect exhibited by ciclosporin is the potent inhibition of T lymphocytes thus suppressing the response to antigen by inhibiting lymphokine secretion and proliferation (Berth-Jones, 2005). The use of ciclosporin has also been shown to have a direct action upon epidermal keratinocytes including inhibition of proliferation (Fisher et al., 1988, Kanitakis and Thivolet, 1990).

As seen with the majority of treatments available for psoriasis there are side effects attributed to the use of ciclosporin. The main side-effects are nephrotoxicity, hypertension and a potential risk of developing non-melanoma skin cancer (Flytstrom et al., 2008), hence close monitoring of patients is required and low doses are often employed.

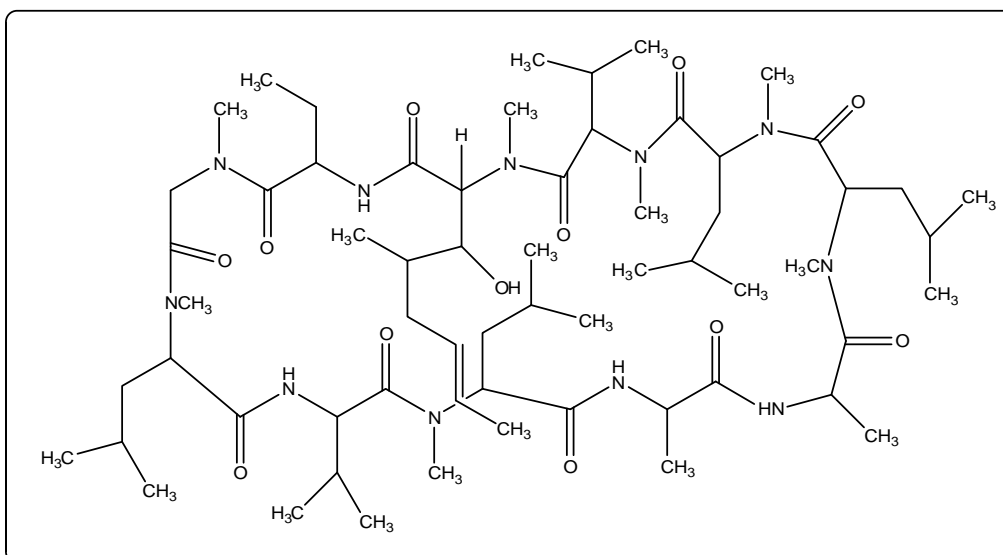


Figure 1-6: The chemical structure of ciclosporin.

1.3.4.3 Biologic Treatments

As detailed above most traditional anti-psoriasis drugs are toxic and so new biologic drugs are being developed to attempt to conquer the problem of side effects. It is expected that these biologics, which are proteins, are target specific and this reduces the possibility of side effects. They include fusion proteins, recombinant proteins (e.g. cytokines, selective receptors), and monoclonal antibodies, and are common forms of treatment for autoimmune diseases such as rheumatoid arthritis and Crohn's disease (Menter and Griffiths, 2007). A recent publication (Papp, 2008) has reviewed the four biologics which are currently available in the UK for the treatment of psoriasis; alefacept, efalizumab, etanercept and infliximab. The biologics are divided into two main groups: T cell modulators and tumour necrosis factor (TNF) inhibitors and their composition details are shown in Table 1-2. A thorough review of these biological treatments is available in (Tzu and Kerdel, 2008) and (Menter and Griffiths, 2007).

Biologic	Target	FDA Approval for Psoriasis Treatment	Composition
Alefacept	T cells modulation	2003	Receptor-Antigen fusion protein
Efalizumab	T cell modulation	2003	Monoclonal Antibody
Etanercept	TNF Inhibition	2004	Receptor-Antigen fusion protein
Infliximab	TNF Inhibition	2006	Chimeric monoclonal antibody

Table 1-2: Summary table of biological treatments, their target, year of approval and biological composition. Summarised from (Sauder and Mamelak, 2004).

The number of patients eligible for treatment by a biological approach is somewhat limited due to costs and availability, however, the impact of biologic treatment has been substantial for the treatment of moderate to severe psoriasis. The inclusion of protein-based treatment could lead to the long term regulation of psoriasis resulting in a significant increase in patient quality of life (van de Kerkhof, 2009). However, for the vast majority of patients a reliance on systemic treatments such as methotrexate and ciclosporin is prevalent.

1.4 Metabolomics

1.4.1 Introduction to Metabolomics.

As the area of metabolomics is relatively new, it was first coined by Oliver and colleagues in 1998, (Oliver et al., 1998) the exact definition and application of metabolomics undergoes frequent discussion, with theories and ideas differing from group to group. The general foundation of a metabolomics-based approach is the holistic and data driven study of the metabolism of both endogenous and exogenous metabolites present in biological systems (Dunn, 2008). A holistic approach investigates a system as a whole, incorporating the complex interactions known to be present into a single problem (Kell and Oliver, 2004). Hypothesis generation can greatly expand the realms of a scientific investigation, and although greatly dependant of the validity of produced data sets can allow hypotheses to be generated through inductive reasoning.

The metabolome is the quantitative complement of all low molecular weight molecules, termed metabolites, present in cells, tissues or organisms in a given physiological or developmental state (Hollywood et al., 2006) that are involved in metabolic processes. The contents of a metabolome denote the cellular processes that control the biochemical phenotype of the cell, tissue or whole organism (Allwood et al., 2008). Metabolites contained within a cell or tissue (endometabolome) or those occupying the extracellular environment (exometabolome) can be studied, either *in situ*, through imaging based analysis or more typically after sampling and extracting the metabolites (Dunn, 2008). The study of the endometabolome is frequently described as metabolic fingerprinting while conversely the study of the exometabolome can be termed metabolic footprinting.

An important factor in any metabolomic-based analysis on a cellular system is the effective quenching of a system. It is imperative that any enzyme action is rapidly and sufficiently halted without the loss of metabolites through leakage. The general method of quenching

involves a rapid change in temperature or pH. The most frequently used quenching method is the addition of 60% aqueous methanol at approximately -50°C. Following the quenching of metabolism it is necessary to extract the metabolites from the cells (Sellick et al., 2009). The aim here is to deactivate endogenous enzymes permanently and make the cell permeable to release the maximum number of cellular metabolites with the highest possible recoveries (Winder et al., 2008). Extraction methods can be sample specific and vary between research groups; however, it usually employs heat or cold and occasionally acid or base to facilitate cell lysis. These additional experimental parameters can be overcome through the use of a metabolite footprinting approach. Probing the exometabolome of a system can be undertaken through the study of culture media. This approach is deemed less technically demanding and is particularly beneficial in high-throughput studies.

In body fluid analysis (e.g., serum or urine) the content of these metabolomes can be greatly influenced by external factors such as food, drugs and alcohol as well as intrinsic factors such as diurnal cycle, age etc (Goodacre, 2007). The effect of external influences is especially noticeable when the metabolomic analysis of urine or serum is undertaken and for this reason experimental design frequently incorporates strict regulations on volunteers including fasting or restricted diet.

It is necessary to apply an element of realism, at present it is impossible to quantify or even detect all the metabolites within any biological system. Limitations arise because of chemical complexity and the large dynamic range of metabolites which has an impact on the analytical capabilities of the platform selected for use and also in the sample preparation conducted prior to analysis.

1.4.2 Analytical Platforms for Metabolomics

There are a number of analytical techniques which can be employed for metabolomic analysis. The emphasis is largely placed on mass spectrometry techniques although Fourier

transform infrared (FT-IR) and Nuclear Magnetic Resonance (NMR) spectroscopies are regularly utilised and Raman spectroscopy is gaining significance in the field. The choice of analytical platform is highly dependent upon the sample being analysed and ultimately the required outcome of the experiment.

1.4.2.1 FT-IR spectroscopy

1.4.2.1.1 General FT-IR Introduction

Infrared (IR) spectroscopy is one of the most common spectroscopic techniques used by scientists and has been proven to be a powerful technique for structural determination and compound identification. FT-IR spectroscopy is a rapid, reagentless, non-destructive analytical technique whose continuing development is resulting in manifold applications across a wide range of biosciences (Ellis et al., 2004). The major advantage associated with infrared spectroscopy is that virtually any sample in almost any given state can be determined with relative ease and minimal sample preparation. There is a vast array of IR based equipment that allows the optimum set-up for a sample to be established. Examples of such equipment include high-throughput analyses as well as microscope and attenuated total reflectance (ATR) based systems. It is also possible within a single system to operate in transmission or reflectance mode which offers further versatility to the user.

FT-IR is based on the principle that when a sample is interrogated with an infrared light beam, specific functional groups within a sample will absorb the infrared radiation at specific wavelengths and vibrate in a variety of manners, *i.e.* bend or stretch corresponding to discrete energy levels. A particular absorption or vibration corresponds directly to a particular chemical species and hence the spectrum produced is specific for that species and can be termed an infrared fingerprint.

A schematic diagram of an FT-IR instrument is shown in Figure 1-7. Infrared light is emitted from a black body source (usually the IR source is a globar) and the beam is focussed through an aperture into the interferometer. The interferometer consists of a beam splitter and two mirrors: one stationary and one moving. As the light enters the interferometer it follows a path until it hits the beam splitter; here the light is split into two. One beam is transmitted through the beam splitter to the moving mirror; which is moving in a “to and fro” manner at a constant velocity determined by the laser wavelength of the system. The second beam is reflected from the beam splitter towards the stationary mirror. The beams are reflected from their corresponding mirrors and the beams recombine at the beam splitter. An interferogram is produced from the interference pattern generated when the beams are combined. Variation occurs due to the difference in the distance travelled between the moving mirror in comparison to the stationary mirror resulting in some wavelengths recombining constructively or destructively. The interferogram leaves the beam splitter and is directed to the sample where the energy is either absorbed or transmitted. The energy which is transmitted reaches the detector and is passed to a computer for interpretation into the infrared spectra *via* the mathematical procedure of Fourier transform. The most common forms of detectors in infrared systems are deuterated triglycine sulphate (DTGS) or HgCdTe (MCT) based. The result of this process is an infrared spectrum of wavenumber (cm^{-1}) vs. absorbance.

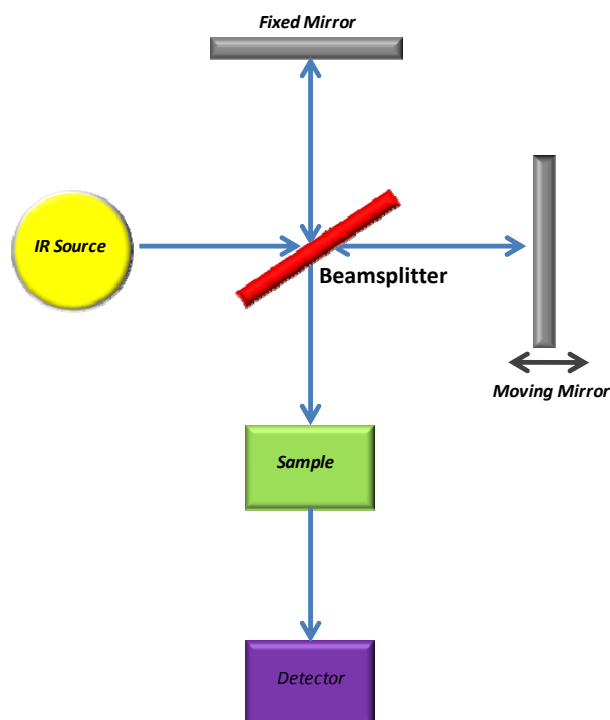


Figure 1-7: A schematic representation of an FT-IR instrument.

1.4.2.1.2 FT-IR Microspectroscopy

The onset of FT-IR microspectroscopy has significantly increased the ability and adaptability of the technique. FT-IR microspectroscopy can incorporate either a single detector element similar to standard FT-IR or a multi-detector element namely a focal plane array (FPA) detector. The incorporation of a single array detector with a light microscopy based system has the distinct advantage that the user can define an exact area of interest from which spectra can be taken. The FPA detector allows the analysis of larger areas again defined by the user through varying sizes of array e.g., 1x16, 32x32, 64x64 or 128x128 pixels. An individual infrared spectrum is collected at each pixel thus generating infrared hypercubes.

1.4.2.1.3 FT-IR applications in Clinical Metabolomics

FT-IR has been utilised as the analytical tool in many biological investigations. It is common that FT-IR is used during the initial stages of investigations as a method to probe global

changes in biochemical composition *i.e.* lipid or amide regulation. FT-IR is regularly used to interrogate variances in cells, tissues and bio-fluids associated with disease.

FT-IR has been used as a tool to distinguish between cell types including discrimination between drug-resistant and non-resistant human melanoma cell line (Zwielly et al., 2009) and the analysis of leucocytes in leukaemia research (Liu et al., 2007). In a recent study Gazi *et al.*, used an FT-IR microscopic approach to investigate the uptake and metabolism of fatty acids by metastatic prostate cancer. In this study PC-3 cells were cultured directly onto IR compatible slides and FT-IR spectra were collected with a 16x1 MCT linear array detector. The study illustrates the benefit of using FT-IR spectroscopy as it eliminates the need to undertake cell isolation or extraction of lipid molecules prior to investigation (Gazi et al., 2009).

The analysis of tissue samples is a useful variation of the technique. A diverse collection of tissue types have been analysed with FT-IR microspectroscopy; examples include a comparative study between normal, benign and malignant ovarian tissues (Krishna et al., 2007), discrimination between normal and malignant human gastric tissues (Fujioka et al., 2004), and the analysis of cervical cancer and melanoma biopsy samples (Mordechai et al., 2004), amongst many others. A study highly related to the work within this thesis is a project undertaken by Pouliot *et al.* (2007). The authors used ATR-FT-IR to analyse the stratum corneum in skin models derived from uninvolved and involved psoriatic cells in a discussion of the use of skin models in dermatological research (Bernard et al., 2007). FT-IR spectroscopy has also been implemented in a collection of studies investigating the diffusion of exogenous molecules/drugs through skin sections (Andanson et al., 2009, Tetteh et al., 2009, Hanh et al., 2000).

1.4.2.2 Mass Spectrometry

1.4.2.2.1 General Overview

Mass spectrometry was first invented in 1912 and is now a mainstay analytical platform for a variety of scientific disciplines. The basic configuration of a mass spectrometry platform is illustrated in Figure 1-8.

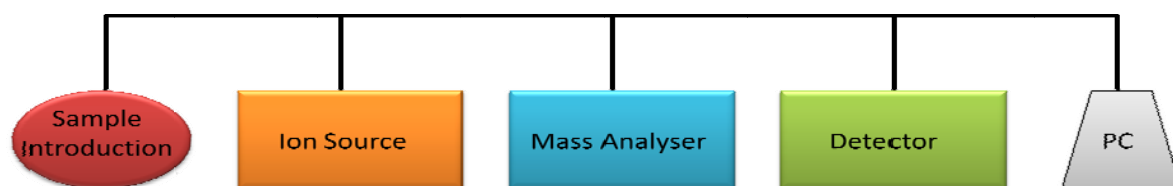


Figure 1-8: Schematic diagram of a mass spectrometer. A sample is introduced into an ion source where positive or negatively charged ions are created, separation of ions according to their mass to charge (m/z) ratio occurs within the mass analyser followed by detection within the detector element. Instrumental components and experimental parameters are controlled computationally and in addition all data is collected and stored on the connected PC. Adapted from (Dunn, 2008).

A sample can be introduced into the system in either a solid, liquid or gas phase depending on the configuration of the system. A major method of sample introduction in metabolomic-based experiments is through a chromatographic approach employing either liquid or gas chromatography (LC- or GC-MS). Upon introduction the sample is passed through to an ionisation source where ions are generated. These ions are subsequently forwarded into a mass analyser where the ions are separated according to their mass to charge (m/z) ratios. The separated ions enter the detector device for required detection and all generated data is passed to a PC for storage.

The configuration of an ideal system can vary greatly. As already mentioned different chromatographic platforms with varying column chemistries are frequently used in GC-MS or LC-MS. In addition there are numerous ionisation sources and mass analysers available. Examples of ionisation sources include electrospray ionisation (ESI), matrix-assisted laser desorption ionisation (MALDI), electron impact (EI), chemical ionisation (CI), atmospheric

pressure chemical ionisation (APCI) and atmospheric pressure photo ionisation (APPI). Additionally, examples of mass analysers include time of flight (TOF), linear quadrupole (Q), quadrupole time of flight (Q-TOF), Fourier transform ion cyclotron resonance (FTICR), triple quadrupole (QQQ) and most recently developed the Orbitrap.

In the following sections a number of systems will be discussed with specific emphasis based on the systems utilised in the work presented within this thesis. In addition, the relevance to metabolomics-based analysis and the advantages and disadvantages associated with the system will also be highlighted.

1.4.2.2.2 GC-MS

GC-MS is a well established technique that is regularly utilised in many analytical fields. GC-MS is a combined system for the analysis of volatile and thermally stable polar and non polar metabolites (Dunn et al., 2005). Compounds are initially separated by GC and eluting analytes detected by mass spectrometry. GC-MS is greatly biased towards the detection of volatile, low molecular weight compounds however the detection of non-volatile, higher molecular weight compounds is possible through employing a chemical derivatisation process prior to analysis. In a metabolomics investigation it is common that a range of metabolites (*i.e.*, amino acids, sugars, alcohols, lipids and phosphorylated metabolites) will be present in a sample and hence derivatisation is readily conducted prior to analysis.

Chemical derivatisation of metabolites is a two stage process which can be used for a variety of classes of compounds. The general process involves oxime formation with *O*-alkylhydroxyamines followed by trimethylsilylation. Oxime formation converts sample carbonyl groups to oximes providing thermal stability while trimethylsilylation replaces active hydrogens on polar functional groups with less polar trimethylsilyl (TMS) groups thus increasing the volatility through the reduction of dipole-dipole interactions. The process of chemical derivatisation is well established and greatly increases the number of metabolite

peaks detected; however, this process is time consuming and sample stability is a concern (Dunn and Ellis, 2005). Samples must be dry prior to derivatisation as the presence of water can result in the reversibility of TMS ester formation. The drying of samples can, however, result in the loss of volatile metabolites which must be considered.

Once any required derivatisation is performed the sample is introduced into a heated injector, where vaporisation of the sample occurs followed by mixing with a carrier gas. The vaporised sample or an aliquot of this gas is introduced onto the top of the chromatography column. The columns employed in GC are silica based with an internal diameter of between 100-500 μm . The column is located within a temperature controlled oven thus regulating the operational temperature. The choice of operational temperature is restricted by the physical properties of the metabolites to be detected. It is common that the starting temperature is approximately 20-30°C below the boiling point of the solvent mobile phase. A temperature program is then utilised to gradually increase the temperature of the oven to temperatures that are often between 300-320°C. This method is used to optimise the chromatographic separations of metabolites. The metabolites elute from the GC column according to volatility and polarity; the most volatile metabolites elute first. Upon elution the metabolites enter the mass spectrometer.

The main sources of ionisation in GC coupled devices are electron impact (EI) or chemical ionisation (CI) (El-Aneed et al., 2009). EI ionisation is performed in a high vacuum ion source where the analyte in vapour form is bombarded with electrons (at 70eV). This transfers sufficient energy to the molecules to allow the formation of fragment ions (Pasikanti et al., 2008). The generation of fragments can provide useful information regarding the structure of an analyte. CI is a relatively soft ionisation approach so the production of fragment ions is reduced. The process of chemical ionisation involves the presence of neutral molecules such as methane or ammonia in great excess to the metabolite. The EI process of bombardment

is conducted creating ionised metabolites through charge transfer but a softer effect is witnessed due to the presence of the additional neutral molecules.

The next stage in the process occurs within a mass analyser. The principle mass analysers employed in GC-MS analysis are quadrupoles (Q) or time of flight (TOF). As previously stated the role of a mass analyser is to separate ions based on their m/z values. Mass analysers offer varying advantages in terms of cost, resolution, mass range and their ability to be used in tandem mass spectrometry platforms.

1.4.2.2.3 Quadrupole

The quadrupole mass analyser consists of four parallel electrical rods. A direct current (DC) field is applied to 2 rods and a radio frequency (RF) field is applied to the other 2 rods. These rods generate an electric field through which the ions can move. The applied potentials are varied thus functioning as a mass filter where ions of a chosen mass have trajectories of amplitude less than half the radius of the quadrupoles and successfully traverse the mass analyser whereas ions of lower and higher mass are lost by collisions with the rods because their amplitudes are too great. A schematic diagram is illustrated in Figure 1-9.

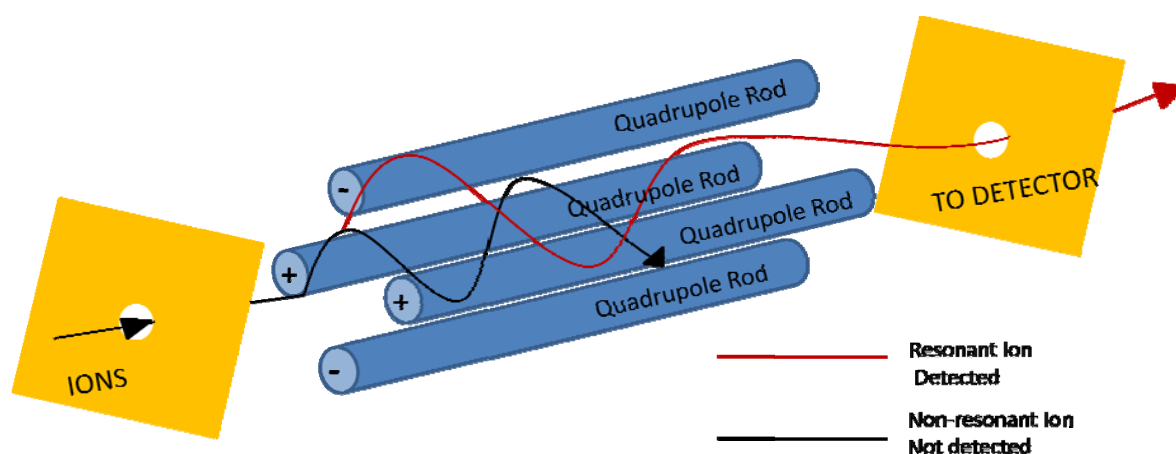


Figure 1-9: Schematic diagram of a quadrupole mass analyser.

The major advantages of quadrupole mass analysers are the relatively low cost, operational robustness and the ease of maintenance and automation. There are however a number of limitations associated with the employment of quadrupoles including the limited mass range and resolution achievable and the inability to perform MS/MS analysis unless a triple quadrupole is used.

1.4.2.2.4 Time of Flight (TOF) Analyser

The TOF analyser is structurally the most basic mass analyser. The TOF system separates ions on the basis of their velocity correlated to the mass of the ion. In general all ions are formed at the same time in the ionisation source and consequently accelerated through a fixed potential into the TOF drift tube. After acceleration all ions have the same amount of kinetic energy, the lower m/z ions achieve higher velocities than the higher m/z ions. In a TOF system all ions will reach the detector but will exhibit varying speeds of travel. A schematic diagram is shown in Figure 1-10.

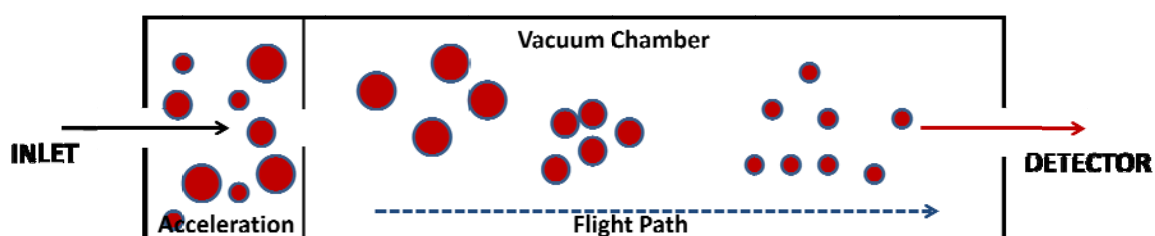


Figure 1-10: Schematic representation of a TOF mass analyser.

The advantage with TOF instruments is the ability to scan a high mass range and the sensitivity of the detector can be greatly increased as the length of drift tube increases.

1.4.2.2.5 Tandem Mass Spectrometry (MS/MS)

A further development in the field of mass spectrometry is the application of tandem mass spectrometry incorporating the use of hybrid mass analysers *i.e.* a quadrupole-time-of-flight (Q-TOF) or ion trapping systems. The general basis of hybrid instrumentation is the selection

of a precursor ion of interest by the first mass analyser followed by the collection of accurate masses of product ions by the second mass analyser. These mass analysers are separated in space by a collision cell or can be separated in time by the use of ion trapping systems. In an ion trapping system the instrumentation has the ability to select the mass of interest, dissociate the molecular ion and analyse the product ions in the same mass analyser. The Orbitrap ion trapping system is discussed in more detail in Section 1.5.2.3.1. The major advantage of these systems is the ability to acquire enhanced structural information and hence this increases the possibility of analyte identification.

1.4.2.2.6 GC-MS Applications in Clinical Metabolomics

GC-MS is at the forefront of analytical techniques utilised in metabolomic studies and as a consequence there is a wealth of literature regarding the application of the technique in clinical metabolomics-based studies. It is common to compare the metabolome of diseased vs. normal control patients *via* the analysis of biofluids including urine, plasma or serum or through investigating disease at a cellular level utilising cell culture techniques or tissue samples.

One of the most significant metabolomics based investigations of recent times was the study conducted by Sreekumar and colleagues whom investigated prostate cancer progression (Sreekumar et al., 2009) using a combination of high-throughput liquid and gas chromatography. The authors probed more than 1,126 metabolites across 262 clinical samples related to prostate cancer including; 42 tissues and 110 each of urine and plasma. The investigation identified sarcosine, a glycine derivative as being a potential biomarker for prostate cancer progression. The metabolite was found to be significantly increased during cancer cell progression to metastasis in tissue studies and was additionally identified non-invasively in urine profiling. To provide an additional example a metabolomics-based study of pre-eclampsia was conducted through the analysis of plasma samples from 87

normal volunteers and 87 diseased patients by GC-TOF-MS in a study conducted by Kenny and co-workers (Kenny et al., 2005). The authors identified three metabolites which could potentially be used in disease diagnostics.

The literature provides numerous additional examples of GC-MS-based metabolomics which are beyond the scope of this introduction. However, to date there are no known metabolomic studies investigating the metabolic variance in psoriasis or its associated co-morbidities.

1.5 Proteomics

1.5.1 Introduction to Proteomics

The global large scale analysis of cellular proteins is termed proteomics. A proteomics protocol involves the separation of complex protein mixtures *via* gel electrophoresis or liquid chromatography followed by protein identification utilising mass spectrometric techniques (Aebersold and Mann, 2003) including matrix assisted laser desorption ionisation (MALDI).

1.5.2 Analytical Platforms for Proteomics

1.5.2.1 2D Gel Electrophoresis

The use of 2D gel electrophoresis is a common tool for the separation of protein mixtures and is a method often used in the initial stages of proteome analysis. The process of high resolution two-dimensional electrophoresis of proteins was first described by O'Farrell in 1975 (O'Farrell, 1975). The process involves the separation of proteins according to the isoelectric point by isoelectric focusing (IEF) in the 1st dimension and according to molecular weight by sodium dodecyl sulfate (SDS) electrophoresis in the 2nd dimension. As these two parameters are uncorrelated it is possible to gain a highly resolved separation across the two dimensions.

As with most analytical techniques there are a number of limitations associated with 2D gel electrophoresis. In a biological sample there are large variations in the magnitude of protein expression. In a typical eukaryotic sample there could be in excess of 10,000 different proteins of which the majority will be housekeeping proteins present in numbers 10^5 to 10^6 copies *per* cell. In addition to these there will be a number of less common proteins such as receptor molecules that are present in much lower concentrations i.e. 100 per cell. In a 2D gel analysis it is possible that proteins present at a lesser magnitude will be masked and

essentially lost from the analysis. Specific proteins have been recognised as being excluded or underrepresented in 2D gels. These include very acidic or basic proteins, excessively large or small proteins and membrane proteins (Peng and Gygi, 2001). The additional limitation associated with 2D gel electrophoresis is the lack of automation available and hence the method can be time consuming and in some cases exhibit low reproducibility. A thorough review discussing the use of 2D gel electrophoresis in proteomics is available for further reading (Gorg et al., 2004).

1.5.2.2 MALDI-MS

Matrix assisted laser desorption ionisation (MALDI) mass spectrometry (MS) is a analytical technique which was conceived in 1987 by Hillenkamp and colleagues (Karas et al., 1987). The incorporation of a matrix (small organic molecule) into the laser desorption (LD) process allowed for the detection of a larger mass range of analytes. The principle of the MALDI process is summarised in Figure 1-11.

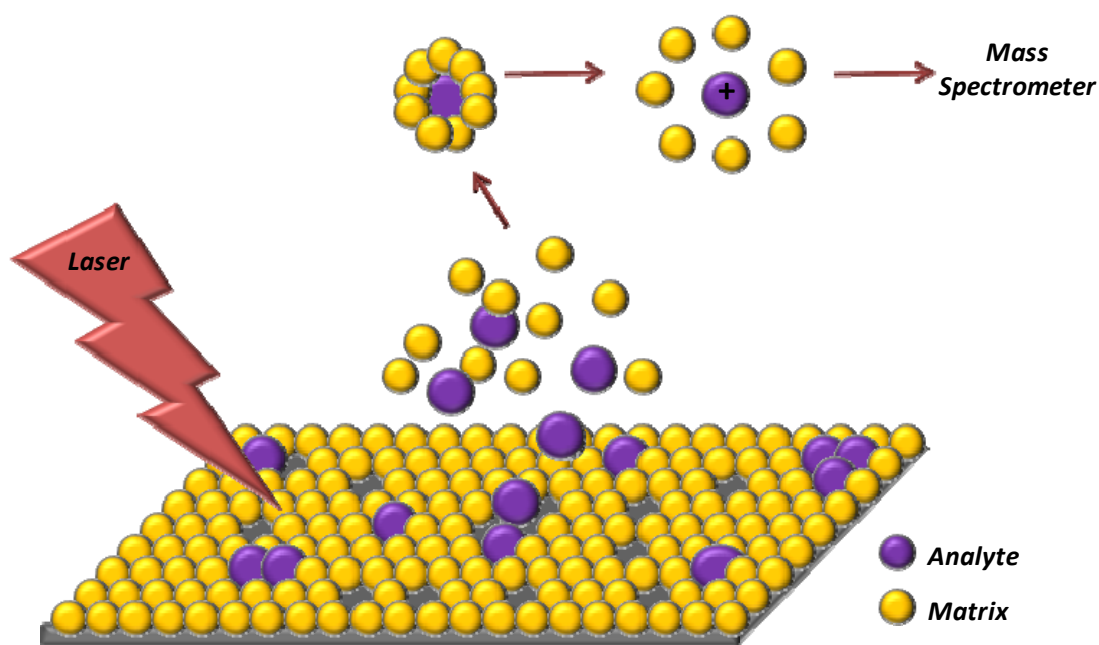


Figure 1-11: Schematic illustration of the MALDI process.

The beginning of the process is to dissolve the sample of interest in an excess of matrix solution; common matrices include α -cyano-4-hydroxycinnamic acid, 3,5-dimethoxy-4-hydroxycinnamic acid (sinapinic acid) or 2,5-dihydroxybenzoic acid (DHB). The sample/matrix solution is applied to a metal target plate where it is irradiated with a pulsed nitrogen laser at 337nm. The UV absorbing matrix molecules absorb the energy from the excitation laser. This energy is then rapidly transferred from the matrix to the analyte to induct vaporisation and ionisation. This leads to the sputtering of pulses of MH^+ ions from each component of the sample. These ions then pass through to the mass analyser which is most commonly a TOF based system (as detailed in section 1.4.2.2.4) in either a linear or reflectron configuration.

MALDI is a soft ionisation method which ensures that, on a whole, fragmentation is minimised. The technique is relatively simple and adaptable and as a consequence is most often the method of choice for high-throughput protein identification. A MALDI-MS approach is compatible with the analysis of an array of sample types. In particular MALDI-MS is used for the identification of protein spots localised within 2D gel analysis. In an identification approach the protein (spot) is often subjected to enzymatic or chemical cleavage and a small aliquot of the sample used. The technique can also be applied to the analysis of bio-fluids or cultured cells and also for the *in situ* analysis of tissue samples. In all approaches a mass spectral fingerprint is produced which can be matched to known libraries to provide a protein identification. A number of protein sequence databases are available including Uni-Prot (pir.georgetown.edu/pirwww) and Swiss-Prot (ca.expasy.org/sprot), (Kris and Joël, 2000).

1.5.2.3 LC-MS

The coupling of liquid chromatography to a mass spectrometer is a well established technique for both proteome and metabolome analysis. The use of LC-MS for the analysis of

complex peptide mixtures was pioneered by Hunt and colleagues in 1992 (Hunt et al., 1992) and is now a core method for MS-based proteomics. LC-MS is beneficial for the analysis of peptides and proteins as the technique is biased towards non-volatile, polar and high molecular weight analytes. In a metabolomics approach LC-MS is applied to allow detection of analytes not usually detectable in GC-MS, or those that are but require complex derivatisation to allow detection. This is particularly prevalent in plant sciences due to the large number of polar/semi-polar compounds (Allwood and Goodacre, 2010).

The configuration of an LC-MS system is highly similar to that of a GC-MS system with the exception of the basis of analyte separation *i.e.* LC. In an LC system the analytes are separated according to their affinities or attraction to either the mobile or stationary phase within the system. Analytes which are attracted to the mobile phase will elute quickly whilst those attracted to the stationary phase will be retained longer and hence elute much slower. Those eluted first will have lower retention times (RT) than those eluted later. Upon eluting the analytes enter the mass spectrometer where they are ionised, analysed and detected as previously discussed.

1.5.2.3.1 Orbitrap

The mass analyser employed in the LC-MS based proteome analysis presented within Chapter 6 was an LTQ-Orbitrap system. The Orbitrap was developed relatively recently by Alexander Makarov (Hardman and Makarov, 2003) and its commercial use in proteomics was quickly established (Scigelova and Makarov, 2006). The Orbitrap is a form of Kingdon trap in which moving ions are trapped by an electrostatic field. Ions are directed in a spiral trajectory around a central electrode and the oscillation frequency is obtained through a Fourier transformation providing the m/z ratio of individual ions. The benefit of an Orbitrap system is its high mass resolution (up to 100,000) and mass accuracy (<1ppm) combined with MS/MS capabilities for improved protein identification.

1.5.3 Proteomics for Dermatological Research

The incorporation of proteomics provides a high-throughput analysis approach for dermatology research (Goldstein, 2003). A proteomic approach has been utilised in a small number of dermatological-based studies. A study undertaken by Park *et al.*, incorporated the use of 2D gel electrophoresis for the analysis of cultured primary keratinocytes from patients with atopic dermatitis and normal controls (Park *et al.*, 2006). Differential gel spots were identified by MALDI-MS analysis and confirmed by LC-MS/MS. The authors successfully identified 18 up-regulated proteins and 27 down-regulated proteins in diseased patients vs. normal controls. A further application of proteomics within dermatology is illustrated by the proteomic analysis of plasma samples from psoriasis and normal control patients (Plavina *et al.*, 2008). This study by Plavina and co-workers investigated the plasma concentrations of cytoskeletal and Ca²⁺ binding proteins and peptides, in which 21 proteins were deemed to be significantly different between control and psoriatic plasma samples. The adaptability of proteomics is illustrated through the analysis of suction blister fluid isolated from normal and non-lesional psoriatic skin (Macdonald *et al.*, 2006). This novel study profiled in excess of 650 proteins of which 9 were identified as differentially expressed between normal and diseased skin.

These examples provide a brief insight into the application of proteomics in dermatology research which is a relatively small area of research. The use of proteomics in clinical research as a whole is highly prevalent and is a successful tool for disease diagnostics through the discovery of potential biomarkers.

Chapter 2: MALDI-MS Based Spatial Proteomic Analysis to Investigate Variances Between Normal and Psoriatic Skin.

2.1 Introduction

Matrix assisted laser desorption/ionisation (MALDI) imaging mass spectrometry (MS) is a relatively new technique first coined by Caprioli and colleagues in 1999 (Chaurand et al., 1999). The great advantage of the technique is the ability for *in situ* measurement of peptides and proteins. The localisation of these peptides and proteins within intact samples is illustrated through the generation of two-dimensional ion image maps which correspond to one or more m/z value (Caprioli et al., 1997). The technique has the ability to detect with high sensitivity with a capability of detecting in the range of femtomole (10^{-15}) to attomole (10^{-18}) levels. The application of the technique to the analysis of intact biological tissue samples was first described in detail by Chaurand (Chaurand et al., 1999) and has since been used in numerous studies.

In this study we have applied a MALDI-MS imaging approach for the comparative analysis of skin tissue samples collected from psoriasis patients and normal control volunteers. It was hoped that we could probe differing localisation and expression of peptides and proteins present within these biopsy samples to provide information regarding the pathogenesis and onset of disease.

2.2 Material and Methods

2.2.1 Sample Collection

In collaboration with the Dermatology Research Centre (Hope Hospital, Manchester, UK) a collection of punch biopsies from the trunk region were collected from psoriatic and non-

psoriatic patients. In total 13 samples were obtained from 9 individual patients. From psoriatic patients two biopsies were collected, one from an involved area and the second from a non-involved area. An involved sample was collected from a site within a present psoriatic lesion and a non-involved sample collected from an area close to but not within a lesion. Normal control samples were age and sex matched as closely as possible to minimise inter-sample variation due to additional external parameters. Normal volunteers provided a single biopsy sample.

Following collection, biopsy samples were bisected and processed. One half was simply snap frozen in liquid nitrogen and stored at -80°C until required. The remaining half was submerged in formalin and embedded in paraffin. An H&E stained section was obtained for each sample to allow detailed visualization of corresponding histology.

Donor	Data number	DOB	Sex	Status
1	001	22.03.78	F	P
2	002	19.07.63	M	P
3	003	13.04.87	F	N
4	004	01.12.63	F	P
5	005	22.12.65	F	N
6	006	29.10.55	M	P
7	007	21.10.68	F	N
8	008	09.60*	M	N
9	009	26.09.76	M	N

Table 2-1: Metadata for samples collected for image analysis. Colour coding indicates the pairing of control and diseased samples. Samples are age and sex matched as closely as possible. *day of birth unavailable.

2.2.2 Sample Preparation

Frozen samples were used for MALDI-MS analysis. The use of paraffin embedded samples can be problematic as the paraffin wax can potentially contaminate the sample even after de-waxing protocols are employed. However there are also potential problems with the use of frozen samples; in cryostat sectioning an optimal cutting temperature (OCT) polymer is used in the process of mounting the sample. This polymer can again potentially contaminate

the sample and consequently impact the quality of resultant spectra. It is imperative that OCT is used carefully and that contact with the cutting edge of the sample minimized. Samples were sectioned in triplicate at 10 μ m using a cryostat (Leica Jung CM1800, Leica Microsystems) and thaw mounted onto a MALDI target plate (microscope slide FlexiMassTM target, Shimadzu Biotech, Manchester, UK).

Sinapinic acid (5mg/mL in 50:50 Acetonitrile/TFA) was directly applied to tissue sections using a Chemical Inkjet Printer (ChIP-1000, Shimadzu Biotech, Manchester, UK). The ChIP delivered matrix solution (100 pL x 5) to each spot and the process repeated 20 times in total (previous work within our research group investigated the optimal quantity of matrix for tissue imaging (Patel et al., 2009)). The result is an array of matrix spots covering the entire surface of the section in an ordered manner. The ChIP operates by piezo-electric print heads that provide a non-contact delivery of matrix solution. The benefit of this approach is that the matrix solution remains spatially localised and hence ensures that distinct areas of interest can be analysed without the possible diffusion of co-located analytes. MALDI spectra are collected for all matrix spots thus providing a profiling image. An example experimental set-up is detailed in Figure 2.1.

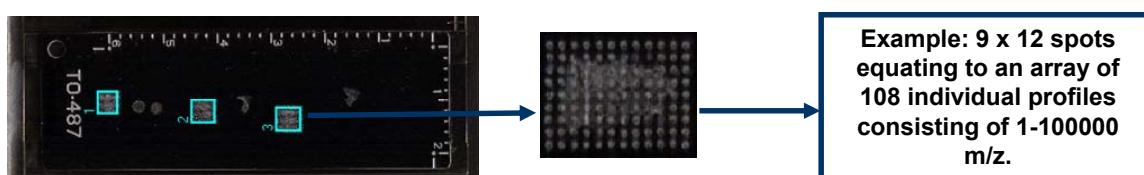


Figure 2-1: Diagram illustrating the experimental set-up for MALDI-MS profiling. Three replicate tissue sections are thaw mounted onto a MALDI target plate. A matrix array is applied through ChIP application providing an array of XxY spots. In the example shown complete matrix coverage requires 9x12 spots equating to 108 individual profiles.

The pitch between matrix spots was 250 μm with an approximate spot diameter of 55 μm which is indicated in the schematic diagram in Figure 2-2. The area of the sample equates to approximately 15 mm^2 .

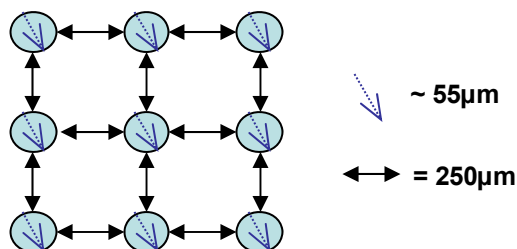


Figure 2-2: Schematic diagram demonstrating the spot size and associated pitch to allow approximation of sample area to be profiled.

2.2.3 MALDI-MS

All MALDI-MS analysis was conducted on a MALDI-TOF mass spectrometer (AXIMA-CFR[™] *plus* (Shimadzu Biotech, Manchester, UK)), equipped with a nitrogen pulsed UV laser (337 nm), and was operated using a positive ion source in linear ion mode. The laser power level was set to 115 mV, each spot was analysed using a random raster of 50 profiles, and each profile contained data from two laser shots.

2.2.4 Data Analysis

All data were collected and viewed within Launch pad 2.7 MALDI-MS imaging software (Shimadzu Biotech).

2.3 Results and Discussion

As detailed above, sinapinic acid was spotted onto the surface of tissue slices using a CHIIP in various arrays. The example shown in Figure 2-3 is a visible image from the scanner within the CHIIP which shows the matrix deposition in a 16x22 configuration, and this is typical of the all the samples that were analysed.

The quality of the mass spectra generated from the tissue region was assessed using software on the mass spectrometer based on number of clearly identifiable peaks and signal to noise ratio; these settings were assessed deterministically on each MS image. As an example, for sample 003 (normal tissue) which consisted of a total of 352 mass spectral profiles the complete dataset was manually searched and a total of 82 spectra were deemed to be of adequate quality (~23%). An example of a spectrum is shown in Figure 2-3, where peaks that have arisen from the surface of the tissue can be clearly seen.

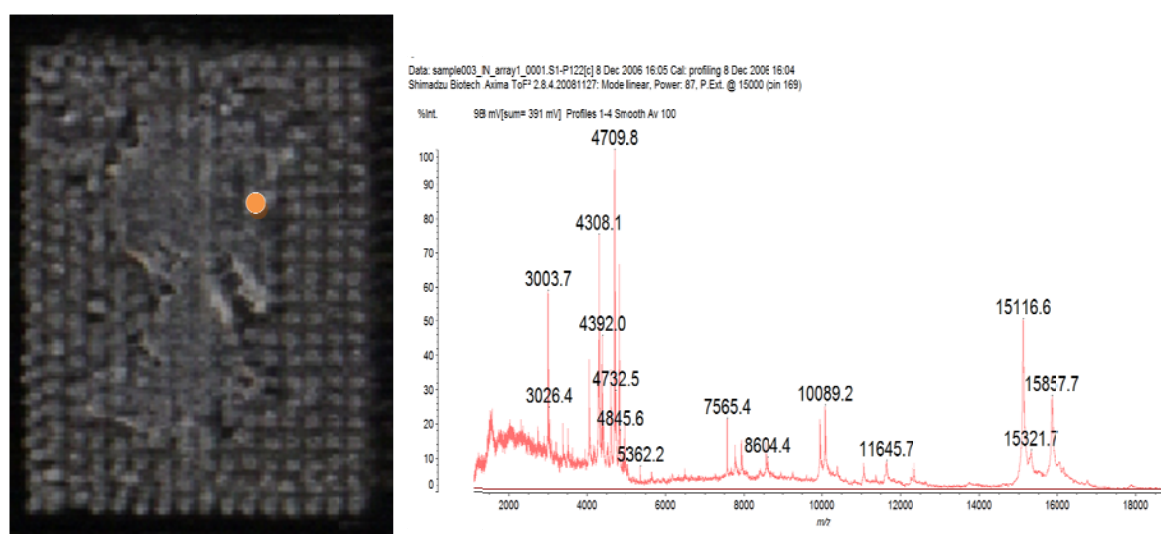


Figure 2-3: A visible image captured by the CHIP scanner illustrating the matrix deposition applied to a normal skin section in a 16x22 array. The example spectrum illustrates a number of peaks which have arisen from the surface of the skin.

However, when this approach was repeated on other normal tissues the spectral quality was significantly lower and the reproducibility of this approach looked poor. Despite this MS data cubes were generated in duplicate from each sample; including involved, non-involved and normal regions. Once the data were collated and processed it became clear that many pixels were of very poor quality even though they came from tissue. On average approximately 20% of the pixels were of sufficient quality and quite often neighboring profiles would show either good mass spectra or no signal. The quality of the data generated was not deemed good enough to construct any chemical maps that could be

related to the anatomy of the skin. For example it was not possible to differentiate between dermis, epidermis and sub-dermal regions.

As the above results were not encouraging this process was repeated with a number of different matrix applications including DHB and α -cyano-4-hydroxycinnamic acid. In addition, the number of repeat spots and matrix concentration was also varied (as in (Patel et al., 2009)). Despite these attempts the data quality remained poor. Subsequent to this we discussed this problem with Prof. Ron Heeren (personal communication) and he reported that his MALDI-MS imaging laboratory had also so far failed to generate good quality MALDI-MS data from skin. Thus the idea of using MS-based protein imaging on skin was abandoned.

Chapter 3: Phenotypic Profiling of Extralesional Keloid Scar Tissue Cross Sections using FT-IR Microspectroscopy Reveals Unique Spectral Signature for Keloid Scars.

3.1 Introduction

Keloid disease (KD) is a benign fibroproliferative tumour affecting the reticular skin, which causes a progressive, recurrent dermal tumor (Brown and Bayat, 2009). Previous studies provide compelling evidence that genetic dysregulation plays an important role in KD development although the exact aetiopathogenesis remains unknown (Brown et al., 2008). These fibrous growths can cause significant disfigurement and unwanted symptoms such as intense itchiness and pain (Brown et al., 2008). The inflammation, itching, and throbbing can be especially severe during the growth phase, but even long-standing lesions may continue to have tender and painful margins compared to a more inactive and often involuting centre (Bayat and McGrouther, 2006). Keloid disease presents a significant burden for patients and a significant therapeutic challenge for clinicians (Durani and Bayat, 2008).

KD results from an abnormal tissue response to dermal injury and is characterized by persistent growth of dermal connective tissue after re-epithelialisation and extension of scar tissue beyond the original borders of the wound (Tan et al., 2010). These scars are raised and spread beyond the margins of the original wound, invade the surrounding normal skin in a site-specific way, in contrast to hypertrophic scars, which are the result of an exaggerated wound healing response and stay confined to the boundaries of the original lesion (Bayat et al., 2003). KD seems to be unique to humans, can occur at any age and affect individuals of all races and both sexes (Bayat et al., 2005). In addition, KD can be identified in most anatomical locations with predisposition to certain sites including the chest, shoulders, upper back, back of the neck, and earlobes (Bayat and McGrouther, 2005, Bayat et al., 2004)

The histological profile of KD is characterized by the presence of thick, hyalinized, homogeneous, strongly eosinophilic bundles of collagen, haphazardly orientated in reticular dermis (Figure 3-1). Keloids have a swirling nodular pattern of collagen fibres and the resulting fibrous growths invade normal dermis which can produce masses in subcutaneous tissue (Shih et al., 2010).

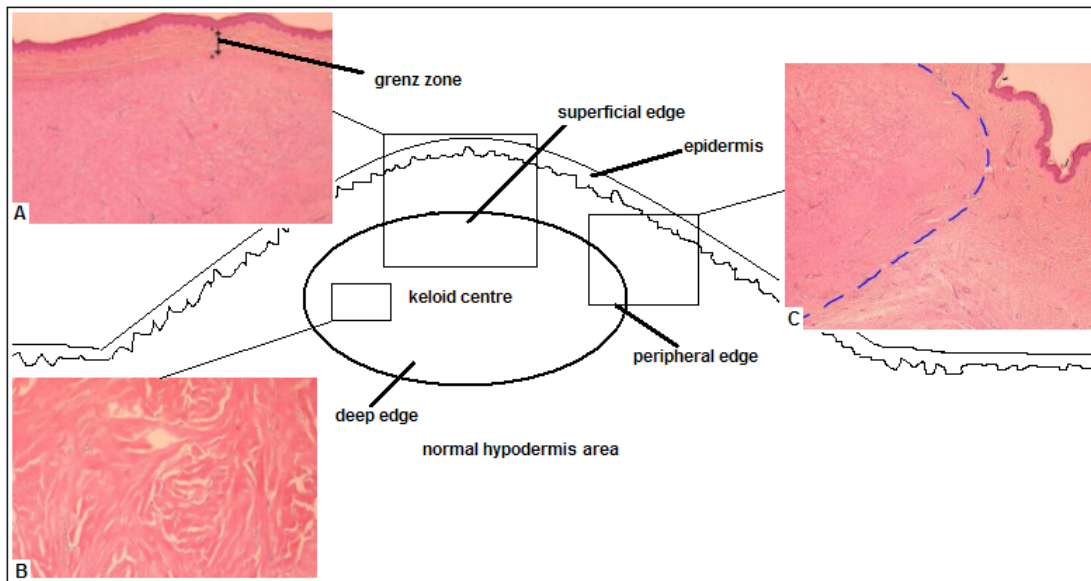


Figure 3-1: Diagrammatic and histological cross section of an extralesional keloid scar including: A: The Grenz zone in a keloid; the histological area corresponding to papillary dermis of normal dermis located between the epidermal basement membrane and the upper edge of the reticular dermis. B: View of thick hyalinized collagen bundles typically found in middle of keloid scars. C: Keloid with circumscribed borders (marked in blue) which are well-demarcated demonstrating the periphery or margin of the keloid scars.

Due to the fact that keloid scars do not regress spontaneously, plus the fact that no plausible long-term effective treatment has yet been found, research on causation, treatment options and prognosis is of great interest. A combination of surgical excision followed by intralesional steroid injection, or other adjuvant therapy, currently appears to be the most effective regimen for clinical management of KD. Surgical excision alone however demonstrates recurrence rates of between 45-100% (Bayat and McGrouther, 2005). It was recently demonstrated that recurrence of keloid lesions can vary according to the extent of surgical excision; keloids excised intralesionally had a higher recurrence compared to those

removed extralesionally (Tan et al., 2010). In addition, there appears to be phenotypic differences between the structurally distinct peripheral margin and the centre of the keloid lesion. The margin is symptomatically more active and hypercellular as opposed to the relatively inactive hypocellular centre (Tan et al., 2010). The aim of this study was to delineate the morphological components of an extralesionally excised keloid tissue by looking at differences in cross sections and comparing different anatomical locations within the keloid tissue using an alternative technique to histology. The main advantage would be to simultaneously image the quantity and quality of multiple components in KD in relation to normal skin using a technique with high molecular sensitivity combined with a spatial resolution down to a few micrometers.

Fourier transform infrared (FT-IR) spectroscopy as previously discussed in Section 1.4.2.1, is a rapid, non-destructive technique which is well suited for the analysis of human tissue samples (Ellis et al., 2007, Ellis and Goodacre, 2006). FT-IR microspectroscopy allows spectral information to be gained while maintaining the morphology of the sample by combining simple light microscopy with infrared instrumentation (Fabian et al., 2006, Sulé-Suso et al., 2005). Sample preparation is minimal and therefore the possibility of losing relevant biochemical information as a function of space is minimised. In FT-IR microspectroscopy there are two general approaches: the coupling of a mercury cadmium telluride (MCT) detector allows the collection of spectra from specific areas to be acquired by combination with a light microscope; by contrast, the incorporation of a focal plane array (FPA) detector (Lewis et al., 1995) permits the production of larger areas to be examined and a variety of arrays exist (e.g., 1×16, 32×32, 64×64 or 128×128 pixels) that allow the generation of infrared hypercubes to be collected in a simultaneous fashion (Fernandez et al., 2005). These hyperspectral data (where each pixel contains an infrared spectrum) can be transformed into chemical maps which allow the spatial distribution of functional groups,

specific chemical species (Patel et al., 2008), or disease areas using chemometrics (Lasch et al., 2004) to be generated.

In this chapter FT-IR microspectroscopy has been applied to investigate the textural morphometric profiling of extralesionally excised keloid scar tissue specimens. Both MCT and FPA detectors were used and coupled to chemometric methods for the classification of keloid vs. normal tissue using partial least squares discriminant analysis (PLS-DA) or for chemical mapping using principal components analysis (PCA).

3.2 Materials and Methods

3.2.1 Patients & Samples

KD cases were recruited at a specialist scar service at the outpatient Department of Plastic and Reconstructive surgery unit in South Manchester University Hospital Foundation Trust (Manchester, England, U.K.). All patients participating in the study were confirmed to have keloid scars both by using stringent clinical criteria in addition to histological confirmation by a pathologist with an interest in dermatopathology. The employment of such rigorous diagnostic criteria in the recruitment protocol assured the correct diagnosis of all recruited individuals. This approach was taken to limit the confounding effects of disease heterogeneity and misdiagnosis potentially inherent in other scarring studies which may fail to differentiate between hypertrophic and KD. Therefore the following clinical criteria were used to identify keloid disease cases as opposed to other forms of skin scarring conditions such as hypertrophic scars. A keloid scar was defined clinically as a dermal tumour that spread beyond the margin of the original wound, continued to grow over time, did not regress spontaneously, and had been present for at least a minimum period of 1 year. In comparison, hypertrophic scars were defined as raised scars that remained within the

boundaries of the original lesion, often regressed spontaneously within several months after the initial injury (Tan et al., 2010).

The local and hospital ethical committees had given approval for the study protocol and proformas. Written consent was obtained from all individuals entered into the study. All cases were personally assessed and examined by Dr Ardeshir Bayat. A full medical history was taken using a proforma and each scar lesion was examined in detail. Extralesional keloid samples were collected post surgery. Each specimen was bisected and one half of the section was snap frozen in liquid nitrogen and the other half placed in formalin fixative.

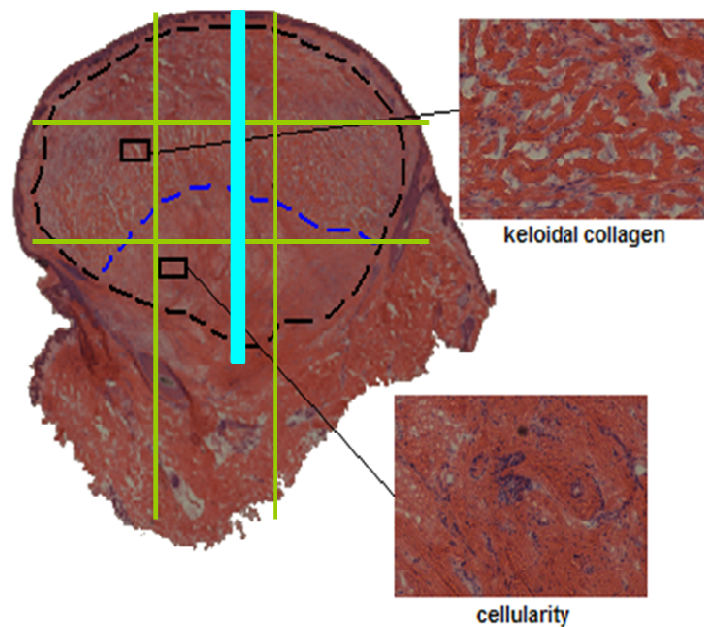


Figure 3-2: This cross section of a typical keloid scar (sample number 3) excised from the chest wall demonstrates anatomical locations within the keloid scar. Lines in green show where line mapping using FT-IR spectroscopy was taken; this resulted in 38 spectra in total: 3 epidermal, 21 normal and 14 from the reticular dermis of the keloid scar. The cyan area shows where FT-IR chemical maps were collected from: this included 14 individual maps containing 64x64 pixels and covered an area of approximately 3.5 x 0.25 mm.

A total of six histologically proven keloid scars (see Figure 3-2 for an example) were excised from four keloid patients. Specimens were collected from a variety of anatomical sites from patients of varying age, sex and ethnicity (Table 3-1). A number of additional features

associated with the causation and appearance of the keloid samples were recorded using a pre-validated scar assessment proforma (Table 3-2) (Beausang et al., 1998).

Patient ID	Sample Number	Age	Sex	Race	Keloid Scar Anatomical Location
KS 28	1	20	Male	Caucasian	Shoulder
KS 33	2	22	Female	Caucasian	Ear
KS 34	3	45	Male	Black African	Sternum
	4	45	Male	Black African	Jaw
KS 35	5	36	Female	Black African	Sternum
	6	36	Female	Black African	Shoulder

Table 3-1: Demographic details of keloid cases involved in the study.

Sample Number	Cause	Onset (yr)	Symptoms	Colour mismatch*	Matt/shiny	Distortion	Texture	Contour
1	Vaccination	3	Itch & pain	Gross	Matt	Severe	Hard	Raised
2	Ear piercing	5	Itch	Slight	Matt	Moderate	Firm	Raised
3	Acne spot	1	Itch	Gross	Shiny	Severe	Hard	Raised
4	Shaving trauma	3	Itch	Gross	Shiny	Severe	Hard	Raised
5	Acne spot	2	Itch	Gross	Shiny	Severe	Hard	Raised
6	Acne spot	2	Itch	Gross	Shiny	Severe	Hard	Raised

Table 3-2: Clinical details (patient history and examination findings) of keloid scars analysed in the study, * represents variation to the surrounding skin.

3.2.2 Fourier Transform infrared (FT-IR) microspectroscopy

The FT-IR data were collected in transmission mode using a Bruker microscope infrared imaging system (Bruker Spectrospin Ltd., Coventry, UK), composed of an Equinox 55 module step scan Fourier transform spectrometer coupled to either (a) mercury cadmium telluride (MCT) single point detector connected to a manually controlled x, y- stage, or (b) a Hyperion 3000 microscope (Bruker Optics Ltd), equipped with a 64×64 liquid nitrogen cooled MCT focal plane array (MCT FPA) detector.

The MCT detector allows for the collection of *single point spectra* at chosen locations. In all MCT driven experiments 64 coadds were collected at a resolution of 4 cm⁻¹ producing

absorbance spectra in the range of 4000-600 cm^{-1} . The FPA detector can be used to collect high resolution images of a large sample area. With a $\times 15$ IR objective lens this allows the analysis of sample areas of approx. $267 \mu\text{m} \times 267 \mu\text{m}$. A pixel area of 64×64 was collected equating to 4096 spectra from each of the detector elements. Tissue mapping was conducted with a spectral resolution of 4 cm^{-1} and a spectral range of $4000-900 \text{ cm}^{-1}$. A single coadd was collected and the typical acquisition time for each image was approximately 12 min.

The data were collected using routines of the OPUS 4.0 IR imaging software (Bruker Optics), and then exported as ASCII files which were subsequently imported into Matlab version 7.1 (The Math Works, Inc., 24 Prime Par Way, Natick, MA, U.S.A.) for analysis (*vide infra*).

3.2.3 Sample Preparation

For FT-IR analysis, specimens were snap frozen in liquid nitrogen and stored at -80°C until analysis. Frozen cross sections from the keloid scars were sectioned using a cryostat microtome (Leica Jung CM1800, Leica Microsystems) at a thickness of $10 \mu\text{m}$ and air dried onto calcium fluoride (CaF_2) IR-transparent windows. Adjacent $5 \mu\text{m}$ sections were collected and air dried onto glass slides for pathological analysis by hematoxylin and eosin (H&E) staining. Digital images were obtained from the H&E stained sections using a Digital Imaging Microscope (Nikon, Eclipse 80i, Japan) at a magnification of 10×4 . Individual images from each section were manually stitched together within GIMP (version 2.2.15) to allow classification of keloid and normal skin cross sections.

3.2.4 FT-IR Data Collection and Chemometric Analyses

3.2.4.1 MCT Infrared Analysis

A total of 22 line mapping experiments were conducted from the six individual keloid slices. Line mapping was conducted in both vertical and horizontal directions. Vertical line maps represented a transition from epidermis, through normal dermis region (termed Grenz zone), into the diseased keloid part (superficial edge → keloid centre → deep edge) and returning to normal dermis region again (See Figure 3-1 and Figure 3-2 for clarification). Similarly, line mapping in a horizontal direction transits from a normal region, into the diseased keloid part (peripheral edge (margin) → keloid centre → peripheral edge (margin)) and finally returning into a normal dermal region. In this way it was possible to categorise our measurements in the following categories, epidermis (e), normal (n), keloid (k) or doubtful provenance (d). Doubtful provenance areas were regions that could not be assigned without an element of doubt from interpretation of corresponding H&E staining or light images from the microscope. Each sample was subject to 3 or 4 line mapping experiments, existing of a number of sampling points (mean of 12 points).

Collected spectra were collated and scaled using extended multiplicative scatter correction (EMSC (Martens et al., 2003)). To eliminate the region of unavoidable baseline drift that occurs between $\sim 1650\text{-}2000\text{ cm}^{-1}$ and the CO_2 absorption in the area of $2350\text{-}2450\text{ cm}^{-1}$ these sections were eliminated from analysis by removing these data regions. Principal component analysis (Jolliffe, 1986) was conducted and typically 3 principal components (PCs) were extracted and PC loading plots were used to study variability within and between the samples and anatomical sites. All data analysis was performed within Matlab version 7.1. Line mapping data were analysed in single line maps, collated per sample and as a large collective dataset.

Partial least squares (PLS) (Martens and Naes, 1989) analysis was conducted on the large collated dataset consisting of 100 spectra from the six locations on the four patients. Spectra were selected based on the collection region being clearly differentiated by microscopy as being normal tissue or keloid. PLS-discriminant analysis (PLS-DA) was performed with defined outputs as 0 = normal and 1 = keloid. In order to validate the classification, so as to avoid false discovery (Broadhurst and Kell, 2006), PLS-DA bootstrapping was performed in PLS-DA using the replacement method (Westerhuis et al., 2008); thus 'on average' 37% of samples were used for testing and 63% samples were used for training. Bootstrapping was performed 10,000 times on the data. On the 10,000 test data only (i.e., the validation data, not the training set) statistics can be performed and this results in a confusion matrix, box and whisker plot and a receiver operator characteristic curve being produced.

3.2.4.2 FPA Image Analysis

The previously obtained H&E stains (Figure 3-2) were used to identify sample KS34 as the best example of a keloid section, and therefore this section was selected for chemical image analysis. A vertical line image was collected by collating 14 individual FPA images (i.e., 14 by 64×64 pixels). The areas were selected using the visible light images provided by the microscope on the Hyperion 3000 and were manual aligned using the x-y stage. The line map incorporates a transition from normal epidermis to dermal keloid areas and returning to normal skin morphology.

Upon collection the individual spectral datacubes were concatenated to produce a single large dataset within Matlab. As some of the pixels were deemed bad (i.e., they were hot and so gave a signal irrespective of whether infrared absorbance was occurring) these were removed by filtering the entire data set and setting any pixels with an absorbance greater than 4.99 recurring to zero (these are later removed prior to PCA; see below). This process

removes large domineering spikes in the data while not blanking the pixel entirely. The spectra were then summed to produce a total intensity image.

To normalise the data for PCA any pixel greater than zero was set to 100% and anything less than zero was set to -100%. This established that 0 is truly zero and its colour will match any other zero in the dataset. Wavenumber regions contributing a high level of varying noise corresponding to water and/or CO₂ interferences were eliminated by removing the wavenumber ranges 4000-3700 cm⁻¹ and 2450-2250 cm⁻¹ respectively. Bad pixels were removed prior to PCA which was performed using MATLAB's "princomp.m" routine. Bad pixels were reinserted into the missing positions in the PC scores matrix with all wavenumber values set to zero. The datacube was reshaped and PC scores false colour coded to generate chemical maps. The corresponding PC loadings plots were produced for the first 9 PC scores.

Finally, nine wavenumber bands were selected as displaying significant variances between normal and keloid tissue regions (see below). The area under the peak of the given wavenumber bands were integrated and the subsequent images plotted.

3.3 Results & Discussion

3.3.1 Histological Findings

The epidermis, the Grenz zone (the intermediate papillary zone between the epidermis and the reticular dermis), the deep reticular dermis of keloid samples ($n=6$) region as well as the equivalent regions in normal skin were identified and confirmed by a histopathologist (e.g., Figure 3-1 A, B & C). The thickness of the Grenz zone varied between the different histological sections (Figure 3-1 A). However, the epidermis remains unaltered at the top in all lesions (Figure 3-1 A & C) and the middle of each keloid scar demonstrated a swirling

nodular pattern of fibres and thick hyalinised collagen bundles (Figure 3-1 B). Figure 3-2 demonstrates a cross section of a keloid lesion which shows the typical, abnormal thick collagen fibres (“keloid collagen”) at the centre of lesion, the lower part however is characterized by a diffuse cellularity. The margin or periphery of the cross sections appeared more cellular.

3.3.2 FT-IR microspectroscopy

Vibrational bands from cellular proteins, membrane lipids and nucleic acids were observed, providing molecular information relating to the structure and concentration of these materials within a cell. Typical representative FT-IR spectra are shown in Figure 3-3. These spectra were obtained from normal regions in the hypodermis or from keloid regions in the cross-section, and the arrows indicate the significant differences between the keloid and the normal skin spectrum. Also included is a spectrum of collagen, which is known to be predominant in skin and in keloid scars.

3.3.3 Chemometric analyses

PCA was carried out on all line mapping experiments to obtain PCA scores plots. A typical PC scores plot is shown in Figure 3-4. In this example, (and others not shown), these scores plots generally show discrimination between normal and keloid tissue; and where present, spectra from the epidermis and dermis were clearly differentiated from normal and keloid tissue. In addition the spectral variance in the keloid areas was less marked than the normal regions (Figure 3-4).

PC loading plots were also generated and these allow the spectral features that are used in the production of the PCA to be revealed. The example shown in Figure 3-4B is typical where spectral features from lipids were larger in the normal tissue (positive in PC1) than in

the keloid tissue (negative in PC1) which seemed to resemble the spectrum of pure collagen (Figure 3-3).

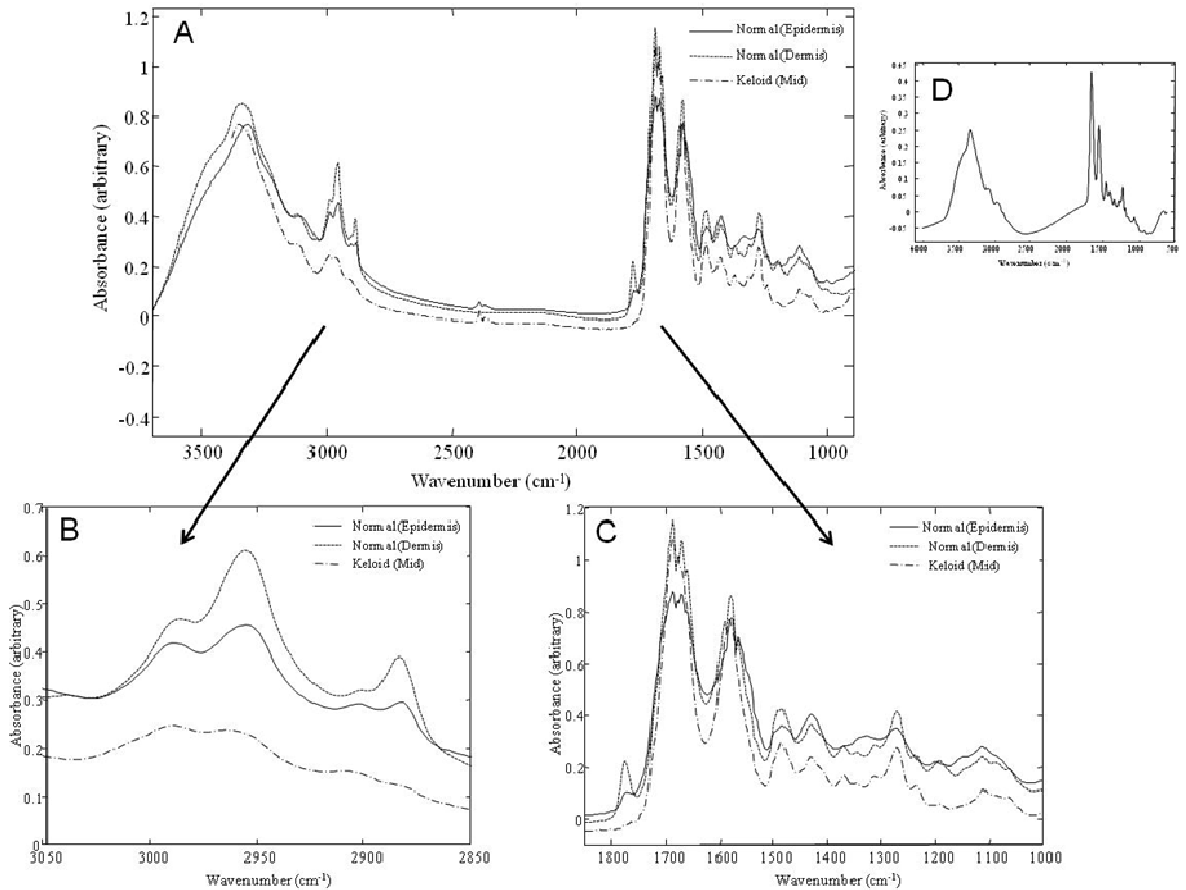


Figure 3-3: A) Typical FT-IR absorbance spectra collected from normal skin tissue, and keloid epidermal and dermal regions. B) Expansion of lipid region C) Expansion of amide region, and D) Offset graph demonstrates a spectrum of collagen.

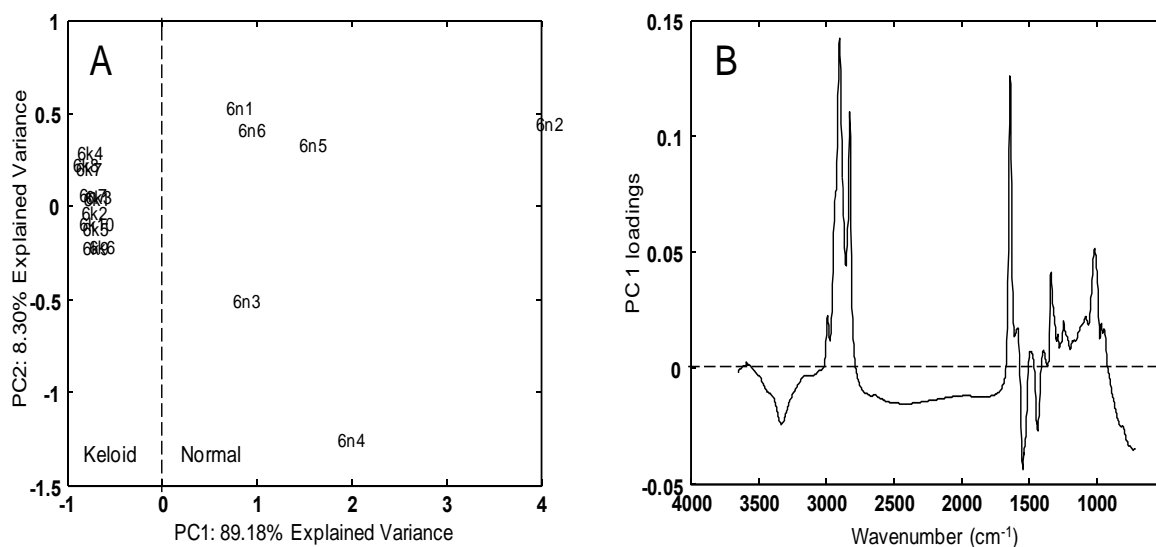


Figure 3-4: (A) PCA scores plot from one of sample no 4 with lines (2nd horizontal line) showing clear differentiation between normal tissue and keloid scar. (B) Corresponding PC1 loadings plots showing features that are discriminatory.

To follow on from this unsupervised learning method, we trained PLS-DA to discriminate between keloid and normal tissue as detailed above. The results from the 10,000 bootstrap analyses for the test data only are shown in Figure 3-5, where it can be seen that the average ROC is 0.922 which is important for differentiation. Moreover the box and whisker plot shows the results for all 10,000 models and also shows that PLS-DA can readily differentiate between normal tissue and keloid scars.

3.3.4 FT-IR microspectroscopic imaging

The results of the spectral area maps correspond well with the tissue histological sections (Figure 3-6). These maps provide detailed biochemical information, not readily available from other techniques (Figure 3-3); these images indicate regions of lipid, amide and phosphate content within different areas in the tissue section (Figure 3-6), and PCA on the total chemical map allowed other features to be revealed by inspecting the corresponding PC loadings matrices (Figure 3-8).

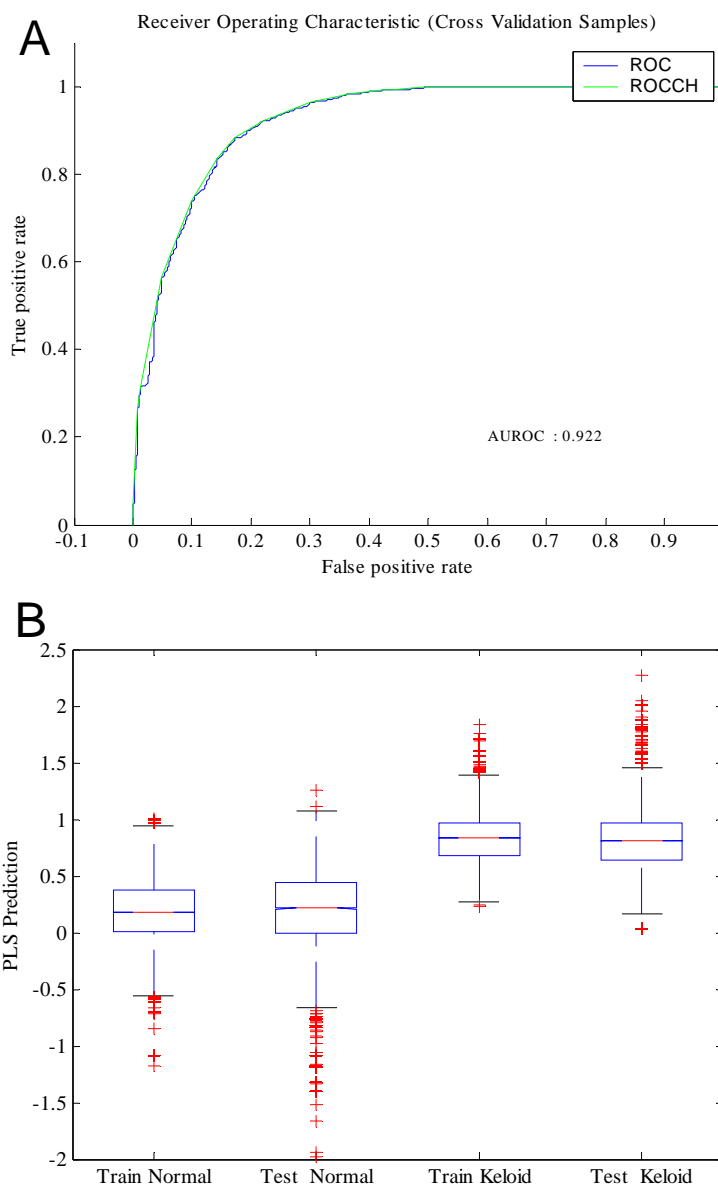


Figure 3-5: Results from PLS-DA bootstrap analysis from 100 spectra selected from six samples. (A) Average receiver operating characteristic plots from the test data only from the 10,000 models and (B) Box whisker plots showing the data from all training and test data from the 10,000 PLS-DA models that were constructed. Boxes represent the lower median and upper quartiles. Whiskers represent the range or 1.5 x the length of the box, whichever is shorter. Outliers (+) are the values out of the whisker range.

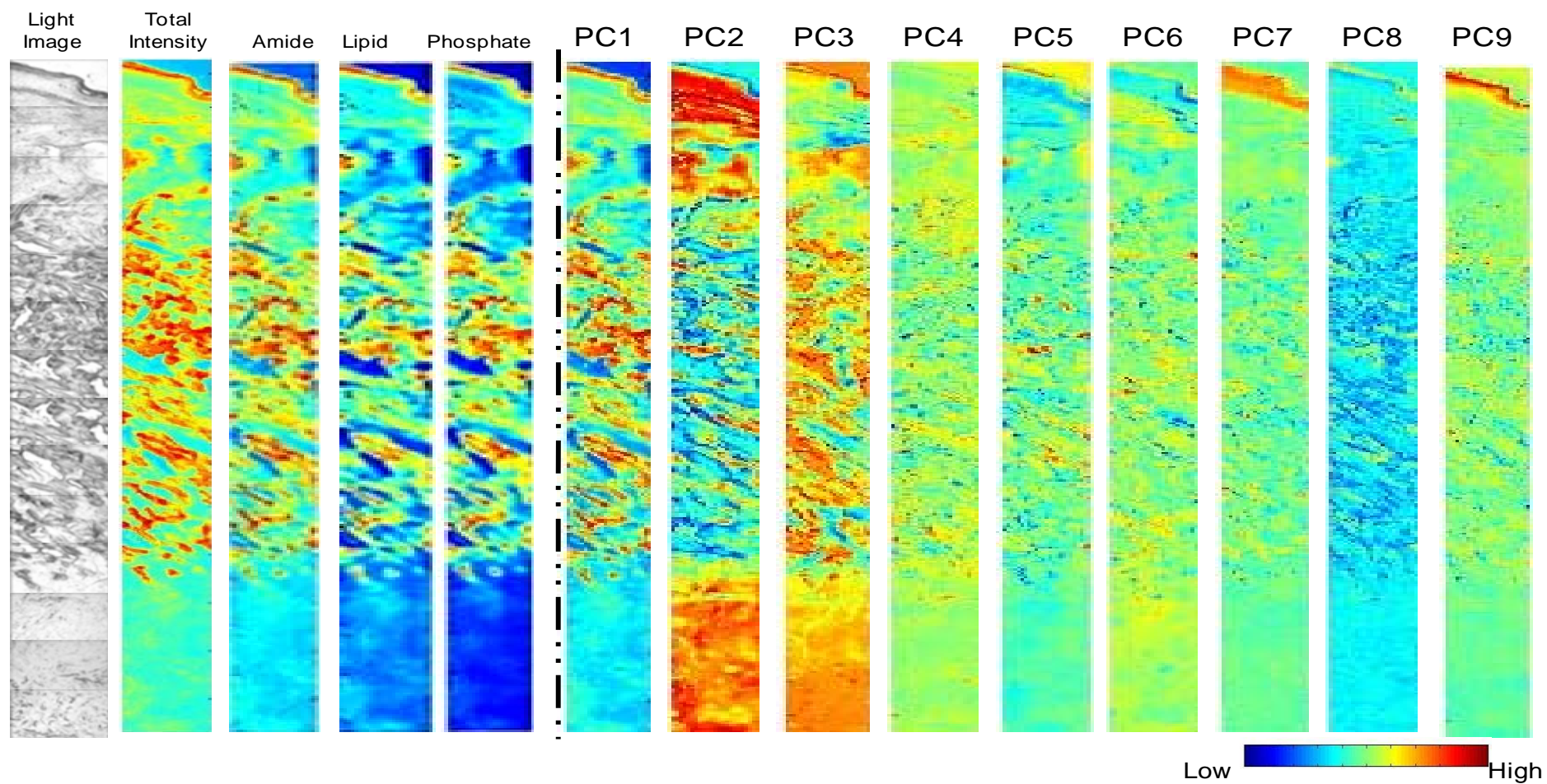


Figure 3-6: Chemical image plots from sample number 3 of chest wall generated from IR microspectroscopy. The light image is shown from the unstained tissue and corresponds to the area detailed in Figure 3-2. The first four false colour coded maps are from the sum of the total IR signal, area under lipid, amide and phosphate bands respectively. The next nine image maps represent the first 9 PC scores.

Region	Wave number Range (cm ⁻¹)	Mid point (cm ⁻¹)	Assignment
1	3030:2995	3012	Amide B (N-H stretching) from protein
2	2990:2880	2935	Asymmetric CH ₂ stretching from lipid
3	2875:2830	2852	Symmetric CH ₂ stretching from lipid
4	1780:1720	1750	C=O stretch from lipid
5	1715:1600	1657	Amide I (80% C=O stretch)
6	1590:1490	1540	Amide II (60% N-H in plane bend, 40% C-N stretch)
7	1480:1430	1455	CH ₂ scissoring from lipid
8	1260:1215	1237	Amide III (40% C-N stretch, 30% N-H in plane bend, 20% methyl-C stretch)
9	1195:1135	1165	Asymmetric PO ₂ ⁻ stretch from nucleic acids

Table 3-3: Tentative infrared vibrational band assignments for regions of interest.

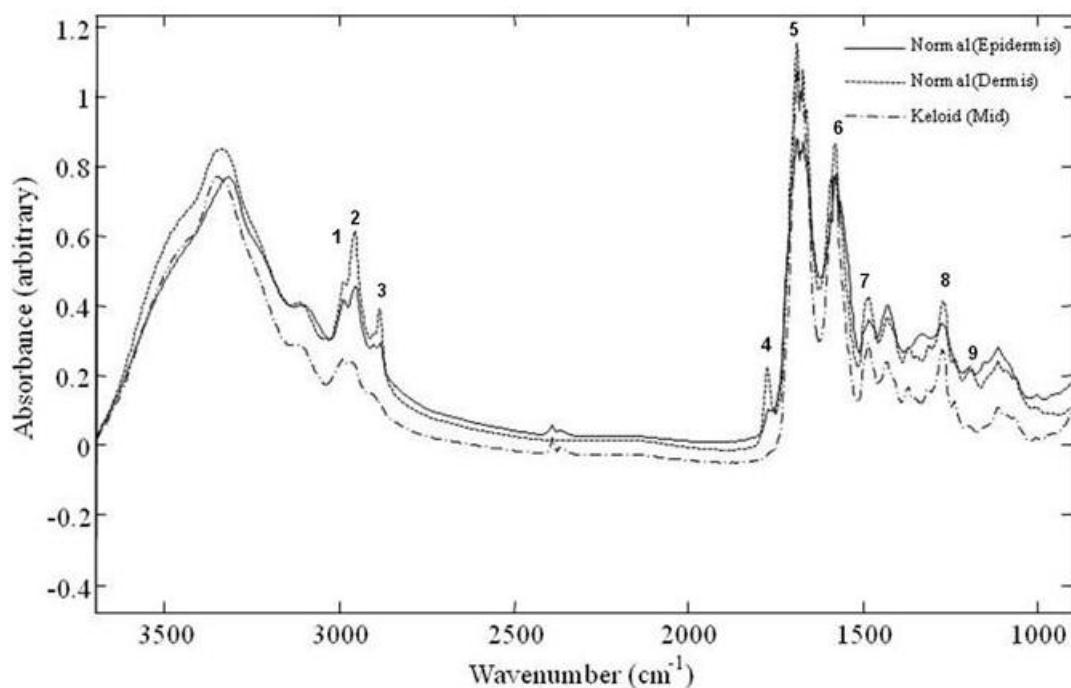


Figure 3-7: Typical FT-IR absorbance spectra collected from normal and keloid skin tissue. The spectra are annotated to illustrate the wavenumber regions of interest highlighted in Table 3-3.

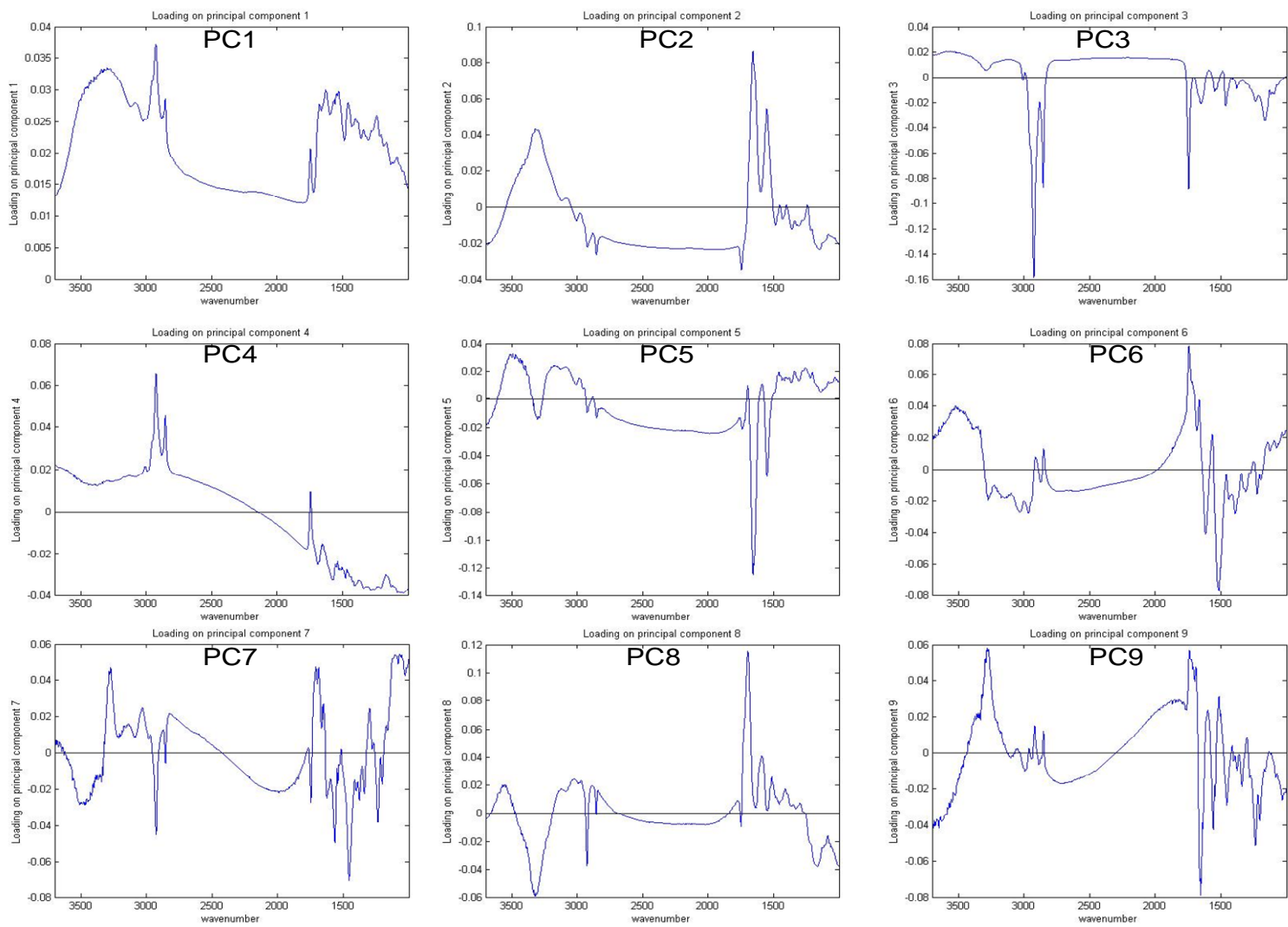


Figure 3-8: Corresponding PC loadings plots from the PCA of IR microspectroscopy in Figure 3-6.

3.4 Discussion

This study for the first time demonstrates that FT-IR microspectroscopy shows significant differences in spectral profiles from keloid tissue in different anatomical locations within a cross section. Distinct vibrational bands (100 spectra from six samples) were observed for each lesion using FT-IR spectroscopy. PLS-DA with appropriate validation using bootstrapping (10, 000 bootstrap analyses), identified whether a spectrum was from the keloid or normal tissue showing an average accuracy of 84.8%, precision of 80.4%, specificity of 76.2% and sensitivity of 92.9%.

FT-IR spectroscopy is a novel and robust approach for keloid disease diagnostics (Ellis and Goodacre, 2006, Hollywood et al., 2006); this has been complemented in this study with the findings verified by routine histopathology. The classification and 'orientation' of the KD tissue slices were confirmed with the aid of complementary H&E stained slides as a direct reference for each KD sample studied. In addition these H&E slides played an important role during the interpretation of the results in particular during the chemical mapping process.

As is common in FT-IR studies the spectra are qualitatively very similar (Figure 3-3) and generally show only subtle quantitative spectral differences between different tissue types or between disease and normal cells. Coupled with the inherent large data size (these FT-IR spectra were typically represented by 1764 data points) there is a reliance on chemometric approaches for analysis of these multivariate data.

The first stage in the chemometric analysis was to analyse each sample individually using an unsupervised method. In such an approach, the algorithm is "unaware" of the data and the main aim is to assess the natural variance in the data presented. PCA is a reliable approach for this and this projection method generates new axes called principal components (PCs) which are non-correlated. PCs summarise the variance in the data and find any natural structure; which in this instance is the difference between KD and normal skin. Figure 3-4 shows an example for sample 4

where the PC scores plot shows clear differentiation between normal tissue and KD in the first PC; that is to say the axes which explain the most natural variance (89.2% total explained variance).

During PCA there is a simultaneous projection in the variable space and these PC loading plots can reveal (bio)chemical information about what features are important for separations in the PC score plots. The resulting loadings plot for sample 3 (KS34) is shown in Figure 3-4B; positive areas are increased in normal tissue (as the samples are located in the positive part of PC scores 1) and *vice versa*, negative loadings are increased in the keloid scar. The negative part of the PC1 loadings plot shows peaks at $\sim 1600\text{ cm}^{-1}$ and $\sim 1450\text{ cm}^{-1}$ which can be attributed to amide I (C=O) and II (N-H), in addition to a broad peak at *ca.* 3250 cm^{-1} which is another N-H stretch from proteins. These correlate well with the FT-IR spectrum of pure collagen type I (Figure 3-3D) which is perhaps not surprising given that collagen is not only found in skin but is densely laid down in KD tissue. By contrast, the positive loadings are predominantly from lipids. The three vibrational bands from $3050\text{-}2750\text{ cm}^{-1}$ are from C-H_x and the very sharp band at 1780 cm^{-1} is from C=O (a constrained carbonyl vibration) from where the acyl chain joins the polar head group.

In order to distinguish tissue spectra from normal skin or KD irrespective of patient or tissue location the supervised learning method of PLS-DA was utilised. In this process the algorithm is given information on the pathological state of the spectrum's location and we encoded normal tissue as a '0' and keloid tissue as '1'. As some of the spectra were of doubtful origin, that is to say the pathological status of the border was difficult to interpret, these were removed from the model, this resulted in 100 spectra in which we had high confidence in their provenance. As only 100 spectra were taken from 6 samples it is possible to over fit the data analysis (Broadhurst and Kell, 2006) and therefore in order to validate the PLS-DA classification model, bootstrapping was performed using the replacement method (Westerhuis et al., 2008). Bootstrapping was performed 10,000 times on the data. Figure 3-5 shows the average ROC curve which has an area of 0.922. In addition, box whisker plots for the training and test data for the normal and keloid tissues are shown from the

10,000 models. This again shows excellent distribution of results and the average statistics on these models were an accuracy of 84.8%, precision of 80.4%, specificity of 76.2% and sensitivity of 92.9%. Finally, the true positive rate was 92.9%, true negative rate 76.2%, false positives were 23.8% and false negative 7.1%.

The H&E section in Figure 3-2 highlighted sample 3, KS34 from the sternum, as the best example of a keloid section, therefore this section was selected for chemical image analysis using FT-IR microspectroscopy. An area of approximately 3.5 x 0.25 mm was analysed by IR and this was achieved by collecting 14 separate 64 x 64 datacubes using the FPA detector on the microscope and aligning the cubes one on top of another (Figure 3-2). In chemical mapping, a derivative value for each spectrum is first generated; thus the whole IR spectrum at each pixel is collapsed into a single value. These are then used to generate false colour maps and in this instance we encoded a high value as red and a low value as blue. In order for the images to look less pixelated we used interpolated shading in the mapping function in Matlab. This is known as Gouraud shading (Gouraud, 1971) and is piecewise linear where the colour in each pixel varies linearly and interpolates with the corner values from the surrounding 8 pixels. The results are displayed as a series of chemical maps and shows these for the total IR signal collected (4000-600 cm^{-1}), the CH_x from the lipid (3000-2750 cm^{-1}), the amide I and II bands (1700-1500 cm^{-1}) and the phosphate content (1350-1250 cm^{-1}) representing predominantly nucleic acids. The total IR signal shows that the keloid scar is very dense in material as is the epidermis, whilst the normal tissue at both interfaces with the keloid is not as rich in spectral features. The lipid, protein and nucleic acid chemical maps show very similar spectral features with the obvious exception of the changes in intensity of these bands. The fact that these images are largely congruent means that alternate methods are needed to reveal any subtle spectral features.

Thus we applied PCA on these images, 57344 spectra were analysed (equating to 14x64x64 spectrax3400 wavenumbers i.e., 194969600 data points), and extracted the first 9 PCs and their

corresponding loadings matrices (Figure 3-8). It is clear from these PC chemical maps that PCs 1, 2, 3, 7 and 9 relate clearly too histological features (Figure 3-2). PC1 highlights the keloid epidermis and dermis as these pixels have high values in PC1, however, this resembles the total IR signal and as no scaling was used prior to PCA this is not surprising. By contrast PC2 highlights the keloid dermal region well as PC2 score is low for the keloid reticular region and positive for normal tissue including the epidermis; the corresponding loadings plot is shown in Figure 3-8(a protein spectrum correlates with collagen). The PC 3 loadings plot corresponds to lipids and the features are similar to those found previously in the analysis of a different tissue (Figure 3-4; sample 4: KS34), the scores plot of this feature is uniformly high in the normal tissue but rather granular within the keloid. PCs 7 and 9 largely highlight the keloid epidermis only and many spectral features are evident in the corresponding loadings plots. From the PCA it is clear that many spectral features are changing within the keloid, and not just collagen alone. In combination with the visible inspection above (lipid, protein, nucleic acid) nine spectral areas of interest are potentially important in this pathological process and these are highlighted in Table 3-3.

3.5 Conclusion

In conclusion, FT-IR spectroscopy is a powerful physicochemical technique which when coupled with microscopy allows detailed chemical maps to be generated from tissues. Strong vibrational bands were observed for each KD section analysed using FT-IR spectroscopy. Keloid scarring is a complex and multifactorial process and such changes were reflected in the complex IR spectra. PCA suggested that on a per sample basis it was possible to delineate between keloid scars and normal tissue (both epidermis and sub-dermal). PLS-DA was used successfully to distinguish between KD and normal skin; irrespective of location or patient. This is the first report of the use of FT-IR spectroscopy in successful differentiation between keloid scars and normal tissue, and the use of chemical imaging may in the future allow more targeted surgical treatment with prognostic information.

Chapter 4: A metabolomic based approach to investigate the response of HaCaT cells upon exposure to three well established anti-psoriatic drugs.

4.1 Introduction

The aim of this work was to apply a metabolomics-based approach to investigate the impact of three well established anti-psoriatic drugs upon direct application to a cellular system at physiologically relevant concentrations.

The HaCaT cell line was chosen as a model system for psoriasis. HaCaTs are a spontaneously transformed human epithelial cell line (Boukamp et al., 1988). HaCaT cells retain a remarkable capacity for normal differentiation even after multiple passages and thus offer a suitable and stable model for keratinisation studies. The HaCaT cell line has been extensively used as an *in vitro* model in a number of psoriasis studies (Farkas et al., 2001, Tse et al., 2006, Belso et al., 2007, Zhang et al., 2008). The cells are quick growing and cultured following a standard procedure as detailed below.

The drugs chosen for study were dithranol, methotrexate and ciclosporin. The background and proposed mechanism of action of these drugs is discussed in Section 1.3.4. These drugs were chosen as they are currently relevant for therapy and in widespread use. Drug selection for treatment is geographically variable however dithranol is popular in some centres in Europe, ciclosporin is used extensively in Italy and methotrexate is used in most European countries and the US (Menter and Griffiths, 2007).

Metabolic profiling was conducted through GC-MS analysis of both the intra-cellular metabolome (fingerprint) and the metabolic footprint. The analysis of the metabolic footprint allows alterations in overflow metabolism to be observed. This can prove useful to substantiate results from within intra-cellular metabolism which can sometimes be compromised by the fast turnover rates observed for some metabolites.

4.2 Materials and Methods

4.2.1 Materials

Drug compounds and reagents were all purchased from Sigma Aldrich, (Gillingham, UK) unless otherwise stated.

4.2.2 Methods

4.2.2.1 Cell Culture

All culture work was conducted within a Microflow biological safety cabinet and all work areas thoroughly cleaned with 70% ethanol before use. Unless otherwise stated, all cell culture consumables were purchased from GIBCO (Invitrogen Group, Paisley UK). The cell culture media utilised in this work was Dulbecco's Modified Eagle Media (DMEM) supplemented with 10% Foetal Bovine Serum (FBS) and 1% Penicillin (5000units/ mL) – Streptomycin (50 mg/ mL). The composition of DMEM media is shown in Table 4-1 while it is important to note that all FBS was chosen from a single tested batch to avoid introduction of variance.

4.2.2.1.1 Resurrection of Frozen Cell Lines

An ampoule of keratinocyte cell line HaCaT was obtained from liquid nitrogen storage. The ampoule was warmed quickly within a water bath heated to 37°C to thaw the cells. Once thawed the cells were added drop wise to a T-25 flask containing 4 mL of warmed complete media and incubated at 37°C and 5% CO₂ for 24 h. Cells were examined microscopically at 24 h periods to assess any morphological changes and nutrient requirements.

4.2.2.1.2 Replacement of Used Media

Cells were routinely fed every 4 days, the media contains phenol red solution, which indicates acidosis in the culture and so allows visual identification of cell stress. With confluence levels of approximately 30-60% a full replacement cycle is completed. All used medium was aspirated and

replaced with new warmed medium (37°C). When confluence levels are below 30% a half replacement of medium was conducted. Replacement of a smaller volume of media allows endogenous growth factors to be maintained in culture to aid cell growth.

Components	Molecular Weight	Concentration (mg/ L)	mM
Amino Acids			
Glycine	75	30	0.4
L-Alanyl-L-Glutamine	217	862	3.97
L-Arginine hydrochloride	211	84	0.398
L-Cystine 2HCl	313	63	0.201
L-Histidine hydrochloride-H ₂ O	210	42	0.2
L-Isoleucine	131	105	0.802
L-Leucine	131	105	0.802
L-Lysine hydrochloride	183	146	0.798
L-Methionine	149	30	0.201
L-Phenylalanine	165	66	0.4
L-Serine	105	42	0.4
L-Threonine	119	95	0.798
L-Tryptophan	204	16	0.0784
L-Tyrosine	181	72	0.398
L-Valine	117	94	0.803
Vitamins			
Choline chloride	140	4	0.0286
D-Calcium pantothenate	477	4	0.00839
Folic Acid	441	4	0.00907
Niacinamide	122	4	0.0328
Pyridoxine hydrochloride	204	4	0.0196
Riboflavin	376	0.4	0.00106
Thiamine hydrochloride	337	4	0.0119
i-Inositol	180	7.2	0.04
Inorganic Salts			
Calcium Chloride (CaCl ₂ 2H ₂ O)	147	264	1.8
Ferric Nitrate (Fe(NO ₃) ₃ 9H ₂ O)	404	0.1	0.000248
Magnesium Sulfate (MgSO ₄ 7H ₂ O)	246	200	0.813
Potassium Chloride (KCl)	75	400	5.33
Sodium Bicarbonate (NaHCO ₃)	84	3700	44.05
Sodium Chloride (NaCl)	58	6400	110.34
Sodium Phosphate monobasic (NaH ₂ PO ₄ 2H ₂ O)	154	141	0.916
Other Components			
D-Glucose (Dextrose)	180	4500	25
HEPES	238	5958	25.03
Phenol Red	376.4	15	0.0399

Table 4-1: DMEM culture media composition.

4.2.2.1.3 Sub-Culturing Monolayer Cell Cultures

HaCaT cells grow as a single thickness cell sheet adherent to the base of the culture flask. As cell growth progresses the base of the culture vessel becomes fully occupied, at which point cell growth slows (contact inhibition). Therefore, in order to maximise the effective growth of healthy cells it was necessary to split the cells within a culture vessel. Incorporating the use of proteolytic enzymes to disrupt the extracellular matrix laid down by the cells on the flask, it was possible to re-distribute cells into sterile larger vessels via a process involving washing and dilution.

Flasks were assessed under inverted phase contrast microscopy (NIKON, Tokyo, Japan) to determine the level of confluency; levels above 80% were selected for sub-culturing. All used cell media was aspirated and 5 mL of 10% calcium and magnesium free phosphate buffered saline (PBS) added to wash the cell monolayer and remove any remaining FBS which can inhibit the action of the proteolytic enzymes to be used. The PBS was removed, 5 mL of trypsin added to the flask and the flask incubated at 37°C for 5 min to increase the performance of the enzyme. Once its incubation time was complete, the flask was agitated slightly to dislodge any remaining attached cells and 5 mL of warmed complete DMEM media was added. The suspended cells were transferred to a centrifuge tube and centrifuged for 5 min at 3080g (Thermo Jouan CR322). The supernatant was removed and 10 mL of new complete DMEM media was added to re-suspend the pellet. This cell mixture was then distributed equally between 10 new T-225 culture flasks and the procedure completed by adding 140 mL of DMEM and incubated at 37°C. The cells required 5-7 days to reach sufficient confluency and media replacement was performed as necessary.

4.2.2.1.4 Cryogenic Preservation of Cell Lines

Cryogenic preservation is a method of retaining cells in a stable condition for an extended period of time without the need for maintenance of the cell conditions through feeding and splitting procedures as detailed above.

The sub-culturing procedure was followed through to the stage where the cell pellet was re-suspended in new DMEM medium after centrifugation. In cryopreservation 100 μ L of dimethyl sulphoxide (DMSO) is added to the cell pellet in addition to the new cell medium. DMSO acted as a cryoprotective medium in the freezing process. The resultant media containing cells was distributed in 1 mL aliquots to labelled ampoules and placed within a cell freezing device (Nalgene, Rochester, NY, USA) containing iso-propanol and stored at -80°C for 24 h. Once frozen, the ampoules were transferred to liquid phase nitrogen storage vessels for long term storage.

4.2.2.2 Drug Exposures

Drug solutions were applied to the samples when the cells were determined by microscope inspection to be 85-90% confluent and incubated for 24 h at various concentrations. The concentration range of the chosen drugs was comparable with the therapeutic doses used during psoriasis treatment. Dithranol was dissolved in 100% acetone to a final concentration range of 0.1-0.5 $\mu\text{g}/\text{mL}$ (corresponding to 4.4×10^{-7} , 8.84×10^{-7} , 1.33×10^{-6} , 1.77×10^{-6} & 2.21×10^{-6} M respectively but for clarity $\mu\text{g}/\text{mL}$ values are used in discussion). Methotrexate was dissolved directly in phosphate buffered saline (PBS) to a concentration range of $1\text{-}5 \times 10^{-7}$ M and finally ciclosporin was also dissolved directly into PBS to a concentration range of $0.5\text{-}2.5 \times 10^{-7}$ M. Each drug range described included a total of 5 concentrations and 1 control. All drug solutions were freshly made before application to the cells. A control exposure was performed for each drug type through application of acetone or PBS. Drug exposures were performed in triplicate for all concentration points and the control.

4.2.2.3 Sample Preparation

It was necessary to develop a sampling protocol that would be optimum for metabolome analysis. The standard process for harvesting adherent cells involves the use of trypsin to detach the cells from the surface of the flask. This incorporates two distinct problems into the experiment. Firstly the use of trypsin can potentially alter the metabolite profile due to its interaction with membrane

proteins. Secondly the process takes a significant proportion of time and includes centrifugation which results in a considerable time lapse between harvesting and quenching of metabolism which is highly likely to result in the loss of significant metabolites. A cell quenching method highly similar to the method developed within this work was recently published (Teng et al., 2009) and a summary diagram of our method is shown in Figure 4-1. The quenching and harvesting method employed differed only through the temperature of the PBS solution used during the washing procedure. Teng *et al.*, used ice cold PBS for the washing stages of the process, however we chose room temperature PBS to reduce cell shock and thus minimise potential cell leakage.

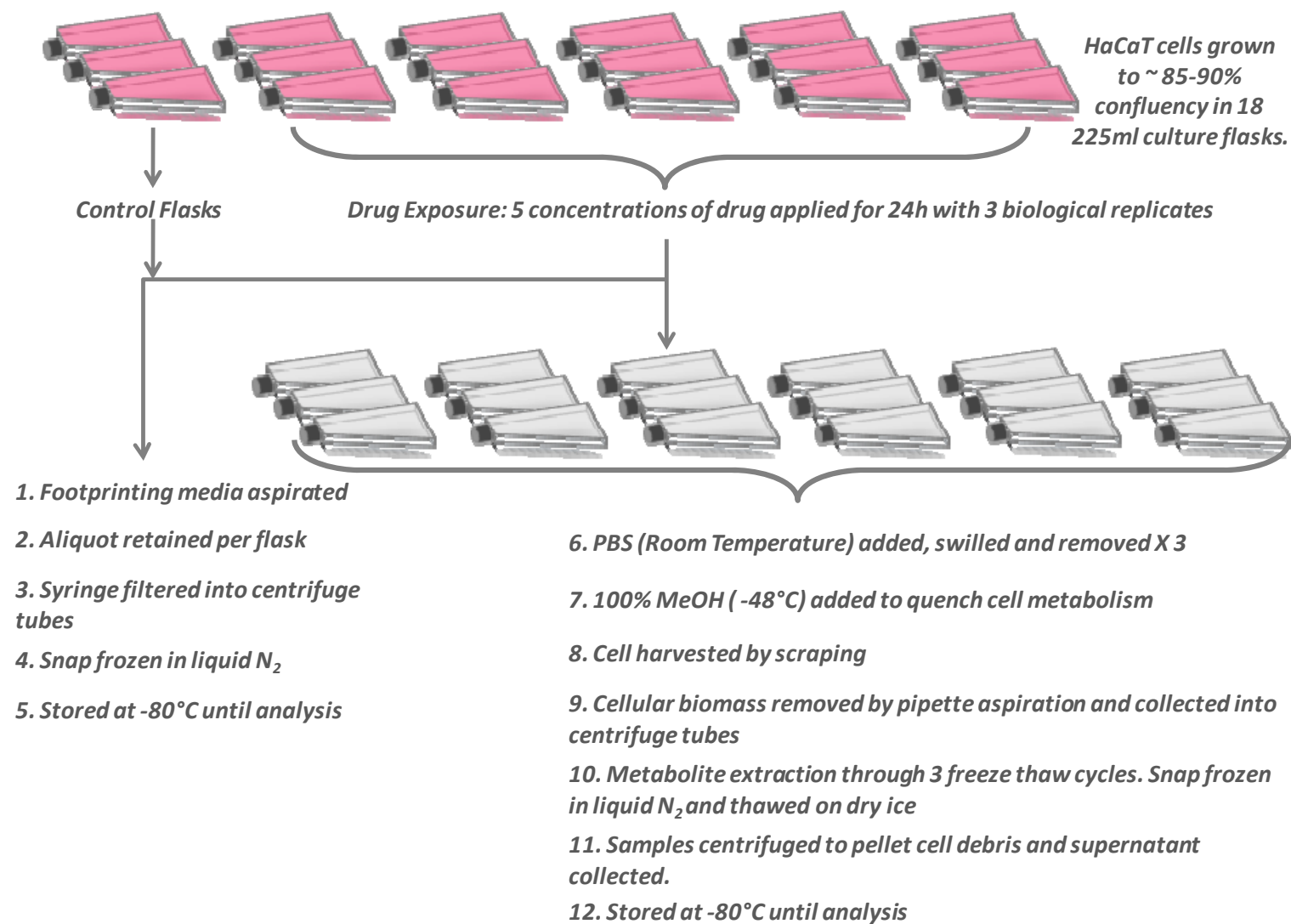


Figure 4-1: A summary diagram to illustrate the successive stages in the collection of fingerprint and footprint samples.

4.2.2.3.1 Metabolomic Footprint Sample Collection

The expired media; to be termed the metabolic footprint was aspirated from each culture flask and filtered through a 0.45 µm pore size cellulose acetate membrane syringe filter to remove any remaining cellular debris. The filtered metabolic footprint samples were aliquoted into centrifuge tubes and immediately snap frozen in liquid nitrogen. All samples were stored at -80°C until GC-MS analysis.

4.2.2.3.2 Metabolomic Fingerprint Sample Collection

After removal of all of the media, PBS (15 mL, room temperature) was applied to the cellular monolayer, swilled and aspirated. This process was performed twice to remove any remaining media. Following this the cell metabolism was quenched by adding 100% methanol (10 mL, -48°C) and harvested by scraping the cells from the flask with a cell scraper. The subsequent biomass was removed by pipette and transferred to centrifuge tubes. To extract the cells the samples were snap frozen in liquid nitrogen and allowed to thaw on dry ice. The extraction procedure was repeated twice to ensure thorough extraction, (Winder et al., 2008). The samples were then centrifuged (-14°C, 5 min, 16200g) to pellet the cell debris. The supernatant was removed and stored at -80°C until analysis. A descriptive summary of this method is supplied in Figure 4-1.

4.2.2.4 Metabolomic GC-MS Analysis

A 1 mL footprint sample was spiked with 100 µL internal standard solution (1.32 mg/ mL succinic d₄ acid, 1.12 mg/ mL malonic d₂ acid, 1.08 mg/ mL glycine d₅, Sigma-Aldrich, Gillingham, UK), vortex-mixed for 20s and lyophilised (Eppendorf Vacufuge Concentrator 5301, Eppendorf, UK). 9 mL of fingerprint extract was lyophilised through successive 1 mL cycles. The final 1 mL extract was spiked with 100 µL internal standard solution (as above), vortex mixed for 20 s and lyophilised (as above).

A two-stage sample chemical derivatisation was performed on the dried sample, 80 µL of 20 mg/ mL O-methylhydroxylamine solution was added and heated at 40°C for 90 min followed by addition of

80 μL MSTFA (N-acetyl-N-[trimethylsilyl]-trifluoroacetamide) and heating at 40°C for 90 min. 20 μL of a retention index solution (4 mg/ mL n-decane, n-dodecane, n-pentadecane, n-nonadecane, n-docosane dissolved in hexane) was added and the samples were analysed in a random order using a Agilent 6890 N gas chromatograph and 7683 autosampler (Agilent Technologies, Stockport, UK) coupled to a LECO Pegasus III electron impact time-of-flight mass spectrometer (LECO Corporation, St Joseph, USA) as detailed in (O'Hagan et al., 2005). Initial data processing of raw data was undertaken using LECO ChromaTof v2.12 software to construct a data matrix (metabolite peak vs. sample no.) including response ratios (peak area metabolite/peak area succinic- d_4 internal standard) for each metabolite peak in each sample. The process of standardising to succinic d_4 acid has previously been reported, details of which can be found in (Pope et al., 2007) and (MacKenzie et al., 2008).

4.2.2.5 GC-MS Data Processing

The data matrix was exported from the GC-MS software and imported into Microsoft Excel. The data were row normalised to total peak area and an analysis of variance (ANOVA) t test based analysis performed. Metabolite peaks were selected as significant with a value of $p < 0.05$. Spring embedded plots were constructed using a correlation threshold of 0.7 (Ebbels et al., 2006).

Metabolite identifications were assigned through searching and matching against an in house constructed library and also the NIST02 and Golm metabolome libraries. A definitive match means that the retention index and mass spectrum match that of an authentic standard analysed on the same instrument (Brown et al., 2009). A putative match implies that the mass spectrum can be matched only to a non-Manchester library and cannot be confirmed via an in-house comparison. This process corresponds with minimum reporting standards proposed for chemical analysis detailed within (Sumner et al., 2007).

4.3 Results and Discussion

4.3.1 Metabolite Detection

The number of metabolite features detected through GC-MS analysis was deemed highly acceptable. The analysis of dithranol treated HaCaT cells yielded 127 metabolite feature peaks from the intra-cellular metabolome (fingerprint) and 107 metabolite features for the metabolic footprint. The analysis of methotrexate and ciclosporin treated cells presented a slightly greater number of metabolite features: the analysis of the intra-cellular metabolome of methotrexate and ciclosporin exposed cells provided 140 and 155 metabolite features respectively; whilst the metabolic footprint for methotrexate and ciclosporin exposure supplied a total of 146 metabolite features each. This information is summarized within Table 4-2.

	Dithranol Fingerprint	Dithranol Footprint	Methotrexate Fingerprint	Methotrexate Footprint	Ciclosporin Fingerprint	Ciclosporin Footprint
Total Metabolite Features Detected	127	107	140	146	155	146
Number of Significant Metabolite Features	75	13	20	59	8	6
% Significant Metabolite Features	59.1	12.1	14.3	40.4	5.2	4.1
Number of Significant Metabolite Features Identified	45	5	10	26	4	1
% Significant Metabolite Features Identified	60.0	38.5	50.0	44.1	50.0	16.7

Table 4-2: A summary of the results gained from the internal and external metabolome of HaCaT cells exposed to dithranol, methotrexate and ciclosporin. The table highlights the overall number of metabolite peaks identified, the number of metabolite peaks declared significant and the number of significant metabolite peaks which were identified.

4.3.2 ANOVA Analysis

Metabolite peaks were selected as significant through the application of an ANOVA-based analysis. Peaks were selected as significant with a value of $p < 0.05$. The number of peaks which were deemed significant varied greatly between each drug exposure and also between the analysis of the internal and external metabolome. A p value limit of < 0.05 was used to allow a greater number of metabolite features to be passed to the correlation analysis stage as discussed in Section 4.3.4.

4.3.2.1 Dithranol Fingerprint

The application of ANOVA analysis to the data acquired from the intra-cellular metabolome of dithranol treated cells highlighted 75 metabolite peaks as statistically significant, Figure 4-2. The number of significant peaks corresponds to approximately 60% of all detected peaks. This represents the greatest number of significant peaks recorded during the experiment which illustrates that dithranol exposure successfully enters the cells and interacts with the internal metabolism of HaCaT cells.

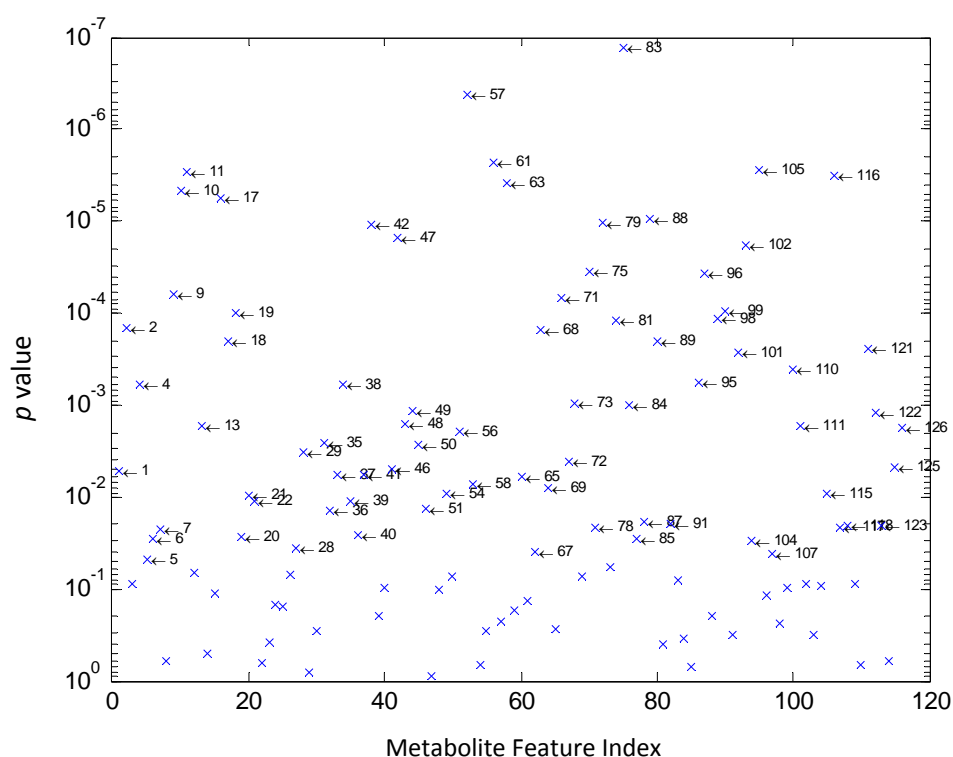


Figure 4-2: A scatter plot of metabolite feature index vs. p value for all metabolite peaks identified for the dithranol fingerprint analysis. Peaks that were identified as significant from ANOVA analysis with a p value < 0.05 are labelled with a number corresponding to feature index to allow identification of the peak.

4.3.2.2 Dithranol Footprint

The ANOVA analysis of the data provided from the metabolic footprint of dithranol treated cells indicated only 13 peaks of significant interest, Figure 4-3. This number of peaks represents only

approximately 12% of the total number of detected peaks. This is a lower recorded proportion to that of the internal metabolome which could indicate that the drug impacts the internal metabolome to such an extent that little external effect is observed. Alternatively it may be possible that the turnover of metabolites within the cells is so rapid that overflow metabolism is not in operation. It is partially expected that the response detected within the footprint media will be reduced due to the nutrient rich nature of the culture media interfering with metabolite detection.

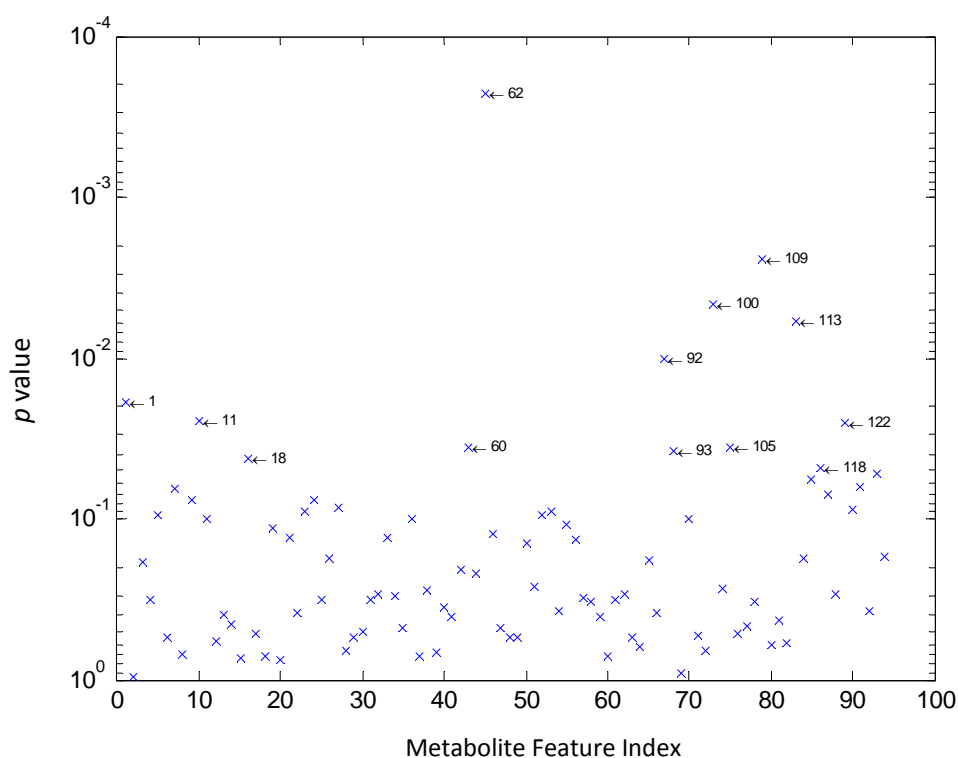


Figure 4-3: A scatter plot of metabolite feature index vs. p value for all metabolite peaks identified for the dithranol footprint analysis. Peaks that were identified as significant from ANOVA analysis with a p value < 0.05 are labelled with a number corresponding to feature index to allow identification of the peak.

4.3.2.3 Methotrexate Fingerprint

A total of 20 metabolite peaks were considered to be significant through ANOVA analysis of the results gained from the intra-cellular metabolome of methotrexate exposure cells, Figure 4-4. This corresponds to approximately 14% of the total number of peaks detected and is in comparison to the results from dithranol fingerprint notably lower. This result suggests that the methotrexate

exposure used in this study has not targeted the internal metabolism of the HaCaT cells or at least has not targeted the metabolites which can be successfully detected through this approach.

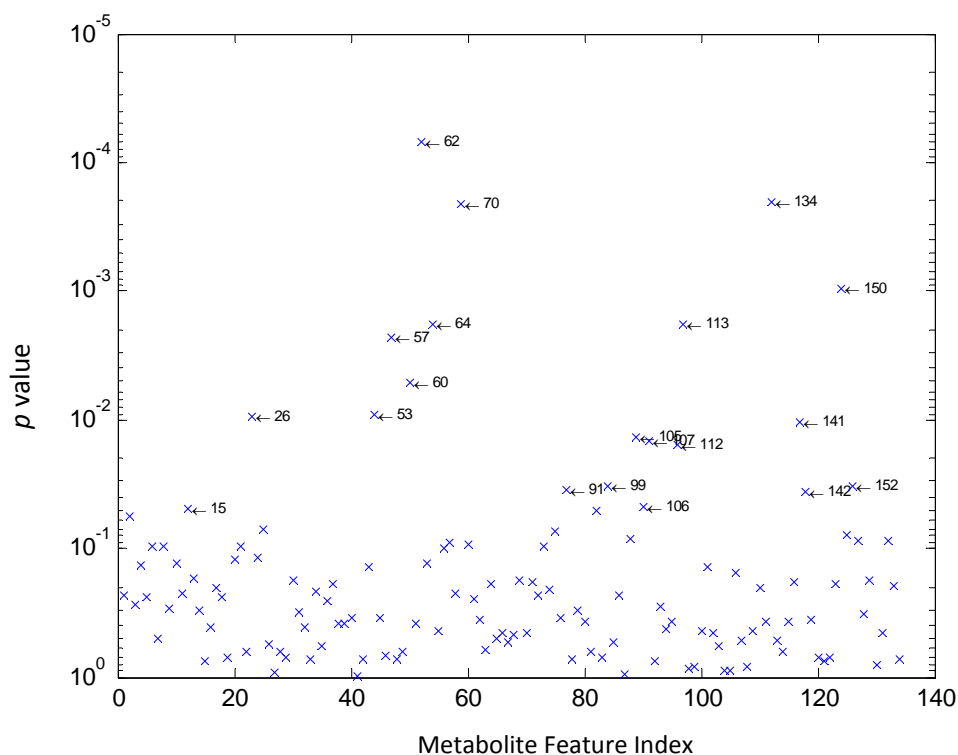


Figure 4-4: A scatter plot of metabolite feature index vs. p value for all metabolite peaks identified for the methotrexate fingerprint analysis. Peaks that were identified as significant from ANOVA analysis with a p value < 0.05 are labelled with a number corresponding to feature index to allow identification of the peak.

4.3.2.4 Methotrexate Footprint

A high proportion of metabolite peaks identified in the metabolic footprint of methotrexate exposed cells were deemed significant by ANOVA analysis illustrated in Figure 4-5. A total of 59 metabolite peaks were selected as significant representing a total of approximately 40% of all peaks identified. The discovery of this high proportion of significantly affected metabolite features infers that methotrexate exposure has to a certain degree altered the cellular metabolism of HaCaT cells.

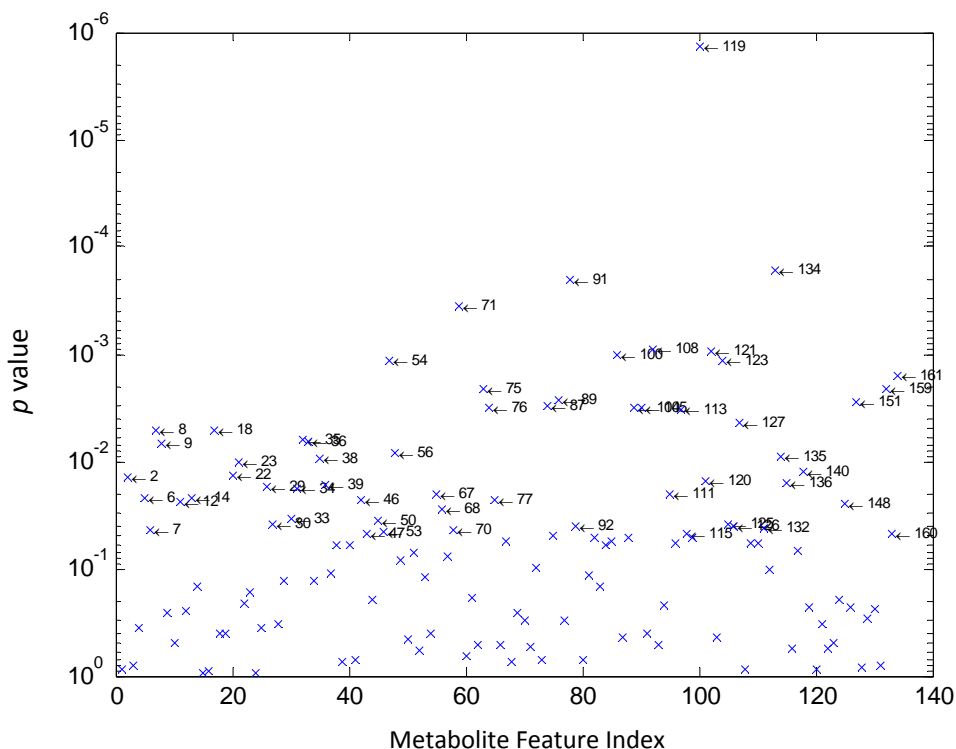


Figure 4-5: A scatter plot of metabolite feature index vs. p value for all metabolite peaks identified for the methotrexate footprint analysis. Peaks that were identified as significant from ANOVA analysis with a p value < 0.05 are labelled with a number corresponding to feature index to allow identification of the peak.

4.3.2.5 Ciclosporin Fingerprint

A very small number of the 155 metabolite features detected were highlighted as significant for ciclosporin exposed cells. In total only 8 peaks were identified as being of significant interest from the internal metabolome of ciclosporin treated cells, Figure 4-6. This represents a percentage of approximately 5% of all identified metabolite peaks. The discovery of such a small proportion of significant features implies that ciclosporin is failing to enforce any affect on the metabolism of HaCaT cells which could be related to the mode of action of the drug or the inability of the drug to penetrate the cells.

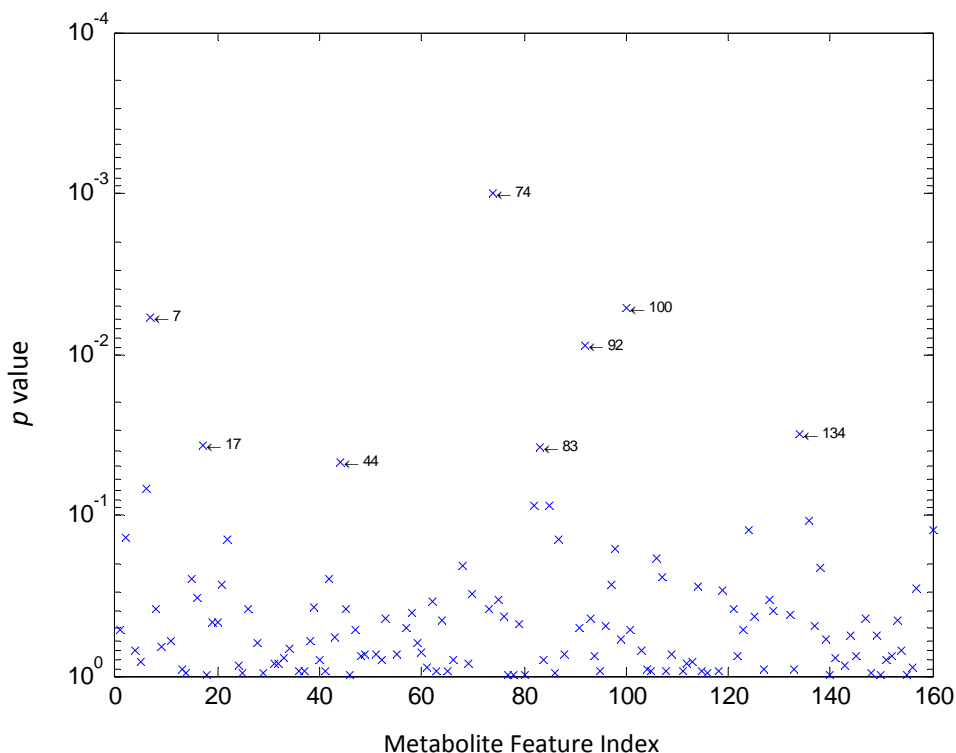


Figure 4-6: A scatter plot of metabolite feature index vs. p value for all metabolite peaks identified for the ciclosporin fingerprint analysis. Peaks that were identified as significant from ANOVA analysis with a p value < 0.05 are labelled with a number corresponding to feature index to allow identification of the peak.

4.3.2.6 Ciclosporin Footprint

In similarity with the results from the intra-cellular analysis of ciclosporin the number of peaks identified as significant for the footprint analysis was low. In total only 6 peaks from the 145 identified were declared to be of significant interest. This is depicted in Figure 4-7 shown below. These results correlate with those of the internal metabolome and again suggest that ciclosporin is failing to target the HaCaT cells or that the metabolites affected by this drug are beyond the metabolite coverage capability of GC-MS.

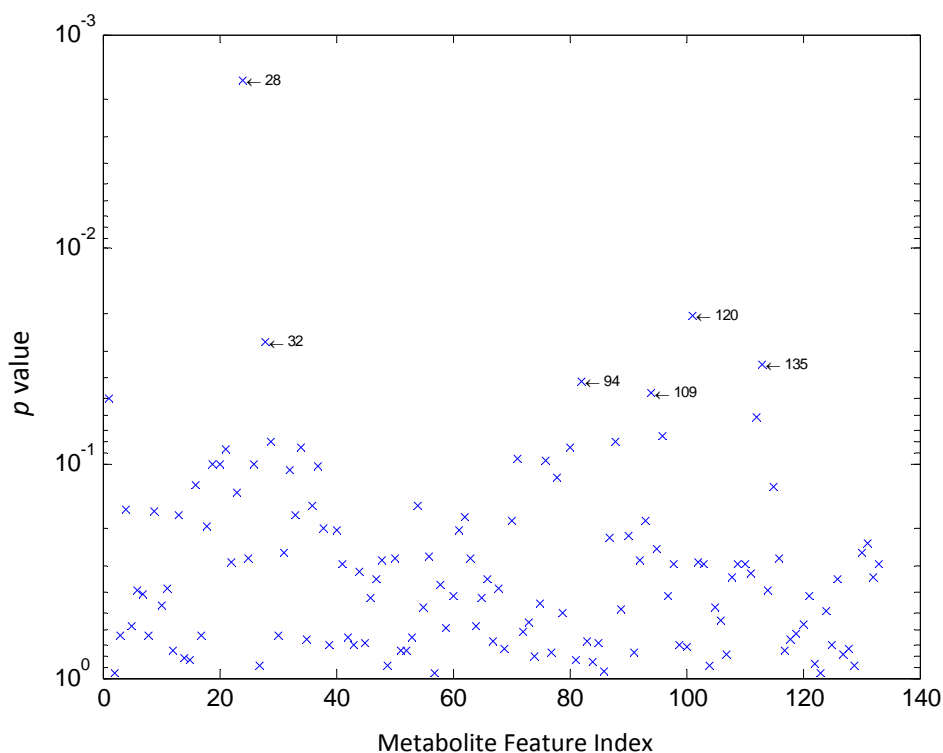


Figure 4-7: A scatter plot of metabolite feature index vs. p value for all metabolite peaks identified for the ciclosporin footprint analysis. Peaks that were identified as significant from ANOVA analysis with a p value < 0.05 are labelled with a number corresponding to feature index to allow identification of the peak.

4.3.3 Identification of Metabolites

The next step of the process requires the metabolites of interest to be identified. The metabolite identifications were assigned through searching and matching against an in-house constructed library and also the NIST02 and Golm metabolome libraries, as outlined in Section 4.2.2.5.

4.3.3.1 Dithranol Identification

A total of 50 metabolites were identified within the internal and external metabolome of dithranol treated cells and are highlighted within Table 4-3 and Table 4-4. The table uses the metabolite mass index number previously used within the ANOVA significance testing stage. The metabolite identification, human metabolome database (HMDB) accession number (Wishart et al., 2007) and

the chemical formula is provided for all metabolites. In addition the table defines the location of the metabolite within the metabolic fingerprint or metabolic footprint.

The majority of metabolites which were identified were present only within the internal metabolome of exposed cells (listed as black within Table 4.3 & 4.4). In addition, three metabolites were identified within the external metabolome (listed as blue in Table 4.3 & 4.4) and two metabolites were identified in both (listed as red within Table 4.3 & 4.4). The percentage of significant metabolites which were successfully identified was approximately 60% for the internal metabolome and approximately 38% for the external metabolome, the data of which is summarised within Table 4-2. Duplicative assignments have occurred for a number of metabolite features due to the formation of multiple products during the derivatisation process. These are indicated by * in Table 4-3 and Table 4-4. The identifications include a variety of metabolites including a number of amino acids and components of central metabolism.

4.3.3.2 Methotrexate & Ciclosporin Identification

The metabolites identified for the analysis of methotrexate and ciclosporin treated cells are shown in Table 4-5. As previous; the table includes the metabolite mass index number and correlating metabolite identifications, HMDB accession number and corresponding chemical formulas. In total 36 and 5 metabolites were identified for methotrexate and ciclosporin treated cells respectively. These numbers are somewhat disappointing and may prove a limiting factor in the analysis of the results.

Metabolite Number	Metabolite ID	HMDB Accession Number	Chemical Formula	Metabolic Footprint or Fingerprint	Metabolic Fingerprint Correlation Group
1	lactic acid	HMDB01311	C ₃ H ₆ O ₃	Footprint & Footprint	B
5	stearate	HMDB00827	C ₁₈ H ₃₆ O ₂	Fingerprint	C
10	glucose-6-phosphate	HMDB01401	C ₆ H ₁₃ O ₉ P	Fingerprint	A
13	leucine*	HMDB00687	C ₆ H ₁₃ NO ₂	Fingerprint	C
17	tryptophan	HMDB00929	C ₁₁ H ₁₂ N ₂ O ₂	Fingerprint	C
35	isoleucine	HMDB00172	C ₆ H ₁₃ NO ₂	Fingerprint	C
36	leucine*	HMDB00687	C ₆ H ₁₃ NO ₂	Fingerprint	C
37	malonate	HMDB00744	C ₄ H ₆ O ₅	Fingerprint	B
38	isoleucine*	HMDB00172	C ₆ H ₁₃ NO ₂	Fingerprint	A
39	isoleucine*	HMDB00172	C ₆ H ₁₃ NO ₂	Fingerprint	C
41	alanine	HMDB00161	C ₃ H ₇ NO ₂	Fingerprint	C
42	glycine	HMDB00123	C ₂ H ₅ NO ₂	Fingerprint	A
46	serine*	HMDB03406	C ₃ H ₇ NO ₃	Fingerprint	C
47	threonine*	HMDB00167	C ₄ H ₉ NO ₃	Fingerprint	B
48	serine*	HMDB03406	C ₃ H ₇ NO ₃	Fingerprint	C
49	urea	HMDB00294	CH ₄ N ₂ O	Fingerprint	B
50	threonine*	HMDB00167	C ₄ H ₉ NO ₃	Fingerprint	C
57	3-ureidopropanoic acid or beta-alanine	HMDB00026/HMDB00056	C ₄ H ₈ N ₂ O ₃ /C ₃ H ₇ NO ₂	Fingerprint	A
58	threitol/erythritol	HMDB04136/HMDB02994	C ₄ H ₁₀ O ₄	Fingerprint	B
61	threonic acid/erythronic acid	HMDB00943/HMDB00613	C ₄ H ₈ O ₅	Fingerprint	A
63	malate	HMDB00744	C ₄ H ₆ O ₅	Fingerprint	A
65	4-hydroxyproline*	HMDB00725	C ₅ H ₉ NO ₃	Fingerprint	C
68	aspartate	HMDB00191	C ₄ H ₇ NO ₄	Fingerprint	A

Table 4-3: Identified metabolites from the internal and external metabolome of dithranol treated HaCaT cells. The majority of metabolites were identified solely within the internal metabolome (indicated in black) while five metabolites were recorded in the external metabolome. A reference number corresponding to the human metabolome database and the chemical formula is given. The correlation group number is supplied for internal metabolites as discussed in Section 4.3.4.1. Metabolite ID's labelled with a * highlight multiple derivatisation products.

Metabolite Number	Metabolite ID	HMDB Accession Number	Chemical Formula	Metabolic Footprint or Fingerprint	Metabolic Fingerprint Correlation Group
69	4-hydroxyproline*	HMDB00725	C ₅ H ₉ NO ₃	Fingerprint	C
72	methionine	HMDB00696	C ₅ H ₁₁ NO ₂ S	Fingerprint	C
78	glutamate*	HMDB03339	C ₅ H ₉ NO ₄	Fingerprint	A
79	glutamate*	HMDB03339	C ₅ H ₉ NO ₄	Fingerprint	A
81	hypotaurine	HMDB00965	C ₂ H ₇ NO ₂ S	Fingerprint	A
83	pyroglutamate	HMDB00267	C ₅ H ₇ NO ₃	Fingerprint	A
84	valine*	HMDB00883	C ₅ H ₁₁ NO ₂	Fingerprint	C
85	fructose*	HMDB00660	C ₆ H ₁₂ O ₆	Fingerprint	B
87	fructose*	HMDB00660	C ₆ H ₁₂ O ₆	Fingerprint	B
88	nicotinamide	HMDB01406	C ₆ H ₆ N ₂ O	Fingerprint	A
89	phenylalanine	HMDB00159	C ₉ H ₁₁ NO ₂	Fingerprint	C
92	phenylalanine	HMDB00159	C ₉ H ₁₁ NO ₂	Footprint	
95	pyruvate	HMDB00243	C ₃ H ₄ O ₃	Fingerprint	B
96	glycerol-3-phosphate	HMDB00126	C ₃ H ₉ O ₆ P	Fingerprint	A
99	ethylphosphate	HMDB12228	C ₂ H ₇ O ₄ P	Fingerprint	A
100	glucose	HMDB00122	C ₆ H ₁₂ O ₆	Footprint	
101	citric acid	HMDB00094	C ₆ H ₈ O ₇	Fingerprint	A
104	glucose	HMDB00122	C ₆ H ₁₂ O ₆	Fingerprint	B
105	myo-inositol	HMDB00211	C ₆ H ₁₂ O ₆	Fingerprint & Footprint	A
107	myo-inositol	HMDB00211	C ₆ H ₁₂ O ₆	Fingerprint	A
110	tyrosine	HMDB00158	C ₉ H ₁₁ NO ₃	Fingerprint	C
111	pantothenate	HMDB00210	C ₉ H ₁₇ NO ₅	Fingerprint	B
113	tyramine	HMDB00306	C ₈ H ₁₁ NO	Footprint	
115	histidine	HMDB00177	C ₆ H ₉ N ₃ O ₂	Fingerprint	C
117	valine*	HMDB00883	C ₅ H ₁₁ NO ₂	Fingerprint	C

Table 4-4: Identified metabolites from the internal and external metabolome of dithranol treated HaCaT cells. The majority of metabolites were identified solely within the internal metabolome (indicated in black) while five metabolites were recorded in the external metabolome. A reference number corresponding to the human metabolome database and the chemical formula is given. The correlation group number is supplied for internal metabolites as discussed in Section 4.3.4.1. Metabolite ID's labelled with a * highlight multiple derivatisation products.

Metabolite Number	Metabolite ID	HMDB Assession Number	Chemical Formula	Fingerprint or Footprint
Methotrexate				
2	Valine	HMDB00883	C ₅ H ₁₁ NO ₂	Footprint
6	myo-inositol *	HMDB00211	C ₆ H ₁₂ O ₆	Footprint
8	myo-inositol*	HMDB00211	C ₆ H ₁₂ O ₆	Footprint
9	pyridoxine	HMDB00239	C ₈ H ₁₁ NO ₃	Footprint
15	pantothenate	HMDB00210	C ₉ H ₁₇ NO ₅	Fingerprint
46	norvaline			Footprint
53	monopalmitin*	HMDB00220	C ₁₆ H ₃₂ O ₂	Fingerprint
62	monopalmitin*	HMDB00220	C ₁₆ H ₃₂ O ₂	Fingerprint
68	leucine*	HMDB00687	C ₆ H ₁₃ NO ₂	Footprint
70	monostearin	HMDB00827	C ₁₈ H ₃₆ O ₂	Footprint
70	monostearin	HMDB00827	C ₁₈ H ₃₆ O ₂	Fingerprint
75	glycerol	HMDB00131	C ₃ H ₈ O ₃	Footprint
76	isoleucine	HMDB00172	C ₆ H ₁₃ NO ₂	Footprint
77	leucine*	HMDB00687	C ₆ H ₁₃ NO ₂	Footprint
87	serine*	HMDB03406	C ₃ H ₇ NO ₃	Footprint
89	glyceric acid	HMDB00139	C ₃ H ₆ O ₄	Footprint
91	threonine	HMDB00167	C ₄ H ₉ NO ₃	Footprint
91	threonine	HMDB00167	C ₄ H ₉ NO ₃	Fingerprint
92	serine*	HMDB03406	C ₃ H ₇ NO ₃	Footprint
104	proline	HMDB00162	C ₅ H ₉ NO ₂	Footprint
105	threitol/erythritol	HMDB04136/HMDB02994	C ₄ H ₁₀ O ₄	Footprint
105	threitol/erthritol	HMDB04136/HMDB02994	C ₄ H ₁₀ O ₄	Fingerprint
111	p-benzoquinone	HMDB03364	C ₆ H ₄ O ₂	Footprint
113	threonic acid/erthronic acid	HMDB00943/HMDB00613	C ₄ H ₈ O ₅	Footprint
113	threonic acid/erythronic acid	HMDB00943/HMDB00613	C ₄ H ₈ O ₅	Fingerprint
115	4-hydroxyproline	HMDB00725	C ₅ H ₉ NO ₃	Footprint
121	3-hydroxybutanoic acid	HMDB00357	C ₄ H ₈ O ₃	Fingerprint
125	methionine*	HMDB00696	C ₅ H ₁₁ NO ₂ S	Footprint
127	methionine*	HMDB00696	C ₅ H ₁₁ NO ₂ S	Footprint
136	creatine	HMDB00064	C ₄ H ₉ N ₃ O ₂	Footprint
140	alanine	HMDB00161	C ₃ H ₇ NO ₂	Footprint
141	pyroglutamic acid	HMDB00267	C ₅ H ₇ NO ₃	Fingerprint
150	fructose	HMDB00660	C ₆ H ₁₂ O ₆	Fingerprint
151	glycine	HMDB00123	C ₂ H ₅ NO ₂	Footprint
152	glycerol-3-phosphate	HMDB00126	C ₃ H ₉ O ₆ P	Fingerprint
Ciclosporin				
17	hexadecanoic acid	HMDB00220	C ₁₆ H ₃₂ O ₂	Fingerprint
44	glucose-6-phosphate	HMDB01401	C ₆ H ₁₃ O ₉ P	Fingerprint
83	glycine	HMDB00123	C ₂ H ₅ NO ₂	Fingerprint
92	serine	HMDB03406	C ₃ H ₇ NO ₃	Fingerprint
94	threonine	HMDB00167	C ₄ H ₉ NO ₃	Footprint

Table 4-5: Identified metabolites from the internal and external metabolome of methotrexate and ciclosporin treated HaCaT cells. A reference number corresponding to the human metabolome database, the chemical formula and corresponding *p* values supplied for all metabolites. Metabolite ID's labelled with a * highlight multiple derivatisation products.

4.3.4 Spring embedded correlation analysis.

Spring embedded correlation analysis was applied to the data corresponding to the metabolite peaks which were judged to be significant (p value < 0.05). Correlation analysis was employed to illustrate similarities and variances in the metabolite response to the exposed drug. A major advantage of this type of analysis is the simplistic schematic manner in which the results are shown.

In the correlation plots (see below) metabolite peaks are represented as circles which are labelled for identification purposes with the metabolite feature index identification number as illustrated in the previous collection of ANOVA scatter plots and identification tables. The size of the circle is representative of the significance of the metabolite peak: the larger the circle the lower the p value associated with the peak and hence the more significance of its presence and *vice versa*. The correlation between metabolites is illustrated by the “spring” element of the plot. The lines or springs link metabolites that are closely correlated. A value is associated with each line which quantifies the level of correlation. The closer the value to 1 the more closely correlated the metabolites are in relationship to each other.

4.3.4.1 Dithranol Fingerprint

The spring embedded correlation plot for the internal metabolome of dithranol treated HaCaT cells shows the 75 significant peaks clustered into three distinct groups as illustrated in Figure 4-8.

The classification of metabolites into the three groups infers that there are variations in response to drug application within the intracellular metabolome of the cells. Figure 4-9 illustrates the typical response exhibited within the three groups; A, B and C. The box and whisker diagrams show dithranol concentration ($\mu\text{g}/\text{mL}$) versus % peak area for a chosen metabolite from each correlation group and all other metabolites within that group exhibited very similar results.

The trend within group A is demonstrated by the response of metabolite feature 63: malate. The metabolite concentration decreases more or less linearly as the concentration of dithranol increases and hence appears to exhibit a down regulated response to the drug.

Group B response is represented by metabolite feature 11: unknown. In response to increasing dithranol concentration the metabolite concentration increases. A slight increase is observed between 0.1 and 0.3 $\mu\text{g}/\text{mL}$ followed by a sharp increase above 0.4 $\mu\text{g}/\text{mL}$.

Metabolite feature 48 , serine; illustrates the parabolic trend associated with group C. Groups B and C consist of an element of common linkage and resultantly shows an increase in metabolite concentration as dithranol concentration increases; although for group C the increase in metabolite concentration is observed much earlier at 0.1 and 0.3 $\mu\text{g}/\text{mL}$. However in comparison to group B metabolites, a decrease in recorded concentration of the metabolite occurs at 0.4 and 0.5 $\mu\text{g}/\text{mL}$.

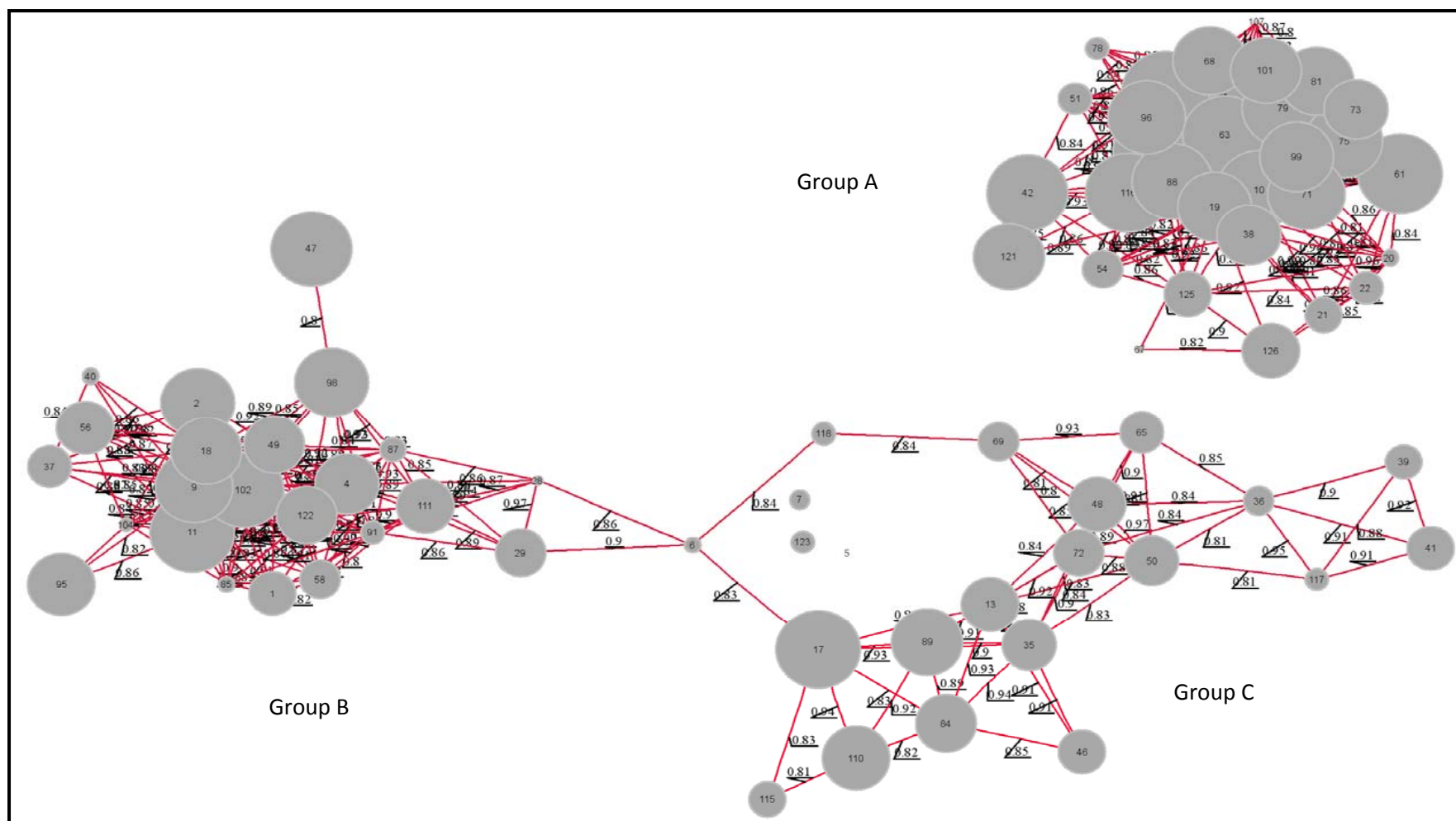


Figure 4-8: Spring embedded correlation plot for the analysis of the internal metabolome of dithranol treated HaCaT cells. The metabolite peaks are represented by the circles and the number within the circle is the metabolite ID. The larger the circle the more significant the metabolite was determined to be by ANOVA analysis. The links shown between metabolites illustrate the correlations present, the magnitude of which is shown by the number. The nearer the number is to 1 the greater the degree of correlation.

Box and whisker plots provide a descriptive summary of the spread of replicate results. The upper and lower whiskers illustrate the sample maximum and sample minimum of the data respectively. The box represents the upper (75th percentile) and lower (25th percentile) quartiles of the data and the middle line indicates the median data value.

Group A metabolites show a gradual decrease over the concentration range of applied dithranol as observed for metabolite 63: malate.

Group B metabolites increase as the concentration of dithranol exposure increases as demonstrated by metabolite 11: unknown.

Group C metabolites demonstrate an initial increase followed by a decrease at the higher concentrations of dithranol exposure. This trend is exhibited by metabolite 48: serine.

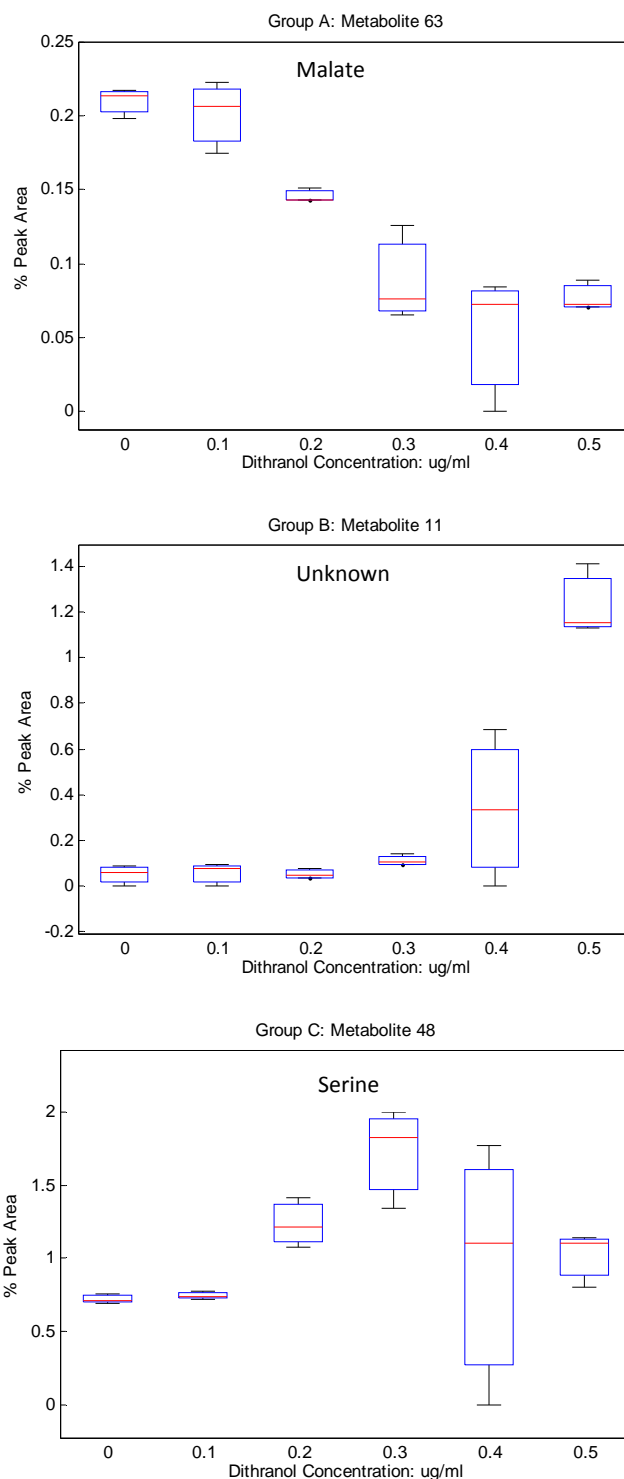


Figure 4-9: Box and whisker plots of dithranol concentration ($\mu\text{g}/\text{mL}$) vs. % peak area to illustrate the general trends observed from the correlation analysis for groups A, B and C.

observed within the dithranol footprint samples are of a lesser magnitude to those from the fingerprint analysis which as previously stated could be attributed to the interference of the media in masking metabolite responses.

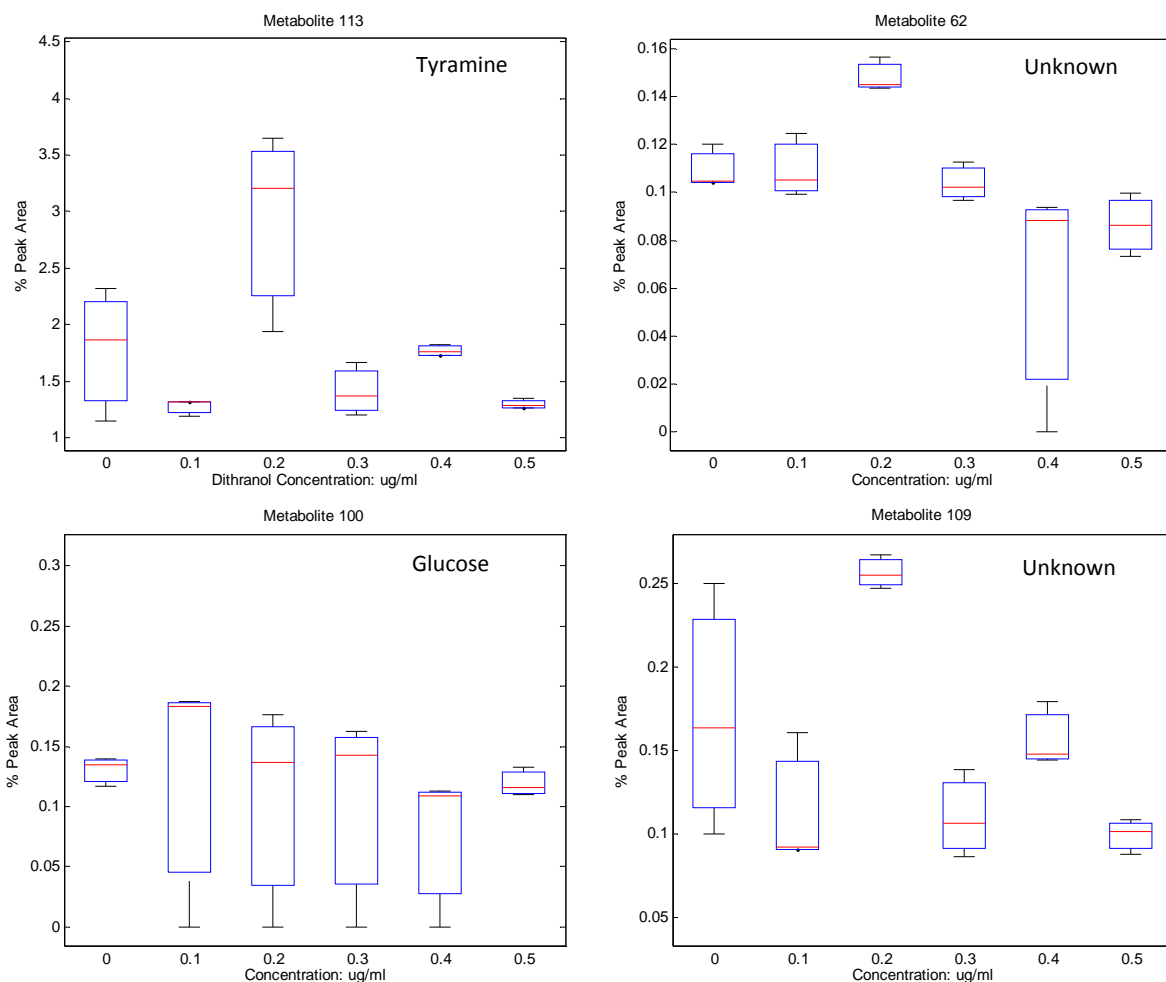


Figure 4-11: Box and whisker diagrams correlating to metabolites 113, 62, 100 and 109 showing dithranol exposure concentration ($\mu\text{g}/\text{mL}$) vs. % peak area for the external metabolome.

4.3.4.3 Methotrexate Fingerprint

The spring embedded correlation plot for the analysis of the internal metabolome of methotrexate treated HaCaT cells is shown in Figure 4-12. The metabolites deemed significant correlate into two loosely connected groups which contain metabolites of ranging significance. The group clustered on the right hand side contains 10 metabolites including metabolites 62 (monopalmitin),

70 (monostearin) and 134 (unknown) which are high in significance. Box and whisker plots for these metabolites which indicate response to methotrexate are shown in Figure 4-13. These metabolites exhibit an up regulated response to the application of methotrexate.

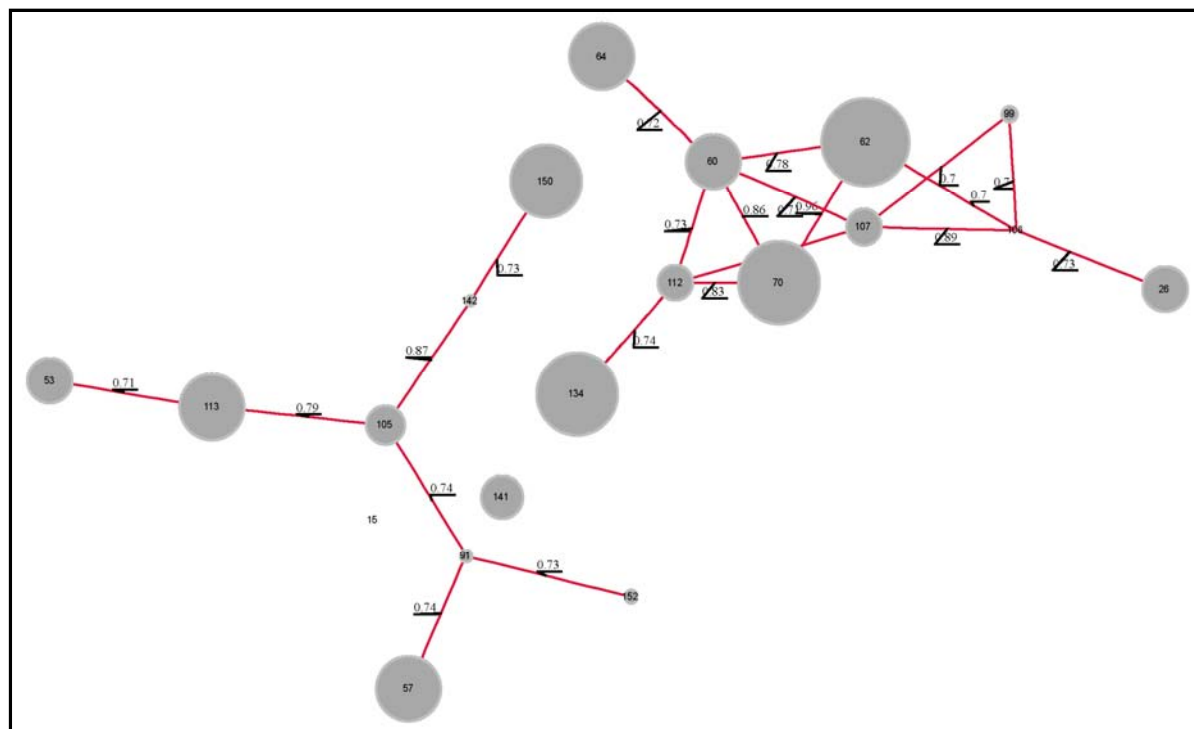


Figure 4-12: Spring embedded correlation plot for the analysis of the internal metabolome of methotrexate treated HaCaT cells. The metabolite peaks are represented by the circles and the number within the circle is the metabolite ID. The larger the circle the more significant the metabolite was determined to be by ANOVA analysis. The links shown between metabolites illustrate the correlations present, the magnitude of which is shown by the number. The nearer the number is to 1 the greater the degree of correlation.

The metabolites which cluster on the left hand of the spring embedded plot include metabolites 57 (unknown), 113 (threonic acid/erythronic acid) and 150 (fructose) which are of the highest significance and 105 (threitol/erythritol) as a central linker in the cluster of metabolites. Box and whisker plots illustrating the response of these metabolites to increasing concentrations of methotrexate are depicted in Figure 4-13. The trend exhibited by the metabolites correlated on the left hand side of Figure 4-12 is less consistent than those previously discussed from the right hand group and their significance could be questioned.

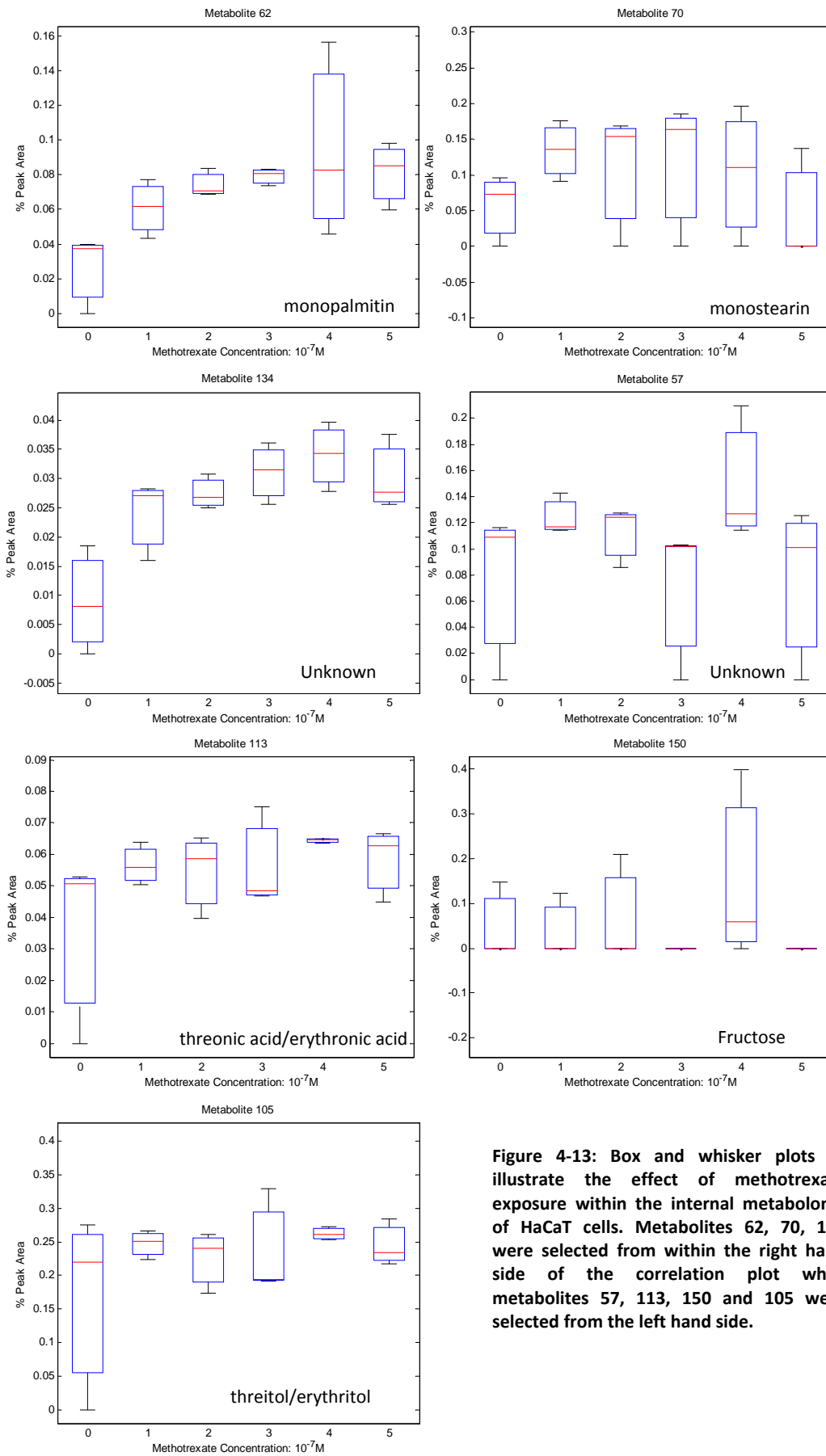


Figure 4-13: Box and whisker plots to illustrate the effect of methotrexate exposure within the internal metabolome of HaCaT cells. Metabolites 62, 70, 134 were selected from within the right hand side of the correlation plot while metabolites 57, 113, 150 and 105 were selected from the left hand side.

4.3.4.4 Methotrexate Footprint

The 59 significant metabolites obtained from the metabolic footprint of methotrexate treated HaCaT cells were subjected to correlation analysis. The metabolites largely cluster into one highly correlated group, while the remaining metabolites form a loosely connected network, Figure 4-14. The most significant metabolite within the large group is metabolite 119; other metabolites of high significance include metabolites 54 (unknown), 71 (unknown), 75 (glycerol) and 123 (unknown). Figure 4-15 indicates the changes in concentration of these metabolites at varying levels of methotrexate exposure. As the most significant metabolite, metabolite 119 (unknown) shows a minor decrease in mean peak area as the concentration of drug exposure increases. Large fluctuations are recorded within the three replicate samples at 2 and 5 $\times 10^{-7}$ M which could indicate a varying biological effect.

Metabolites 54 (unknown) and 75 (unknown) exhibit the large fluctuations amongst replicates at 2 and 5 $\times 10^{-7}$ M exposure however while metabolite 54 (unknown) shows a general decrease as concentration increases, metabolite 75 (unknown) remains relatively constant with proportional down-regulation at 4 $\times 10^{-7}$ M. Metabolites 71 (unknown) and 123 (unknown) show similar responses. An initial increase in concentration is observed between 1-3 $\times 10^{-7}$ M followed by a decrease at 4 $\times 10^{-7}$ M. In comparison to the previously mentioned metabolites, metabolites 71 and 123 show large fluctuations between replicates at 4 $\times 10^{-7}$ M which could be a response to the fluctuations mentioned above.

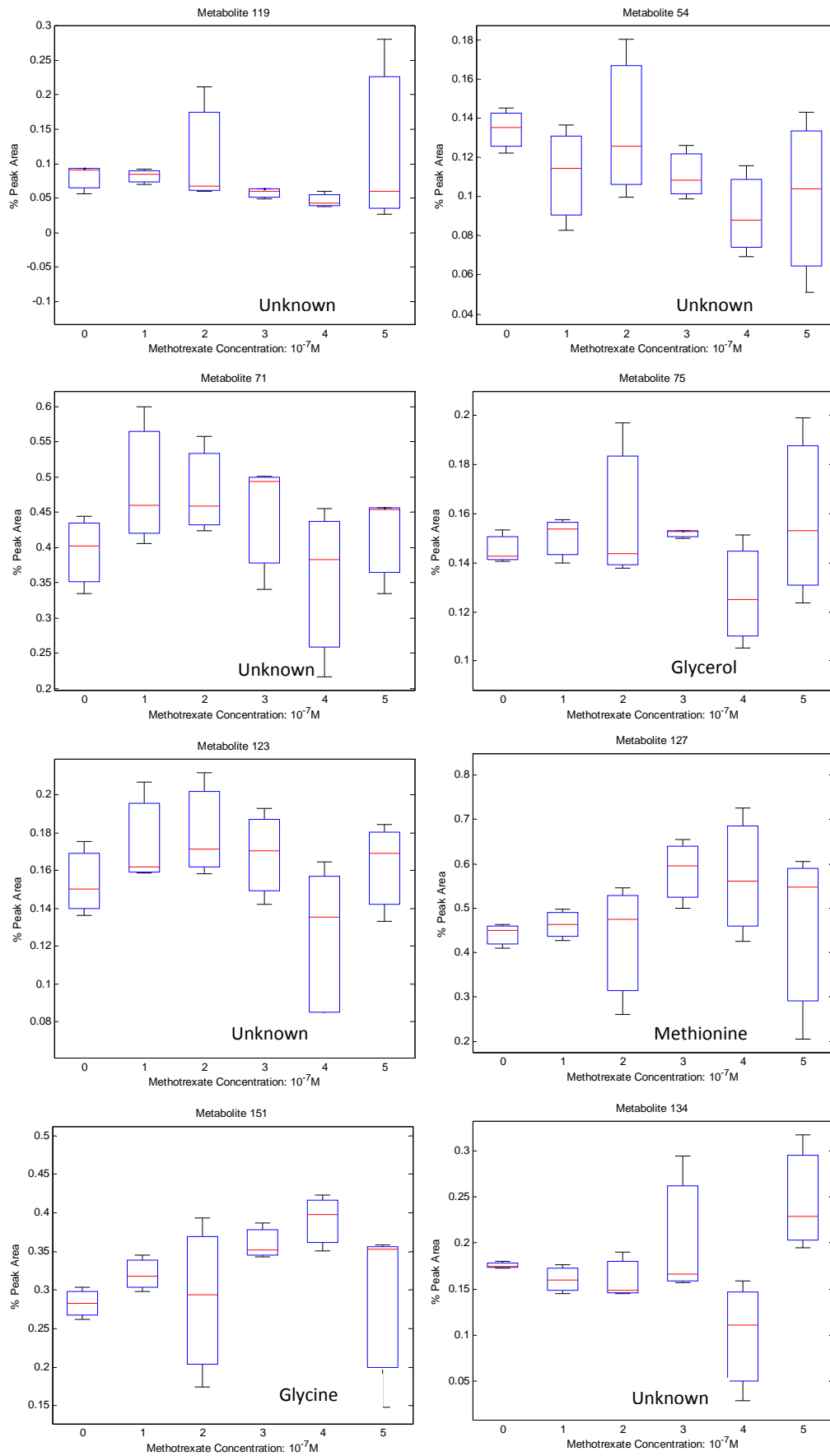


Figure 4-15: Box and whisker plots to illustrate the effect of methotrexate exposure within the metabolic footprint of HaCaT cells.

Metabolite 119 is depicted as the most significant metabolite within the correlation analysis and shows a gradual decrease increase over concentration increase. Large fluctuations are observed at 2 & 5 x10⁻⁷ M.

The other metabolites exhibit varying responses to methotrexate exposure.

4.3.4.5 Ciclosporin Fingerprint

As a consequence of the limited number of metabolites deemed significant for the fingerprint analysis of ciclosporin treated cells, the correlation plot shown in Figure 4-16 is very limited in information. The majority of metabolites which were deemed significant remained unidentified with the exception of metabolite 83 which was identified as glycine. Metabolites 7, 83, 100 and 134 were chosen as example metabolites and box and whisker plots were generated which are shown in Figure 4-17.

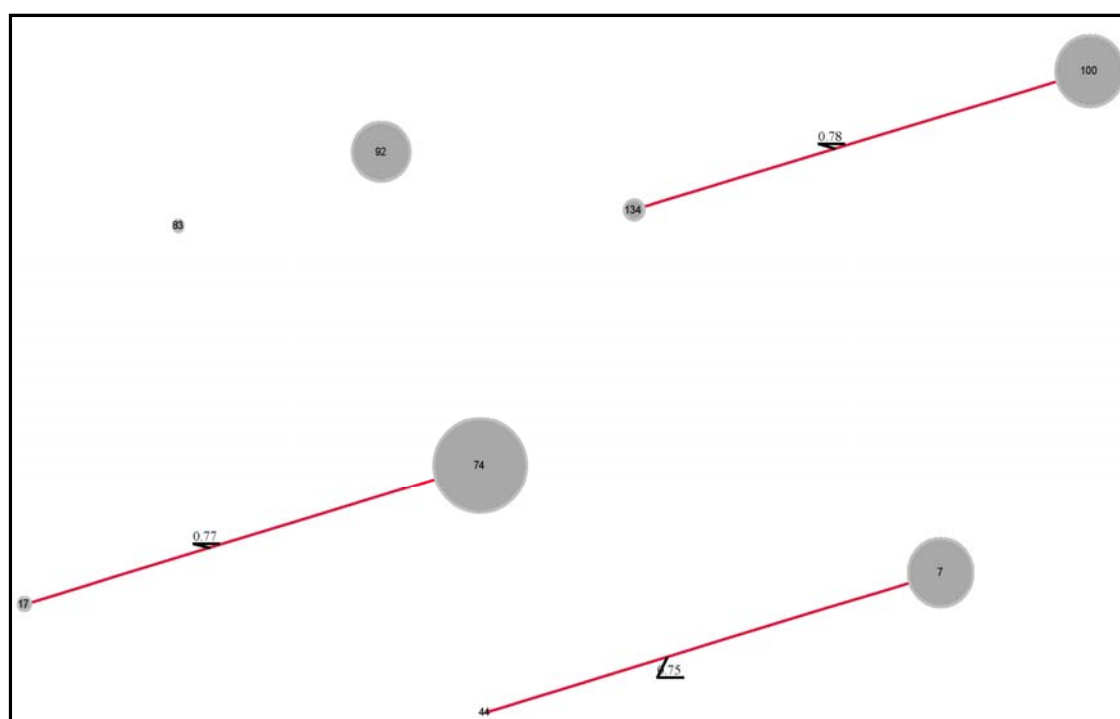


Figure 4-16: Spring embedded correlation plot for the analysis of the internal metabolome of ciclosporin treated HaCaT cells. The metabolite peaks are represented by the circles and the number within the circle is the metabolite ID. The larger the circle the more significant the metabolite was determined to be by ANOVA analysis. The links shown between metabolites illustrate the correlations present, the magnitude of which is shown by the number. The nearer the number is to 1 the greater the degree of correlation.

The metabolites exhibit varying responses to the drug. Metabolites 7 and 134 increase steadily in concentration until $2 \times 10^{-7} \text{M}$, and follow by a notable decrease in concentration at $2.5 \times 10^{-7} \text{M}$. In comparison metabolite 83 increases slightly and plateaus over the drug exposure range. Metabolite 100 reaches the highest concentration at $1.5 \times 10^{-7} \text{M}$ and decreases slightly thereafter.

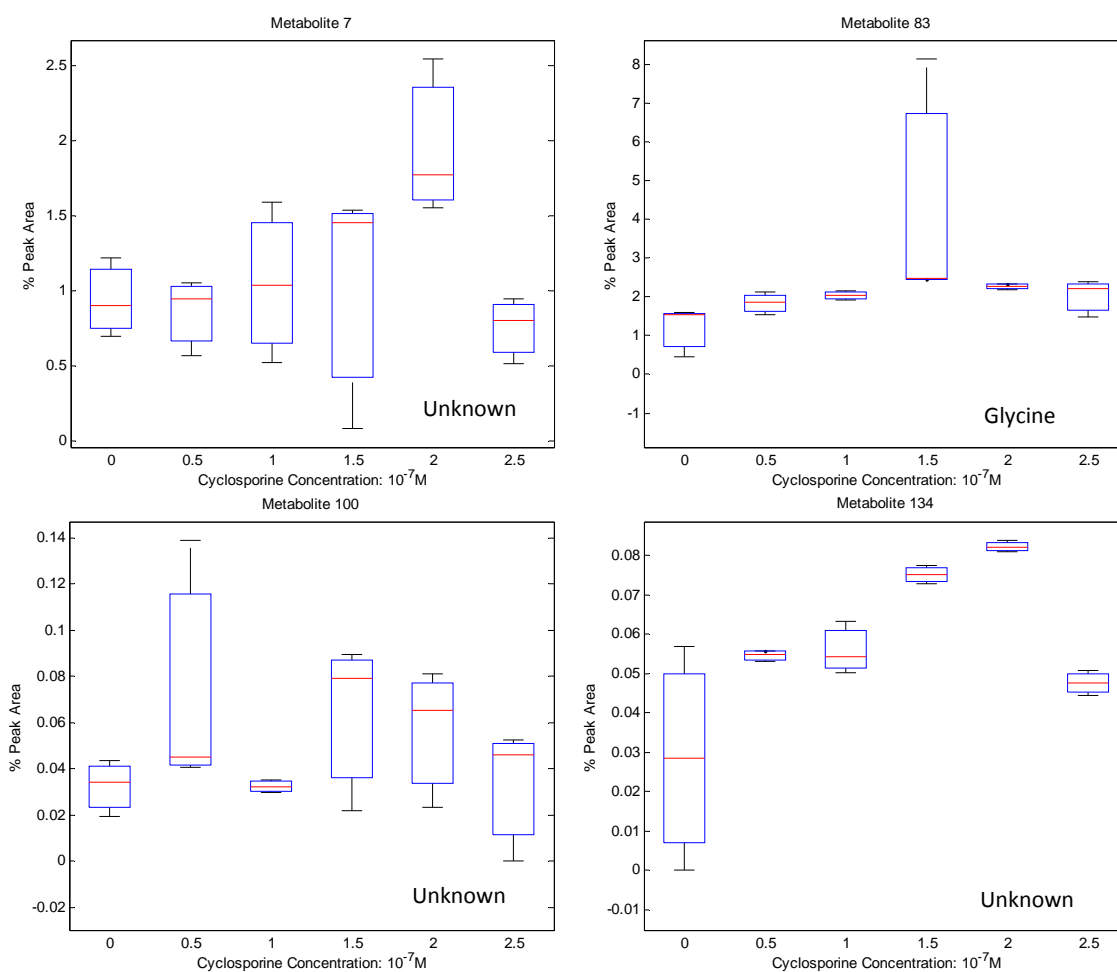


Figure 4-17: Box and whisker plots to illustrate the affect of ciclosporin exposure within the internal metabolome of HaCaT cells. Metabolites 7, 83, 100 and 134 were chosen as example metabolites. The metabolites exhibit varying responses to the drug. Metabolites 7 and 134 increase steadily in concentration until $2 \times 10^{-7} \text{M}$, and follow by a notable decrease in concentration at $2.5 \times 10^{-7} \text{M}$. In comparison metabolite 83 increases slightly and plateaus over the drug exposure range. Metabolite 100 reaches the highest concentration at $1.5 \times 10^{-7} \text{M}$ and decreases slightly thereafter.

4.3.4.6 Ciclosporin Footprint

The spring embedded correlation plot for the metabolic footprint of HaCaT cells treated with ciclosporin displayed in Figure 4-18 also incorporates a limited number of metabolites. However the metabolites presented exhibit a trend upon exposure to the drug. An increase in metabolite concentration is observed between 0- $1 \times 10^{-7} \text{M}$ exposures to reach a plateau at $1 \times 10^{-7} \text{M}$. All metabolites present within the correlation plot remained unidentified. Metabolites 28, 32 and 120 subsequently decrease in concentration following an almost linear reduction from 1- $2.5 \times 10^{-7} \text{M}$.

Metabolite 135 also shows a decrease in concentration from $1 \times 10^{-7} \text{M}$ however, the box and whisker plot is distorted due to the inclusion of zero values in some replicate samples. This information is displayed in Figure 4-19.

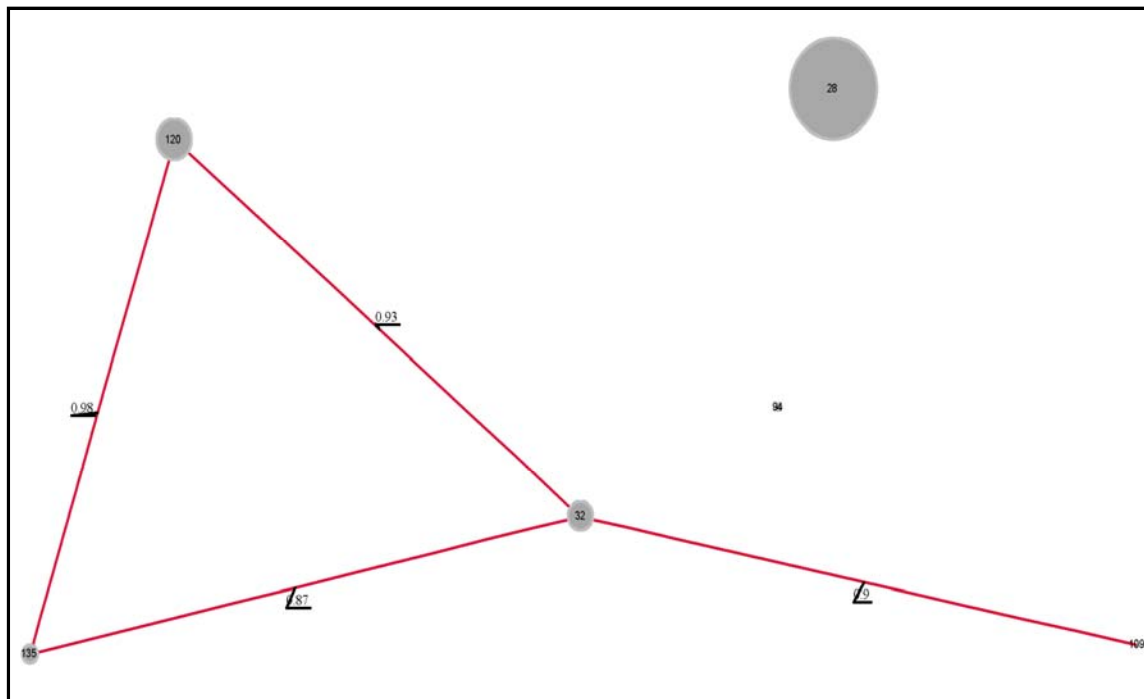


Figure 4-18: Spring embedded correlation plot for the analysis of the metabolic footprint of ciclosporin treated HaCaT cells. The metabolite peaks are represented by the circles and the number within the circle is the metabolite ID. The larger the circle the more significant the metabolite was determined to be by ANOVA analysis. The links shown between metabolites illustrate the correlations present, the magnitude of which is shown by the number. The nearer the number is to 1 the greater the degree of correlation.

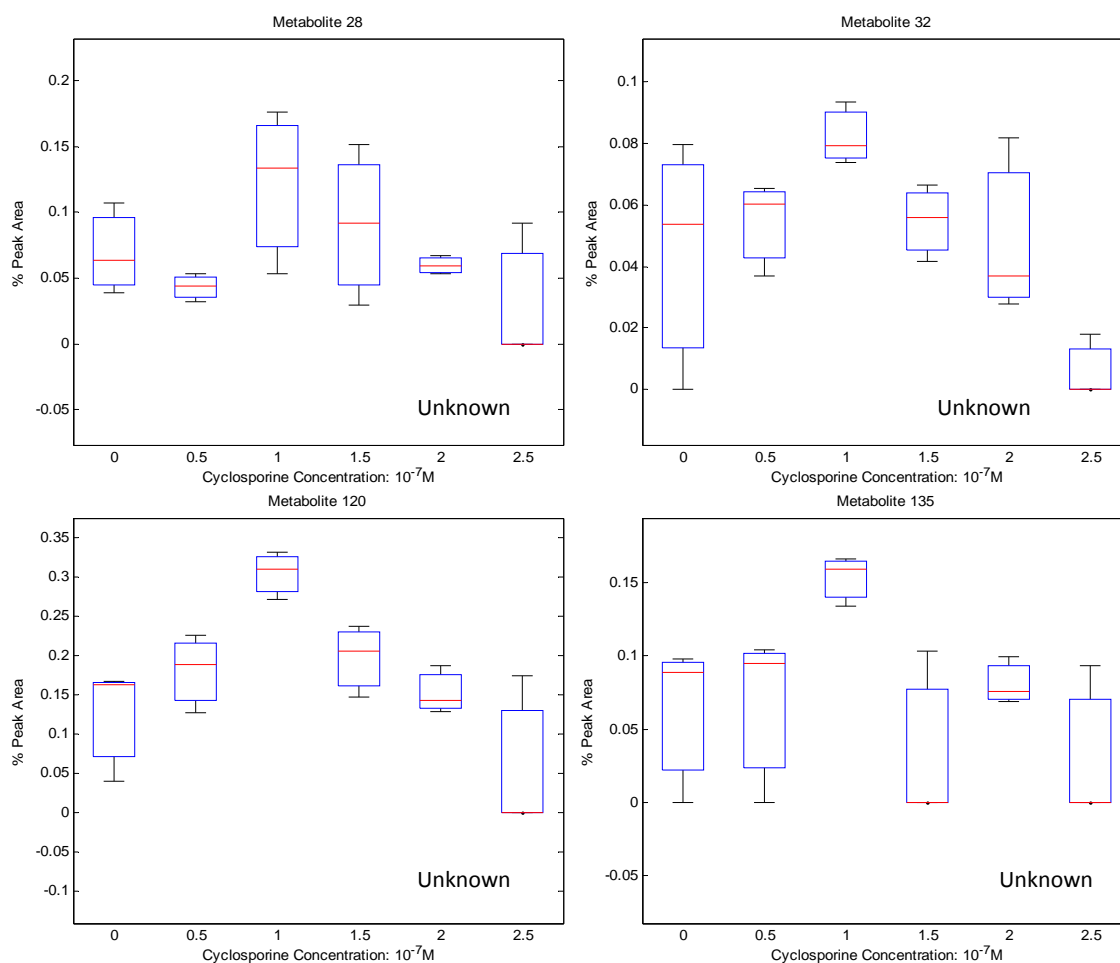


Figure 4-19: Box and Whisker plots for metabolites 28, 32, 120 and 135 to illustrate a degree of metabolic response to cyclosporin exposure within the metabolic footprint. All metabolites show a positive response to initial treatment through an increase in concentration between 0-1x10⁻⁷ M followed by a decrease in concentration between 1-2.5x10⁻⁷ M.

4.3.5 Dithranol Interpretation

As a consequence of the large number of metabolites identified for the dithranol treated cells it would be unrealistic to interpret individual box and whisker plots for each metabolite without the inclusion of additional biochemical information. It was for this reason that a metabolic map illustrated in Figure 4-20 was constructed utilising information gained from within the KEGG database.

The metabolite map presents a series of metabolites linked according to the biochemical steps within their metabolism and degradation. The levels of several intermediates of central metabolism were affected by exposure to dithranol including a number associated with the TCA cycle and amino acid metabolism. The use of solid arrows indicates a direct linkage of metabolites while a dashed arrow corresponds to a pathway including a limited number of undetected metabolites. The metabolites in black are those which were successfully identified and those in red are included as a reference. Metabolites highlighted in orange are metabolites which are actively present in the DMEM growth media employed in the growth of the HaCaT cells. All box and whisker plots represent metabolites detected in the internal metabolome unless highlighted accordingly, **. To accommodate the multiple derivatisation products the metabolite feature which was deemed to show the best trend response was incorporated into the metabolite map.

The concluding part of metabolite analysis is to begin to understand and interpret the role of these metabolites that vary and are co-correlated upon drug exposure. It is clearly evident from the results discussed that dithranol has a pronounced affect on the metabolism of HaCaT cells, and it is necessary to combine *a priori* literature based information with the current results to develop an understanding of the mode of action of dithranol on psoriasis treatment.

As previously mentioned the mode of action of dithranol during anti-psoriatic treatment is not fully understood. One major theory is that dithranol accumulates in the mitochondria of cells thus inhibiting mitochondrial oxidative respiration. Components of the respiratory chain are reduced and hence ATP synthesis is restricted (McGill et al., 2005). As the TCA cycle occurs within the mitochondrial matrix of cells, the down-regulation of TCA intermediates is anticipated and this is observed within the constructed metabolite map, Figure 4-20. It was relatively disappointing that the number of TCA intermediates detected was low, however, the concentration of citrate significantly decreases at 0.2 $\mu\text{g}/\text{mL}$ and malate concentration decreases at 0.3 $\mu\text{g}/\text{mL}$. A collection of additional metabolites exhibit a trend associated with this down-regulation of TCA intermediates in association with the increasing concentration of dithranol exposure. These metabolites include nicotinamide, aspartate, glutamate, pyro-glutamate, β -alanine and hypotaurine, all of which exhibit a similar decreasing trend in concentration as the concentration of drug application increases.

Nicotinamide concentration decreases as the concentration of dithranol exposure increases. Nicotinamide is a form of niacin, a vitamin B₃, and has recently been implemented in a number of new patents aimed at psoriasis treatment. However a publication by Lim and colleagues indicated that within primary human neonatal skin fibroblasts (type 82-6) an increase in nicotinamide concentration greatly increased the rate of cell proliferation (Lim et al., 2006). This result seems to correspond with our results that infer that through dithranol exposure a decrease in cell proliferation would be observed and hence a decrease in nicotinamide.

Nicotinamide metabolism is directly related to nicotinamide adenine dinucleotide (NAD^+) and nicotinamide adenine dinucleotide phosphate (NADP^+). The response of NAD^+ and NADP^+ to dithranol treatment has previously been discussed (Hammar, 1975). In the first

instance the concentration of NAD^+ and NADP^+ was shown to be greater within psoriatic lesions than normal control skin. This observation can be back correlated to the effect observed for nicotinamide concentration within the HaCaT treated cells. It was additionally reported that dithranol decreased the level of NAD^+ towards control levels however the affect upon NADP^+ levels was not significant.

NADH is generated in small amounts during glycolysis and is readily produced during the TCA cycle through the inter-conversion of NAD to NADH *via* reduction. We are aware from this study and the literature above that the TCA stage of metabolism is compromised by the application of dithranol and as a consequence the balance of co-factor production and usage will be altered. The combination of the skew in co-factor balance and the requirement for an alternative route for carbon metabolism to bypass TCA implies that an alternative route occurs for the generation of cofactors and biomass. A possible alternative route is *via* the pentose phosphate pathway which is an alternative to glycolysis and occurs in the cytosol of the cell so is less likely to be affected by the drug. The pentose phosphate pathway begins with an irreversible oxidation stage converting glucose-6-phosphate to ribulose-5-phosphate (undetected in this analysis) generating NADPH . This theory would help to explain the trend observed for glucose-6-phosphate and glycerol-3-phosphate; a linear decrease in concentration as the concentration of dithranol exposure increases.

A decrease in glutamate concentration was also observed in line with the altered TCA intermediates. Glutamate as a key metabolite is highly involved in a number of cellular processes including histidine, nitrogen and glutathione metabolism. Glutamate is closely linked to glutamine which was undetected in our analysis. It is believed that glutamate has a relatively low turnover resulting in high quantity pools within the cell, while glutamine has a relatively fast turnover and thus pools of low quantity (Rivett, 1985) (Darmaun et al., 1988). Darmaun *et al.*, consistently observed that human fibroblast cells contained more free

glutamate than free glutamine. This theory helps to explain why glutamine remains undetected. The significance of glutamine is its associated role within purine and pyrimidine metabolism and hence a down regulation in glutamine would infer a reduction in DNA synthesis. This would correlate with the anti-proliferative role of dithranol as replication and growth would be impaired, which may result in a decrease in cellular proteins as well as metabolites and nucleic acids. A discussion of the effect of dithranol on cellular protein content is available in Chapter 5.

The effect of dithranol observed through the response of the central metabolism intermediates glucose, pyruvate and lactate is varied. During respiration the fate of pyruvate is largely either to oxidative phosphorylation within the mitochondria being converted by pyruvate dehydrogenase into citrate, or alternatively pyruvate can undergo fermentation and be converted to lactate *via* lactate dehydrogenase. The general response of these metabolites is independent to the increasing concentration of dithranol treatment. Glucose was successfully detected within the internal and external metabolome of the HaCaT cells and appears to be maintained at all levels of treatment possibly through the inter-conversion of myo-inositol supplies. Pyruvate was shown to be significantly affected by dithranol treatment within the metabolic fingerprint. The presence of pyruvate is at its maximum at 0.3 $\mu\text{g}/\text{mL}$ which correlates with the concentration minimum of citrate downstream in the TCA cycle. The fermentative product lactate was additionally detected within the internal and external metabolome of the analysis. The response of lactate within the internal metabolome correlates well with the response observed for pyruvate in that the concentration of lactate dipped significantly at 0.3 $\mu\text{g}/\text{mL}$ dithranol exposure when the highest concentration of pyruvate is also present. This observation is complemented by the response of lactate within the external metabolome where the maximum concentration is observed at 0.3 $\mu\text{g}/\text{mL}$. The response relationship exhibited between these three metabolites indicates the effect of dithranol on central metabolism of the HaCaT cells and

illustrates that the drug has successfully penetrated the cells, and again seems to be targeting the mitochondria.

The results discussed above have partially confirmed the primary mode of action of dithranol upon HaCaT cells through describing the alteration of the TCA cycle and additional respiration linked metabolites. The metabolite map also indicates a response by a number of amino acids which could provide a potential alternative route of action of the drug. As building blocks for protein synthesis amino acid regulation or alteration could be deemed influential in the treatment of psoriasis.

The amino acid metabolite tyrosine is of particular interest. The concentration of tyrosine increases sharply from the control sample through to 0.3 $\mu\text{g}/\text{mL}$ dithranol exposure. This rise is subsequently followed by a decrease at 0.4 and 0.5 $\mu\text{g}/\text{mL}$. The down regulation of phosphotyrosine within HaCaT cells has previously been reported upon exposure to 0.5 $\mu\text{g}/\text{mL}$ of dithranol. The intracellular concentration of phosphotyrosine was determined by six independent assays and was reported to be 59% lower compared to cells cultured in 100% pure media (Ockenfels et al., 1995). The authors reported that this reduction in intracellular phosphotyrosine may be one reason for the therapeutic effect of dithranol on psoriasis.

Tyrosine can be directly linked to tyramine and phenylalanine within the metabolic map. The external metabolome content of tyramine and phenylalanine is illustrated within the box and whisker diagrams in Figure 4-20 . The concentrations of these metabolites remain fairly constant with the exception of a sharp increase at 0.2 $\mu\text{g}/\text{mL}$. This increase can be correlated to the step prior to the maximum concentration of tyrosine being recorded within the internal metabolome. This could suggest the pathways are triggered in response to the increasing cellular content of tyrosine. Interestingly the internal composition of

phenylalanine follows a trend greatly similar to that of tyrosine. This infers that the internal and external metabolome is acting independently in this region of the metabolite map.

A collection of amino acids are found on the right hand side of the metabolite map including the linked metabolites serine, glycine and threonine which originally branch from pyruvate and leucine, isoleucine and valine which metabolise *via* 2-oxobutanoate. These metabolites with the exception of isoleucine exhibit a parabolic trend upon exposure to increasing concentrations of dithranol. The parabolic trend associated with these amino acids indicates a concentration maximum of 0.3 µg/ mL in the case of serine, threonine, leucine and valine; and a concentration maximum of 0.2 µg/ mL for glycine. Isoleucine shows a negative correlation to increasing dithranol concentration. These results provide evidence that dithranol is altering the foundations of growth metabolism (in terms of precursors for protein production) which successfully implies that dithranol is inhibiting growth. The parabolic trend is somewhat difficult to explain. It is possible that at mid concentrations of exposure the cells are able to retrieve supplies of these amino acids from the growth media in a recovery type mechanism to replenish diminishing energy supplies. The variation in response exhibited by isoleucine is unexplained and could incorporate a number of factors.

4.3.6 Methotrexate and Ciclosporin Interpretation

The results gained from the metabolomic analysis of methotrexate and ciclosporin treated HaCaT cells are considerably less noteworthy than those found from the analysis of dithranol treatment. The most accountable reason for this can be attributed to the variety and mode of action of the drugs. These two drugs are immunosuppressant's which are administered systemically to patients and hence in hindsight it seems unlikely that we would observe a notable change in metabolites which are detectable using GC-MS analysis over a 24h period. The observed cellular growth rate and cell viability was deemed unaffected during drug exposure and the final cellular biomass recorded did not differ from the dithranol samples.

The target of these drugs is unlikely to be directly upon the keratinocyte cells but on immune cells associated with the disease. This would give reason for the large variation in the success of this experiment.

However in spite of this, we do have a limited number of metabolite features that have been highlighted as being significantly affected by treatment and have been successfully identified. The box and whisker plots have been individually assessed but in large the results were deemed unworthy of individual discussion. The box and whisker plots generated are available within Appendix A-D.

4.4 Conclusion and Further work

The use of a metabolomics approach for the investigation of the mode of action of anti-psoriatic drugs has been deemed successful. The application of GC-MS analysis has provided information regarding the response of key metabolites located within the central metabolism of HaCaT cells. The results generated for dithranol treated cells were of much greater significance and magnitude than those received for methotrexate and ciclosporin treated cells. This was attributed to the mode of action of the drugs; in that methotrexate and ciclosporin are immuno-regulators and hence observing an effect on metabolites would seem unlikely. Moreover, these are administered either orally or intravenously.

Dithranol is usually administered as a topical agent and is applied directly to the skin of a patient. In this capability we might expect to observe a direct response within HaCaT cells, and this was indeed the case. A vast number of metabolites were deemed to be significantly affected by dithranol treatment compared to controls when ANOVA analysis was conducted. Correlation analysis of these significant metabolites classified these metabolites into three distinct groups and upon production of representative box and whisker plots it was possible to observe the individual trends of metabolites as the concentration of treatment increased.

These box and whisker plots were overlaid onto a metabolite map of central metabolism and could be used to investigate the response of metabolism.

The approach supplies a list of metabolites which could potentially be used as indicators of successful treatment. Dithranol is known to accumulate in the mitochondria of cells and hence an effect on the concentration of glycolysis and TCA intermediates is expected. The concentration of glucose 6-phosphate, glycerol 3-phosphate, citrate and malate show a linear reduction in concentration as the concentration of dithranol increases. This response is also observed for isoleucine, nicotinamide, aspartate and glutamate. An interesting response was observed for a number of amino acids which provides evidence that dithranol is altering the foundations of growth metabolism and hence implies that dithranol is inhibiting internal growth mechanisms, despite the fact that growth rate was not altered.

Armed with the above knowledge a more targeted metabolite profiling approach could be adopted to investigate dithranol treatment. This would attempt to detect and quantify more accurately a larger number of glycolysis and TCA metabolites and hence expand and validate the results displayed in the metabolite map.

In addition to the changes in metabolome detailed above, this work has established a successful sampling protocol for the analysis of adherent mammalian cells by GC-MS. It is envisaged that this method is transferable and reproducible for the analysis of varying cell lines and conditions and other group members have adopted this strategy.

Chapter 5: A proteomic-based approach to investigate the response of HaCaT cells upon exposure to three well established anti-psoriatic drugs.

5.1 Introduction

In a complementary approach to the work depicted in Chapter 4: the cellular response of HaCaT cells to treatment by dithranol, methotrexate and ciclosporin exposure leading to differences in the proteome was investigated. As previously stated there is limited understanding regarding the precise mechanism of action of these anti-psoriatic drugs and therefore vital information may be gained through proteomic profiling, and combining this knowledge with metabolomics. The initial stages of this work incorporated the use of 2D gel electrophoresis; however, due to problems with gel reproducibility LC-MS was ultimately used for the generation of results.

5.2 Materials and Methods

5.2.1 Materials

Drug compounds and reagents were all purchased from Sigma Aldrich, Gillingham, UK unless otherwise stated.

5.2.2 Methods

5.2.2.1 Cell Culture and Drug Exposure

The HaCaT cell culture protocol and method of drug exposure was conducted as detailed in section 4.2.2.1 & 4.2.2.2.

5.2.2.2 Sample Collection

In a similar approach to metabolomic sample preparation, culture media was removed and the cellular monolayer was washed with three applications of PBS (15 mL, room temperature). To minimise the potential loss of any protein, extraction buffer (5 mL, 50 mM Tris-HCl pH 7.5, 750 mM NaCl, 4mM MgCl₂ and 5mM DTT, room temperature) was added directly to each flask and cells harvested by cell scraping. Extraction was conducted via 4 cycles of sonification (15 min) followed by centrifugation (5°C, 15 min, 16200g). The supernatant was collected and stored at -80°C until further use.

5.2.2.3 Sample Clean Up

A sample clean up protocol was conducted employing the use of a ReadyPrep™ 2-D Cleanup Kit (Bio-Rad Laboratories, Inc. Hercules, CA, USA). The procedure works by quantitatively precipitating and concentrating proteins in a sample while leaving behind and subsequently washing away substances including salts, nucleic acids and lipids. The inclusion of this step helps to eliminate streaking and improve spot detection for 2D gel electrophoresis and can help to minimise adduct formation in LC-MS analysis.

In short; 100 µL of sample was transferred to a clean low bind microcentrifuge tube (Eppendorf®). 300 µL of precipitating agent 1 was added, mixed well by vortexing and incubated on ice for 15 min. Precipitating agent 2 (300 µL) was then added to the mixture, vortexed and centrifuged at 16200g for 5 min. The supernatant was removed and a series of wash steps performed. Firstly 40 µL of wash reagent 1 was added to the pellet, centrifuged at 13000 rpm for 5 min and the wash removed. To the protein pellet, 25 µL of HPLC grade water was added and vortexed to ensure thorough mixing. Finally 1 mL of wash reagent 2 (with added additive) was added, vortexed briefly and incubated at -20°C for 30 min. After the incubation period the sample was centrifuged at 13000 rpm for 5 min and the

consequent supernatant removed. The pellet was re-suspended in 1mL of rehydration buffer (8M Urea / 0.5% CHAPS / 10mM DTT / 0.2% biolyte ampholytes).

5.2.2.4 Protein Quantification

It was necessary to quantify the amount of protein present within the cellular extracts of treated cells to ensure that no bias was introduced due to biomass. A RC-DC protein assay (Bio-Rad Laboratories, Inc. Hercules, CA, USA) was employed for protein quantification. The standard protocol was as follows. In brief, 5 μ L of DC reagent S was added to each 250 μ L of DC reagent A which would be needed for each run; i.e., for 18 samples corresponding to 1 drug exposure 65 μ L of DC reagent S was added to 3250 μ L of DC reagent A. This solution was referred to as reagent A'.

A number of protein standards were prepared through serial dilution of serum albumin stock of concentration 1.42 mg/ mL. Protein standards were 0.355, 0.710, 0.852, 1.065 and 1.42 mg/ mL diluted with rehydration buffer as above. 25 μ L of samples and standards were transferred into clean, dry microcentrifuge tubes and 125 μ L of RC reagent 1 was added, vortexed and incubated for 1 min at room temperature. 125 μ L of RC reagent 2 was subsequently added, vortexed thoroughly and centrifuged (16200g for 5 min). The supernatant was completely removed and 127 μ L of reagent A' added and vortex mixed. The sample was incubated at room temperature for 5 min to dissolve and remaining precipitate. Finally 1 mL of DC reagent B was added, vortex mixed and incubated at room temperature for 15 min. The absorbance maxima at 750 nm were recorded for all samples and the resultant protein concentration extrapolated.

5.2.2.5 1D Gel Electrophoresis

5.2.2.5.1 Separating Buffer

A separating buffer was prepared by dissolving Tris Buffer (18.2 g) and SDS (0.4 g) into ddH₂O (80 mL). The pH was adjusted to pH 8.8 by addition of HCl (5M). The volume was increased to 100 mL by addition of ddH₂O. Separating buffer can be stored for up to 1 month; however the pH should be checked.

5.2.2.5.2 Separating Gel

A 12% separating gel was composed of 40% Acrylamide (10 mL), separating buffer (8.34 mL), ddH₂O (14.82 mL), 10% ammonium persulphate (AMPS, 167 µL) and tetramethylethylenediamine (TEMED, 17 µL).

5.2.2.5.3 Stacking Gel

A 4% stacking buffer was composed of 40% Acrylamide (2.5 mL), separating buffer (6.25 mL), ddH₂O (16.1 mL), 10% AMPS (125 µL) and TEMED (25 µL).

5.2.2.5.4 Pouring of Gel

Separating gel mixture was poured into the gel cassette until approximately two thirds of the way to the top. A layer of butanol (50%) was added to ensure a straight edge was achieved. The butanol was removed once the gel had set and the stacking gel mixture added. A comb insert was added to form wells within the gel to allow application of sample. Once the gel was set the comb was removed and the gel was ready for sample addition.

5.2.2.5.5 Sample Cracking

Cracking buffer was composed of Tris buffer (0.5M, 3.75 mL), SDS (0.6 g), glycerol (3.0 g), DTT (0.154 g) and bromophenol blue (1%, 1 mL); made up to 10 mL at pH 6.6.

30 μ L of each sample was added to 30 μ L of cracking buffer, vortexed and heated at 98°C for 5 min. 20 μ L of cracked sample was added to each well.

5.2.2.5.6 Running Buffer

Glycine (14.4 g), Tris buffer (3 g) and SDS (1 g) were dissolved in 800 mL of ddH₂O to form a running buffer solution.

5.2.2.5.7 Gel Running

The sample laden gel cassettes were placed into a running chamber and sufficient running buffer added to cover the gels. Electrodes were connected and a current of 35 mA was applied. This process was conducted until the blue colouration from the bromophenol blue was seen to be ~ 1 cm away from the end of the gel.

5.2.2.6 2D Gel Electrophoresis

5.2.2.6.1 Rehydration of Immobilised pH Gradient (IPG) Strip and isoelectric focussing.

Rehydration and isoelectric focussing was conducted using a PROTEAN IEF cell (Bio-Rad Laboratories, Inc. Hercules, CA, USA). An isoelectric focussing tray was used to actively rehydrate the IPG strip (pH 7-12) when the sample was maintained within rehydration buffer. 600 μ L of rehydration buffer containing sample was added to each channel within the focussing tray. The IPG strip was removed from its plastic cover and placed gel side down into the tray channels. To ensure complete coverage the strip was gently lowered into the sample solution and slid from side to side making certain that no air bubbles were introduced. The strip was aligned with the acidic (+) end at the anode and the basic (-) end at the cathode. An aliquot of mineral oil was applied to each channel containing an IPG strip, ensuring that the strip was completely covered and the chamber was approximately half full.

The lid was reapplied to the isoelectric tray and the tray placed on the peltier platform aligned with the electrode. The initial rehydration with the sample was conducted at 50 V, 20°C for 12 h.

Once rehydrated, wicks were placed between the IPG strip and the electrode to provide protection from the high voltage to be applied. Addition mineral oil was overlayed to completely cover the strips. The IEF cell was programmed and the isoelectric focussing process started. The programme incorporated a conditioning step; 250 V, 20°C for 15 min followed by a voltage ramp. The voltage ramp began at 250 V and ended at 4000 V over a period of 2h at 20°C. The final focussing step was conducted at 4000 V, 20°C for 5h. The sample is now separated in the 1st dimension according to pH.

IPG strips were stored at ~5°C for a maximum of 1 month prior to use.

5.2.2.6.2 Equilibration Buffer I

Prior to using the IPG strips it is necessary for them to be equilibrated in SDS based buffer. Equilibration buffer I was prepared with urea (6M, 3.6 g), SDS (0.2 g), Tris HCl (0.375M, 2.5 mL, pH 8.8), glycerol (2 mL) and DTT (0.02 g) made up to 10 mL with ddH₂O. Equilibration buffer (2 mL) was added to the IPG strips, shaken, left for 10 min and removed.

5.2.2.6.3 Equilibration Buffer II

Equilibration II was prepared with urea (6M, 3.6 g), SDS (0.2 g), Tris-HCl (0.375M, 2.5 mL, pH 8.8), glycerol (2 mL) and iodoacetamide (0.481 g) made up into 10 mL with ddH₂O. Equilibration buffer (2 mL) was added to the IPG strip, shaken, left for 10 min and removed.

5.2.2.6.4 Gel Preparation and Running Procedure

The preparation of gel solutions for 2D analysis is highly similar to the details listed above for the production of a 1D gel, however; for 2D gels the use of a stacking gel is not required. In short a 12% separating gel was produced in larger quantities to that shown in Sections 5.2.2.5.1 & 5.2.2.5.2. The running buffer was as detailed in Section 5.2.2.5.6.

The gel solution was poured into the gel cassette until approximately 1 cm from the top. Butanol (50%) was applied to ensure a straight gel edge was achieved. Once the gel was set the butanol was removed and the IPG strip mounted on top of the gel. It was imperative that the strip was placed in a straight manner and in direct contact with the gel. The strip was overlaid and set in place with 1% lowmelt agarose containing bromophenol blue.

The gel cassette was placed within the running chamber and sufficient running buffer added. The electrodes were attached and a constant current of 35 mA was applied. The procedure was stopped when the bromophenol blue was ~ 1 cm from the bottom edge of the gel.

5.2.2.7 Coomassie Stain

All gels were stained using colloidal Coomassie staining. Dye stock solution was prepared by adding phosphoric acid (13.52 mL) and ammonium sulphate (100 g) to ddH₂O (800 mL) with thorough mixing. While stirring Coomassie dye (1 g) was added and the solution made up to 1 L. The stock solution was left for at least 24 h before use. Dye working solution was prepared by adding dye stock solution (80%) to methanol (20%) while stirring. The dye working solution was always prepared directly before use.

5.2.2.8 Staining Procedure

All steps were performed on a shaking table at room temperature ensuring that the gel was completely covered at each stage. The first stage of the procedure is the fixing of the gel. A fixing solution of ethanol (40%), acetic acid (10%) and ddH₂O (50%) was prepared and

applied to the gel for a minimum of 60 min. The gel was washed with water twice for a period of 10 min then the Coomassie stain was applied. The stain was left for a minimum of 24 h. Finally the gel was washed with acetic acid (1%) until all Coomassie particles were removed.

5.2.2.9 Visualisation of Gels

The gels were imaged using a Syngene Gene Genius bio imaging system (Syngene, Cambridge, UK).

5.2.2.10 LC-MS

5.2.2.10.1 Sample Preparation

Stock solutions of ammonium bicarbonate (Ambic/50 mM), Dithiothreitol (DTT/20 mM) and Iodoacetamide (10 mM) were prepared immediately before the sampling protocol was begun. 10 μ L of extract (from 5.2.2.3) was added to 10 μ L DTT (20 mM) and incubated at 56°C for 1 h. Upon cooling 20 μ L of iodoacetamide was added and the sample was incubated at room temperature for 30 min in the dark. An ampoule of lyophilised trypsin (20 μ g) was reconstituted with buffer (20 μ L) and Ambic (180 μ L) and 10 μ L aliquots added to each sample. Multiple ampoules of trypsin were used as required. The tryptic digest was left overnight at 37°C.

5.2.2.10.2 Nano-LC-MS/MS

The digested samples were diluted 1/50 in 95% water/5% acetonitrile (MeCN)/0.1% formic and resolved by LC-MS using a nanoACQUITY chromatograph (Waters MS technologies, Manchester, UK), coupled to an LTQ Orbitrap XL (ThermoFisher Scientific, Bremen, Germany), equipped with the manufacturer's nanospray source fitted with a PicoTip Emitter (New Objective, MA, USA).

The sample temperature was maintained at 10°C, and 4 µL of sample was injected onto a trapping column (Waters C18 180 µm X 20 mm), using the partial loop mode of injection, at a flow rate of 18 µL/ min 95% A1/5% B1 (where A1 is 100% water/0.1% formic, and B1 corresponds to 100% MeCN/0.1%FA), prior to valve switching to the analytical column. The analytical column (nanoACQUITY UPLC™ BEH C18 75 µm x 150 mm 1.7 µm column) was maintained at a temperature of 35°C, and at a constant flow rate of 300 nL/ min. The gradient conditions were as follows: 0.33 min - 95% A1/5% B1, 30 min - 50% B1, 31 min - 85% B1, 50 min, 95% A1/5% B1 (equilibration).

5.2.2.10.3 Mass Spectrometry

Full scan MS spectra (m/z 300-1600) were acquired in an LTQ-Orbitrap XL with the Orbitrap operating at a resolution of 30,000 (defined at m/z 400) in data-dependent mode. The top five most intense ions from the MS1 scan were selected for tandem MS by collision induced dissociation (CID) in the LTQ, at a normalized collision energy of 30%, and an activation q of 0.25. Dynamic exclusion was applied for duration of 30 s, with a repeat count of two and an exclude duration width of 40 s, and all product ion spectra were acquired in the LTQ.

5.2.2.10.4 Data analysis

Data was searched with Sequest (version 28, rev. 12; Thermo Fisher Scientific Inc.) against human-specific version of the nrdb database. The digest enzyme was set to trypsin, fixed modification of carbamidomethylation of cysteine and variable modification of methioinine oxidisation were selected, and with peptide tolerance and fragment tolerance set to 2.0 Da and 1.0 Da respectively. Utilising these criteria provided a list of proteins present within each sample.

5.3 Results & Discussion

5.3.1 Protein Quantification

As detailed in Section 5.2.2.4 protein quantification was performed on all samples prior to analysis *via* gel electrophoresis or LC-MS.

The amount of protein was determined for all dithranol exposed cells used in this work. The results shown below correspond to the samples analysed by LC-MS but are highly similar to other quantification results. A standard curve was produced of known protein concentration vs. UV absorbance. Through the determination of the equation of the line as shown in Figure 5.1 it is possible to estimate the concentration of protein within the samples to be analysed (Table 5-1).

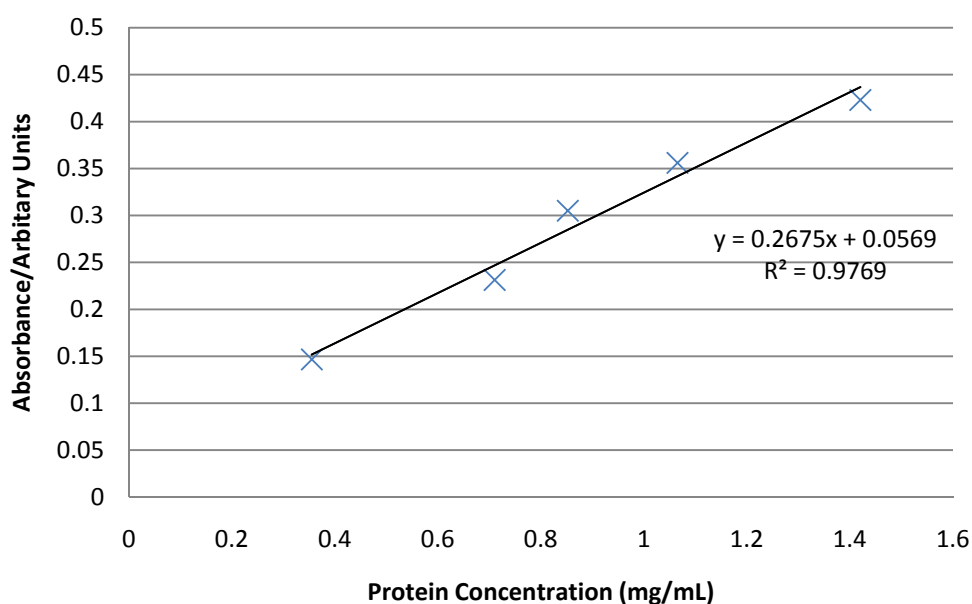


Figure 5-1: Protein quantification standard curve for dithranol treated HaCaT cells.

Three UV measurements were conducted per sample and the average UV absorbance is shown in column two. Protein content was calculated for each replicate and the average protein content was elucidated. The average protein content results clearly show that dithranol is directly affecting the cellular protein content as a reduction is observed as the concentration of dithranol increases.

Sample Name	Average Absorbance	Protein Content (mg/mL)	Average Protein Content (mg/mL)
c1	0.267	0.785	0.766
c2	0.275	0.815	
c3	0.244	0.698	
0.1_1	0.181	0.465	0.573
0.1_2	0.219	0.607	
0.1_3	0.230	0.646	
0.2_1	0.220	0.610	0.575
0.2_2	0.199	0.531	
0.2_3	0.213	0.584	
0.3_1	0.244	0.699	0.489
0.3_2	0.158	0.377	
0.3_3	0.162	0.392	
0.4_1	0.165	0.405	0.313
0.4_2	0.126	0.257	
0.4_3	0.131	0.277	
0.5_1	0.094	0.137	0.074
0.5_2	0.067	0.037	
0.5_3	0.070	0.048	

Table 5-1: A table to illustrate the protein content of HaCaT cells exposed to dithranol. The sample name prefix corresponds to the concentration of dithranol ($\mu\text{g/mL}$) or control (c). The sample name suffix corresponds to the replicate number.

The amount of protein was also determined for all methotrexate and ciclosporin exposed cells, again the results shown correspond to the samples which were used for LC-MS analysis but they are indicative of all samples which were quantified. The results of protein quantification are illustrated in Table 5-2 and Table 5-3. The estimated protein quantification for methotrexate shows minimal change over the increasing concentration

range of drug exposure. This could imply that the drug is failing to penetrate the cell membrane and hence little effect is recorded or that methotrexate alters the protein content instead of diminishing it. Finally the amount of estimated protein recorded for HaCaT cells exposed to ciclosporin showed a similar trend to that of methotrexate. The lowest concentrations of ciclosporin exhibit minimal alteration of protein quantification in comparison to the control sample; however at concentrations of $1.5 \times 10^{-7} \text{M}$ upwards there is a small reduction in protein content however this could be minimal in significance.

Sample Name	Average Absorbance	Protein Content (mg/mL)	Average Protein Content (mg/mL)
c1	0.239	0.759	0.809
c2	0.25	0.798	
c3	0.27	0.869	
1_1	0.258	0.827	0.801
1_2	0.229	0.724	
1_3	0.265	0.852	
2_1	0.273	0.880	0.865
2_2	0.267	0.859	
2_3	0.266	0.855	
3_1	0.301	0.979	0.826
3_2	0.169	0.511	
3_3	0.303	0.986	
4_1	0.271	0.873	0.612
4_2	0.089	0.228	
4_3	0.232	0.735	
5_1	0.272	0.876	0.893
5_2	0.252	0.805	
5_3	0.306	0.997	

Table 5-2: A table to illustrate the protein content of HaCaT cells exposed to methotrexate. The sample name prefix corresponds to the concentration of methotrexate ($\times 10^{-7} \text{M}$) or control (c). The sample name suffix corresponds to the replicate number.

Sample Name	Average Absorbance	Protein Content (mg/mL)	Average Protein Content (mg/mL)
c1	0.286	0.875	0.770
c2	0.252	0.738	
c3	0.242	0.697	
0.5_1	0.248	0.721	0.701
0.5_2	0.232	0.657	
0.5_3	0.249	0.726	
1_1	0.284	0.867	0.797
1_2	0.242	0.697	
1_3	0.274	0.826	
1.5_1	0.219	0.605	0.683
1.5_2	0.271	0.814	
1.5_3	0.225	0.629	
2_1	0.246	0.713	0.668
2_2	0.23	0.649	
2_3	0.228	0.641	
2.5_1	0.214	0.584	0.648
2.5_2	0.226	0.633	
2.5_3	0.249	0.726	

Table 5-3: A table to illustrate the protein content of HaCaT cells exposed to ciclosporin. The sample name prefix corresponds to the concentration of ciclosporin ($\times 10^{-7}$ M) or control (c). The sample name suffix corresponds to the replicate number.

5.3.2 Gel Electrophoresis

The gel electrophoresis results were variable in their success. The major drawback associated with the gel approach was the apparent lack of correlation between protein quantification and density of proteins present on the gel. A 1D gel approach was employed to check that protein was present in the sample; Figure 5-2 is an example of a 1D gel produced. This figure illustrates that sufficient protein appears to be present and that a wide range of protein mass is incorporated.

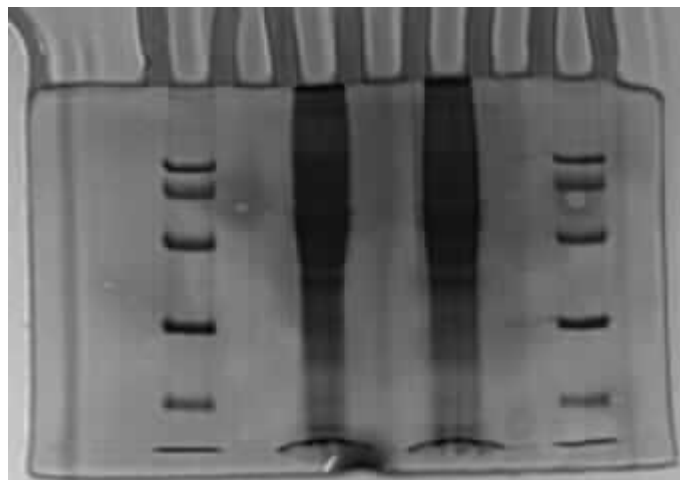


Figure 5-2: An example result for 1D gel electrophoresis analysis of the proteome of control HaCaT cells.

1D gels can not readily be used for protein quantification and identification so 2D gel electrophoresis was undertaken; example images illustrating the 2D gel results are shown in Figure 5.5.

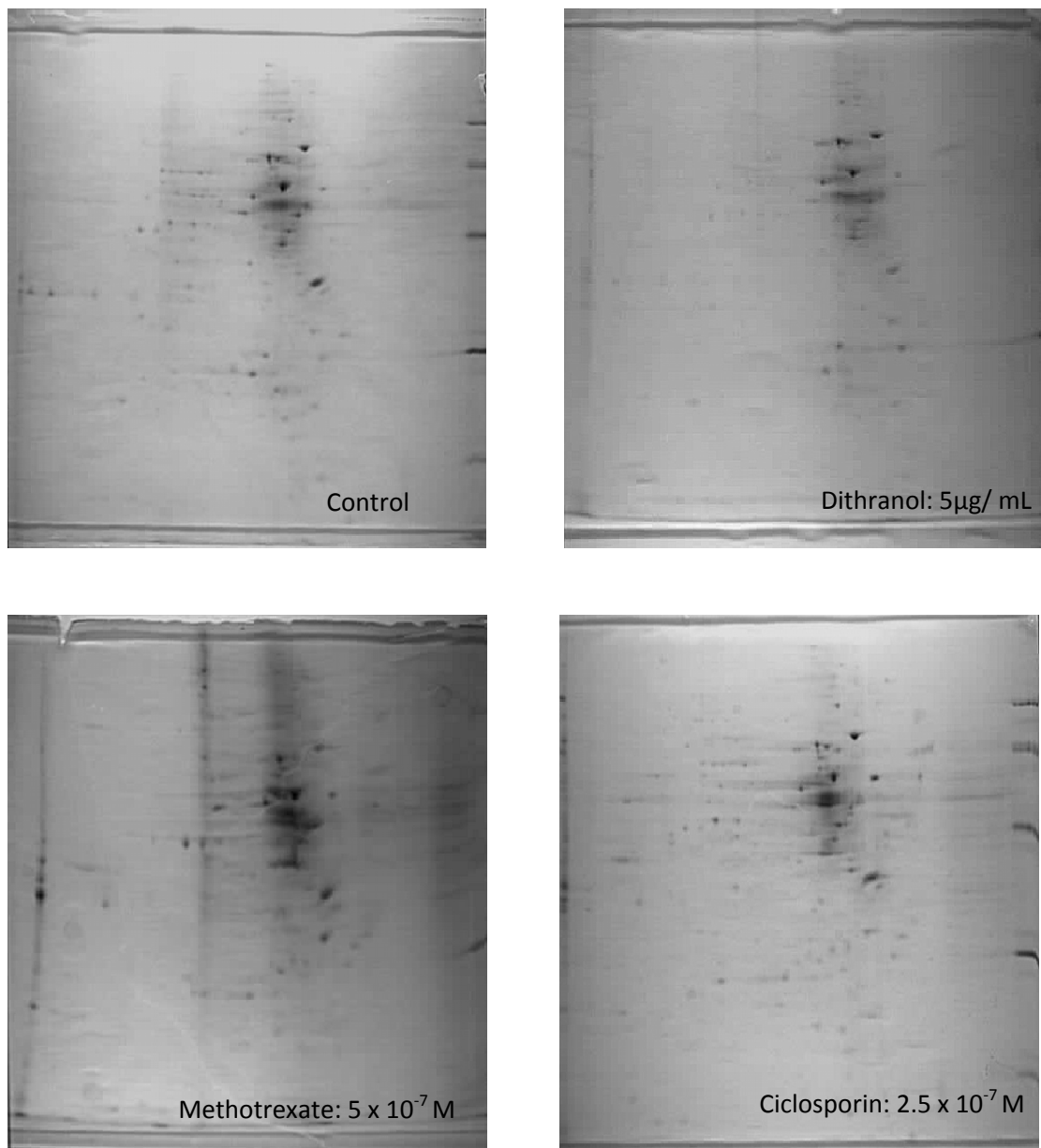


Figure 5-3: 2D gel electrophoresis results illustrating the protein presence and localisation within a control, dithranol treated, methotrexate treated and a ciclosporin treated sample.

Whilst these images indicate that a degree of protein separation was achieved, the quantity of protein present is minimal. Moreover, in a comparative sense it is possible to see some variation between the localisation of proteins within the gels, and this would make protein identification problematic. Although the amount of protein analysed was equivalent, the gel produced from the HaCaT cells treated with dithranol shows a marked decrease in protein spots when compared to the control gel. Even taking in to consideration the protein normalisation prior to analysis, this result correlates well with the protein quantification

results previously discussed. In contrast the gels gained from the analysis of methotrexate and ciclosporin treated cells are highly similar to that of the control. This again corresponds well with the total protein quantification results.

Despite these general trends, the qualities of these gels (and the many others run) were deemed of insufficient quality to be used for protein identification and quantification purposes. The combination of this problem and the time taken in the production of gels meant that it was decided that an alternative approach was necessary. It was at this stage that the use of LC-MS based analysis was incorporated.

5.3.3 LC-MS Results

The results from LC-MS analysis were obtained in Excel format upon being exported from Sequest. An Excel file was retrieved for each individual sample: 18 individual Excel files per drug corresponding to the 6 drug concentrations and the 3 replicate samples taken. The Excel array included information regarding the individual peptides generated and the subsequent matched protein identification name. As the results gained were qualitative (protein detected or not) rather than quantitative, only the protein name was extracted from the Excel file and used in further discussion. The protein ID list was alphabetised for each sample and the three replicate data from each sample was manually mined to match the presence or absence of the particular protein within these replicates. A selection criteria was defined that required a protein to be present within at least two out of three replicates, however a greater degree of confidence was associated with those proteins which were successfully detected within all three replicates. This process was repeated for each concentration of drug exposure; in that protein identifications were matched and the presence or absence of these proteins at each concentration was noted. This process generated a matrix of protein name vs. drug concentration colour coded to indicate the

presence of the protein in all three replicates (green), two replicate (blue) or less than two (red) and thus creating a scoring system.

Using this approach it was possible to begin to understand the effect imposed by the drugs as it was possible to assign whether proteins were up-regulated, down regulated, equivalent throughout the concentration range or exhibit a non-correlated response and hence were deemed non significant. It is at this stage that it is possible to begin to probe the proteome response of HaCaT cells to anti-psoriatic treatment.

5.3.3.1 Dithranol

A total of 162 proteins were identified in the dithranol treated samples of which 18% were deemed to be down-regulated and 4% up-regulated. A total of 40% were shown to be equivalent in that they were present at all concentrations of the drug and in the control. In addition 38% of proteins were classified as not significant as their presence was highly variable over the concentration range, and did not correlate with drug level.

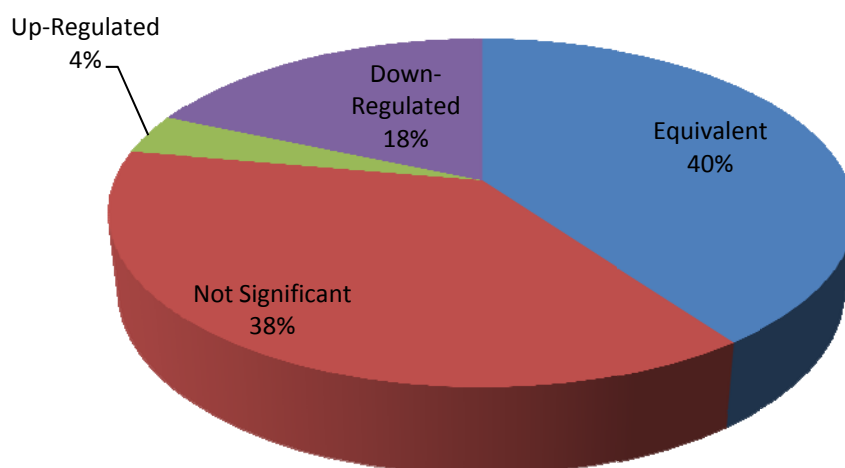


Figure 5-4: Schematic representation indicating the proportion of proteins which were up-regulated, down-regulated, deemed equivalent or non significant within the proteome of dithranol treated HaCaT cells.

The proteins which were successfully identified within the internal proteome of dithranol treated HaCaT cells vary greatly in their cellular role and function, and can be classified into an array of groups.

Firstly there are a number of identified proteins which can be assigned as enzymes located within central metabolism pathways and in particular glycolysis. These proteins are summarised in Table 5-4.

Protein Name	EC Number	C	0.1	0.2	0.3	0.4	0.5	Metabolism Location
argininosuccinate synthetase 1	6.3.4.5	Green	Red	Red	Red	Red	Red	Urea Cycle
cytosolic malate dehydrogenase	1.1.1.37	Green	Green	Green	Green	Red	Green	TCA
enolase 1	4.2.1.11	Green	Green	Green	Green	Green	Green	Glycolysis
enolase 2	4.2.1.11	Green	Green	Green	Blue	Red	Red	Glycolysis
enolase 3	4.2.1.11	Green	Green	Green	Green	Green	Red	Glycolysis
fructose-bisphosphate aldolase C	4.1.2.13	Red	Red	Red	Blue	Red	Red	Glycolysis
glucose-6-phosphate isomerase	5.3.1.9	Green	Green	Green	Green	Blue	Green	Glycolysis
glutathione transferase	2.5.1.18	Green	Green	Green	Green	Blue	Blue	Gluthionine Metabolism
glyceraldehyde-3-phosphate dehydrogenase	1.2.1.12	Green	Green	Green	Green	Green	Green	Glycolysis
isocitrate dehydrogenase 1 (NADP+), soluble	1.1.1.42	Green	Green	Green	Green	Green	Blue	TCA
lactate dehydrogenase A	1.1.1.27	Green	Green	Green	Green	Blue	Red	Glycolysis
lactate dehydrogenase B	1.1.1.27	Blue	Blue	Green	Green	Red	Blue	Glycolysis
lactate dehydrogenase C	1.1.1.27	Blue	Green	Green	Green	Red	Green	Glycolysis
phosphogluconate dehydrogenase	1.1.1.44	Red	Blue	Red	Red	Red	Red	Pentose Phosphate Pathway
phosphoglycerate kinase 1	2.7.2.3	Green	Green	Green	Green	Green	Green	Glycolysis
phosphoglycerate kinase 2	2.7.2.3	Green	Blue	Blue	Red	Red	Red	Glycolysis
pyruvate kinase, liver and RBC isoform 1	2.7.1.40	Green	Green	Green	Green	Green	Green	Glycolysis
transaldolase 1	2.2.1.2	Blue	Blue	Red	Red	Red	Red	Pentose Phosphate Pathway
transketolase	2.2.1.1	Green	Blue	Green	Green	Green	Green	Pentose Phosphate Pathway
triosephosphate isomerase 1	5.3.1.1	Green	Green	Green	Green	Green	Green	Glycolysis

Table 5-4: Summary table illustrating the proteins identified within the proteome of dithranol treated HaCaT cells. The protein name, associated EC number and the metabolism location is provided. The colour scheme dictates the presence or omission of a protein at the given drug treatment concentration. Green implies that the protein was present within all three replicate samples, blue indicates that the protein was detected within two replicates and red indicates that the protein was not detected.

It is possible in a similar manner to the analysis of the metabolome data discussed in Chapter 4: to reconstruct a metabolite map combining the enzyme information provided within Table 5-4. This metabolite map is shown in Figure 5-5.

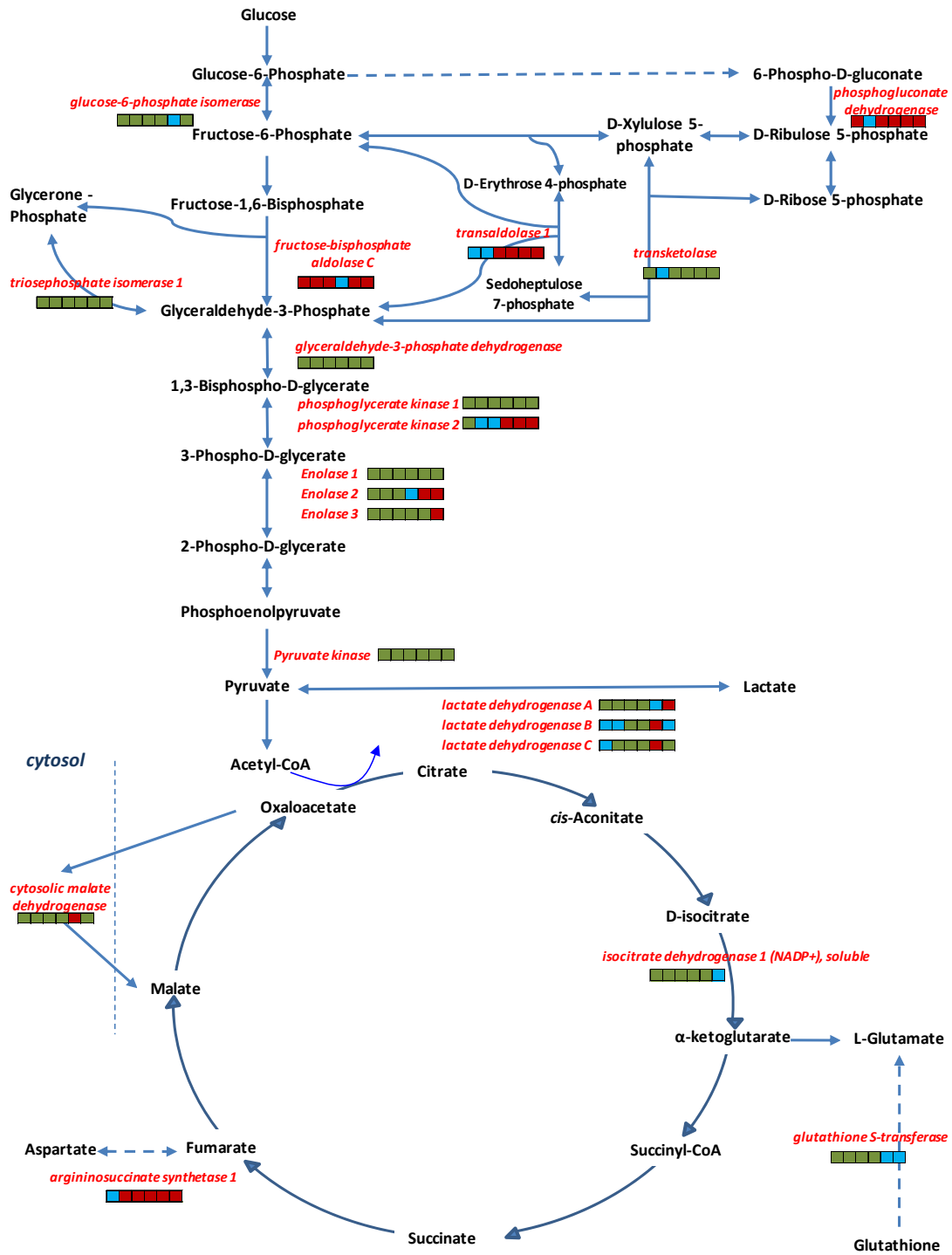


Figure 5-5: Reconstructed metabolite map depicting the proteins (*red italics*) successfully identified within dithranol treated HaCaT cells and the corresponding linked metabolites (black normal font). Adjacent metabolites are linked with block lines while pathways with some metabolites omitted are linked with dashed lines. The presence of proteins over the concentration range is summarised within the box diagrams whereby green implies that the protein was present within all three replicate samples, blue indicates that the protein was detected within two replicates and red indicates that the protein was not detected. The control sample is the left hand box and the highest concentration the right hand box.

The metabolite map illustrates that a number of proteins located within central metabolism are affected by dithranol treatment. The effect observed for phosphoglycerate kinase 2 and enolase 2 & 3 is of particular interest. These enzymes are down-regulated at the highest concentrations of dithranol treatment and hence will lead to impaired glycolytic function. This result could help to explain the decreasing presence of pyruvate at 0.4 & 0.5 $\mu\text{g}/\text{mL}$ illustrated within the metabolite map shown in Figure 4-20. The response observed for lactate dehydrogenase is also of interest; lactate dehydrogenase A is down-regulated at 0.4 & 0.5 $\mu\text{g}/\text{mL}$ dithranol treatment, lactate dehydrogenase B & C are initially of variable presence within the three replicate samples, then become stable at mid-range concentrations and become down-regulated at 0.4 $\mu\text{g}/\text{mL}$. This is a variable response over the concentration range of dithranol treatment and was also observed in the level of lactate from metabolite measures (Figure 4-20). The inclusion of the pentose phosphate enzymes is an interesting feature as this pathway has been flagged as a possible route of metabolism from the analysis of the metabolome data in Chapter 4. The number of enzymes detected within this cycle is limited however; the down-regulation of transaldolase 1 is noteworthy.

Aside from the above proteins associated with central metabolism, there is a large array of additional proteins that were identified within the dithranol treated HaCaT cells, and these are summarised in Appendix E. A number of proteins were observed as being down-regulated upon exposure to dithranol treatment and could be placed into context with what is known in the literature about these anti-psoriasis drugs. These proteins are summarised in Table 5-5.

Protein Name	C	0.1	0.2	0.3	0.4	0.5
acidic (leucine-rich) nuclear phosphoprotein 32 family, member A	Red	Red	Red	Red	Red	Blue
acidic (leucine-rich) nuclear phosphoprotein 32 family, member B	Red	Red	Red	Blue	Green	Blue
albumin precursor	Red	Red	Blue	Blue	Blue	Blue
annexin 5	Blue	Blue	Green	Red	Red	Red
annexin 4	Green	Green	Green	Blue	Red	Red
calmodulin 2	Blue	Blue	Green	Red	Red	Red
gelsolin-like capping protein	Blue	Green	Green	Red	Red	Red
S100 calcium binding protein A11	Green	Green	Green	Green	Green	Blue
S100 calcium binding protein A14	Green	Green	Green	Green	Green	Red
tubulin, alpha, ubiquitous	Green	Green	Green	Green	Red	Red
tubulin, beta polypeptide	Green	Green	Green	Green	Blue	Red
tubulin, beta, 2	Green	Green	Green	Blue	Blue	Red

Table 5-5: Summary table illustrating additional identified proteins within the proteome of dithranol treated HaCaT cells. The colour scheme dictates the presence or omission of a protein at the given drug treatment concentration. Green implies that the protein was present within all three replicate samples, blue indicates that the protein was detected within two replicates and red indicates that the protein was not detected.

The members of the S100 protein family, A11 and A14, display potential down-regulation and down-regulation at 0.5µg/ mL dithranol exposure respectively. The S100 family of proteins is the largest sub-set of proteins within the EF-hand protein superfamily. S100 proteins are small, acidic proteins of 10-12kDa and contain 2 distinct EF-hands. Similarly to most other EF-hand proteins, S100 proteins act intracellularly as Ca²⁺ -signalling or Ca²⁺ -buffering proteins. However, the most unusual characteristic of certain S100 proteins is their occurrence in the extracellular space, where they act in a cytokine-like manner (Marenholz et al., 2004). These S100 proteins have been implemented in a number of potential roles in epidermal wound repair, cancer, differentiation, and response to stress (Eckert et al., 2004). S100 proteins are calcium-responsive signalling proteins that are over-expressed in cancer and inflammatory diseases. They act by forming complexes with target proteins to modify target protein function (Ruse et al., 2003).

A number of these S100 proteins have also been implemented in psoriasis. Broome *et al.* (2003) provided a summary of the involvement of five of these S100 proteins in psoriasis. S100A7 was found to be expressed in both normal and psoriatic epidermis; however levels

were markedly increased in psoriatic epidermis. It was postulated that this increased expression could be related to the cytokine function of S100A7. The co-expression of S100A8 and S100A9 was determined to be greatly over-expressed in psoriasis. These proteins are active as a heterodimer and hence co-expression is common. In normal epidermis these proteins are expressed at minimal levels. It was suggested that S100A8 and S100A9 may have roles in promoting and/or responding to the hyper-proliferative state observed in psoriasis. The expression of S100A10 and S100A11 was not noted as different in normal or psoriatic skin however their association with annexin molecules was noted (Broome et al., 2003). Upon formation of heterodimers, S100A10 binds two copies of annexin II in a calcium independent manner to form a heterotetramer called calpactin (Nakata et al., 1990). Alternatively, S100A11 interacts with annexin I in a calcium dependant manner (Seemann et al., 1997).

The over-expression of S100A15 was also recorded in psoriasis and in particular in the epidermis of diseased skin. The observation of an up-regulation of S100A15 by calcium and pro-inflammatory cytokines in human keratinocytes suggests that both epidermal maturation and cytokine environment contribute to the elevated S100A15 levels in the diseased skin (Wolf et al., 2007). Most recently the significance of S100A4 in psoriasis has been discussed (Zibert et al., 2009); S100A4 was observed as being over-expressed in upper dermal regions of psoriatic skin. The authors suggest that S100A4 is an essential contributor to the pathogenesis of psoriasis.

Table 5-5 also highlights an up-regulation in three proteins: acidic (leucine-rich) nuclear phosphoprotein 32 family, member A; acidic (leucine-rich) nuclear phosphoprotein 32 family, member B; and albumin precursor. However, minimal information is available regarding the association of these proteins with psoriasis.

The calcium binding protein calmodulin is observed to be down-regulated upon exposure to dithranol treatment of 0.3 µg/ mL (Table 5-5). This is highly similar to results described by Tucker et al., whereby dithranol was found to be a potent competitive inhibitor of calmodulin at clinically relevant concentrations (Tucker et al., 1986). Similarly both involved plaque and uninvolved epidermis levels of calmodulin activity were determined to be significantly greater than in normal epidermis (Tucker et al., 1984).

The microtubule cytoskeleton plays roles in determining cell shape, cell polarity, vesicle trafficking, and cell division and as a consequence microtubule reorganization during cell differentiation is believed to be essential for cell morphogenesis (Lechler and Fuchs, 2007). Upon exposure to dithranol three components of microtubules were determined to be down-regulated within the proteome of HaCaT cells and hence it would be down-regulated in successful treatment. The up-regulation of class II tubulin has been demonstrated during keratinocyte differentiation *in vivo* and *in vitro* (Lee et al., 2005) and hence we can propose in this study that it is likely that a high quantity of tubulin would be present within rapidly differentiating HaCaT cells. The presence of tubulin entities have also been co-localised with S100 proteins; it was suggested that S100A11 associates with microtubules and that microtubules mediate movement of S100A11 to the cell periphery (Broome and Eckert, 2004).

The down-regulation of annexin IV and annexin V was recorded at 0.3 and 0.2µg/mL respectively (Table 5-5). Annexins are a structurally related family of calcium binding proteins implicated in a number of intracellular processes involving the action of calcium. Annexins contain calcium-binding sites distinct from the 'E-F hand' calcium-binding domain seen in other calcium-binding proteins such as calmodulin and S-100 (Barwise and Walker, 1996). The involvement of annexin I with S100A11 and annexin II with S100A10 has previously been discussed; however, there is minimal information available within the

literature to link the involvement of annexin IV and V with psoriasis and/or dithranol treatment. In a separate recent study the expression of annexin II has been shown to be significantly increased within involved atopic dermatitis skin in comparison to normal control skin (Yamane et al., 2009). This result is highly similar to those found by Bastian et al., whereby the presence and localisation of a variety of annexins in normal and psoriatic skin was discussed. The authors found annexin I and annexin II to be significantly increased in diseased skin however the other annexins remained more or less unchanged in comparison to normal skin (Bastian et al., 1993). The authors stated that the expression of annexin I is linked to a distinct state of cell differentiation and noted a high expression of annexin I in keratinocytes of proliferating pathological conditions including psoriasis.

The down-regulation of the gelsolin-like capping protein is also noted. An association between this protein and psoriasis has previously not been established. Gelsolin-like capping proteins are cytosolic factors that have been implicated in a number of physiological functions requiring rapid actin cytoskeleton reorganization such as cell locomotion or signal transduction. Gelsolin-like capping proteins interfere with the growth of actin filaments *in vitro* by severing actin filaments and capping their barbed ends through formation of an actin-capping protein dimer in a Ca^{2+} dependent manner (Constantin et al., 1998).

Clearly there are many other proteins that are altered with respect to drug concentration, and the findings above discuss those that have been reported before as being involved in psoriasis. These discussions highlight the complex interplay occurring between calcium regulating entities which upon treatment with the anti-psoriatic treatment dithranol become down-regulated. This implies that during a psoriatic outbreak, an over-expression of calcium regulatory processes occur which are consequently minimised during successful treatment.

5.3.3.2 Methotrexate

A total of 336 proteins were identified in the methotrexate treated cell samples of which 11% were shown to be down-regulated and 5% up-regulated. A total of 41% were equivalent in that they were present at all concentrations of the drug and in the control. In addition 43% of proteins were classified as not significant.

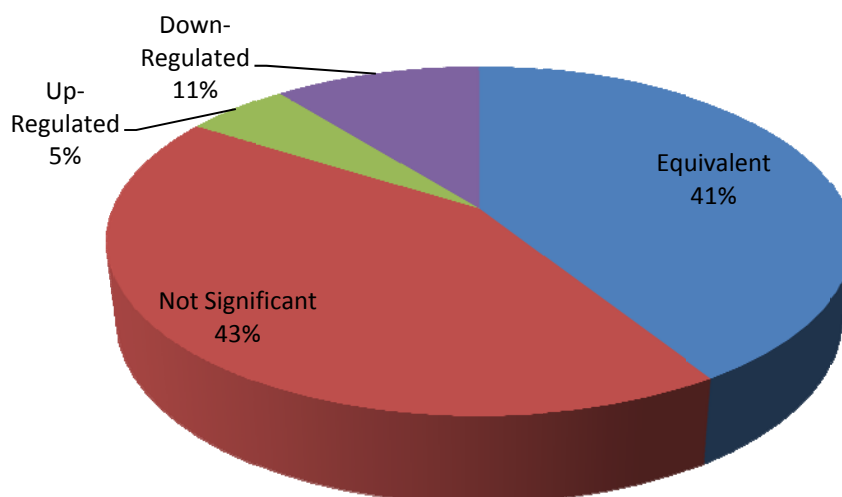


Figure 5-6: Schematic representation indicating the proportion of proteins which were up-regulated, down-regulated, deemed equivalent or not significant within the proteome of methotrexate treated HaCaT cells.

As was observed for the dithranol treated HaCaT cells the proteins identified within the proteome of methotrexate exposed cells vary greatly in their functional classes. The first subset of proteins to be discussed is those associated with central metabolism. These proteins are summarised in Table 5-6. In comparison to dithranol treated cells a greater number of proteins were identified and hence the number of associated with central metabolism also increased.

Protein Name	EC Number	C	1	2	3	4	5	Metabolism Location
argininosuccinate synthetase 1	6.3.4.5							Urea Cycle
aspartate aminotransferase 1	2.6.1.1							Alanine, Aspartate and Glutamate Metabolism
cytosolic malate dehydrogenase	1.1.1.37							TCA
enolase 1	4.2.1.11							Glycolysis
enolase 2	4.2.1.11							Glycolysis
enolase 3	4.2.1.11							Glycolysis
fructose-1,6-bisphosphatase 1	3.1.3.11							Glycolysis
fructose-bisphosphate aldolase C	4.1.2.13							Glycolysis
glucose-6-phosphate isomerase	5.3.1.9							Glycolysis
glucose-6-phosphate dehydrogenase	1.1.1.49							Pentose Phosphate Pathway
glutathione transferase	2.5.1.18							Gluthionine Metabolism
glyceraldehyde-3-phosphate dehydrogenase	1.2.1.12							Glycolysis
glycogen phosphorylase, liver	2.4.1.1							Starch and Sucrose Metabolism
glyoxalase I	4.4.1.5							Pyruvate Metabolism
isocitrate dehydrogenase 1 (NADP+), soluble	1.1.1.42							TCA
lactate dehydrogenase A	1.1.1.27							Glycolysis
lactate dehydrogenase B	1.1.1.27							Glycolysis
lactate dehydrogenase C	1.1.1.27							Glycolysis
phosphofructokinase, platelet	2.7.1.11							Glycolysis
phosphogluconate dehydrogenase	1.1.1.44							Pentose Phosphate Pathway
phosphoglycerate dehydrogenase	1.1.1.95							Glycine, Serine and Threonine Metabolism
phosphoglycerate kinase 1	2.7.2.3							Glycolysis
phosphoglycerate kinase 2	2.7.2.3							Glycolysis
sorbitol dehydrogenase	1.1.1.14							Fructose and Mannose Metabolism
transaldolase 1	2.2.1.2							Pentose Phosphate Pathway
transketolase	2.2.1.1							Pentose Phosphate Pathway
triosephosphate isomerase 1	5.3.1.1							Glycolysis

Table 5-6: Summary table illustrating the proteins identified within the proteome of methotrexate treated HaCaT cells. The protein name, associated EC number and the metabolism location is provided. The colour scheme dictates the presence or omission of a protein at the given drug treatment concentration. Green implies that the protein was present within all three replicate samples, blue indicates that the protein was detected within two replicates and red indicates that the protein was not detected.

To summarise the response of the proteins present within the central metabolism of methotrexate treated HaCaT cells a further metabolite map was constructed as shown in Figure 5-7.

Most interestingly it is observed that the central glycolysis enzymes are unaffected by methotrexate treatment in comparison to the results observed for dithranol treatment. This trend is also observed for the recorded TCA enzymes. A number of peripheral enzymes are noted within the proteome of methotrexate treated HaCaT cells including glycogen phosphorylase, sorbitol dehydrogenase, phosphoglycerate dehydrogenase, glyoxalase I and aspartate aminotransferase. These enzymes show varied responses to methotrexate treatment but in the majority of cases are down-regulated at high concentrations of treatment.

With approximate twice as many proteins being detected and identified within the methotrexate treated HaCaT proteome compared to dithranol there is consequently a far greater number of proteins that could be discussed. The complete list of these proteins is available in Appendix F. As in the previous section a small subset of these proteins were selected for discussion, in most cases these selected proteins or variants of have previously been noted as significant in psoriatic cases. This subset of proteins is summarised in Table 5-7.

Protein Name	C	1	2	3	4	5
actinin, alpha 1	Green	Blue	Blue	Blue	Red	Red
annexin A3	Blue	Red	Red	Red	Red	Red
annexin IV	Green	Blue	Green	Blue	Green	Red
chaperonin containing TCP1, subunit 2	Green	Green	Green	Blue	Green	Red
gelsolin isoform b	Blue	Blue	Green	Red	Red	Red
high mobility group AT-hook 1 isoform a	Green	Green	Green	Blue	Blue	Red
high-mobility group box1	Blue	Blue	Blue	Red	Red	Red
high-mobility group box2	Green	Blue	Blue	Red	Red	Red
ribosomal protein L5	Green	Green	Blue	Green	Blue	Red
ribosomal protein L9	Blue	Blue	Blue	Blue	Green	Red
ribosomal protein S20	Green	Blue	Green	Green	Blue	Red
ribosomal protein S4, X-linked X isoform	Blue	Blue	Green	Green	Red	Red
ribosomal protein S5	Blue	Green	Green	Blue	Blue	Red

Table 5-7: Summary table illustrating additional identified proteins within the proteome of methotrexate treated HaCaT cells. The colour scheme dictates the presence or omission of a protein at the given drug treatment concentration. Green implies that the protein was present within all three replicate samples, blue indicates that the protein was detected within two replicates and red indicates that the protein was not detected.

α -Actinin-1 is shown to be down-regulated in HaCaT cells upon methotrexate treatment. α -Actinin-1 has been implemented in a number of functions of migrating cells; it links the cytoskeleton to many different transmembrane proteins in a collection of junctions, it regulates the activity of a variety of receptors, and it serves as a scaffold to connect the cytoskeleton to diverse signalling pathways (Otey and Carpen, 2004). It has been shown that the binding of α -Actinin-1 to actin is essential for the migration of T-cells (Stanley et al., 2008) and as psoriasis is a T cell mediated disease this could provide a potential mode of action for methotrexate, especially since it is known that methotrexate is an immune-suppressor. A down-regulation of α -Actinin-1 has been reported in methotrexate treated human osteogenic sarcoma cells (malignant bone tumour) whereby the down-regulated expression is proposed to imply the involvement of α -Actinin-1 in the regulation of cell rounding and detachment that represent early events in drug-induced apoptosis (Fellenberg et al., 2003).

Similarly to the results received during dithranol treatment, a down-regulation in the expression of some annexins is observed. The importance of a down-regulation of annexin IV has been discussed previously in Section 5.3.3.1. The significance of annexin A3 in psoriasis has also been highlighted previously where it has been reported that it is up-regulated in patients with active psoriasis in comparison to normal patients (Koczan et al., 2005).

A down-regulation is observed in the expression of chaperonin containing TCP1 (subunit 2). The chaperonins are key molecular complexes that ensure the correct folding of proteins to produce energetically stable and functionally competent protein conformations, which are essential for cell growth and survival. The primary substrates for TCP1 appear to be the cytoskeletal proteins, the tubulins, and actins. Disruption of TCP1 function to down-regulate expression of TCP1 alpha is associated with inhibition of cell proliferation, a decrease in cell viability, cell cycle arrest with hyperdiploid DNA content, and cellular apoptosis (Liu et al., 2005). Whilst the over expression of TCP1 has recently been correlated to a poorer prognosis of patients with colonic cancer (Coghlin et al., 2006), an association with psoriasis is yet to be presented.

A down-regulation in expression of gelsolin is observed upon exposure to methotrexate, which was also shown in this study during dithranol exposure. Gelsolin is an actin-severing protein which breaks the non-covalent bonds between actin subunits, reducing F-actin to its component parts (Suhler et al., 1997). An increase in gelsolin expression has been associated with Crohn's disease; in this immuno-based co-morbidity it has been suggested that increased concentrations of gelsolin in Crohn's muscle cells is consistent with enhanced cell migration as a consequence of the inflammatory cell state (Ehrlich et al., 2000).

We have detected a down-regulation in three high-mobility group proteins; box 1, box 2 and AT-hook 1 isoform a. Box 1 type is an extracellular protein which acts as a cytokine by

binding to the receptor for advanced glycation end products (RAGE) and initiates a positive feedback autocrine loop that maintains the inflammatory cascade (Straino et al., 2008). It also elicits pro-inflammatory responses in endothelial cells by increasing the expression of vascular adhesion molecules as well as secretion of cytokines (TNF- α) and chemokines (IL-8) (Fiuza et al., 2003). High levels of high-mobility group box 1 have been detected in the synovial fluid of patients with rheumatoid arthritis (Taniguchi et al., 2003). There is no direct correlation between these proteins and psoriasis or methotrexate treatment however; we can deduce that these proteins are linked to the inflammatory response observed during a psoriasis outbreak and hence during successful treatment protein expression is reduced.

In addition to the protein listed above, we have also noted a down-regulation in a number of ribosomal proteins upon methotrexate exposure. Whilst there is no direct correlation in the literature between these specific ribosomal proteins and psoriasis, a link has been made between ribosomal protein S6 kinase and psoriasis (Choi et al., 1997). In this study ribosomal protein S6 kinase was found to be increased 4-fold in involved psoriatic skin in comparison to non-lesional and normal epidermis.

5.3.3.3 Ciclosporin

A total of 342 proteins were identified in the ciclosporin treated samples of which 6% were deemed to be down-regulated and 8% up-regulated. A total of 47% were proven to be equivalent in that they were present at all concentrations of the drug and in the control. Finally 43% of proteins were classified as not significant as their presence varied over the concentration range.

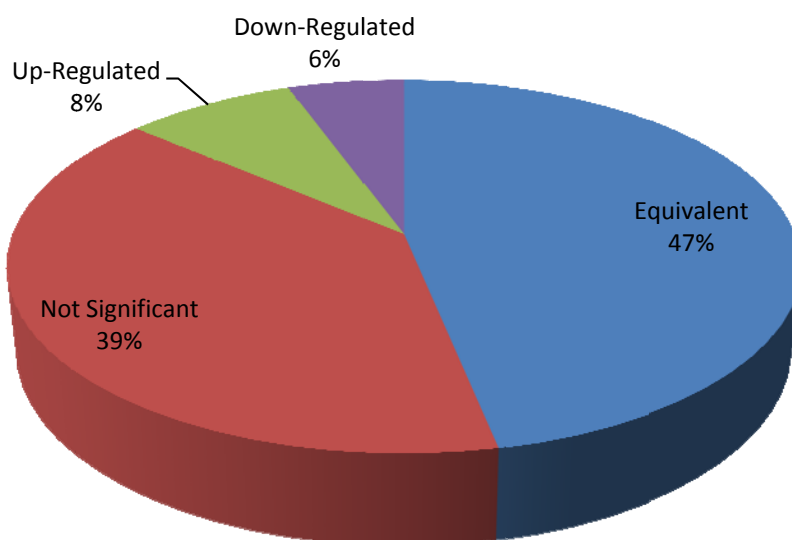


Figure 5-8: Schematic representation indicating the proportion of proteins which were up-regulated, down-regulated, deemed equivalent or non significant within the proteome of ciclosporin treated HaCaT cells.

A final metabolite map was constructed to illustrate the response of enzymes associated with the central metabolism from ciclosporin treated HaCaT cells. The list of enzymes is summarised in Table 5-8 and the resultant metabolite map depicted in Figure 5-9.

Protein Name	EC Number	C	0.5	1	1.5	2	2.5	Metabolism Location
argininosuccinate synthetase 1	6.3.4.5	Green	Green	Green	Green	Green	Green	Urea Cycle
aspartate aminotransferase 1	2.6.1.1	Red	Red	Blue	Blue	Green	Green	Alanine, Aspartate and Glutamate Metabolism
cytosolic malate dehydrogenase	1.1.1.37	Green	Green	Green	Green	Green	Green	TCA
cytosolic malic enzyme 1	1.1.1.40	Red	Red	Blue	Red	Red	Red	Pyruvate Metabolism
enolase 1	4.2.1.11	Green	Green	Green	Green	Green	Green	Glycolysis
enolase 2	4.2.1.11	Green	Green	Green	Green	Green	Green	Glycolysis
enolase 3	4.2.1.11	Green	Green	Green	Green	Green	Green	Glycolysis
fructose-1,6-bisphosphatase 1	3.1.3.11	Blue	Green	Green	Green	Green	Green	Glycolysis
fructose-bisphosphate aldolase C	4.1.2.13	Green	Green	Green	Green	Green	Green	Glycolysis
glucose phosphate isomerase	5.3.1.9	Green	Green	Green	Green	Green	Green	Glycolysis
glucose-6-phosphate dehydrogenase isoform a	1.1.1.49	Red	Red	Blue	Blue	Red	Red	Pentose Phosphate Pathway
glutathione transferase	2.5.1.18	Green	Green	Green	Green	Green	Green	Glutathione Metabolism
glyceraldehyde-3-phosphate dehydrogenase	1.2.1.12	Green	Green	Green	Green	Green	Green	Glycolysis
glyoxalase I	4.4.1.5	Blue	Red	Red	Red	Blue	Green	Pyruvate Metabolism
hydroxypyruvate isomerase homolog	5.3.1.22	Blue	Red	Green	Blue	Red	Red	Glyoxylate and dicarboxylate metabolism
isocitrate dehydrogenase 1 (NADP+), soluble	1.1.1.42	Green	Green	Green	Green	Green	Green	TCA
lactate dehydrogenase A	1.1.1.27	Green	Green	Green	Green	Green	Green	Glycolysis
lactate dehydrogenase B	1.1.1.27	Green	Blue	Green	Green	Green	Green	Glycolysis
lactate dehydrogenase C	1.1.1.27	Blue	Blue	Green	Red	Blue	Green	Glycolysis
phosphofructokinase, platelet	2.7.1.11	Blue	Blue	Green	Green	Blue	Red	Glycolysis
phosphogluconate dehydrogenase	1.1.1.44	Green	Green	Green	Green	Green	Green	Pentose Phosphate Pathway
phosphoglycerate dehydrogenase	1.1.1.95	Blue	Green	Green	Blue	Green	Green	Glycine, Serine and Threonine Metabolism
phosphoglycerate kinase 1	2.7.2.3	Green	Green	Green	Green	Green	Green	Glycolysis
phosphoglycerate kinase 2	2.7.2.3	Green	Green	Blue	Green	Green	Green	Glycolysis
phosphoserine aminotransferase isoform 1	2.6.1.52	Blue	Red	Red	Blue	Red	Red	Glycine, serine and threonine metabolism
sorbitol dehydrogenase	1.1.1.14	Red	Red	Red	Red	Red	Blue	Fructose and Mannose Metabolism
transaldolase 1	2.2.1.2	Blue	Red	Red	Red	Red	Blue	Pentose Phosphate Pathway
transketolase	2.2.1.1	Green	Green	Green	Green	Green	Green	Pentose Phosphate Pathway
triosephosphate isomerase 1	5.3.1.1	Green	Green	Green	Green	Green	Green	Glycolysis

Table 5-8: Summary table illustrating the proteins identified within the proteome of ciclosporin treated HaCaT cells. The protein name, associated EC number and the metabolism location is provided. The colour scheme dictates the presence or omission of a protein at the given drug treatment concentration. Green implies that the protein was present within all three replicate samples, blue indicates that the protein was detected within two replicates and red indicates that the protein was not detected.

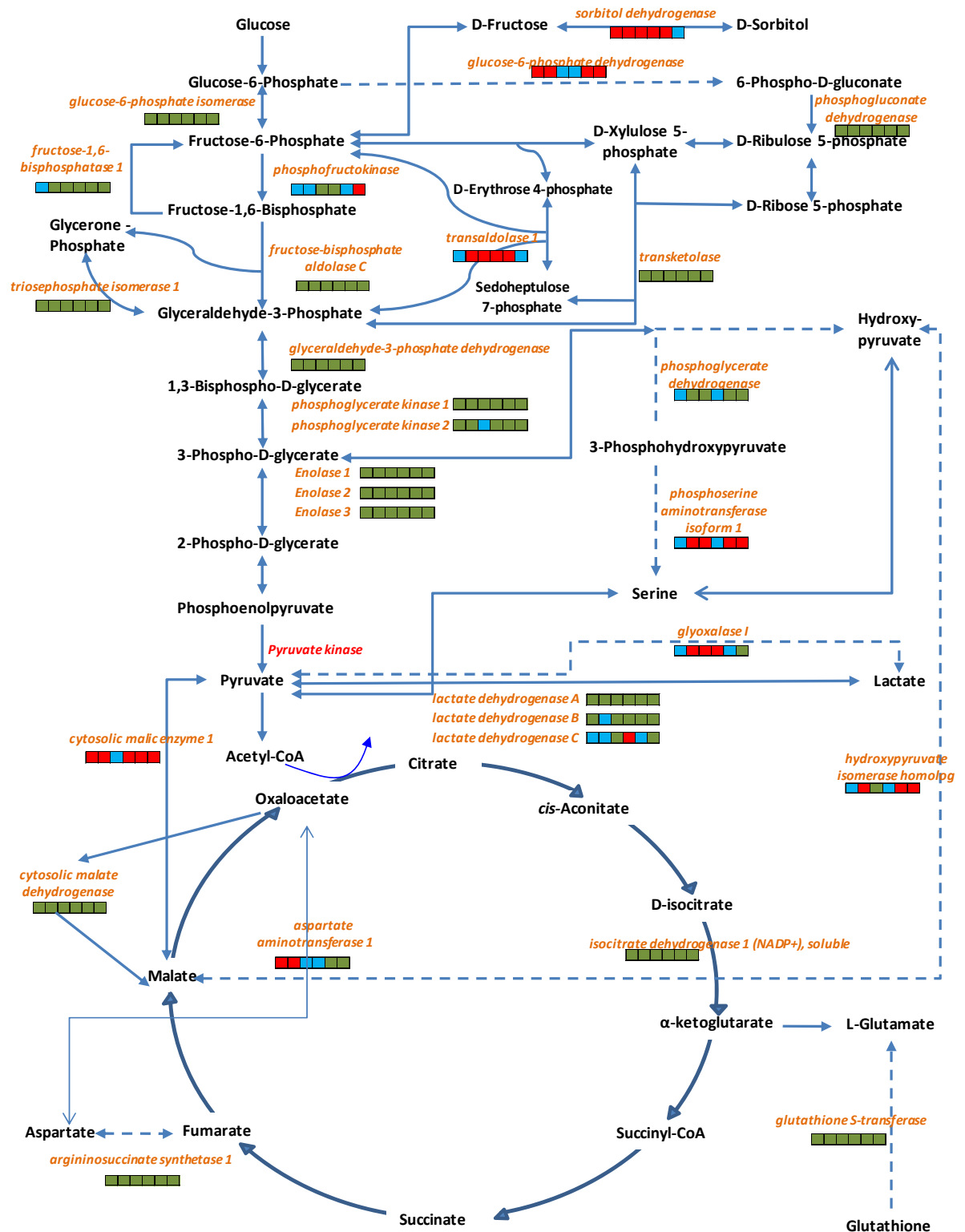


Figure 5-9: Reconstructed metabolite map depicting the proteins (orange) successfully identified within ciclosporin treated HaCaT cells and the corresponding linked metabolites (black). Adjacent metabolites are linked with block lines while pathways with some metabolites omitted are linked with dashed lines. The presence of proteins over the concentration range is summarised within the box diagrams whereby green implies that the protein was present within all three replicate samples, blue indicates that the protein was detected within two replicates and red indicates that the protein was not detected. The control sample is the left hand box and the highest concentration the right hand box.

The metabolite map illustrates many similarities between the central metabolism proteome responses of ciclosporin and methotrexate treated HaCaT cells. The main glycolysis and TCA enzymes are unaffected by ciclosporin treatment, however a variation in the expression of some linking proteins is observed. Although up-regulation in aspartate aminotransferase 1 and glyoxylase expression is recorded, the majority of proteins show a variable response to ciclosporin treatment. These results imply that ciclosporin has a minimal effect on central metabolism; this correlates well with the metabolome results highlighted in Chapter 4 which failed to show a significant impact on metabolites localised within principal metabolism pathways.

In addition to these central enzymes, a large number of additional proteins were detected within the proteome of ciclosporin treated HaCaT cells. Table 5-9 summarises a subset of proteins which can be linked to ciclosporin treatment, psoriasis or linked inflammatory disorders and a complete list is available for reference in Appendix G.

Protein Name	C	0.5	1	1.5	2	2.5
chaperonin containing TCP1, subunit 8 (theta)	Red	Red	Red	Red	Red	Red
chaperonin containing TCP1, subunit 5 (epsilon)	Red	Red	Red	Red	Red	Blue
chaperonin containing TCP1, subunit 7 isoform a	Red	Red	Red	Red	Red	Blue
ribosomal protein S2	Blue	Red	Red	Red	Red	Red
ribosomal protein L11	Red	Red	Red	Red	Red	Blue
ribosomal protein L12	Red	Red	Red	Red	Blue	Blue
ribosomal protein S17	Red	Red	Red	Red	Red	Blue
histone H2a	Green	Blue	Blue	Green	Green	Red
keratin 20	Blue	Red	Red	Red	Red	Red
myotrophin	Blue	Red	Red	Red	Red	Red
tumor protein, translationally-controlled 1 (TPT1)	Green	Blue	Red	Red	Red	Red
actinin, alpha 2	Red	Red	Red	Red	Red	Blue
gelsolin-like capping protein	Red	Red	Red	Red	Red	Blue
karyopherin beta 1	Red	Red	Red	Red	Red	Green
myristoylated alanine-rich protein kinase C substrate (MARCKS)	Red	Green	Green	Green	Blue	Blue
tubulin, beta, 2	Red	Blue	Green	Blue	Blue	Green

Table 5-9: Summary table illustrating additional identified proteins within the proteome of ciclosporin treated HaCaT cells. The colour scheme dictates the presence or omission of a protein at the given drug treatment concentration. Green implies that the protein was present within all three replicate samples, blue indicates that the protein was detected within two replicates and red indicates that the protein was not detected.

On a whole these results appear ambiguous when compared to the results found for dithranol or methotrexate treatments, as a greater quantity of proteins are up-regulated upon ciclosporin treatment. These proteins include actinin, gelsolin-like capping protein and tubulin which were found to be down-regulated by dithranol or methotrexate treatment which could suggest a completely different mode of action for ciclosporin or potentially highlight experimental error. A series of chaperonin containing TCP1 subunits were detected within the proteome of ciclosporin treated HaCaT cells; of which one appeared potentially down-regulated and two appeared potentially up-regulated upon treatment. A similar observation is recorded in the response of a series of ribosomal proteins, one ribosomal protein is down-regulated and three are up-regulated. These results are difficult to explain as it seems highly unlikely that proteins from the same family could exhibit such varying responses to treatment by the same drug. The combination of these findings reduces the amount of confidence associated with these results and hence a reduced amount of discussion is provided. Briefly, down-regulation of histone H2a, keratin 10, myotrophin and tumor protein (translationally-controlled 1) was observed and an up-regulation of karyopherin beta 1 and myristoylated alanine-rich protein kinase C substrate (MARCKS) was recorded, again this may be because ciclosporin modulates the immune system and so is difficult to correlate to any clear metabolic effects.

5.4 Conclusions

An investigation of the response of HaCaT cells to treatment with three anti-psoriatic drugs has been probed at the proteome level. LC-MS was utilised in a qualitative approach to identify changes in the expression of proteins over the concentration ranges of treatment. A scoring system was established to quantify the presence of a specific protein within three biological replicates leading to three classification groups. Firstly those which were present within all three replicates and hence a large amount of confidence can be associated with

this observation, secondly those which were present in two out of three replicates and finally those which were present in a single replicate or not observed at all. Through incorporating this semi-quantitative approach it was possible to identify proteins which were up-regulated, down-regulated and unaffected by treatment.

A number of enzymes from central metabolism were identified within the proteome of HaCaT cells exposed to dithranol, methotrexate and ciclosporin. Metabolite maps were constructed to illustrate changes in enzyme expression with treatment. These maps demonstrated that dithranol treatment has a greater pronounced effect of the central metabolism enzymes. In particular a number of enzymes associated with glycolysis and the TCA cycle were down-regulated with increasing concentrations of dithranol exposure (*viz.* enolase 2 & 3 and phosphoglycerate kinase 2). These results correlate well with the findings gained from the metabolomic analysis discussed previously. Conversely the results from methotrexate and ciclosporin treatment demonstrate that they imposed a minimal effect upon central metabolism and as previously stated this is perhaps expected as these drugs are immuno-suppressants. In addition, a variety of proteins that are not primarily associated with central metabolism were identified in the proteome of the drug treated cells. These proteins varied greatly between treatment type indicating variable drug mode of actions or targets. In some cases these proteins had previously been indicated in psoriasis or in similar disorders with highly proliferating cell processes. However some proteins highlighted in this study are potential novel biomarkers for psoriasis onset or conversely drug mode of action, and would need to be investigated further using a more quantitative proteomics approach such as iTRAQ or SILAC.

The results presented in this chapter illustrate that these anti-psoriatic drugs induce global changes in the proteome of HaCaT cells. In the future work it would be necessary to investigate quantitative protein changes; *i.e.*, by incorporating the use of isotope labelling

techniques which would increase the confidence in the proposed biomarkers, and by also using transcriptomics or qPCR as complementary approaches

Chapter 6: Metabolomic analysis of plasma samples collected from psoriasis patients during methotrexate treatment: A short study.

6.1 Introduction

The analysis of plasma using a metabolomics approach is a well established procedure. A number of studies have used this approach to assign potential biomarkers for a number of diseases including; diabetes mellitus (Li et al., 2009), ankylosing spondylitis; a form of chronic inflammatory arthritis (Gao et al., 2008), preeclampsia (Kenny et al., 2008), Parkinsons' disease (Bogdanov et al., 2008), schizophrenia (Kaddurah-Daouk et al., 2007) and coronary heart disease (Sabatine et al., 2005).

In this study plasma samples were collected from a cohort of psoriasis patients preselected for a research project undertaken by Dr RB Warren at The Dermatology Centre, The University of Manchester, Salford Royal Foundation Hospital, Manchester with required ethics approved (05/Q1407/120). The samples were collected during a routine day clinic and hence the samples provide a real-life analysis scenario incorporating all the variance associated with a lack of fasting prior to sample collection.

The general scope of patient selection criteria was beyond our immediate control and hence the clinical metadata is rather limited in terms of age of patient, height, weight, BMI and any other pathology. However as the samples do represent a 'real life scenario' it was deemed important to assess whether a metabolomics-based investigation could play a role in predicting drug responders and also to investigate if any link could be made with previous findings in Chapter 4 & 5.

The patients selected were orally administered with methotrexate and given folic acid supplements. Folic acid has been proven to increase the likelihood of efficacious, longterm, tolerable and toxicity free therapy for patients receiving methotrexate (Gisondi et al., 2007,

Strober and Menon, 2005). The severity of the psoriasis and the outcome of the treatment were graded according to the psoriasis area severity index (PASI) score, a method used worldwide to evaluate the severity and effectiveness of treatment in psoriasis patients (Exum et al., 1996). The PASI system evaluates the affected body area and the individual lesional characteristics to produce an overall score. The procedure begins by assessing four separate areas of the body and calculating the area of involvement; the head (Ah), the upper extremities (Au), the trunk (At) and the lower extremities (Al) which account for 10%, 20%, 30% and 40% of the total body respectively. Each area is assigned a value between 0-6 where 0 is equivalent to no involvement, 1 = <10%, 2 = 10-<30%, 3 = 30-<50%, 4 =50-<70%, 5 = 70-<90% and 6 = 90-100%. The next stage establishes the type of lesions present in each region; erythema (E), infiltration (I), and desquamation (D). These three types of lesions are quantified for each separate region using a five point scale; where 0 = no involvement, 1 = slight, 2 = moderate, 3 = striking, and 4 = exceptionally striking involvement. To compile all this information a final equation is generated:

$$\text{PASI} = 0.1\text{Ah} (\text{Eh} + \text{Ih} + \text{Dh}) + 0.2\text{Au} (\text{Eu} + \text{IU} + \text{Du}) + 0.3\text{At} (\text{Et} + \text{It} + \text{Dt}) + 0.4\text{Al} (\text{El} + \text{Il} + \text{Dl}).$$

PASI scores can range from 0.0-72.0 and the greater the value the more severe the psoriasis outbreak. This summary is adapted from (Exum et al., 1996). Whilst the PASI score is relatively subjective and dependent upon the assessment by a dermatologist, it is a valid and tested method which will be used in this study as a quantitative indicator of psoriasis severity and treatment success. The difference between the PASI score before treatment and after treatment was calculated and the magnitude of the result was related to responsiveness.

The samples were analysed *via* GC-MS to investigate the presence of plasma-based metabolites. The results were analysed to probe inter-sex and inter-response variations in metabolite composition. Kruskal-Wallis was the primary tool used within this analysis; an

element of predictive modelling was undertaken however the outcome was of minimal validity.

6.2 Material and Methods

6.2.1 Materials

Drug compounds and reagents were all purchased from Sigma Aldrich, Gillingham, UK unless otherwise stated.

6.2.2 Methods

6.2.2.1 Patient Selection

Patients were recruited from a psoriasis clinic at Salford Royal Foundation Hospital, Manchester. In total 26 patients of varying age and sex were involved in the study. As previously stated the PASI score was calculated for each patient prior to methotrexate treatment. All patient information known prior to treatment is summarised in Table 6-1. The table shows that the PASI scores ranged from 8.8 to 28.2 indicating that the patients involved were low to moderate sufferers. Plasma samples were prepared and separated following blood collection and all samples stored at -80 °C until analysis.

6.2.2.2 GC-MS Sample Preparation

All samples were thawed on ice and randomised prior to analysis. The internal standard solution was initially composed of 10 mg succinic d4 acid dissolved in 10 mL ddH₂O followed by a further dilution of 2 mL dissolved in 10 mL of ddH₂O. Plasma samples were vortexed for approximately 20s. To a clean labelled centrifuge tube 100 µL of internal standard, 200 µL of plasma sample and 60 µL of HPLC grade methanol was added to deproteinize the sample. The mixture was vortexed for 15s and then centrifuged at 16200g for 15min. The supernatant was removed and transferred to a clean centrifuge tube. The sample was finally

lyophilised (Eppendorf Vacufuge Concentrator 5301, Eppendorf, UK) overnight at a low temperature. A two-stage sample chemical derivatisation was performed on the dried sample 80 μ L of 20 mg/mL O-methylhydroxylamine solution was added and heated at 40°C for 90 min followed by addition of 80 μ L MSTFA (N-acetyl-N-[trimethylsilyl]-trifluoroacetamide) and heating at 40°C for 90 min. 20 μ L of a retention index solution (4 mg/mL n-decane, n-dodecane, n-pentadecane, n-nonadecane, n-docosane dissolved in hexane) was added and the samples were analysed in a random order using a Agilent 6890 N gas chromatograph and 7683 autosampler (Agilent Technologies, Stockport, UK) coupled to a LECO Pegasus III electron impact time-of-flight mass spectrometer (LECO Corporation, St Joseph, USA) as detailed in (O'Hagan et al., 2005). Initial data processing of raw data was undertaken using LECO ChromaTof v2.12 software to construct a data matrix (metabolite peak vs. sample no.) including response ratios (peak area metabolite/peak area succinic-d₄ internal standard) for each metabolite peak in each sample. The process of standardising to succinic-d₄ acid has previously been reported, details of which can be found in (Pope et al., 2007) and (MacKenzie et al., 2008).

6.2.2.3 Quality Control Samples

Quality control (QC) samples were prepared by combining 100 μ L of each plasma sample into a pooled QC sample. This sample was vortexed for 30s and separated into 10 individual QC samples. These samples were prepared as above for GC-MS analysis and were analysed intermittently during the experiment to quantify process variability. The incorporation of QC samples acts as an internal reference amongst the individual samples, (Dunn et al., 2008). At present there are no exact criteria for the assessment of reproducibility in metabolomics data-sets however the inclusion of QC samples allows the data quality and sample variance to be quantified often through the application of a standard deviation limit (Begley et al., 2009).

6.2.2.4 GC-MS Data Analysis

The data matrix generated within the GC-MS software was exported to Microsoft Excel where it was normalised to total peak area. A Kruskal-Wallis analysis was performed on the data. Kruskal-Wallis was employed in the analysis as no assumptions could be made about the data distributions of the classes. Kruskal-Wallis is a non-parametric equivalent to ANOVA. ANOVA in comparison assumes that the class populations have normal distributions, *i.e.* a parametric test (Hollander and Wolfe, 1999).

Metabolites were identified in the same manner as discussed in Section 4.3.3. Metabolites were defined as a definitive match if the retention time and mass spectrum matched that of a standard analysed on the same instrument. In comparison a putative match can be matched by mass spectrum to that from a non-in house library and cannot be matched by retention time.

Patient Code	Sex	Age of Onset	PASI Baseline Score
99	F	13	22.4
100	M	21	16
101	F	15	14.2
105	F	18	17.4
108	F	43	22.4
109	F	30	16.4
110	M	28	15.6
111	M	22	10
112	M	22	16
113	F	39	12.8
114	F	24	18.5
115	M	18	9.6
116	M	33	15.6
117	M	28	9.8
119	F	13	15.4
120	F	30	16.8
121	M	32	8.8
122	F	16	12.8
123	M	19	14.6
124	M	50	18.6
125	F	2	13.7
126	F	30	28.2
127	M	24	21.2
128	M	12	10.6
129	F	4	13
130	M	15	12.6

Table 6-1: Patient metadata collected prior to treatment with methotrexate. The table illustrates the patient identification code, sex, age and baseline PASI score.

6.3 Results and Discussion

6.3.1 Post treatment metadata

After treatment with methotrexate the patients were reassessed and a new PASI score generated. The % change in PASI score was calculated and the patients assigned as a responder, non-responder or intermediate responder using the following criteria. A PASI score reduction of >75 % was deemed to be a successful response, a PASI score reduction of between 50-75% was determined as an intermediate response and a response of < 50% was declared as a non-response. This information is summarised in Table 6-2.

Patient Code	Sex	Age of Onset	PASI Baseline	Weekly Dose at 3/12 mg	PASI 3/12	% PASI Change	Response status
99	F	13	22.4	17.5mg	3.6	83.93	Responder
100	M	21	16	N/A	N/A	N/A	N/A Severe GI AE
101	F	15	14.2	20mg	3.1	78.17	Responder
105	F	18	17.4	10mg	4.1	76.44	Responder
108	F	43	22.4	N/A	N/A	N/A	N/A Severe GI AE
109	F	30	16.4	10mg	3.8	76.83	Responder
110	M	28	15.6	15mg	11.2	28.21	Non-responder
111	M	22	10	10mg	2.4	76.00	Responder
112	M	22	16	17.5mg	3.9	75.63	Responder
113	F	39	12.8	30mg	6.1	52.34	Intermediate response
114	F	24	18.5	10mg	3.9	78.92	Responder
115	M	18	9.6	12.5mg	4.5	53.13	Intermediate response
116	M	33	15.6	15mg	11.2	28.21	Non-responder
117	M	28	9.8	10mg	8.5	13.27	Non-responder
119	F	13	15.4	10mg	3.8	75.32	Responder
120	F	30	16.8	25mg	4.1	75.60	Responder
121	M	32	8.8	17.5mg	9.2	-4.55	Non-responder
122	F	16	12.8	N/A	N/A	N/A	N/A MTX stomatitis
123	M	19	14.6	7.5mg	2.9	80.14	Responder
124	M	50	18.6	7.5mg	4.5	75.81	Responder
125	F	2	13.7	17.5mg	9.6	29.93	Non-responder
126	F	30	28.2	20mg	5.6	80.14	Responder
127	M	24	21.2	10mg	4.5	78.77	Responder
128	M	12	10.6	17.5mg	8.5	19.81	Non-responder
129	F	4	13	17.5mg	3.2	75.38	Responder
130	M	15	12.6	12.5mg	6	52.38	Intermediate response

Table 6-2: Patient information illustrating the dose of methotrexate administered, the starting PASI score, the PASI score post treatment and the corresponding response rate and status.

From the total of 26 participating patients; 14 patients showed a response, 3 showed an intermediate response and 6 were non-responders to methotrexate treatment in this instance. Three individuals were excluded from the study as they exhibited side effects. Two patients presented with a severe gastrointestinal adverse effect and one presented with methotrexate associated stomatitis; an inflammation of the mouth. The patients with attributed side effects were declined further treatment but plasma samples were still collected and included in the study.

An interesting feature presented within the table is the non-correlation between dosage and response which indicates the varied successfulness achieved by methotrexate treatment. This factor is further highlighted by the response recorded for patient 121 who demonstrated an increased level of psoriasis involvement after methotrexate treatment.

6.3.2 Principal Components Analysis

The initial stage of data analysis incorporated the use of principal components analysis (PCA) to identify any trends within the data which could potentially be associated with methotrexate response. Additionally PCA is utilised to visualise the repeatability and correlation between QC samples. Figure 6-1 illustrates the PCA plot generated for the complete data set using the first two principal components which account for 76.82% of the total explained variance. The plot shown in Figure 6-1A indicates the spread of data in terms of response whereby the following identifications are observed; response (R), intermediate response (I), non-response (N), severe (S) and finally the QC samples (Q). The plot highlights a lack of clustering within response classes and shows a large amount of variance. This finding is additionally evident for the QC samples. The QC samples although biologically identical fail to cluster together in an acceptable manner. A large majority of QC samples are localised around the origin of PC1 and PC2; however a sub-set are visible outliers. The plot presented in Figure 6-1B was constructed using an identification number corresponding to

the order in which the samples were analysed. This plot eliminates sample drift over time as a reason for the dispersive presence of the QC samples within the PCA analysis. Over time results from the analysis of complex samples can differ as a function of time and not as a function of biological variance but this can be discounted as no relationship between location in PCA space and sample order is observed.

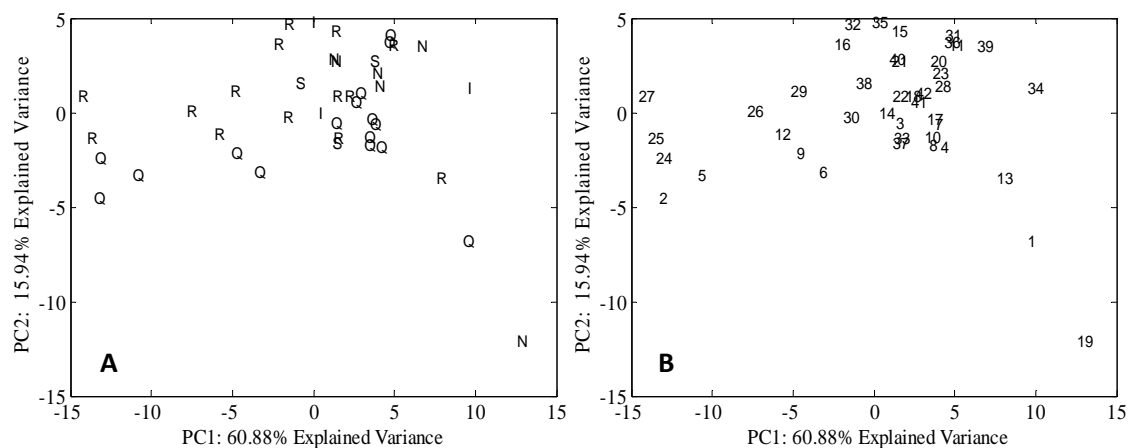


Figure 6-1: PCA plots of PC1 vs PC2 accounting for 76.82% total explained variance from the complete data set. Plot A illustrates the variance within the data in terms of response; responder (R), intermediate responder (I), non-responder (N) and QC sample (Q). Plot B illustrates the variance using the sample order as the naming structure.

6.3.3 Kruskal-Wallis Analysis

Kruskal-Wallis analysis was used to provide corresponding p values for the metabolites identified within the plasma samples. The analysis was conducted twice, to identify metabolites related to response to treatment and also to sex. The first class structure was generated according to the outcome of the treatment providing three classes; response, intermediate response, non-response. The second class structure was generated according to male or female. Given the small sample size and heterogeneity of patients; metabolites with a p value <0.08 were considered. This p value is rather high and was chosen as a threshold value to allow the top proportion of metabolites to be taken into the discussion stage of the analysis. Table 6-3 shows the metabolites which fit the p value criteria and the corresponding identifications according to response. A couple of metabolites were not

identified, in that it was not possible to match them to known metabolites in our in house libraries.

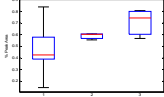
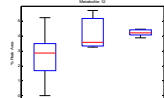
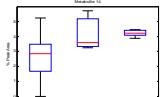
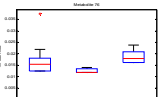
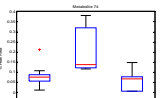
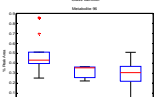
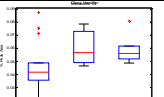
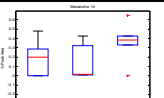
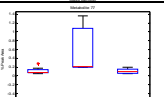
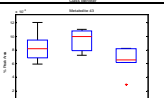
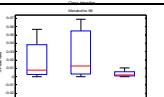
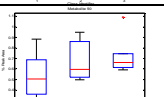
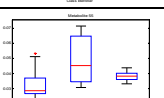
<i>Metabolite ID</i>	<i>p value</i>	Metabolite	Box and Whisker
103	0.0138	uric acid	
12	0.0279	valine	
14	0.0279	valine	
76	0.0348	unidentified	
74	0.0503	fructose	
96	0.0556	hexadecanoic acid	
54	0.0568	methionine	
10	0.057	p cymene/EDTA	
77	0.0598	monosaccharide	
43	0.0742	succinic acid	
98	0.0746	unidentified	
90	0.0782	tyrosine	
55	0.0795	cysteine	

Table 6-3: Kruskal-Wallis results table identifying metabolites significantly related to response to treatment. The metabolite identification and subsequent *p* value is shown. The box & whisker plot illustrates the metabolite level in responders (left), intermediate responders (middle) and non-responders (right).

The table shows a number of metabolites which vary according to response. The metabolites uric acid, valine, methionine, tyrosine and cysteine are observed to be reduced in responders in comparison to non-responders. In comparison fructose, hexadecanoic acid and succinic acid appear elevated in responding patients when compared to non-responding patients. These metabolites could be potential markers for predicting response to treatment, but this of course would need further validation. Interestingly in most cases the variation associated with metabolite concentration is much greater in responders in comparison to non-responders. This observation could correlate to the varying magnitude of response. The derivatisation products of valine help to indicate the reproducibility associated with the analysis and the two metabolite features illustrate almost identical trends.

The above 'markers' may be generated by chance due to the small number of samples and the sample collection methods (*i.e.* the omission of a fasting period). Therefore it was decided to attempt a prediction where known biological effects have been reported in the literature. Thus, as previously stated it is also possible to probe the variability of plasma metabolites according to sex. Table 6-4 shows the metabolites which fit the *p* value criteria and the corresponding identifications according to response. All the identified metabolites were observed to be at an increased concentration in male patients in comparison to female patients. The selection of metabolites which were significantly altered between sexes includes creatinine. Serum creatinine levels have previously been investigated in a large survey of the US population involving 18,723 participants (Jones, 2000). In this study the mean serum creatinine levels were found to be significantly higher in male vs. females through a variety of races. The other metabolites include the amino acids, 4-hydroxyproline, threonine, tryptophan and methionine whose increased concentration in males can be attributed to increased protein turnover in comparison to females. A similar trend was

observed by Kochhar and colleagues who screened urine and plasma samples using NMR (Kochhar et al., 2006).

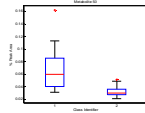
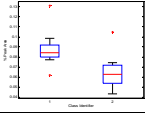
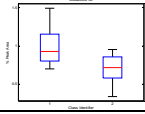
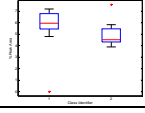
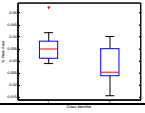
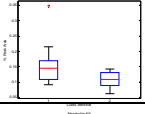
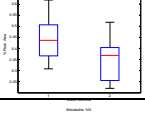
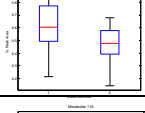
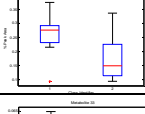
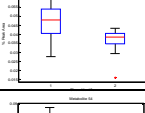
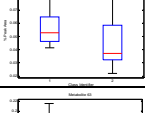
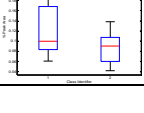
Metabolite ID	<i>p</i> value	Metabolite	Box & Whisker
50	0.0011	4-hydroxyproline	
60	0.0021	creatinine	
38	0.0068	threonine	
64	0.0078	glutamic acid and/or pyroglutamic acid	
86	0.0116	hydrocinnamic acid	
71	0.0228	ornithine and/or arginine	
69	0.0267	ornithine and/or arginine	
103	0.0489	uric acid	
115	0.0564	tryptophan	
33	0.0564	unidentified	
54	0.0564	methionine	
63	0.0783	glutamic acid and/or glutamine	

Table 6-4: Kruskal-Wallis results table identifying metabolites significantly related to sex of patient. The metabolite identification and subsequent *p* value is shown. The box & whisker plot illustrates the metabolite level in male patients (left) and female patients (right).

6.3.4 Multivariate Predictive Analysis

To analyse these data further and to investigate whether it was possible to discriminate between responders and non-responders to methotrexate treatment successfully and differentiate between male and female patients we conducted PLS-DA and support vector machine (SVM) analyses. For both these analyses bootstrapping was performed. Unfortunately both PLS-DA and SVMs failed to discriminate between the defined classes. PLS results were particularly disappointing for gender classification and provided a correct classification result (CCR) of approximately 56%. Gender classification utilising SVM provided a slightly better CCR of 59% from an average of 1000 bootstraps. Finally, predictive modelling was incorporated to investigate drug response, again this method failed. The difficulty in modelling drug response can be specifically related to the unbalanced class structure. In total there were 14 responders, 6 non-responder and 3 intermediate and severe responders.

6.4 Conclusions & Future Work

This work was conducted to investigate the application of a metabolomics-based study in a 'real life scenario' in which samples were collected from patients without the incorporation of a fasting period, during normal clinical practice. The aim was to investigate whether we could identify potential markers to predict a patient's response to methotrexate treatment by plasma-based metabolomics using GC-MS analysis.

Initial PCA indicated minimal separation between responders and non-responders and also illustrated an unusual amount of variation in the QC samples which itself is difficult to explain. Kruskal-Wallis analysis was successful in identifying a small number of significant metabolites (from a total of 121 metabolite features detected) which seem to be correlated to response and also a number of metabolites related to gender. Metabolites linked to methotrexate response included uric acid, valine, methionine, tyrosine and cysteine which

were recorded at a reduced level in responders when compared to non-responders. In these cases we could potentially imply that these metabolites could be used as indicators of response, but this of course needs validation in a larger more controlled study. The results gained for gender analysis were relatively promising and correlated well with previous findings in the literature. As expected a number of metabolites associated with protein turnover and muscle growth were detected at increased levels in plasma collected from males in comparison to females.

This study helps to confirm the importance of experimental design and the regulation of external parameters when undertaking a clinical metabolomics study in particular those including human samples.

Chapter 7: Monitoring the succinate dehydrogenase activity isolated from mitochondria by surface enhanced Raman scattering.

7.1 Introduction

The main aims of this thesis have been the investigation of bioanalytical approaches to understanding psoriasis and other skin pathologies. This has involved the development of imaging approaches based on vibrational spectroscopy, and in depth metabolomics and proteomics studies using mass spectrometry coupled to gas chromatography and liquid chromatography respectively. These studies have involved static snapshots of pathology and drug interactions and therefore in order to investigate highly dynamic processes Raman spectroscopy was developed to analyse enzymatic activity. This work has transferable potential into areas of human metabolism research and may be useful for metabolomics studies.

The theory of Raman spectroscopy was first discovered by CV Raman in 1928 (Raman and Krishnan, 1928). The technique is often used in a complementary approach to infrared spectroscopy and is applicable to a wide array of samples including solids, liquids and gases. The basis of Raman spectroscopy is the scattering of light from a molecule. In normal cases for Rayleigh scattering the light is elastically scattered in which the photons have the same energy/frequency and hence wavelength as the incident light. However in Raman spectroscopy a small fraction of photons are inelastically scattered at different frequencies than the incident photons. Light scattered with a frequency lower than that of the incident beam of radiation is referred to as Stokes radiation, while light scattered with a higher frequency is termed anti-Stokes radiation. Stokes radiation involves an increase in photon energy while anti-Stokes radiation involves a decrease in energy. Similar to IR, Raman spectra include a number of distinctive peaks which can be attributed to specific functional

group vibrations; however, as Raman is complementary to IR, peaks which are weak in IR can be strong within Raman and *vice versa*.

The analysis of metabolic processes is important in all areas of biochemistry and particular interest is shown in the analysis of succinate dehydrogenase, the enzyme involved in the electron transfer reactions in all kingdoms of life as documented by (Reichmann and Wildenauer, 1991, Peterson et al., 1994, Trumpower and Gennis, 1994, Dautry et al., 1999). Succinate dehydrogenase is responsible for catalyzing the oxidation of succinate to fumarate within the citric acid cycle as illustrated in Figure 7-1C and Figure 7-2A. In higher organisms all enzymes within the cycle are located within the mitochondrial matrix; however an exception to this is succinate dehydrogenase and its coenzyme flavin adenine dinucleotide (FAD). The enzyme complex (often represented by E-FAD) is tightly bound to the inner membrane of the mitochondrion allowing its easy isolation.

Upon isolation of this E-FAD it is possible to measure the succinate to fumarate reaction by monitoring the reduction of an artificial electron acceptor; for example, the Hill reagent 2,6-dichlorophenolindophenol (DCPIP). When this redox dye is oxidised it is blue and when reduced it is colourless (See Figure 7-1 A&B for reactions), thus simple spectrophotometry can be employed to follow this redox change. In order to use this artificial electron acceptor, the normal path of electrons in the electron transport chain must be blocked (Nelson and Cox, 2008). This is accomplished by adding sodium azide to the reaction mixture (Figure 7-2B).

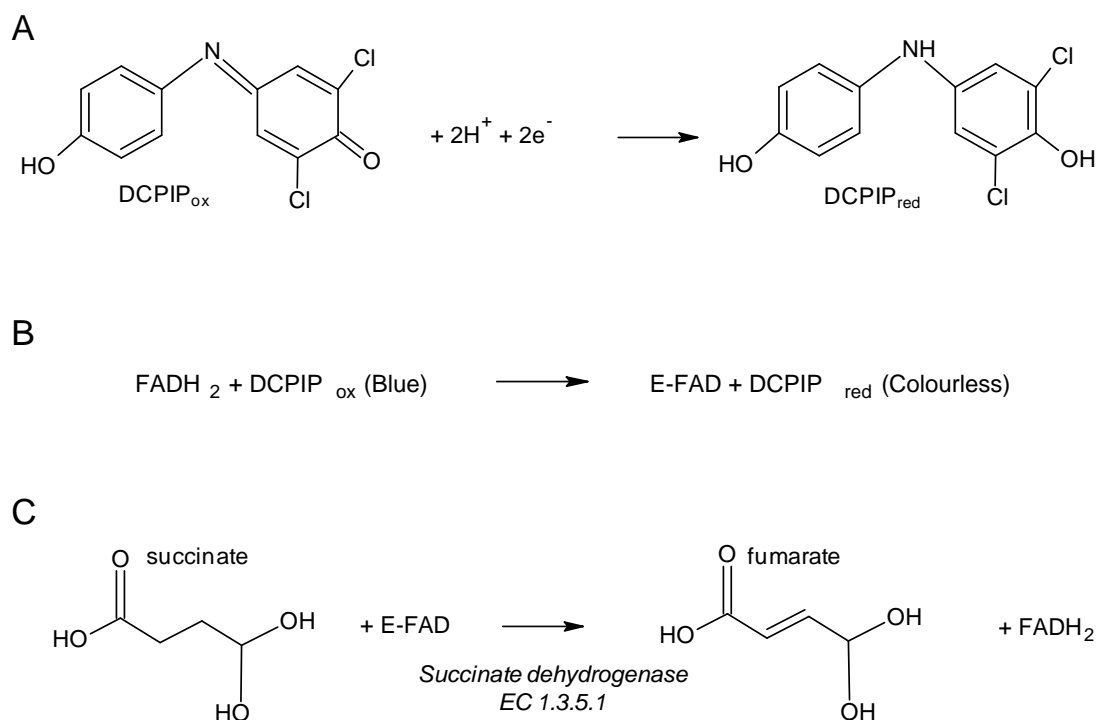


Figure 7-1: Detection of enzyme activity and reactions involved. (A) Schematic drawing of DCPIP (the final electron acceptor) in its oxidised and reduced form. (B) Representation of the reduction of DCPIP by FADH_2 from its oxidised blue form of the dye to the reduced colourless form. (C) The reaction catalysed by the enzyme succinate dehydrogenase (EC 1.3.5.1).

This poison inhibits the transfer of electrons from Complex IV (cytochrome a_3) to the final acceptor, oxygen, so that the electrons cannot be passed along the preceding cytochromes and ubiquinone (also called co-enzyme Q). Instead these electrons are picked up by DCPIP. The reduction of DCPIP by E- FADH_2 can then be measured at 600nm (Figure 7-1A) through the observed blue to colourless colour change (Nelson and Cox, 2008). However, one of the problems with spectrophotometry is that no chemical information on the reporter is available which means that the method potentially lacks specificity. By contrast, Raman spectroscopy yields information rich spectral fingerprints due to specific vibrational band frequencies being probed from the molecules under interrogation (Ferraro and Nakamoto, 1994).

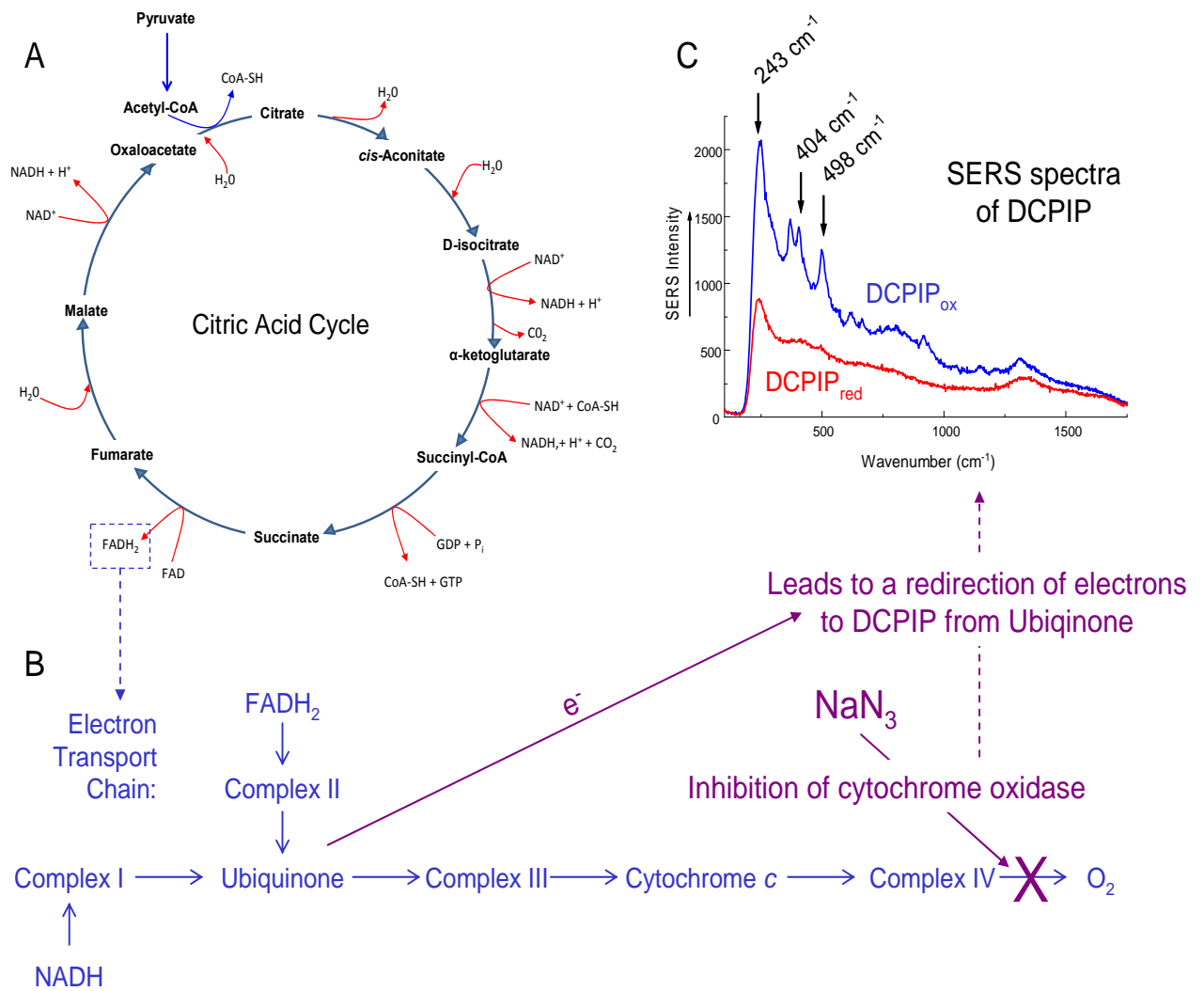


Figure 7-2: Schematic representations of (A) the citric acid cycle showing where succinate is converted into fumarate, and (B) the electron transport chain detailing where sodium azide inhibits cytochrome oxidase. (C) SERS spectra of the artificial electron acceptor DCPIP in its oxidised and reduced forms which occurs due to the redirection of electrons from the electron transport chain.

However, this inelastic scattering of light is usually very weak (typically 1 in $10^6 - 10^8$ photons), and Raman spectra can often be difficult to obtain from organic molecules because of the presence of fluorescence, which is further compounded in biological matrices. These shortcomings in Raman spectroscopy can be largely overcome by surface enhanced Raman scattering (SERS (Moskovits, 1985)), including both fluorescence (Shadi et al., 2009) and signal enhancement, which for certain molecules allows single molecule detection (Kneipp et al., 2002, Moskovits et al., 2002). Thus SERS has found wide utility as a

sensitive analytical and bioanalytical technique (Bailo and Deckert, 2008, Graham and Faulds, 2008, Jarvis and Goodacre, 2008, Qian and Nie, 2008)

Recently there has been interest in applying SERS to monitor kinetics of reactions particularly those concerned with metabolism. Success in monitoring kinetics of synthetic chemical reactions using SERRS (a variant of SERS which includes a resonance enhancement) has been reported in (Shadi et al., 2004), as well as those detailing general enzyme activity (Moore et al., 2004), (Ingram et al., 2008). Therefore the aim of the present study was to investigate whether SERS could be used to gain quantitative enzyme information from succinate dehydrogenase isolated from mitochondria.

7.2 Materials & Methods

7.2.1 Chemical and reagents

All chemicals and reagents were purchased from Sigma (D-mannitol KOH, sodium azide, sodium succinate, malonic acid, $\text{MgCl}_2 \cdot 6\text{H}_2\text{O}$, poly L-lysine hydrobromide, gold tetra chloride, tri-sodium citrate) with the exception of DCPIP (Acros), KH_2PO_4 , K_2HPO_4 , (BDH) and hydrochloric acid (Fisher). All chemicals were used without further purification. Double de-ionised water was used for all experiments.

7.2.2 Extraction of mitochondria

Cauliflowers were obtained from a national retail outlet. 20 g from the 2-3 mm of the surface of cauliflower florets was added to 40 mL of ice cold grinding media (0.3 mol dm^{-3} mannitol, $0.006 \text{ mol dm}^{-3}$ KH_2PO_4 , $0.014 \text{ mol dm}^{-3}$ K_2HPO_4 , adjusted to pH 7.2) and blended in a Ferretti FEBL10 food processor for 5 min. The ground material was filtered through a muslin cloth and the supernatant transferred into chilled centrifuge tubes and centrifuged (Sorvall RC-5B refrigerated superspeed centrifuge) at 1778 *g* for 10 min. The post-nuclear supernatant was decanted into clean chilled centrifuge tubes and centrifuged (Sorvall RC-5B

refrigerated superspeed centrifuge) at 23042g for 30 min. The mitochondria pellet was recovered and resuspended in manitol assay medium (0.3 mol dm^{-3} mannitol, $0.006 \text{ mol dm}^{-3} \text{ KH}_2\text{PO}_4$, $0.014 \text{ mol dm}^{-3} \text{ K}_2\text{HPO}_4$, $0.005 \text{ mol dm}^{-3} \text{ MgCl}_2$, adjusted to pH 7.2).

7.2.3 Monitoring enzyme activity

In a test tube, 0.5 mL of sodium azide (0.04 mol dm^{-3}), 0.5 mL ($5 \times 10^{-4} \text{ mol dm}^{-3}$) DCPIP, 0.5 mL of succinate (0.02 mol dm^{-3}) and 0.9 mL of mitochondrial suspension was added to 3.2 mL of assay media and mixed. The mixture was allowed to equilibrate for 5 min after mitochondria addition. The kinetics of the reaction was subsequently measured over a period of 5 to 30 min using a Thermo-2 UV-VIS spectrophotometer set at 600 nm as well as by SERS.

For SERS measurements an aliquot of 150 μL of the above mixture was taken at 5 min intervals and added immediately to the gold SERS colloid (*vide infra*) with subsequent collection of SERS spectra. In addition to the above reaction mixture, controls were also incorporated into the analysis and included:

- Removing only the sodium azide inhibitor. This is the negative control so that the electron transport chain functions normally and the terminal electron acceptor is oxygen (Figure 7-2B).
- Removing only the sodium succinate. This is another negative control where as there is no substrate no electron transport will occur.
- Adding 2 mL of malonic acid (0.2 mol dm^{-3}). This was included as malonic acid is a competitive inhibitor for succinate dehydrogenase.
- Reducing the volume of the mitochondria preparation to 0.3 mL or 0.6 mL.

7.2.4 Surface enhanced Raman scattering

7.2.4.1 Colloid preparation

A gold colloid was prepared by Dr Iqbal Shadi using the Lee and Meisel method as detailed in (Lee and Meisel, 1982). All glassware were acid washed with *aqua regia* [HNO_3/HCl (1:3 v/v)] followed by gentle scrubbing with a soap solution. Colloid was prepared by reduction of HAuCl_4 by sodium citrate. Briefly, 250 mL of 1 mM solution of HAuCl_4 was brought to the boil followed by addition of 25 mL of 38.8 mM solution of sodium citrate. The mixture was boiled for 30 min followed by cooling at room temperature. The quality of the resulting colloid was checked by determining the wavelength of the absorption maximum in the visible region on a Thermo-2 UV-VIS spectrophotometer. The nature of the colloid often used for SERS, has been examined using visible absorption, photon correlation and NMR spectroscopic techniques (performed by Dr Shadi; data not shown) which confirm that the surface of the gold particles are covered with a layer of citrate with pendent negatively charged groups. However, the subsequent addition of poly L-lysine which coats the surface, results in the presence of pendent positively charged groups on the colloidal surface (Chaudry et al., 1996).

The citrate-reduced sols gave an absorption maximum at ~ 529 nm. An acceptable gold sol is one which not only absorbed at 529 nm but has an absorption band at this wavelength with a half height width of ~ 50 nm, and this was the case for this preparation (data not shown). TEM of the gold sols showed that the particles had a mean diameter of 20 nm and had good uniformity (Figure 7-3).

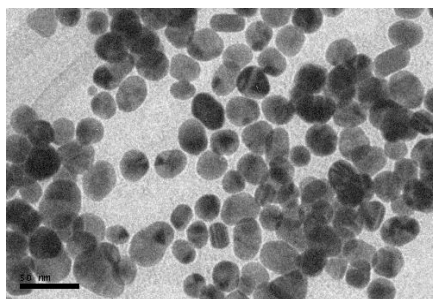


Figure 7-3: Transmission electron micrograph of citrate reduced Au colloids showing good homogeneity. The scale bar is 50nm.

7.2.4.2 Aggregation

In initial experiments the aggregation of the citrate reduced gold colloid particles was induced by the addition of poly L-lysine as this has been found by use to be very important for SERS of dye molecules (Shadi et al., 2009). In this process 150 μL of a 0.01 % aqueous solution of poly L-lysine was added to 1 mL of gold colloid, which had been diluted with 1 mL of de-ionised water, followed by 150 μL of the dye solution. The pH was then adjusted to enhance SERS (Whitney et al., 2006) by the addition of 35 μL of hydrochloric acid, 1 mol dm^{-3} of KOH, or 10 μL of 1 mol dm^{-3} KOH.

The above was found to give very little SERS (see below) so for subsequent experiments poly-L-lysine was excluded with the rest of the analysis mixture as detailed above; a phenomenon that has been previously observed (Shadi et al., 2003). For the enzyme reactions the 150 μL of the dye solution was replaced with 150 μL of the enzyme reaction.

7.2.4.3 Instrumentation

Raman analysis spectra were collected using an Ahura Defender system (Ahura Scientifics, Wilmington, MA, USA), a hand held, portable Raman spectrometer (using back scattered geometry) with a built in 4 mL sample chamber which provided at the sample 300 mW laser power at 785 nm \pm 0.5 nm laser excitation and 2 cm^{-1} line width. The spectrometer has a

monochromatic spectral range of 781 – 1014 nm, a Raman spectrum range of 250 – 2875 cm^{-1} and a spectral resolution of 7-10.5 cm^{-1} (full width at half maximum; FWHM). Built into the Ahura spectrometer are Rayleigh rejection filters of OD 7, a silicon CCD 2048 pixels detector in direct dispersive detection mode and a dispersion mode which is a single pass spectrometer (1200 grooves/mm blazed at 900 nm).

The SERS colloid-analyte aggregate was analysed by placing the sample into a 4 mL sample chamber. All samples were analysed three times to give three machine replicate measurements.

7.3 Results and discussion

7.3.1 Validation of the enzyme systems under study

Before any SERS analyses took place it was important to make sure that the succinate dehydrogenase assay using an artificial electron acceptor with visible spectrophotometry as detailed in Figure 7-1 & Figure 7-2 was functioning. Therefore as detailed above a series of positive and negative controls were conducted. The positive controls included varying the volume of the mitochondria preparation used (0.3, 0.6 or 0.9 mL), whilst the negative controls included not having any succinate substrate present or any sodium azide inhibitor. In addition, malonic acid was added with succinic acid in the reaction mixture as malonate is a competitive inhibitor for succinate dehydrogenase.

The results of these preliminary experiments are shown in Figure 7-4 where the absorbance of DCPIP at 600 nm is plotted against reaction time. It can be seen that there was no enzyme reaction measured in the negative control that contained no succinic acid substrate (symbols = pluses) as the slope of the time reaction is more or less flat. This slope was also very close to the reaction that contained malonic acid which inhibited the succinate dehydrogenase enzyme (downward pointing triangles). The reaction mixture containing no

sodium azide (diamonds) still allowed some of the DCPIP to become reduced as this artificial electron acceptor likely accepted excessive electrons generated from the electron transport chain; the slope of this line was identical to the reaction mixture with 0.3 mL of mitochondria preparation, which suggests that the concentration of succinate dehydrogenase in this preparation was too low. By contrast, when the volume of mitochondria preparation was increased to 0.6 mL (upward pointing triangles) and 0.9 mL (circles) the slope decreased further showing that the enzyme reaction was faster as more enzyme was used. From these experiments we decided that as the enzyme reaction occurred fastest with 0.9 mL of mitochondria preparation this was to be used for the SERS experiments.

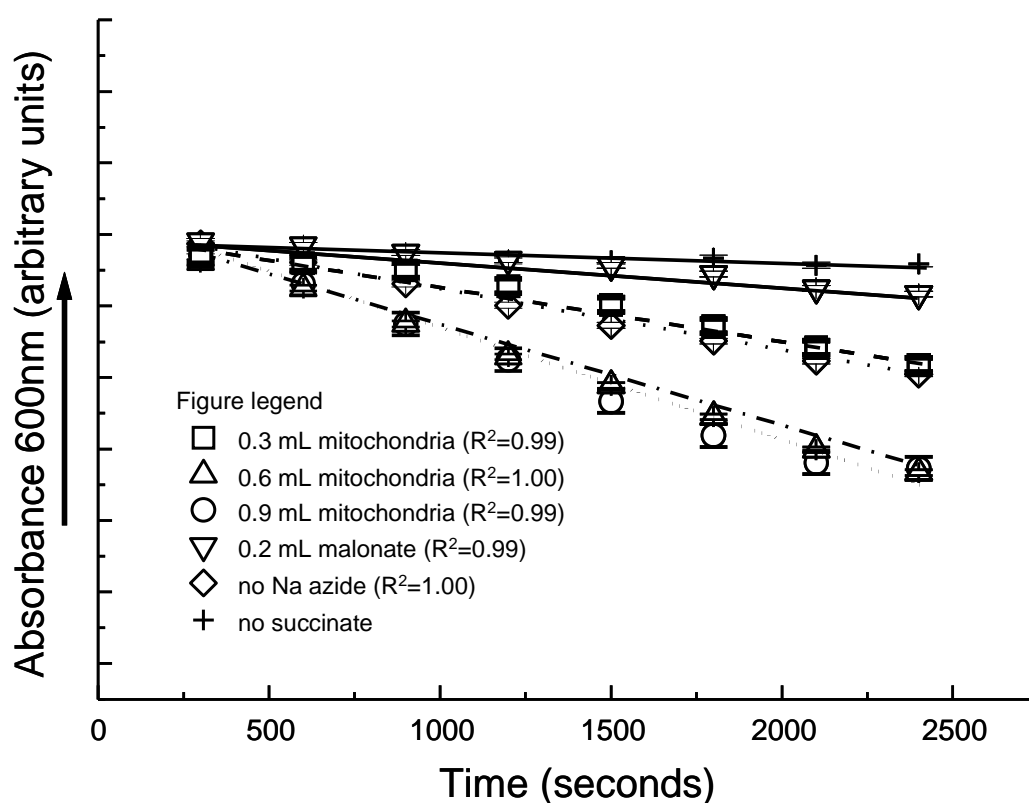


Figure 7-4: Graph representing the kinetic experiments (DCPIPox \rightarrow DCPIPred) monitored spectrophotometrically. The wavelength used for analysis is 600 nm. From the top to bottom are the controls employed to assay the enzyme activity; see text for full details. Correlations coefficients (R^2) are also shown in the inset.

7.3.2 SERS optimisation

The Raman spectrum of powdered samples of DCPIP collected with an integration time of 10 s using full laser power (300 mW) is shown in Figure 7-5 and this an information-rich spectrum contains plenty of molecular vibrations. However, whilst solution state spectra of DCPIP could also be collected at high concentrations, the signal was very low at $3.3 \times 10^{-5} \text{ mol dm}^{-3}$ (data not shown) which was the concentration used in the enzyme reaction (*vide supra*), therefore without very long collection times SERS would need to be employed.

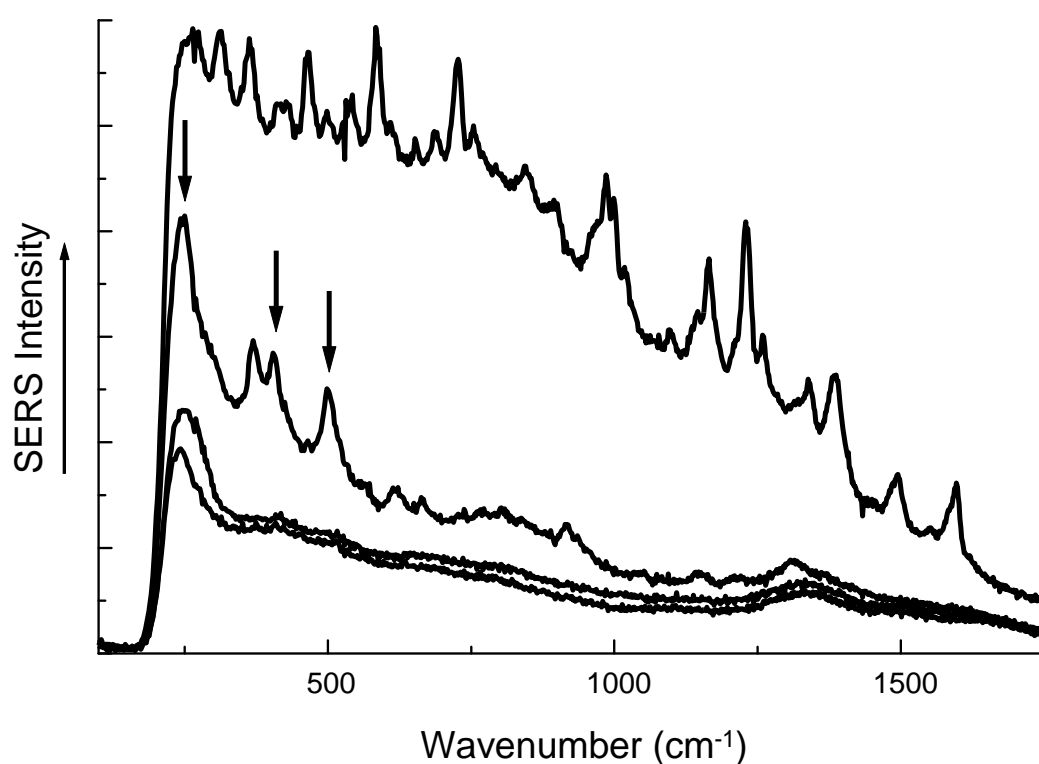


Figure 7-5: Representative raw Raman and SERS spectra, from top to bottom: Raman spectra of DCPIP in the solid state; followed by SERS spectra collected after 5 min aggregation at pH 7.2, pH 5.5 and pH 2.2 respectively. The three vibrational bands from SERS that were used for kinetic analysis are indicated by arrows and these are at 243, 404 and 498 cm^{-1} .

One advantage of SERS is that intense Raman signals enable analyte concentrations well below monolayer coverage of the (gold) sol to be readily examined. Since aggregation is essential for obtaining enhanced intensities, control of the aggregation process has to be achieved if SERS is to be used. Based on previous studies (Shadi et al., 2009) we decided to

use poly L-lysine, which contains both positive and negative charged groups as well as HCl (which maintains an acidic environment), as this combination provides a less dynamic and thus more controllable aggregation procedure (Sirlin et al., 1990).

For optimisation of the SERS signal a dilute solution of the dye (150 μL ; resulting in a final concentration of $3.3 \times 10^{-5} \text{ mol dm}^{-3}$) was added to an aliquot of gold sol (1 mL) diluted with 1 mL of H_2O to which was added 150 μL poly-L-lysine (0.01 %) and either HCl or KOH to achieve the optimum solution pH. After this induction of colloid aggregation with poly-L-lysine, subsequent collection of SERS occurred after 5 min. Unfortunately, the spectra collected did not reveal vibrational bands attributed to DCPIP regardless of whether we increased further aggregation time or investigating other pH conditions. It therefore appeared that the addition of poly-L-lysine prevented collection of SERS spectra.

A subsequent set of experiments in the absence of poly-L-lysine were conducted as described above. The pH conditions that were tested included pH 7.2, pH 5.5 and pH 2.2 and the resultant SERS spectra of $3.3 \times 10^{-5} \text{ mol dm}^{-3}$ DCPIP collected with an integration time of 10 s using full laser power (300 mW) are shown in Figure 7-5. It can be seen in this figure that the best SERS spectrum (in terms of vibrational features) was when the pH of the aggregating reaction was conducted at pH 7.2, with very few discernible features were obtained from DCPIP under acidic conditions other than gold sol band at $\sim 250 \text{ cm}^{-1}$.

7.3.3 Monitoring succinate dehydrogenase activity using SERS

Despite the above pH optimisation, for monitoring the reduction of DCPIP by electron transfer the SERS aggregation was still assessed at the three different pH conditions as the dye could exist in either the protonated or deprotonated forms (see Figure 7-1 for the structure of DCPIP).

For SERS analysis at pH 5.5 (the natural pH of the aggregating reaction) no vibrational bands could be seen, with the exception of the sol band at 238 cm^{-1} (Figure 7-6A) and it was

therefore not surprising that no enzyme activity could be observed by plotting the intensity of this band against time at this pH (Figure 7-6B). When the experiment was repeated and the pH adjusted to 2.2 (Figure 7-6C) a direct correlation could be seen between the data acquired using UV/Vis (Figure 7-5) and SERS with the disadvantage that only the sol vibrational band at 257 cm^{-1} was suitable for analysis of enzyme activity by SERS. A plot of SERS peak area *versus* time (Figure 7-6D) provided a good correlation coefficient ($R^2=0.983$), but this is likely to be impractical as no spectral features from DCPIP were involved in this correlation.

By contrast, by adjusting the pH to 7.2 the most marked SERS effect was observed which resulted in strong vibrational bands (Figure 7-6E) where the bands at 243, 404 and 498 cm^{-1} could be used for quantitative analysis (Figure 7-6F) providing good correlation coefficients of 0.952, 0.976 and 0.939, respectively. In addition, whilst these fits are calculated from linear regression it is clear from Figure 7-6F that as expected the enzyme kinetics measured are not really linear and are decaying as a function of time as the succinate substrate is being converted into the product fumarate (Figure 7-2).

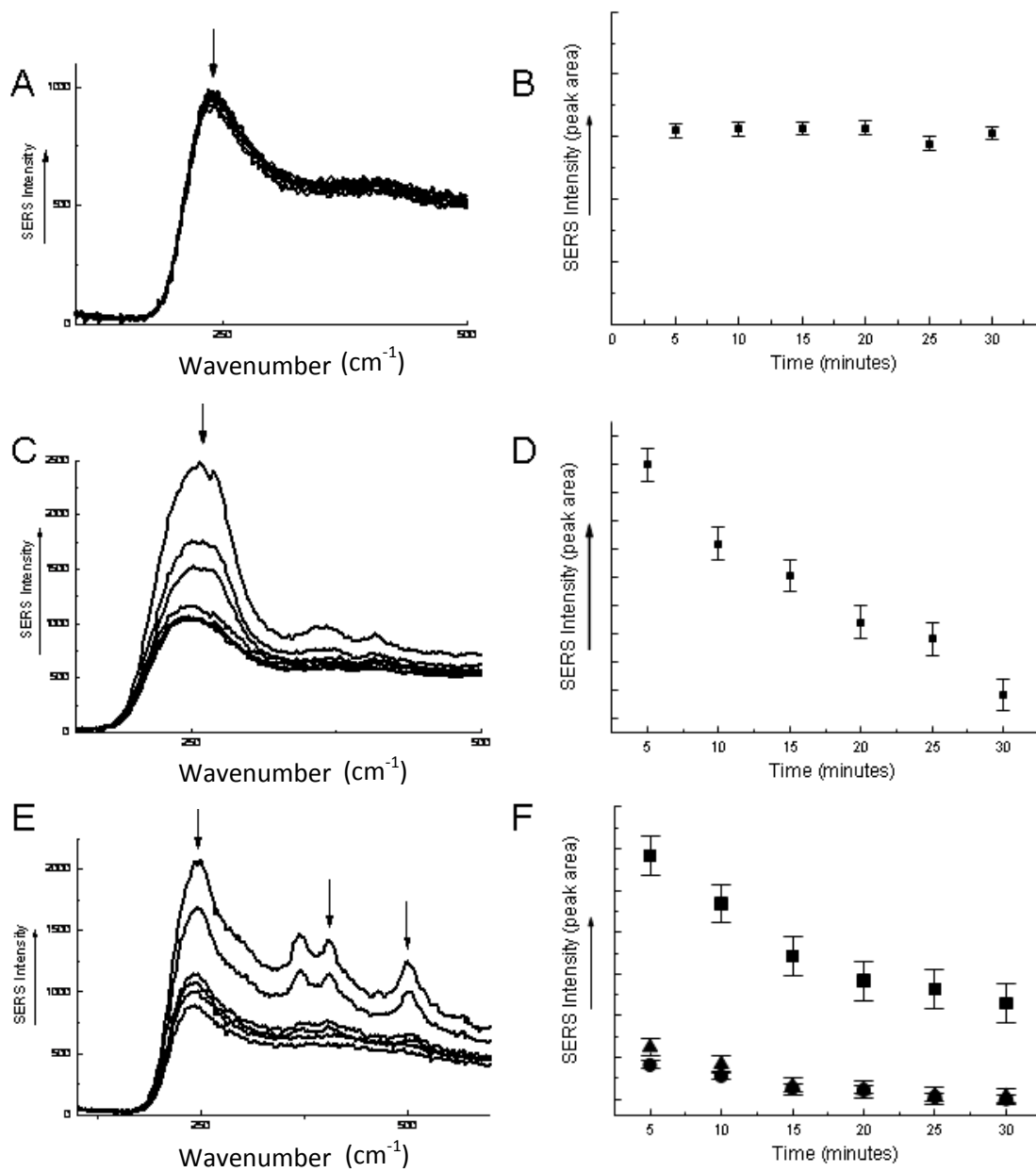


Figure 7-6: SERS spectra of the succinate dehydrogenase enzyme reaction. Aggregation was performed without poly L-lysine at (A) pH 5.5, (C) pH 2.2 and (E) pH 7.2 - from top to bottom the spectra shown were collected after 5, 10, 15, 20, 25 and 30 min of enzyme reaction. Plots of \log_{10} peak area *versus* time for the vibrational bands at (B) 238 cm⁻¹ for measurements conducted at pH 5.5, (D) 257 cm⁻¹ ($R^2 = 0.983$) for SERS at pH 2.2, and (F) for readings at pH 7.2 for bands 243, 404 and 498 cm⁻¹ ($R^2 = 0.952, 0.976$ and 0.939 , respectively); error bars show standard deviations from the three replicate measurements.

An interesting physical chemistry observation relates to the quantitative decrease in the peak areas of the SERS vibrational bands vs. time when comparison is made of the two experiments conducted at acid and neutral pH (pH 2.2 and 7.2) see Figure 7-6D and Figure 7-6E. These data potentially suggest that two forms of the dye, protonated and deprotonated, are present, and this is feasible when the structure of DCPIP is inspected (see Figure 7-1). It can be hypothesized that the decrease in intensity (peak area) of the “sol” bands, as a function of time, for SERS experiments conducted at pH 2.2 and 7.2 (*viz.*, 257 and 243 cm^{-1} respectively) may be due to the packing effects of either competing species of DCPIP or artefacts of enzyme activity competing for the surface sites on gold. Packing effects (excess of monolayer coverage) on the surface would almost certainly decrease the signal intensity and at the start of the enzymatic reaction the DCPIP concentration is $3.3 \times 10^{-5} \text{ mol dm}^{-3}$. Successive layers of molecules on the surface of the nanoparticles would most likely be a contributory factor and appear to be the logical reason for the results observed; e.g., an excess of monolayer coverage is being observed as enzyme activity proceeds. The effect of packing effects when collecting SERS spectra have been reported and this is a similar phenomenon that was observed in a separate study where it was shown that an excess of monolayer coverage led to a proportional decrease in signal intensity (Shadi et al., 2001). Close inspection of the two sol bands for pH 2.2 (Figure 7-6D) and pH 7.2 (Figure 7-6F) show that the reduction of this band at pH 2.2 is linear, which would support the above packing hypothesis. By contrast, at pH 7.2 the decrease is non-linear which shows that packing is not occurring and follows the classic enzyme kinetic reactions; due to depletion of substrate as detailed above. An observation that is also observed during the conversion of DCPIP from its oxidised to reduced forms for the other two peaks at 404 and 498 cm^{-1} (Figure 7-6D). These bands certainly arise from the DCPIP molecule itself and are possibly from C-Cl stretches (498 cm^{-1}) and skeletal vibrations (404 cm^{-1}) (Degan, 1997) and

the additional small intensity band at *ca.* 800 cm⁻¹ (Figure 7-5) originates from ring breathing (Degan, 1997) further highlighting that the reporter molecule itself is being measured.

7.4 Concluding remarks

The main objective of this work was to monitor a metabolic pathway utilising SERS as the reporting tool. For the first time a widely studied pathway, the kinetics of succinate dehydrogenase activity, is reported employing Raman spectroscopy to monitor this enzyme activity using a SERS reporter dye as a model system probe. The data reported clearly show a direct correlation between acquisition of SERS spectra at specific time intervals and that obtained using classical spectrophotometric techniques. Very good correlations were observed for quantitative analysis as the reaction proceeded and the SERS aggregation protocol developed was pH dependent. In the future we plan to investigate the multiplexing of SERS where different reporter molecules are used which are 'tuned' into different metabolic processes, as detailed for DNA sequence detection by Graham, Faulds and colleagues (Graham et al., 2002, Faulds et al., 2007, MacAskill et al., 2009). In conclusion, we believe that SERS has considerable potential for being applied to the analysis of metabolic processes, and to our knowledge this is the first study of a metabolic pathway that has been monitored by SERS.

Chapter 8: Overall Summary and Conclusions

The aim of the work undertaken in this course of research was to incorporate the use of bio-analytical techniques into dermatology research. It is common place that patients who are suffering from skin disorders are diagnosed and the extent of the disease assessed by a dermatologist and hence an element of subjective human error can be involved. This is extremely prevalent when you consider the PASI scoring system for psoriasis as described in Chapter 6: and the importance associated with the complete removal of a keloid scar in keloid patients undergoing surgery (Chapter 3:). The availability and application of methods to screen patients and hence potentially quantify the level of disease or response to treatment could provide beneficial routes in disease management.

The application of these bio-analytical approaches began with an attempt to analyse human skin biopsy samples from psoriatic patients using MALDI-MS. Whilst this technique has been regularly utilised for the imaging of intact tissue, when applied to skin tissue the results were disappointing. Although it was possible to gain some mass spectra of sufficient quality, the reproducibility of the method was poor. It was common that a good spectrum would be neighboured by mass spectra of poor signal-to-noise and minimal peak presence. The reason for these poor results is as yet unknown and personal communication with Prof. Ron Heeren confirmed that similar problems associated with imaging skin are occurring in other MALDI-MS laboratories. Perhaps in the future this method may be applicable for the study of skin disorders through further development of the technique.

FT-IR microspectroscopy was the next approach to be applied to the analysis of skin samples. In this study the technique was used for the analysis of keloid scars which had been surgically excised from patients with keloid disease. The major advantage of analysing keloid sections is the unique morphology of the sample. Upon excision it is common that the

surgeon will remove the surrounding normal tissue in an attempt to prolong the time taken for the keloid tumour to return. The samples that were available therefore contained both normal and diseased areas in the same section, thus eliminating inter-sample variation often incorporated when using control samples. On a case to case basis it was possible through PCA to discriminate between normal and keloid areas successfully using FT-IR microscopy. Through the application of PLS-DA it was possible to further validate this result to include 100 spectra collected from a collection of patients and sample locations. This model gave a positive result which can suggest that FT-IR spectroscopy could be readily used to discriminate between keloid and normal tissue and has potential to be transferable to other skin conditions. Furthermore the method of FT-IR imaging was applied to a keloid sample; by collating 14 individual FT-IR images it was possible to investigate the cellular composition and variation in keloid skin and the surrounding tissue. This method illustrated the complex cellular composition present within a keloid scar, with increased lipid, amide and phosphate levels being observed. This measurable variation could, in the future, be incorporated into surgical procedures to allow targeted excision ensuring all keloid areas were removed.

In an alternative approach the response of HaCaT cells upon exposure to three anti-psoriatic drugs was investigated. The response was probed by the analysis of the internal and external metabolome and the internal proteome of the cells. The use of a metabolomic and proteomic approach allowed for the holistic, high-throughput analysis of a wide array of metabolites and proteins. The metabolome analysis was particularly successful for the analysis of dithranol treated cells. In this analysis a vast number of metabolites were deemed to be significantly affected upon drug exposure. It was possible to reconstruct a metabolite map which began to depict the biological effect of the drug. It became clear that the drug was successfully targeting principal pathways in central metabolism including glycolysis and the TCA cycle. In addition, the concentrations of a number of amino acids were significantly altered by dithranol which implies that growth metabolism is an

additional/connected target. This method was successful in highlighting a number of metabolites which could potentially be used as indicators of successful treatment. It was however relatively disappointing that the results gained for methotrexate and ciclosporin treatment failed to provide significant insight into the exposure targets. This was attributed to the mode of action of these drugs and highlights that although metabolomics is a powerful method of analysis its application can in some cases be limited.

The complementary qualitative proteomic analysis also provided useful information regarding the mode of action of these anti-psoriatic drugs. The development of a scoring system assessing the presence or absence of a protein allowed for a semi-quantitative approach which identified proteins as up-regulated, down-regulated or unaffected by treatment. A number of enzymes from central metabolism were identified within the proteome of HaCaT cells exposed to dithranol, methotrexate and ciclosporin. Dithranol was found to have a greater pronounced affect on the enzymes of central metabolism. A down-regulation of enzymes located within glycolysis and the TCA was noted which correlated well with the previous results from metabolome analysis. In addition, vast arrays of proteins which are not primarily associated with central metabolism were identified within the proteome of HaCaT cells exposed to the drugs. The findings varied greatly from drug to drug therefore suggesting varying modes of action. The analysis highlighted a number of novel proteins which have previously not been linked to anti-psoriatic treatment methods which could, with further quantitative validation prove to be novel biomarkers of successful treatment.

The investigation of methotrexate treated cells utilising both a metabolomic and proteomic approach was somewhat hindered by the mechanism of action of the drug; i.e., acting as an immunosuppressant. Therefore when the opportunity arose to analyse a number of plasma samples from patients undergoing methotrexate treatment a further metabolomic-based

analysis was conducted. This study was not without its limitations and the experimental design was not optimal for metabolomic profiling. In particular a vast amount of metadata was unavailable including BMI and age and there was no regulation of diet prior to sample collection. It was not possible to discriminate between responders and non-responders using PCA however a collection of metabolites were deemed to be significant using Kruskal-Wallis analysis. These metabolites could potentially be used as indicators of response; however these results would require significant validation in a larger and more strictly controlled study. Interestingly, in addition to these indicators of response it was also possible to identify metabolites correlated to gender of patient. Ultimately this study was useful to demonstrate the importance of experimental design but also illustrated the successful technique of plasma analysis in a metabolomics-based analysis.

The final approach adopted in this thesis was to investigate the dynamic enzymatic succinate dehydrogenase reaction using SERS as a reporting tool. The enzyme is responsible for catalyzing the oxidation of succinate to fumarate in the TCA cycle of metabolism, an area which has been highlighted in the metabolomic and proteomic investigations previously discussed. The data reported clearly indicates a direct correlation between acquisition of SERS spectra at specific time intervals and that obtained using classical UV-VIS spectrophotometric techniques. The success of this experiment could imply that further enzymatic reactions could be tracked utilising SERS with a variety of different reporter molecules. This approach would be a beneficial addition to the analysis of metabolic process.

This project has successfully used a number of bio-analytical techniques to investigate dermatological problems. While the ultimate goal would be the application of a single analytical technique to provide answers to biological questions, it has been found that a number of complementary techniques and statistical data handling approaches can provide a valuable insight into the problems posed.

Chapter 9: References

- AEBERSOLD, R. & MANN, M. (2003) Mass spectrometry-based proteomics. *Nature*, 422, 198-207.
- ALLWOOD, J. W., ELLIS, D. I. & GOODACRE, R. (2008) Biomarker metabolites capturing the metabolite variance present in a rice plant developmental period. *Physiologia Plantarum*, 132, 117-135.
- ALLWOOD, J. W. & GOODACRE, R. (2010) An Introduction to Liquid Chromatography-Mass Spectrometry Instrumentation Applied in Plant Metabolomic Analyses. *Phytochemical Analysis*, 21, 33-47.
- ALTMAN, E. M. & KAMINO, H. (1999) Diagnosis: Psoriasis or not? What are the clues? *Seminars in Cutaneous Medicine and Surgery*, 18, 25-35.
- ANDANSON, J. M., HADGRAFT, J. & KAZARIAN, S. G. (2009) In situ permeation study of drug through the stratum corneum using attenuated total reflection Fourier transform infrared spectroscopic imaging. *Journal of Biomedical Optics*, 14, 8.
- BAILO, E. & DECKERT, V. (2008) Tip-enhanced Raman scattering. *Chemical Society Reviews*, 37, 921-930.
- BARWISE, J. L. & WALKER, J. H. (1996) Annexins II, IV, V and VI relocate in response to rises in intracellular calcium in human foreskin fibroblasts. *Journal of Cell Science*, 109, 247-255.
- BASTIAN, B. C., VAN DER PIEPEN, U., ROEMISCH, J., PAQUES, E.-P. & BROECKER, E.-B. (1993) Localization of annexins in normal and diseased human skin. *Journal of Dermatological Science*, 6, 225-234.
- BAYAT, A., ARSCOTT, G., OLLIER, W. E. R., FERGUSON, M. W. J. & MC GROUTHER, D. A. (2004) Description of site-specific morphology of keloid phenotypes in an Afrocaribbean population. *British Journal of Plastic Surgery*, 57, 122-133.
- BAYAT, A., ARSCOTT, G., OLLIER, W. E. R., MC GROUTHER, D. A. & FERGUSON, M. W. J. (2005) Keloid disease: clinical relevance of single versus multiple site scars. *British Journal of Plastic Surgery*, 58, 28-37.
- BAYAT, A. & MCGROUTHER, D. A. (2005) Clinical management of skin scarring. *Skinmed*, 4, 165-73.
- BAYAT, A. & MCGROUTHER, D. A. (2006) Spectrum of abnormal skin scars and their clinical management. *British Journal of Hospital Medicine*, 67, 527-532.
- BAYAT, A., MCGROUTHER, D. A. & FERGUSON, M. W. J. (2003) Skin scarring. *British Medical Journal*, 326, 88-92.
- BEAUSANG, E., FLOYD, H., DUNN, K. W., ORTON, C. I. & FERGUSON, M. W. J. (1998) A new quantitative scale for clinical scar assessment. *Plastic and Reconstructive Surgery*, 102, 1954-1961.
- BEGLEY, P., FRANCIS-MCINTYRE, S., DUNN, W. B., BROADHURST, D. I., HALSALL, A., TSENG, A., KNOWLES, J., GOODACRE, R., KELL, D. B. & CONSORTIUM, H. (2009) Development and Performance of a Gas Chromatography-Time-of-Flight Mass Spectrometry Analysis for Large-Scale Nontargeted Metabolomic Studies of Human Serum. *Analytical Chemistry*, 81, 7038-7046.
- BELSO, N., SZELL, M., PIVARCSI, A., KIS, K., KORMOS, B., KENDERESSY, A. S., DOBOZY, A., KEMENY, L. & BATA-CSORGO, Z. (2007) Differential Expression of D-Type Cyclins in HaCaT Keratinocytes and in Psoriasis. *J Invest Dermatol*, 128, 634-642.
- BERNARD, G., AUGER, M., SOUCY, J. & POULIOT, R. (2007) Physical characterization of the stratum corneum of an in vitro psoriatic skin model by ATR-FTIR and Raman spectroscopies. *Biochimica Et Biophysica Acta-General Subjects*, 1770, 1317-1323.
- BERTH-JONES, J. (2005) The use of ciclosporin in psoriasis. *Journal of Dermatological Treatment*, 16, 258-277.

- BHALERAO, J. & BOWCOCK, A. M. (1998) The genetics of psoriasis: a complex disorder of the skin and immune system. *Human Molecular Genetics*, 7, 1537-1545.
- BOEHNCKE, S., THACI, D., BESCHMANN, H., LUDWIG, R. J., ACKERMANN, H., BADENHOOP, K. & BOEHNCKE, W. H. (2007) Psoriasis patients show signs of insulin resistance. *British Journal of Dermatology*, 157, 1249-1251.
- BOGDANOV, M., MATSON, W. R., WANG, L., MATSON, T., SAUNDERS-PULLMAN, R., BRESSMAN, S. S. & BEAL, M. F. (2008) Metabolomic profiling to develop blood biomarkers for Parkinson's disease. *Brain*, 131, 389-396.
- BOS, J. D. & SPULS, P. I. (2008) Topical treatments in psoriasis: today and tomorrow. *Clinics in Dermatology*, 26, 432-437.
- BOUKAMP, P., PETRUSSEVSKA, R. T., BREITKREUTZ, D., HORNING, J., MARKHAM, A. & FUSENIG, N. E. (1988) NORMAL KERATINIZATION IN A SPONTANEOUSLY IMMORTALIZED ANEUPLOID HUMAN KERATINOCYTE CELL-LINE. *Journal of Cell Biology*, 106, 761-771.
- BOWCOCK, A. M. & KRUEGER, J. G. (2005) Getting under the skin: The immunogenetics of psoriasis. *Nature Reviews Immunology*, 5, 699-711.
- BRENELLI, S. L., MORAES, A. M., MONTEALEGRE, S., CARVALHO, O. M. F. & SAAD, M. J. A. (1995) Insulin-Resistance in Psoriasis. *Brazilian Journal of Medical and Biological Research*, 28, 297-301.
- BROADHURST, D. & KELL, D. B. (2006) Statistical strategies for avoiding false discoveries in metabolomics and related experiments. *Metabolomics*, 2, 171-196.
- BROOME, A. M. & ECKERT, R. L. (2004) Microtubule-dependent redistribution of a cytoplasmic cornified envelope precursor. *Journal of Investigative Dermatology*, 122, 29-38.
- BROOME, A. M., RYAN, D. & ECKERT, R. L. (2003) S100 protein subcellular localization during epidermal differentiation and psoriasis. *Journal of Histochemistry & Cytochemistry*, 51, 675-685.
- BROWN, B. C., MCKENNA, S. P., SIDDHI, K., MCGROUTHER, D. A. & BAYAT, A. (2008) The hidden cost of skin scars: quality of life after skin scarring. *Journal of Plastic Reconstructive and Aesthetic Surgery*, 61, 1049-1058.
- BROWN, J. J. & BAYAT, A. (2009) Genetic susceptibility to raised dermal scarring. *British Journal of Dermatology*, 161, 8-18.
- BROWN, M., DUNN, W. B., DOBSON, P., PATEL, Y., WINDER, C. L., FRANCIS-MCINTYRE, S., BEGLEY, P., CARROLL, K., BROADHURST, D., TSENG, A., SWAINSTON, N., SPASIC, I., GOODACRE, R. & KELL, D. B. (2009) Mass spectrometry tools and metabolite-specific databases for molecular identification in metabolomics. *Analyst*, 134, 1322-1332.
- CAPRIOLI, R. M., FARMER, T. B. & GILE, J. (1997) Molecular imaging of biological samples: Localization of peptides and proteins using MALDI-TOF MS. *Analytical Chemistry*, 69, 4751-4760.
- CHAUDRY, M. A., AMIN, S. & MALIK, M. T. (1996) Tri-n-octylamine-xylene-based supported liquid membranes and transport of Ce(IV) ions. *Separation Science and Technology*, 31, 1309-1326.
- CHAURAND, P., STOECKLI, M. & CAPRIOLI, R. M. (1999) Direct profiling of proteins in biological tissue sections by MALDI mass spectrometry. *Analytical Chemistry*, 71, 5263-5270.
- CHOI, J. H., OCONNOR, T. P., KANG, S., VOORHEES, J. J. & FISHER, G. J. (1997) Activation of ribosomal protein S6 kinase in psoriatic lesions and cultured human keratinocytes by epidermal growth factor receptor ligands. *Journal of Investigative Dermatology*, 108, 98-102.

- COGHLIN, C., CARPENTER, B., DUNDAS, S. R., LAWRIE, L. C., TELFER, C. & MURRAY, G. I. (2006) Characterization and over-expression of chaperonin t-complex proteins in colorectal cancer. *Journal of Pathology*, 210, 351-357.
- COHEN, A. D., DREIHER, J. & BIRKENFELD, S. (2009) Psoriasis associated with ulcerative colitis and Crohn's disease. *Journal of the European Academy of Dermatology and Venereology*, 23, 561-565.
- CONSTANTIN, B., MEERSCHAERT, K., VANDEKERCKHOVE, J. & GETTEMANS, J. (1998) Disruption of the actin cytoskeleton of mammalian cells by the capping complex actin-fragmin is inhibited by actin phosphorylation and regulated by Ca²⁺ ions. *Journal of Cell Science*, 111, 1695-1706.
- CUMBERBATCH, M., SINGH, M., DEARMAN, R. J., YOUNG, H. S., KIMBER, I. & GRIFFITHS, C. E. M. (2006) Impaired Langerhans cell migration in psoriasis. *Journal of Experimental Medicine*, 203, 953-960.
- DARMAUN, D., MATTHEWS, D. E., DESJEUX, J. F. & BIER, D. M. (1988) GLUTAMINE AND GLUTAMATE NITROGEN EXCHANGEABLE POOLS IN CULTURED FIBROBLASTS - A STABLE ISOTOPE STUDY. *Journal of Cellular Physiology*, 134, 143-148.
- DAUTRY, C., CONDE, F., BROUILLET, E., MITTOUX, V., BEAL, M. F., BLOCH, G. & HANTRAYE, P. (1999) Serial 1H-NMR spectroscopy study of metabolic impairment in primates chronically treated with the succinate dehydrogenase inhibitor 3-nitropropionic acid. *Neurobiology of Disease*, 6, 259-268.
- DEGAN, I. A. (1997) *Tables of characteristic group frequencies for the interpretation of infrared and Raman spectra*, Acolyte Publications.
- DUNN, W. B. (2008) Current trends and future requirements for the mass spectrometric investigation of microbial, mammalian and plant metabolomes. *Physical Biology*, 5.
- DUNN, W. B., BAILEY, N. J. C. & JOHNSON, H. E. (2005) Measuring the metabolome: current analytical technologies. *Analyst*, 130, 606-625.
- DUNN, W. B., BROADHURST, D., BROWN, M., BAKER, P. N., REDMAN, C. W. G., KENNY, L. C. & KELL, D. B. (2008) Metabolic profiling of serum using Ultra Performance Liquid Chromatography and the LTQ-Orbitrap mass spectrometry system. *Journal of Chromatography B-Analytical Technologies in the Biomedical and Life Sciences*, 871, 288-298.
- DUNN, W. B. & ELLIS, D. I. (2005) Metabolomics: Current analytical platforms and methodologies. *Trac-Trends in Analytical Chemistry*, 24, 285-294.
- DURANI, P. & BAYAT, A. (2008) Levels of evidence for the treatment of keloid disease. *Journal of Plastic Reconstructive and Aesthetic Surgery*, 61, 4-17.
- DUVIC, M., NAGPAL, S., ASANO, A. T. & CHANDRARATNA, R. A. S. (1997) Molecular mechanisms of tazarotene action in psoriasis. *Journal of the American Academy of Dermatology*, 37, S18-S24.
- EBBELS, T. M. D., BUXTON, B. F. & JONES, D. T. (2006) springScape: visualisation of microarray and contextual bioinformatic data using spring embedding and an 'information landscape'. *Bioinformatics*, 22, E99-E107.
- ECKERT, R. L., BROOME, A. M., RUSE, M., ROBINSON, N., RYAN, D. & LEE, K. (2004) S100 proteins in the epidermis. *Journal of Investigative Dermatology*, 123, 23-33.
- EHRlich, H. P., ALLISON, G. M., PAGE, M. J., KOLTON, W. A. & GRAHAM, M. (2000) Increased gelsolin expression and retarded collagen lattice contraction with smooth muscle cells from Crohn's diseased intestine. *Journal of Cellular Physiology*, 182, 303-309.
- EL-ANEED, A., COHEN, A. & BANOUB, J. (2009) Mass Spectrometry, Review of the Basics: Electrospray, MALDI, and Commonly Used Mass Analyzers. *Applied Spectroscopy Reviews*, 44, 210-230.

- ELLIS, D. I., BROADHURST, D. & GOODACRE, R. (2004) Rapid and quantitative detection of the microbial spoilage of beef by Fourier transform infrared spectroscopy and machine learning. *Analytica Chimica Acta*, 514, 193-201.
- ELLIS, D. I., DUNN, W. B., GRIFFIN, J. L., ALLWOOD, J. W. & GOODACRE, R. (2007) Metabolic fingerprinting as a diagnostic tool. *Pharmacogenomics*, 8, 1243-1266.
- ELLIS, D. I. & GOODACRE, R. (2006) Metabolic fingerprinting in disease diagnosis: biomedical applications of infrared and Raman spectroscopy. *Analyst*, 131, 875-885.
- EXUM, M. L., RAPP, S. R., FELDMAN, S. R., FLEISCHER, A. B., REBOUSSIN, D. M. & CLARK, A. R. (1996) Measuring severity of psoriasis: Methodological issues. *Journal of Dermatological Treatment*, 7, 119-124.
- FABIAN, H., THI, N. A. N., EIDEN, M., LASCH, P., SCHMITT, J. & NAUMANN, D. (2006) Diagnosing benign and malignant lesions in breast tissue sections by using IR-microspectroscopy. *Biochimica et Biophysica acta. Biomembranes*, 1758, 874-882.
- FARKAS, A., KEMENY, L., SZONYI, B. J., BATA-CSORGO, Z., PIVARCSI, A., KISS, M., SZELL, M., KORECK, A. & DOBOZY, A. (2001) Dithranol upregulates IL-10 receptors on the cultured human keratinocyte cell line HaCaT. *Inflammation Research*, 50, 44-49.
- FAULDS, K., MCKENZIE, F., SMITH, W. E. & GRAHAM, D. (2007) Quantitative simultaneous multianalyte detection of DNA by dual-wavelength surface-enhanced resonance Raman scattering. *Angewandte Chemie-International Edition*, 46, 1829-1831.
- FELLENBERG, J., DECHANT, M. J., EWERBECK, V. & MAU, H. (2003) Identification of drug-regulated genes in osteosarcoma cells. *International Journal of Cancer*, 105, 636-643.
- FERNANDEZ, D. C., BHARGAVA, R., HEWITT, S. M. & LEVIN, I. W. (2005) Infrared spectroscopic imaging for histopathologic recognition. *Nature Biotechnology*, 23, 469-474.
- FERRARO, J. R. & NAKAMOTO, K. (1994) *Introductory Raman Spectroscopy*, London, Academic Press.
- FISHER, G. J., DUELL, E. A., NICKOLOFF, B. J., ANNESLEY, T. M., KOWALKE, J. K., ELLIS, C. N. & VOORHEES, J. J. (1988) LEVELS OF CYCLOSPORIN IN EPIDERMIS OF TREATED PSORIASIS PATIENTS DIFFERENTIALLY INHIBIT GROWTH OF KERATINOCYTES CULTURED IN SERUM FREE VERSUS SERUM CONTAINING MEDIA. *Journal of Investigative Dermatology*, 91, 142-146.
- FITZGERALD, O. & WINCHESTER, R. (2009) Psoriatic arthritis: from pathogenesis to therapy. *Arthritis Research & Therapy*, 11.
- FIUZA, C., BUSTIN, M., TALWAR, S., TROPEA, M., GERSTENBERGER, E., SHELHAMER, J. H. & SUFFREDINI, A. F. (2003) Inflammation-promoting activity of HMGB1 on human microvascular endothelial cells. *Blood*, 101, 2652-2660.
- FLYTSTROM, I., STENBERG, B., SVENSSON, A. & BERGBRANT, I. M. (2008) Methotrexate vs. ciclosporin in psoriasis: effectiveness, quality of life and safety. A randomized controlled trial. *British Journal of Dermatology*, 158, 116-121.
- FUCHS, J., NITSCHMANN, W. H. & PACKER, L. (1990) THE ANTIPSORIATIC COMPOUND ANTHRALIN INFLUENCES BIOENERGETIC PARAMETERS AND REDOX PROPERTIES OF ENERGY TRANSDUCING MEMBRANES. *Journal of Investigative Dermatology*, 94, 71-76.
- FUJIOKA, N., MORIMOTO, Y., ARAI, T. & KIKUCHI, M. (2004) Discrimination between normal and malignant human gastric tissues by Fourier transform infrared spectroscopy. *Cancer Detection and Prevention*, 28, 32-36.
- GAO, P., LU, C., ZHANG, F. X., SANG, P., YANG, D. W., LI, X., KONG, H. W., YIN, P. Y., TIAN, J., LU, X., LU, A. P. & XU, G. W. (2008) Integrated GC-MS and LC-MS plasma metabonomics analysis of ankylosing spondylitis. *Analyst*, 133, 1214-1220.

- GAZI, E., HARVEY, T. J., BROWN, M. D., LOCKYER, N. P., GARDNER, P. & CLARKE, N. W. (2009) A FTIR microspectroscopic study of the uptake and metabolism of isotopically labelled fatty acids by metastatic prostate cancer. *Vibrational Spectroscopy*, 50, 99-105.
- GIROLOMONI, G. & GISONDI, P. (2008) Psoriasis and metabolic comorbidities: The importance of well-designed prospective studies. *Dermatology*, 217, 222-224.
- GISONDI, P., FANTUZZI, F., MALERBA, M. & GIROLOMONI, G. (2007) Folic acid in general medicine and dermatology. *Journal of Dermatological Treatment*, 18, 138-146.
- GOLDSTEIN, A. M. (2003) Changing paradigms in dermatology: Proteomics: A new approach to skin disease. *Clinics in Dermatology*, 21, 370-374.
- GOODACRE, R. (2007) Metabolomics of a superorganism. *Journal of Nutrition*, 137, 259S-266S.
- GORG, A., WEISS, W. & DUNN, M. J. (2004) Current two-dimensional electrophoresis technology for proteomics. *Proteomics*, 4, 3665-3685.
- GOTTLIEB, A. B., CHAO, C. & DANN, F. (2008) Psoriasis comorbidities. *Journal of Dermatological Treatment*, 19, 5-21.
- GOTTLIEB, A. B. & DANN, F. (2009) Comorbidities in Patients with Psoriasis. *American Journal of Medicine*, 122, 9.
- GOURAUND, H. (1971) Continuous shading of curved surfaces. *IEEE Trans Computers*, C-20, 623-629.
- GRAHAM, D. & FAULDS, K. (2008) Quantitative SERRS for DNA sequence analysis. *Chemical Society Reviews*, 37, 1042-1051.
- GRAHAM, D., MALLINDER, B. J., WHITCOMBE, D., WATSON, N. D. & SMITH, W. E. (2002) Simple multiplex genotyping by surface-enhanced resonance Raman scattering. *Analytical Chemistry*, 74, 1069-+.
- GRIFFITHS, C. E. M. & BARKER, J. (2007) Psoriasis 1 - Pathogenesis and clinical features of psoriasis. *Lancet*, 370, 263-271.
- HAMMAR, H. (1975) EPIDERMAL NICOTINAMIDE ADENINE DINUCLEOTIDES IN PSORIASIS DURING TREATMENT WITH DITHRANOL. *Archiv Fur Dermatologische Forschung*, 252, 229-236.
- HANH, B. D., NEUBERT, R. H. H., WARTEWIG, S., CHRIST, A. & HENTZSCH, C. (2000) Drug penetration as studied by noninvasive methods: Fourier transform infrared-attenuated total reflection, Fourier transform infrared, and ultraviolet photoacoustic spectroscopy. *Journal of Pharmaceutical Sciences*, 89, 1106-1113.
- HARDMAN, M. & MAKAROV, A. A. (2003) Interfacing the orbitrap mass analyzer to an electrospray ion source. *Analytical Chemistry*, 75, 1699-1705.
- HENSELER, T. & CHRISTOPHERS, E. (1995) Disease Concomitance in Psoriasis. *Journal of the American Academy of Dermatology*, 32, 982-986.
- HOLLANDER, M. & WOLFE, D. A. (1999) *Nonparametric Statistical Methods*, Hoboken, NJ, John Wiley & Sons.
- HOLLYWOOD, K., BRISON, D. R. & GOODACRE, R. (2006) Metabolomics: current technologies and future trends. *Proteomics*, 6, 4716-4723.
- HUNT, D. F., HENDERSON, R. A., SHABANOWITZ, J., SAKAGUCHI, K., MICHEL, H., SEVILIR, N., COX, A. L., APPELLA, E. & ENGELHARD, V. H. (1992) CHARACTERIZATION OF PEPTIDES BOUND TO THE CLASS-I MHC MOLECULE HLA-A2.1 BY MASS-SPECTROMETRY. *Science*, 255, 1261-1263.
- INGRAM, A., BYERS, L., FAULDS, K., MOORE, B. D. & GRAHAM, D. (2008) SERRS-based enzymatic probes for the detection of protease activity. *Journal of the American Chemical Society*, 130, 11846-11847.
- JARVIS, R. M. & GOODACRE, R. (2008) Characterisation and identification of bacteria using SERS. *Chemical Society Reviews*, 37, 931-936.

- JOLLIFFE, I. T. (1986) *Principal Component Analysis*, New York, Springer-Verlag.
- JONES (2000) Serum creatinine levels in the US population: Third national health and nutrition examination survey (vol 32, pg 992, 1998). *American Journal of Kidney Diseases*, 35, 178-178.
- KADDURAH-DAOUK, R., MCEVOY, J., BAILLIE, R. A., LEE, D., YAO, J. K., DORAISWAMY, P. M. & KRISHNAN, K. R. R. (2007) Metabolomic mapping of atypical antipsychotic effects in schizophrenia. *Molecular Psychiatry*, 12, 934-945.
- KALB, R. E., STROBER, B., WEINSTEIN, G. & LEBWOHL, M. (2009) Methotrexate and psoriasis: 2009 National Psoriasis Foundation Consensus Conference. *Journal of the American Academy of Dermatology*, 60, 824-837.
- KALTWASSER, J. P., NASH, P., GLADMAN, D., ROSEN, C. F., BEHRENS, F., JONES, P., WOLLENHAUPT, J., FALK, F. G. & MEASE, P. (2004) Efficacy and safety of leflunomide in the treatment of psoriatic arthritis and psoriasis - A multinational, double-blind, randomized, placebo-controlled clinical trial. *Arthritis and Rheumatism*, 50, 1939-1950.
- KANITAKIS, J. & THIVOLET, J. (1990) CYCLOSPORINE - AN IMMUNOSUPPRESSANT AFFECTING EPITHELIAL-CELL PROLIFERATION. *Archives of Dermatology*, 126, 369-375.
- KARAS, M., BACHMANN, D., BAHR, U. & HILLENKAMP, F. (1987) MATRIX-ASSISTED ULTRAVIOLET-LASER DESORPTION OF NONVOLATILE COMPOUNDS. *International Journal of Mass Spectrometry and Ion Processes*, 78, 53-68.
- KELL, D. B. & OLIVER, S. G. (2004) Here is the evidence, now what is the hypothesis? The complementary roles of inductive and hypothesis-driven science in the post-genomic era. *Bioessays*, 26, 99-105.
- KENNY, L. C., BROADHURST, D., BROWN, M., DUNN, W. B., REDMAN, C. W. G., KILL, D. B. & BAKER, P. N. (2008) Detection and identification of novel metabolomic biomarkers in preeclampsia. *Reproductive Sciences*, 15, 591-597.
- KENNY, L. C., DUNN, W. B., ELLIS, D. I., MYERS, J., BAKER, P. N. & KELL, D. B. (2005) Novel biomarkers for pre-eclampsia detected using metabolomics and machine learning. *Metabolomics*, 1, 227-234.
- KNEIPP, K., KNEIPP, H., ITZKAN, I., DASARI, R. R., FELD, M. S. & DRESSELHAUS, M. S. (2002) Nonlinear Raman probe of single molecules attached to colloidal silver and gold clusters. *Optical Properties of Nanostructured Random Media*, 82, 227-247.
- KOCHHAR, S., JACOBS, D. M., RAMADAN, Z., BERRUX, F., FUERHOZ, A. & FAY, L. B. (2006) Probing gender-specific metabolism differences in humans by nuclear magnetic resonance-based metabolomics. *Analytical Biochemistry*, 352, 274-281.
- KOCZAN, D., GUTHKE, R., THIESEN, H. J., IBRAHIM, S. M., KUNDT, G., KRENTZ, H., GROSS, G. & KUNZ, M. (2005) Gene expression profiling of peripheral blood mononuclear leukocytes from psoriasis patients identifies new immune regulatory molecules. *European Journal of Dermatology*, 15, 251-257.
- KRIS, G. & JOËL, V. (2000) Protein identification methods in proteomics. *Electrophoresis*, 21, 1145-1154.
- KRISHNA, C. M., SOCKALINGUM, G. D., BHAT, R. A., VENDEO, L., KUSHTAGI, P., PLUOT, M. & MANFAIT, M. (2007) FTIR and Raman microspectroscopy of normal, benign, and malignant formalin-fixed ovarian tissues. *Analytical and Bioanalytical Chemistry*, 387, 1649-1656.
- KRUEGER, G., KOO, J., LEBWOHL, M., MENTER, A., STERN, R. S. & ROLSTAD, T. (2001) The impact of psoriasis on quality of life - Results of a 1998 National Psoriasis Foundation Patient-Membership Survey. *Archives of Dermatology*, 137, 280-284.
- KRUEGER, J. G. & BOWCOCK, A. (2005) Psoriasis pathophysiology: current concepts of pathogenesis. *Annals of the Rheumatic Diseases*, 64, 30-36.

- LAPORTE, M., GALAND, P., FOKAN, D., DE GRAEF, C. & HEENEN, M. (2000) Apoptosis in established and healing psoriasis. *Dermatology*, 200, 314-316.
- LASCH, P., HAENSCH, W., NAUMANN, D. & DIEM, M. (2004) Imaging of colorectal adenocarcinoma using FT-IR microspectroscopy and cluster analysis. *Biochimica Et Biophysica Acta-Molecular Basis of Disease*, 1688, 176-186.
- LECHLER, T. & FUCHS, E. (2007) Desmoplakin: An unexpected regulator of microtubule organization in the epidermis. *Journal of Cell Biology*, 176, 147-154.
- LEE, P. C. & MEISEL, D. (1982) ADSORPTION AND SURFACE-ENHANCED RAMAN OF DYES ON SILVER AND GOLD SOLS. *Journal of Physical Chemistry*, 86, 3391-3395.
- LEE, W. H., KIM, J. Y., KIM, Y. S., SONG, H. J., KI-JOON, S., SONG, J. W., BAEK, L. J., SEO, E. Y., KIM, C. D., LEE, J. H. & KEE, S. H. (2005) Upregulation of class II beta-tubulin expression in differentiating keratinocytes. *Journal of Investigative Dermatology*, 124, 291-297.
- LEWIS, E. N., TREADO, P. J., REEDER, R. C., STORY, G. M., DOWREY, A. E., MARCOTT, C. & LEVIN, I. W. (1995) Fourier transform spectroscopic imaging using an infrared focal-plane array detector. *Analytical Chemistry*, 67, 3377-3381.
- LI, X., XU, Z. L., LU, X., YANG, X. H., YIN, P. Y., KONG, H. W., YU, Y. & XU, G. W. (2009) Comprehensive two-dimensional gas chromatography/time-of-flight mass spectrometry for metabonomics: Biomarker discovery for diabetes mellitus. *Analytica Chimica Acta*, 633, 257-262.
- LIM, C. S., POTTS, M. & HELM, R. E. (2006) Nicotinamide extends the replicative life span of primary human cells. *Mechanisms of Ageing and Development*, 127, 511-514.
- LIU, K. Z., XU, M. Q. & SCOTT, D. A. (2007) Biomolecular characterisation of leucocytes by infrared spectroscopy. *British Journal of Haematology*, 136, 713-722.
- LIU, X. Q., LIN, C. Y., LEI, M., YAN, S., ZHOU, T. H. & ERIKSON, R. L. (2005) CCT chaperonin complex is required for the biogenesis of functional Plk1. *Molecular and Cellular Biology*, 25, 4993-5010.
- LOWES, M. A., BOWCOCK, A. M. & KRUEGER, J. G. (2007) Pathogenesis and therapy of psoriasis. *Nature*, 445, 866-873.
- MACASKILL, A., CRAWFORD, D., GRAHAM, D. & FAULDS, K. (2009) DNA Sequence Detection Using Surface-Enhanced Resonance Raman Spectroscopy in a Homogeneous Multiplexed Assay. *Analytical Chemistry*, 81, 8134-8140.
- MACDONALD, N., CUMBERBATCH, M., SINGH, M., MOGGS, J. G., ORPHANIDES, G., DEARMAN, R. J., GRIFFITHS, C. E. M. & KIMBER, I. (2006) Proteomic analysis of suction blister fluid isolated from human skin. *Clinical and Experimental Dermatology*, 31, 445-448.
- MACKENZIE, D. A., DEFERNEZ, M., DUNN, W. B., BROWN, M., FULLER, L. J., DE HERRERA, S., GUENTHER, A., JAMES, S. A., EAGLES, J., PHILO, M., GOODACRE, R. & ROBERTS, I. N. (2008) Relatedness of medically important strains of *Saccharomyces cerevisiae* as revealed by phylogenetics and metabolomics. *Yeast*, 25, 501-512.
- MADAN, V. & GRIFFITHS, C. E. M. (2007) Systemic ciclosporin and tacrolimus in dermatology. *Dermatologic Therapy*, 20, 239-250.
- MALLBRIS, L., AKRE, O., GRANATH, F., YIN, L., LINDELOF, B., EKBOM, A. & STAHL-BACKDAHL, M. (2004) Increased risk for cardiovascular mortality in psoriasis inpatients but not in outpatients. *European Journal of Epidemiology*, 19, 225-230.
- MARENHOLZ, I., HEIZMANN, C. W. & FRITZ, G. (2004) S100 proteins in mouse and man: from evolution to function and pathology (including an update of the nomenclature). *Biochemical and Biophysical Research Communications*, 322, 1111-1122.
- MARTENS, H. & NAES, T. (1989) *Multivariate Calibration*, Chichester, UK, John Wiley & Sons.
- MARTENS, H., NIELSEN, J. P. & ENGENLSEN, S. B. (2003) Light Scattering and Light Absorbance Separated by Extended Multiplicative Signal Correction. Application to

- Near-Infrared Transmission Analysis of Powder Mixtures. *Analytical Chemistry*, 75, 394-404.
- MCGILL, A., FRANK, A., EMMETT, N., LEECH, S. N., TURNBULL, D. M., BIRCH-MACHIN, M. A. & REYNOLDS, N. J. (2005) The antipsoriatic drug anthralin accumulates in keratinocyte mitochondria, dissipates mitochondrial membrane potential, and induces apoptosis through a pathway dependent on respiratory competent mitochondria. *FASEB Journal*, 19, 1012-+.
- MENTER, A. & GRIFFITHS, C. E. M. (2007) Psoriasis 2 - Current and future management of psoriasis. *Lancet*, 370, 272-284.
- MOORE, B. D., STEVENSON, L., WATT, A., FLITSCH, S., TURNER, N. J., CASSIDY, C. & GRAHAM, D. (2004) Rapid and ultra-sensitive determination of enzyme activities using surface-enhanced resonance Raman scattering. *Nature Biotechnology*, 22, 1133-1138.
- MORDECHAI, S., SAHU, R. K., HAMMODY, Z., MARK, S., KANTAROVICH, K., GUTERMAN, H., PODSHYVALOV, A., GOLDSTEIN, J. & ARGOV, S. (2004) Possible common biomarkers from FTIR microspectroscopy of cervical cancer and melanoma. *Journal of Microscopy-Oxford*, 215, 86-91.
- MOSKOVITS, M. (1985) SURFACE-ENHANCED SPECTROSCOPY. *Reviews of Modern Physics*, 57, 783-826.
- MOSKOVITS, M., TAY, L. L., YANG, J. & HASLETT, T. (2002) SERS and the single molecule. *Optical Properties of Nanostructured Random Media*, 82, 215-226.
- MUELLER, W. & HERRMANN, B. (1979) CYCLOSPORIN A FOR PSORIASIS. *New England Journal of Medicine*, 301, 555-555.
- NAKATA, T., SOBUE, K. & HIROKAWA, N. (1990) CONFORMATIONAL CHANGE AND LOCALIZATION OF CALPACTIN-I COMPLEX INVOLVED IN EXOCYTOSIS AS REVEALED BY QUICK-FREEZE, DEEP-ETCH ELECTRON-MICROSCOPY AND IMMUNOCYTOCHEMISTRY. *Journal of Cell Biology*, 110, 13-25.
- NELSON, D. L. & COX, M. M. (2008) *Lehninger: Principles of Biochemistry*, Freeman, W.H.
- NEVITT, G. J. & HUTCHINSON, P. E. (1996) Psoriasis in the community: Prevalence, severity and patients' beliefs and attitudes towards the disease. *British Journal of Dermatology*, 135, 533-537.
- NICKOLOFF, B. J., XIN, H., NESTLE, F. O. & QIN, J. Z. (2007) The cytokine and chemokine network in psoriasis. *Clinics in Dermatology*, 25, 568-573.
- O'HAGAN, S., DUNN, W. B., BROWN, M., KNOWLES, J. D. & KELL, D. B. (2005) Closed-loop, multiobjective optimization of analytical instrumentation: Gas chromatography/time-of-flight mass spectrometry of the metabolomes of human serum and of yeast fermentations. *Analytical Chemistry*, 77, 290-303.
- OCKENFELS, H. M., NUSSBAUM, G., SCHULTEWOLTER, T., BURGER, P. M. & GOOS, M. (1995) CYCLOSPORINE-A, FH506 AND DITHRANOL ALTER TYROSINE-SPECIFIC PROTEIN-PHOSPHORYLATION IN HACAT KERATINOCYTES. *Archives of Dermatological Research*, 287, 304-309.
- OFARRELL, P. H. (1975) HIGH-RESOLUTION 2-DIMENSIONAL ELECTROPHORESIS OF PROTEINS. *Journal of Biological Chemistry*, 250, 4007-4021.
- OLIVER, S. G., WINSON, M. K., KELL, D. B. & BAGANZ, F. (1998) Systematic functional analysis of the yeast genome. *Trends in Biotechnology*, 16, 373-378.
- OTEY, C. A. & CARPEN, O. (2004) alpha-actinin revisited: A fresh look at an old player. *Cell Motility and the Cytoskeleton*, 58, 104-111.
- PAPP, K. A. (2008) Monitoring biologics for the treatment of psoriasis. *Clinics in Dermatology*, 26, 515-521.
- PARK, Y. D., JANG, H. S., KIM, S. Y., KO, S. K., LYOU, Y. J., LEE, D. Y., PAIK, Y. K. & YANG, J. M. (2006) Two-dimensional electrophoretic profiling of atopic dermatitis in primary cultured keratinocytes from patients. *Proteomics*, 6, 1362-1370.

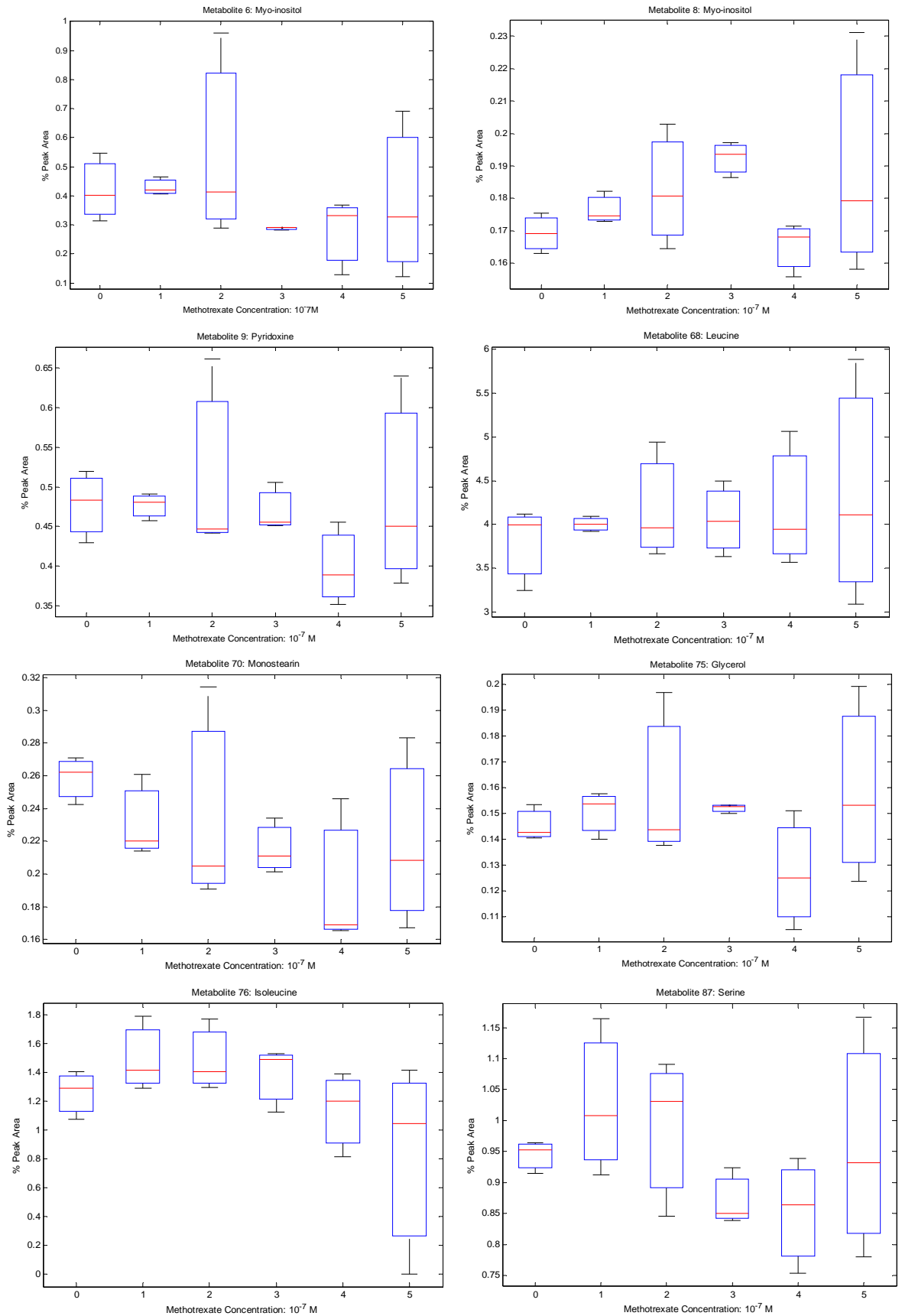
- PASIKANTI, K. K., HO, P. C. & CHAN, E. C. Y. (2008) Gas chromatography/mass spectrometry in metabolic profiling of biological fluids. *Journal of Chromatography B-Analytical Technologies in the Biomedical and Life Sciences*, 871, 202-211.
- PATEL, S. A., BARNES, A., LOFTUS, N., MARTIN, R., SLOAN, P., THAKKER, N. & GOODACRE, R. (2009) Imaging mass spectrometry using chemical inkjet printing reveals differential protein expression in human oral squamous cell carcinoma. *Analyst*, 134, 301-307.
- PATEL, S. A., CURRIE, F., THAKKER, N. & GOODACRE, R. (2008) Spatial metabolic fingerprinting using FT-IR spectroscopy: investigating abiotic stresses on *Micrasterias hardyi*. *Analyst*, 133, 1707-1713.
- PENG, J. M. & GYGI, S. P. (2001) Proteomics: the move to mixtures. *Journal of Mass Spectrometry*, 36, 1083-1091.
- PETERSON, J., VIBAT, C. & GENNIS, R. B. (1994) IDENTIFICATION OF THE AXIAL HEME LIGANDS OF CYTOCHROME B(556) IN SUCCINATE - UBIQUINONE OXIDOREDUCTASE FROM ESCHERICHIA-COLI. *Febs Letters*, 355, 155-156.
- PLAVINA, T., HINCAPIE, M., WAKSHULL, E., SUBRAMANYAM, M. & HANCOCK, W. S. (2008) Increased Plasma Concentrations of Cytoskeletal and Ca²⁺-Binding Proteins and Their Peptides in Psoriasis Patients. *Clinical Chemistry*, 54, 1805-1814.
- POPE, G. A., MACKENZIE, D. A., DEFEMEZ, M., AROSO, M., FULLER, L. J., MELLON, F. A., DUNN, W. B., BROWN, M., GOODACRE, R., KELL, D. B., MARVIN, M. E., LOUIS, E. J. & ROBERTS, I. N. (2007) Metabolic footprinting as a tool for discriminating between brewing yeasts. *Yeast*, 24, 667-679.
- QIAN, X. M. & NIE, S. M. (2008) Single-molecule and single-nanoparticle SERS: from fundamental mechanisms to biomedical applications. *Chemical Society Reviews*, 37, 912-920.
- RAJ, D., BRASH, D. E. & GROSSMAN, D. (2006) Keratinocyte apoptosis in epidermal development and disease. *Journal of Investigative Dermatology*, 126, 243-257.
- RAMAN, C. & KRISHNAN, K. (1928) A new type of secondary radiation. *Nature Biotechnology*, 121, 501-502.
- RAPP, S. R., FELDMAN, S. R., EXUM, M. L., FLEISCHER, A. B. & REBOUSSIN, D. M. (1999) Psoriasis causes as much disability as other major medical diseases. *Journal of the American Academy of Dermatology*, 41, 401-407.
- REICHMANN, H. & WILDENAUER, D. (1991) QUANTITATIVE SUCCINATE-DEHYDROGENASE ANALYSIS IN NORMAL AND RAGGED-RED MUSCLE-FIBERS. *Histochemistry*, 96, 251-253.
- RIVETT, A. J. (1985) PREFERENTIAL DEGRADATION OF THE OXIDATIVELY MODIFIED FORM OF GLUTAMINE-SYNTHEASE BY INTRACELLULAR MAMMALIAN PROTEASES. *Journal of Biological Chemistry*, 260, 300-305.
- RUSE, M., BROOME, A. M. & ECKERT, R. L. (2003) S100A7 (psoriasin) interacts with epidermal fatty acid binding protein and localizes in focal adhesion-like structures in cultured keratinocytes. *Journal of Investigative Dermatology*, 121, 132-141.
- SABATINE, M. S., LIU, E., MORROW, D. A., HELLER, E., MCCARROLL, R., WIEGAND, R., BERRIZ, G. F., ROTH, F. P. & GERSZTEN, R. E. (2005) Metabolomic identification of novel biomarkers of myocardial ischemia. *Circulation*, 112, 3868-3875.
- SAPORITO, F. C. & MENTER, M. A. (2004) Methotrexate and psoriasis in the era of new biologic agents. *Journal of the American Academy of Dermatology*, 50, 301-309.
- SAUDER, D. N. & MAMELAK, A. J. (2004) Understanding the new clinical landscape for psoriasis: A comparative review of biologics. *Journal of Cutaneous Medicine and Surgery*, 8, 205-212.
- SCIGELOVA, M. & MAKAROV, A. (2006) Orbitrap mass analyzer - Overview and applications in proteomics. *Proteomics*, 16-21.

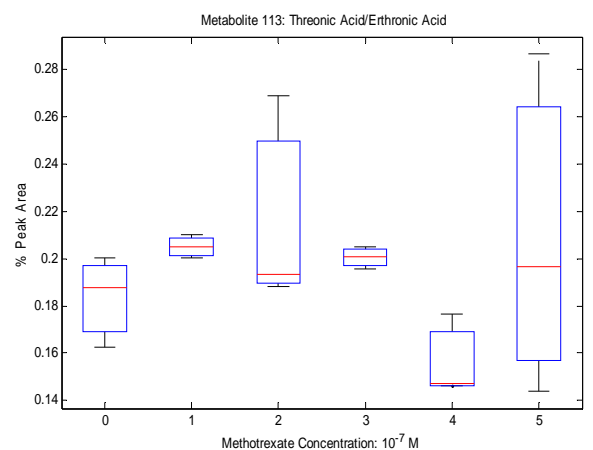
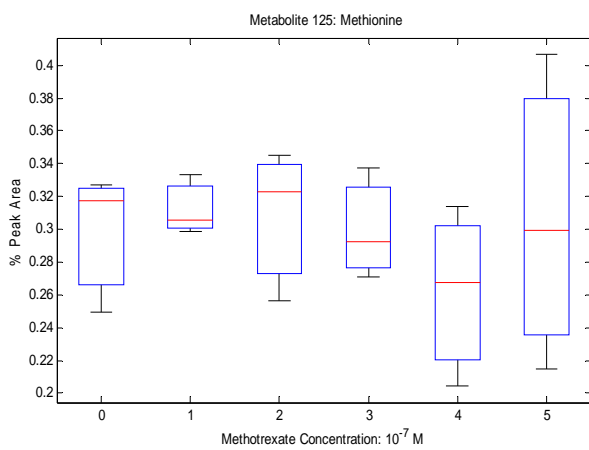
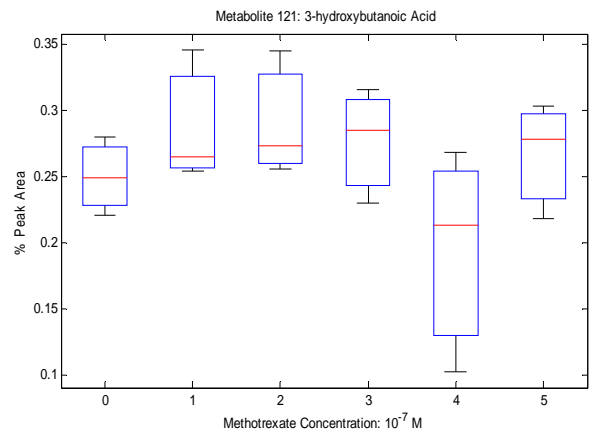
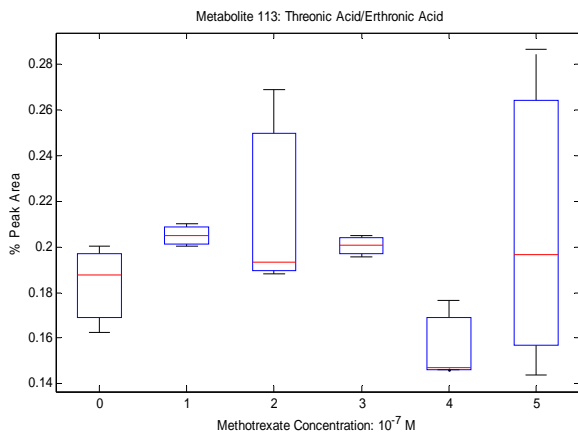
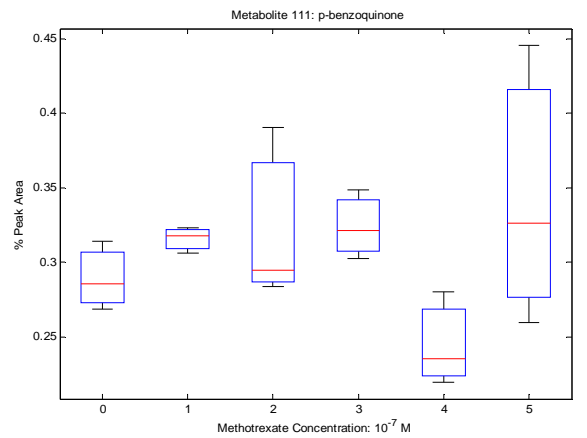
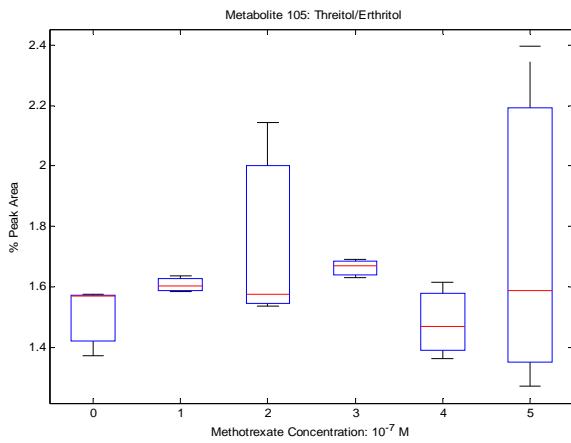
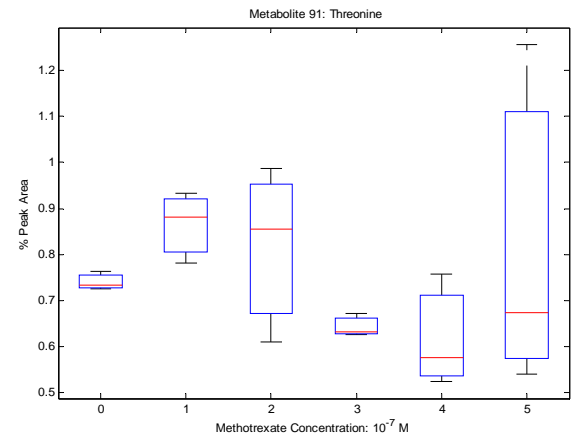
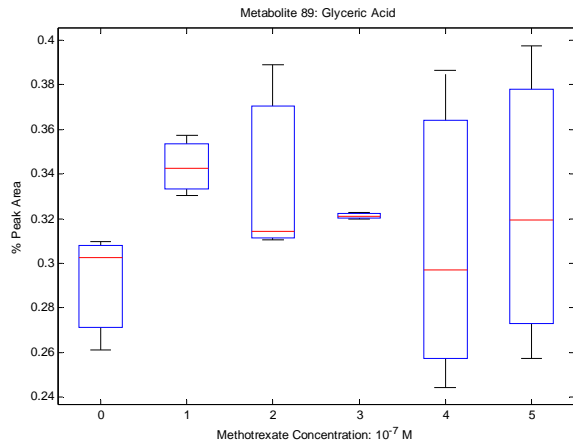
- SEEMANN, J., WEBER, K. & GERKE, V. (1997) Annexin I targets S100C to early endosomes. *Febs Letters*, 413, 185-190.
- SELLICK, C. A., HANSEN, R., MAQSOOD, A. R., DUNN, W. B., STEPHENS, G. M., GOODACRE, R. & DICKSON, A. J. (2009) Effective Quenching Processes for Physiologically Valid Metabolite Profiling of Suspension Cultured Mammalian Cells. *Analytical Chemistry*, 81, 174-183.
- SHADI, I. T., CHEUNG, W. & GOODACRE, R. (2009) Quantitative analysis of methyl green using surface-enhanced resonance Raman scattering. *Analytical and Bioanalytical Chemistry*, 394, 1833-1838.
- SHADI, I. T., CHOWDHRY, B. Z., SNOWDEN, M. J. & WITHNALL, R. (2001) Semi-quantitative trace analysis of nuclear fast red by surface enhanced resonance Raman scattering. *Analytica Chimica Acta*, 450, 115-122.
- SHADI, I. T., CHOWDHRY, B. Z., SNOWDEN, M. J. & WITHNALL, R. (2003) Semi-quantitative analysis of indigo by surface enhanced resonance Raman spectroscopy (SERRS) using silver colloids. *Spectrochimica Acta Part a-Molecular and Biomolecular Spectroscopy*, 59, 2213-2220.
- SHADI, I. T., CHOWDHRY, B. Z., SNOWDEN, M. J. & WITHNALL, R. (2004) Analysis of the conversion of indigo into indigo carmine dye using SERRS. *Chemical Communications*, 1436-1437.
- SHIH, B., GARSIDE, E., MCGROUTHER, D. A. & BAYAT, A. (2010) Molecular dissection of abnormal wound healing processes resulting in keloid disease. *Wound Repair and Regeneration*, 18, 139-153.
- SIRLIN, C., BURGARD, M., LEROY, M. J. F. & PREVOST, M. (1990) SILVER-NITRATE REFINING USING SUPPORTED LIQUID MEMBRANES. *Journal of Membrane Science*, 54, 299-305.
- SPULS, P. I., WITKAMP, L., BOSSUYT, P. M. M. & BOS, J. D. (1997) A systematic review of five systemic treatments for severe psoriasis. *British Journal of Dermatology*, 137, 943-949.
- SREEKUMAR, A., POISSON, L. M., RAJENDIRAN, T. M., KHAN, A. P., CAO, Q., YU, J. D., LAXMAN, B., MEHRA, R., LONIGRO, R. J., LI, Y., NYATI, M. K., AHSAN, A., KALYANA-SUNDARAM, S., HAN, B., CAO, X. H., BYUN, J., OMENN, G. S., GHOSH, D., PENNATHUR, S., ALEXANDER, D. C., BERGER, A., SHUSTER, J. R., WEI, J. T., VARAMBALLY, S., BEECHER, C. & CHINNAIYAN, A. M. (2009) Metabolomic profiles delineate potential role for sarcosine in prostate cancer progression. *Nature*, 457, 910-914.
- STANLEY, P., SMITH, A., MCDOWALL, A., NICOL, A., ZICHA, D. & HOGG, N. (2008) Intermediate-affinity LFA-1 binds alpha-actinin-1 to control migration at the leading edge of the T cell. *Embo Journal*, 27, 62-75.
- STRAINO, S., DI CARLO, A., MANGONI, A., DE MORI, R., GUERRA, L., MAURELLI, R., PANACCHIA, L., DI GIACOMO, F., PALUMBO, R., DI CAMPLI, C., UCCIOLI, L., BIGLIOLI, P., BIANCHI, M. E., CAPOGROSSI, M. C. & GERMANI, A. (2008) High-mobility group box 1 protein in human and murine skin: Involvement in wound healing. *Journal of Investigative Dermatology*, 128, 1545-1553.
- STROBER, B. E. & MENON, K. (2005) Folate supplementation during methotrexate therapy for patients with psoriasis. *Journal of the American Academy of Dermatology*, 53, 652-659.
- SUHLER, E., LIN, W., YIN, H. L. & LEE, W. M. (1997) Decreased plasma gelsolin concentrations in acute liver failure, myocardial infarction, septic shock, and myonecrosis. *Critical Care Medicine*, 25, 594-598.

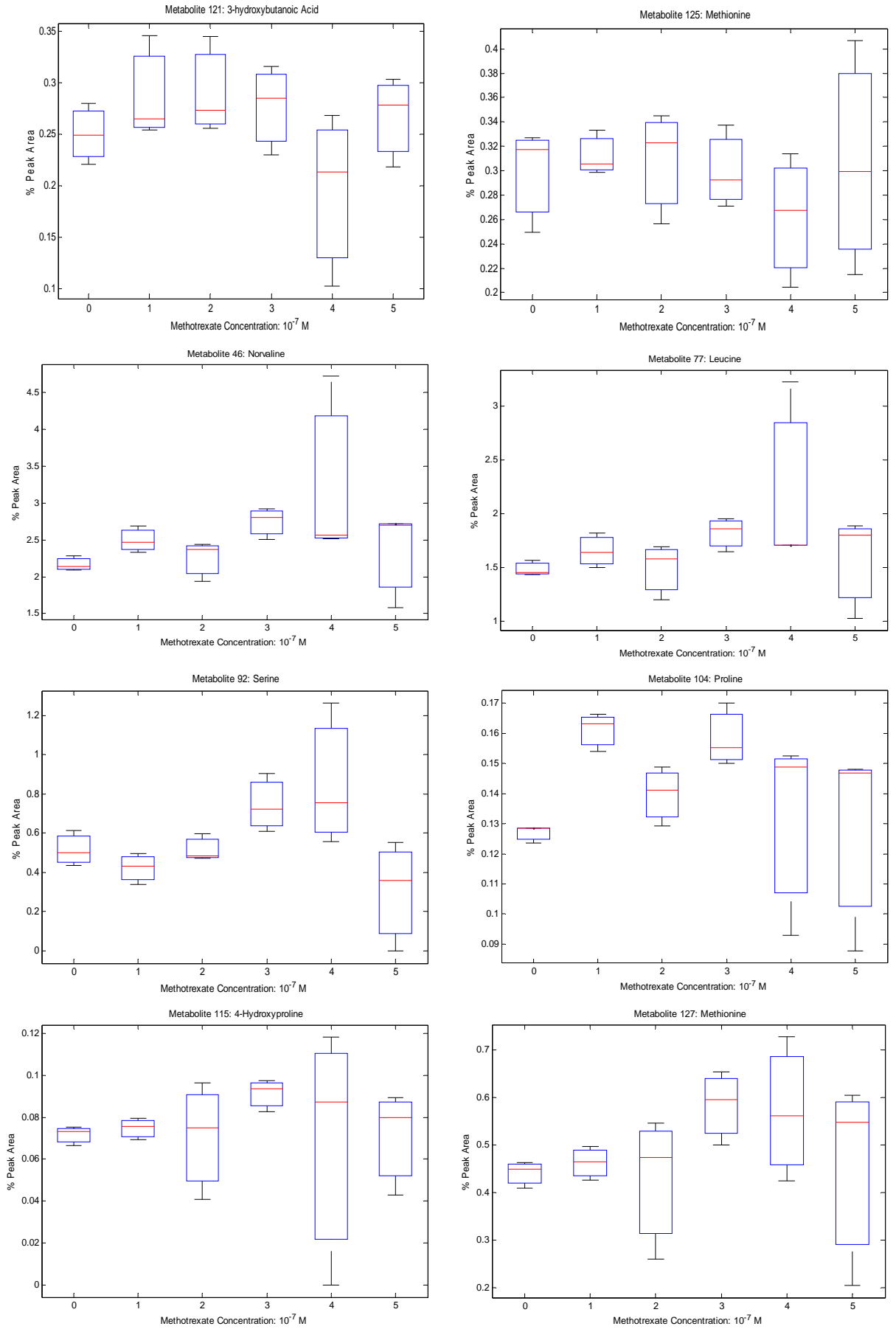
- SULÉ-SUSO, J., SKINGSLEY, D., SOCKALINGUM, G. D., KOHLER, A., KEGELAER, G., MANFAIT, M. & EL HAJ, A. J. (2005) FT-IR microspectroscopy as a tool to assess lung cancer cells response to chemotherapy. *Vibrational Spectroscopy*, 38, 179-184.
- SUMNER, L. W., AMBERG, A., BARRETT, D., BEALE, M. H., BEGER, R., DAYKIN, C. A., FAN, T. W. M., FIEHN, O., GOODACRE, R., GRIFFIN, J. L., HANKEMEIER, T., HARDY, N., HARNLY, J., HIGASHI, R., KOPKA, J., LANE, A. N., LINDON, J. C., MARRIOTT, P., NICHOLLS, A. W., REILY, M. D., THADEN, J. J. & VIANT, M. R. (2007) Proposed minimum reporting standards for chemical analysis. *Metabolomics*, 3, 211-221.
- TAN, K. T., SHAH, N., PRITCHARD, S. A., MCGROUTHER, D. A. & BAYAT, A. (2010) The Influence of Surgical Excision Margins on Keloid Prognosis. *Annals of Plastic Surgery*, 64, 55-58.
- TANIGUCHI, N., KAWAHARA, K., YONE, K., HASHIGUCHI, T., YAMAKUCHI, M., GOTO, M., INOUE, K., YAMADA, S., IJIRI, K., MATSUNAGA, S., NAKAJIMA, T., KOMIYA, S. & MARUYAMA, I. (2003) High mobility group box chromosomal protein 1 plays a role in the pathogenesis of rheumatoid arthritis as a novel cytokine. *Arthritis and Rheumatism*, 48, 971-981.
- TENG, Q., HUANG, W. L., COLLETTE, T. W., EKMAN, D. R. & TAN, C. (2009) A direct cell quenching method for cell-culture based metabolomics. *Metabolomics*, 5, 199-208.
- TETTEH, J., MADER, K. T., ANDANSON, J. M., MCAULEY, W. J., LANE, M. E., HADGRAFT, J., KAZARIAN, S. G. & MITCHELL, J. C. (2009) Local examination of skin diffusion using FTIR spectroscopic imaging and multivariate target factor analysis. *Analytica Chimica Acta*, 642, 246-256.
- TRUMPOWER, B. L. & GENNIS, R. B. (1994) ENERGY TRANSDUCTION BY CYTOCHROME COMPLEXES IN MITOCHONDRIAL AND BACTERIAL RESPIRATION - THE ENZYMOLOGY OF COUPLING ELECTRON-TRANSFER REACTIONS TO TRANSMEMBRANE PROTON TRANSLOCATION. *Annual Review of Biochemistry*, 63, 675-716.
- TSE, W.-P., CHE, C.-T., LIU, K. & LIN, Z.-X. (2006) Evaluation of the anti-proliferative properties of selected psoriasis-treating Chinese medicines on cultured HaCaT cells. *Journal of Ethnopharmacology*, 108, 133-141.
- TUCKER, W. F. G., MACNEIL, S., BLEEHEN, S. S. & TOMLINSON, S. (1984) BIOLOGICALLY-ACTIVE CALMODULIN LEVELS ARE ELEVATED IN BOTH INVOLVED AND UNINVOLVED EPIDERMIS IN PSORIASIS. *Journal of Investigative Dermatology*, 82, 298-299.
- TUCKER, W. F. G., MACNEIL, S., DAWSON, R. A., TOMLINSON, S. & BLEEHEN, S. S. (1986) AN INVESTIGATION OF THE ABILITY OF ANTIPSORIATIC DRUGS TO INHIBIT CALMODULIN ACTIVITY - A POSSIBLE MODE OF ACTION OF DITHRANOL (ANTHRALIN). *Journal of Investigative Dermatology*, 87, 232-235.
- TZU, J. & KERDEL, F. (2008) From conventional to cutting edge: the new era of biologics in treatment of psoriasis. *Dermatologic Therapy*, 21, 131-141.
- VAN DE KERKHOF, P. C. M. (2009) The relevance of biologics for the treatment of patients with psoriasis. *British Journal of Dermatology*, 161, 1213-1214.
- VAN DE KERKHOF, P. C. M., BARKER, J., GRIFFITHS, C. E. M., KRAGBALLE, K., MASON, J., MENTER, A. & PAPP, K. (2008) Psoriasis: consensus on topical therapies. *Journal of the European Academy of Dermatology and Venereology*, 22, 859-870.
- WARREN, R. B., CHALMERS, R. J. G., GRIFFITHS, C. E. M. & MENTER, A. (2008) Methotrexate for psoriasis in the era of biological therapy. *Clinical and Experimental Dermatology*, 33, 551-554.
- WESTERHUIS, J. A., HOEFSLOOT, H. C. J., SMIT, S., VIS, D. J., SMILDE, A. K., VAN VELZEN, E. J. J., VAN DUIJNHOFEN, J. P. M. & VAN DORSTEN, F. A. (2008) Assessment of PLSDA cross validation. *Metabolomics*, 4, 81-89.

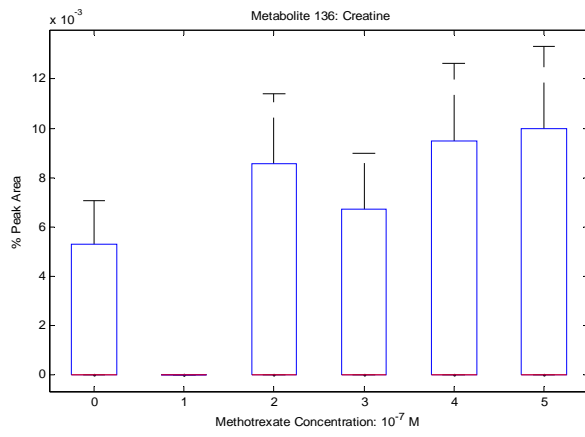
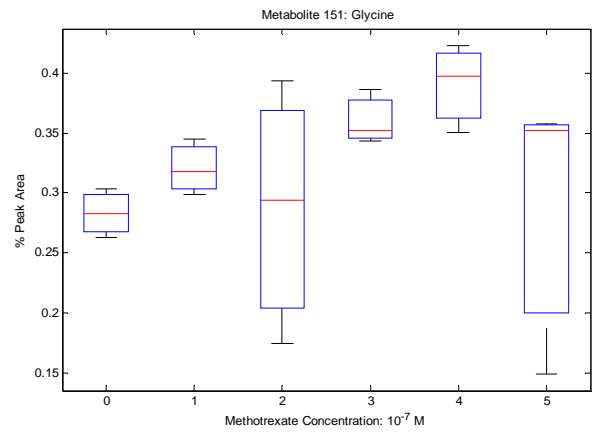
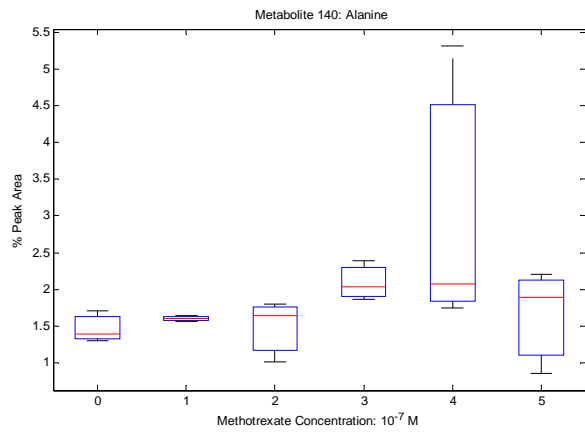
- WHITNEY, A. V., VAN DUYN, R. P. & CASADIO, F. (2006) An innovative surface-enhanced Raman spectroscopy (SERS) method for the identification of six historical red lakes and dyestuffs. *Journal of Raman Spectroscopy*, 37, 993-1002.
- WINDER, C. L., DUNN, W. B., SCHULER, S., BROADHURST, D., JARVIS, R., STEPHENS, G. M. & GOODACRE, R. (2008) Global metabolic profiling of *Escherichia coli* cultures: An evaluation of methods for quenching and extraction of intracellular metabolites. *Analytical Chemistry*, 80, 2939-2948.
- WISHART, D. S., TZUR, D., KNOX, C., EISNER, R., GUO, A. C., YOUNG, N., CHENG, D., JEWELL, K., ARNDT, D., SAWHNEY, S., FUNG, C., NIKOLAI, L., LEWIS, M., COUTOULY, M. A., FORSYTHE, I., TANG, P., SHRIVASTAVA, S., JERONCIC, K., STOTHARD, P., AMEGBEY, G., BLOCK, D., HAU, D. D., WAGNER, J., MINIACI, J., CLEMENTS, M., GEBREMEDHIN, M., GUO, N., ZHANG, Y., DUGGAN, G. E., MACINNIS, G. D., WELJIE, A. M., DOWLATABADI, R., BAMFORTH, F., CLIVE, D., GREINER, R., LI, L., MARRIE, T., SYKES, B. D., VOGEL, H. J. & QUERENGESSER, L. (2007) HMDB: the human metabolome database. *Nucleic Acids Research*, 35, D521-D526.
- WOLF, R., LEWERENZ, V., BUCHAO, A. S., WALZ, M. & RUZICKA, T. (2007) Human S100A15 splice variants are differentially expressed in inflammatory skin diseases and regulated through Th1 cytokines and calcium. *Experimental Dermatology*, 16, 685-691.
- YAMANE, Y., MORIYAMA, K., YASUDA, C., MIYATA, S., AIHARA, M., IKEZAWA, Z. & MIYAZAKI, K. (2009) New Horny Layer Marker Proteins for Evaluating Skin Condition in Atopic Dermatitis. *International Archives of Allergy and Immunology*, 150, 89-101.
- ZHANG, M., ZHU, L., FENG, Y., YANG, Y. X., LIU, L. & RAN, Y. P. (2008) Effects of acitretin on proliferative inhibition and RANTES production of HaCaT cells. *Archives of Dermatological Research*, 300, 575-581.
- ZIBERT, J. R., SKOV, L., THYSSEN, J. P., JACOBSEN, G. K. & GRIGORIAN, M. (2009) Significance of the S100A4 Protein in Psoriasis. *Journal of Investigative Dermatology*, 130, 150-160.
- ZWIELLY, A., GOPAS, J., BRKIC, G. & MORDECHAI, S. (2009) Discrimination between drug-resistant and non-resistant human melanoma cell lines by FTIR spectroscopy. *Analyst*, 134, 294-300.

Appendix A Additional Metabolite Box Plots for Methotrexate Treatment: Fingerprint

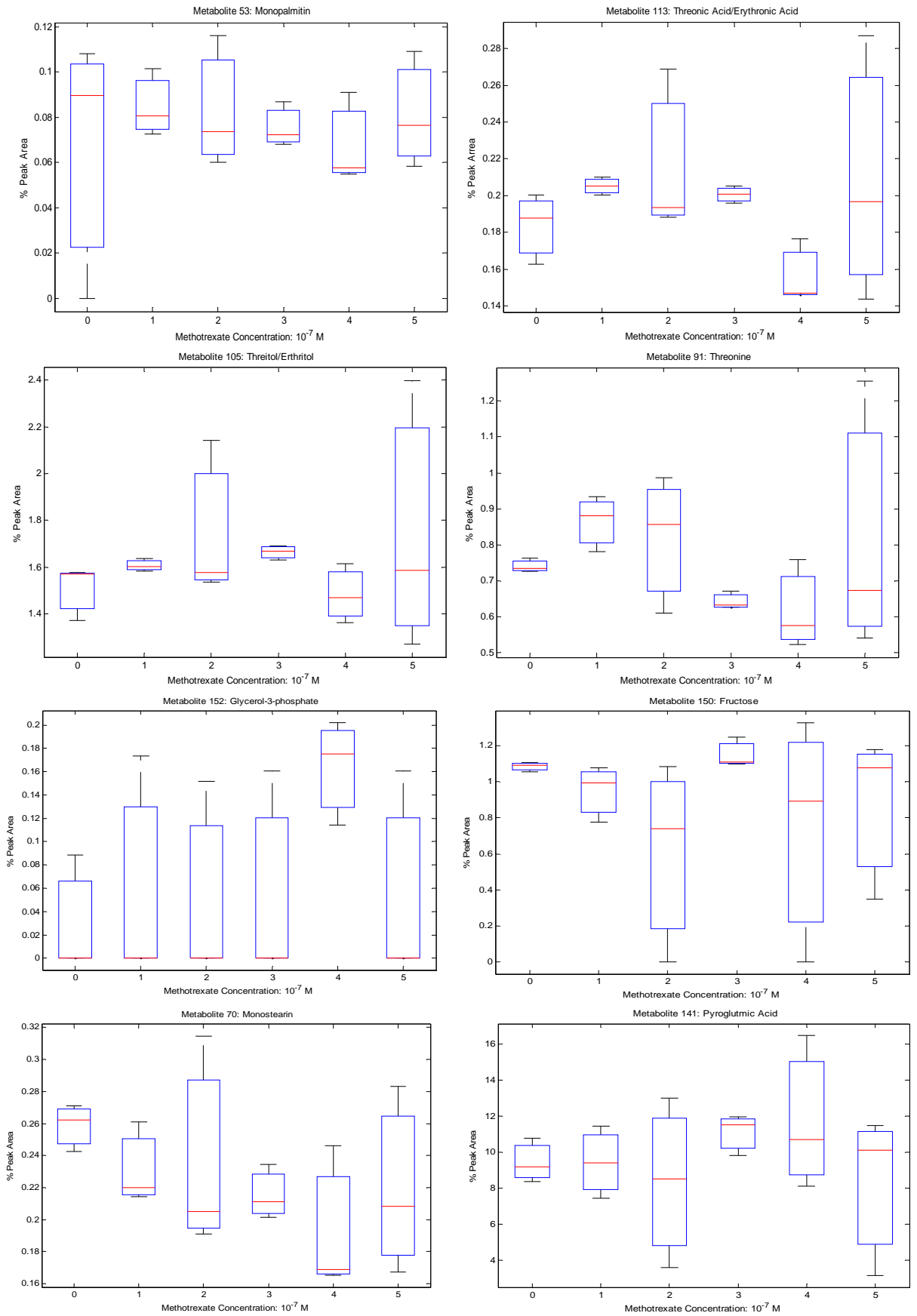


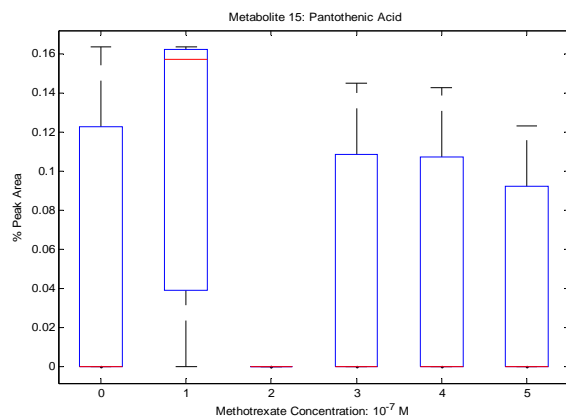




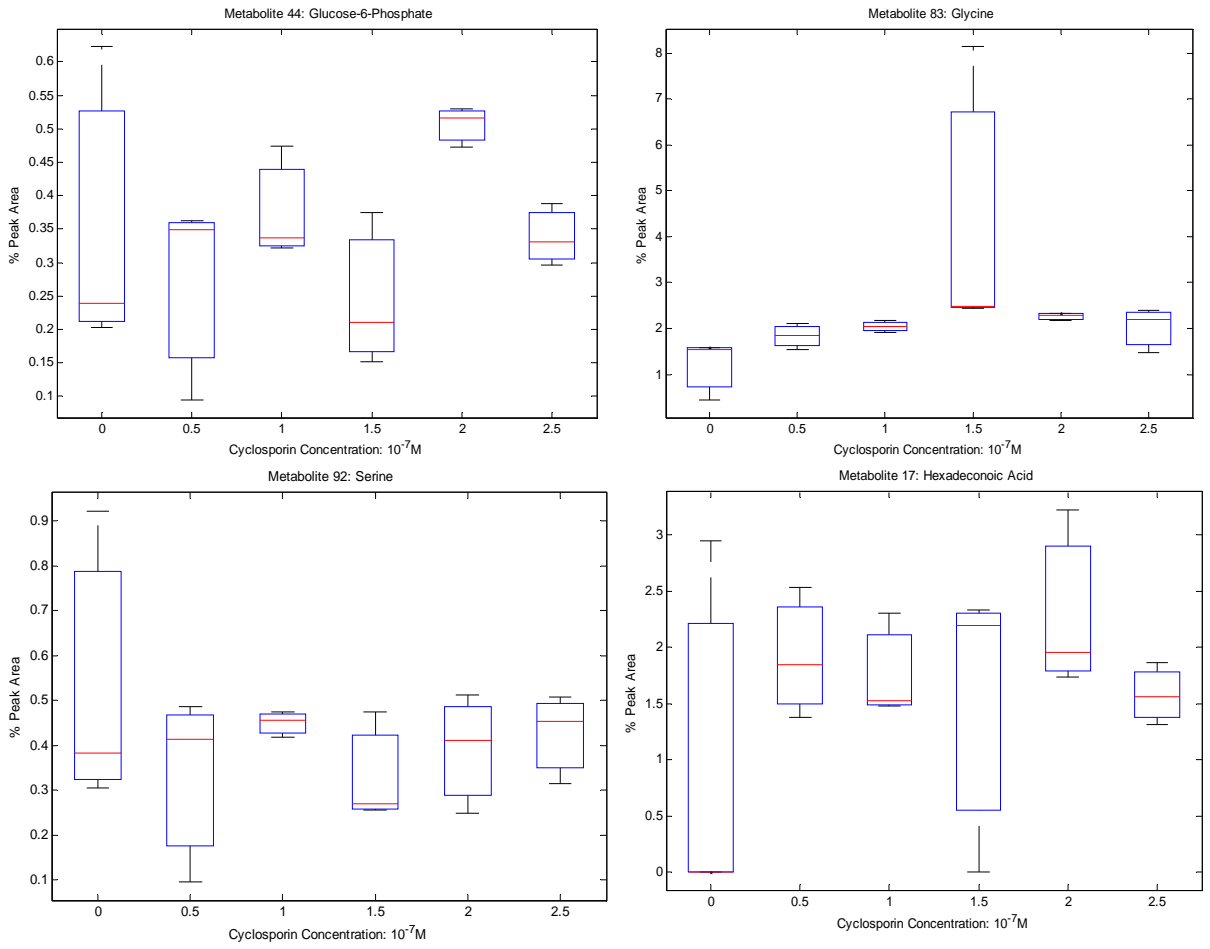


Appendix B Additional Metabolite Box Plots for Methotrexate Treatment: Footprint

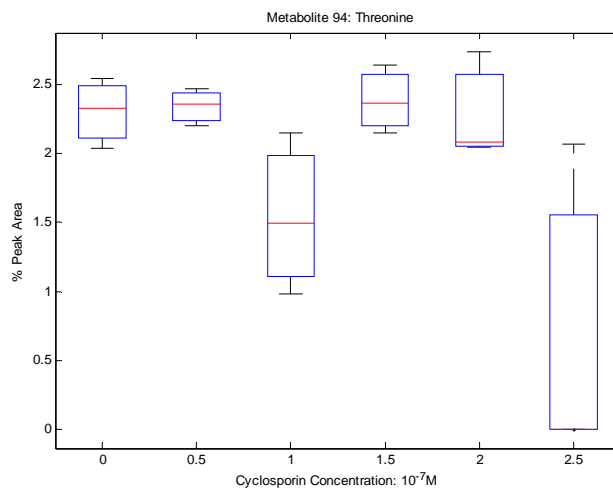




Appendix C Additional Metabolite Box Plots for Cyclosporin Treatment: Fingerprint



Appendix D Additional Metabolite Box Plots for Cyclosporin Treatment: Footprint



Appendix E Proteome Results for Dithranol Treatment

Protein Identification	C	0.1	0.2	0.3	0.4	0.5
annexin 5	Blue	Blue	Green	Red	Red	Red
annexin IV	Green	Green	Green	Blue	Red	Red
argininosuccinate synthetase 1	Blue	Red	Red	Red	Red	Red
calmodulin 2	Blue	Green	Green	Red	Red	Red
DEAH (Asp-Glu-Ala-His) box polypeptide 15	Green	Blue	Blue	Blue	Red	Red
enolase 2	Green	Green	Green	Blue	Red	Red
enolase 3	Green	Green	Green	Green	Green	Red
eukaryotic translation elongation factor 1 alpha 1	Green	Green	Green	Green	Blue	Red
eukaryotic translation initiation factor 4A2	Green	Green	Green	Green	Green	Red
gelsolin-like capping protein	Blue	Green	Green	Red	Red	Red
heterogeneous nuclear ribonucleoprotein A1 isoform a	Blue	Red	Red	Red	Red	Red
lactate dehydrogenase A	Green	Green	Green	Green	Blue	Red
nascent-polypeptide-associated complex alpha polypeptide-like	Blue	Red	Red	Red	Red	Red
nucleophosmin 1 isoform 1	Blue	Blue	Blue	Red	Red	Red
phosphoglycerate kinase 2	Green	Blue	Blue	Red	Red	Red
poly(rC) binding protein 3	Blue	Green	Green	Red	Red	Red
PREDICTED: similar to Heterogeneous nuclear ribonucleoprotein A1	Green	Green	Green	Blue	Blue	Red
PREDICTED: similar to nascent polypeptide-associated complex alpha polypeptide	Blue	Red	Red	Red	Red	Red
PREDICTED: similar to Phosphoglycerate mutase 1 (Phosphoglycerate mutase isozyme B)	Green	Green	Green	Green	Green	Red
PREDICTED: similar to Protein SET (Phosphatase 2A inhibitor I2PP2A)	Green	Green	Blue	Blue	Blue	Red
PREDICTED: similar to ribosomal protein S18 isoform 4	Blue	Red	Red	Red	Red	Red
pyruvate kinase 3 isoform 1	Green	Green	Green	Green	Green	Red
ribosomal protein S14	Green	Green	Blue	Red	Red	Red
S100 calcium binding protein A14	Green	Green	Green	Green	Green	Red
synaptotagmin binding, cytoplasmic RNA interacting protein	Blue	Green	Blue	Blue	Red	Red
transaldolase 1	Blue	Blue	Red	Red	Red	Red
tubulin, alpha, ubiquitous	Green	Green	Green	Green	Red	Red
tubulin, beta polypeptide	Green	Green	Green	Green	Blue	Red
tubulin, beta, 2	Green	Green	Green	Blue	Blue	Red
ubiquitin and ribosomal protein L40 precursor	Blue	Blue	Blue	Blue	Red	Red
adipose specific 2	Green	Green	Green	Green	Green	Green
ADP-ribosylation factor 1	Green	Green	Green	Blue	Red	Red
aldolase A	Green	Green	Green	Green	Green	Red
alpha 2 actin	Green	Green	Green	Green	Green	Red
annexin A2 isoform 2	Green	Green	Green	Green	Green	Red
annexin I	Green	Green	Green	Green	Green	Red
chloride intracellular channel 1	Green	Green	Green	Green	Blue	Red
cofilin 1 (non-muscle)	Green	Green	Green	Green	Green	Red
enolase 1	Green	Green	Green	Green	Green	Red
eukaryotic translation elongation factor 1 alpha 2	Green	Green	Green	Blue	Red	Red
eukaryotic translation elongation factor 2	Green	Green	Green	Green	Green	Red
glucose phosphate isomerase	Green	Green	Green	Green	Blue	Red
glutathione transferase	Green	Green	Green	Green	Blue	Red
glyceraldehyde-3-phosphate dehydrogenase	Green	Green	Green	Green	Blue	Red
H2B histone family, member C	Blue	Green	Green	Green	Blue	Red
H4 histone family, member B	Blue	Green	Green	Green	Blue	Red
heat shock 27kDa protein 1	Green	Blue	Blue	Green	Green	Red
heat shock 70kDa protein 1A	Green	Green	Green	Green	Green	Red
heat shock 70kDa protein 8 isoform 2	Green	Green	Green	Green	Green	Red
heat shock 90kDa protein 1, beta	Green	Green	Green	Green	Green	Red
heat shock protein 90kDa alpha (cytosolic), class A member 1 isoform 2	Green	Green	Green	Green	Green	Red
heterogeneous nuclear ribonucleoprotein A2/B1 isoform A2	Green	Green	Green	Green	Green	Red
heterogeneous nuclear ribonucleoprotein D isoform c	Green	Green	Blue	Green	Green	Red
heterogeneous nuclear ribonucleoprotein K isoform a	Green	Green	Green	Green	Green	Red
histone cluster 1, H1b	Green	Green	Green	Green	Green	Red
histone cluster 1, H1c	Green	Green	Green	Green	Green	Red
histone H2a	Blue	Green	Blue	Green	Green	Red
isocitrate dehydrogenase 1 (NADP+), soluble	Green	Green	Green	Green	Green	Blue
lactate dehydrogenase C	Blue	Green	Green	Green	Green	Red
lamin A/C isoform 1 precursor	Green	Green	Green	Blue	Blue	Red
lamin A/C isoform 3	Green	Green	Green	Green	Green	Red
LIM and SH3 protein 1	Green	Green	Green	Green	Green	Red
nucleolin	Green	Green	Green	Green	Green	Red
peroxiredoxin 1	Green	Green	Green	Green	Green	Red
peroxiredoxin 6	Green	Green	Green	Green	Blue	Red

phosphoglycerate kinase 1						
PREDICTED: hypothetical protein						
PREDICTED: similar to 60S ribosomal protein L23a						
PREDICTED: similar to actin-like protein						
PREDICTED: similar to cytoplasmic beta-actin						
PREDICTED: similar to peptidylprolyl isomerase A (cyclophilin A)-like 4						
PREDICTED: similar to peptidylprolyl isomerase A isoform 1						
PREDICTED: similar to peptidylprolyl isomerase A isoform 1						
profilin 1						
pyruvate kinase 3 isoform 2						
pyruvate kinase, liver and RBC isoform 1						
ribosomal protein P2						
S100 calcium binding protein A11						
serine (or cysteine) proteinase inhibitor, clade B (ovalbumin), member 5						
stratifin						
thioredoxin						
TNF receptor-associated protein 1						
transgelin 2						
transketolase						
triosephosphate isomerase 1						
tropomyosin 2 (beta) isoform 2						
tubulin, alpha 1a						
tubulin, beta 2B						
tubulin, beta, 4						
tumor rejection antigen (gp96) 1						
tyrosine 3/tryptophan 5 -monooxygenase activation protein, epsilon polypeptide						
tyrosine 3/tryptophan 5 -monooxygenase activation protein, theta polypeptide						
tyrosine 3/tryptophan 5 -monooxygenase activation protein, zeta polypeptide						
tyrosine 3-monooxygenase/tryptophan 5-monooxygenase activation protein, beta polypeptide						
villin 2						
actin, gamma 1 propeptide						
actinin, alpha 4						
adenylyl cyclase-associated protein						
AHNAK nucleoprotein isoform 1						
aldo-keto reductase family 1, member B1						
aldo-keto reductase family 1, member B1						
annexin A11						
annexin A8-like 1						
autoantigen La						
chaperonin containing TCP1, subunit 5 (epsilon)						
ciliary rootlet coiled-coil, rootletin						
cytochrome P450, family 24 precursor						
cytosolic malate dehydrogenase						
ErbB3-binding protein 1						
eukaryotic translation initiation factor 3, subunit 10 theta, 150/170kDa						
fructose-bisphosphate aldolase C						
GDP dissociation inhibitor 2						
heat shock 70kDa protein 6 (HSP 70B')						
heat shock 70kDa protein 8 isoform 1						
heterogeneous nuclear ribonucleoprotein C isoform b						
heterogeneous nuclear ribonucleoprotein F						
heterogeneous nuclear ribonucleoprotein H2						
heterogeneous nuclear ribonucleoprotein R						
heterogeneous nuclear ribonucleoprotein U isoform b						
hypothetical protein LOC345651						
IQ motif containing GTPase activating protein 1						
karyopherin beta 1						
keratin 1						
keratin 10						
keratin 1B						
keratin 13 isoform a						
keratin 2						
keratin 5						
keratin 6B						
lactate dehydrogenase B						
myristoylated alanine-rich protein kinase C substrate						

nascent-polypeptide-associated complex alpha polypeptide	Blue	Red	Red	Blue	Red	Red
PDZ and LIM domain 1 (elfin)	Blue	Red	Red	Blue	Blue	Blue
peroxiredoxin 5 precursor, isoform b	Green	Red	Red	Red	Red	Green
phosphogluconate dehydrogenase	Red	Blue	Red	Red	Red	Red
polypyrimidine tract binding protein 2	Red	Red	Green	Blue	Blue	Red
polypyrimidine tract-binding protein 1 isoform c	Red	Red	Green	Blue	Blue	Red
PREDICTED: hypothetical protein	Red	Red	Green	Red	Blue	Red
PREDICTED: similar to 40S ribosomal protein S16 isoform 2	Red	Red	Red	Blue	Blue	Red
PREDICTED: similar to 40S ribosomal protein S28	Green	Red	Red	Red	Blue	Blue
PREDICTED: similar to 60S ribosomal protein L22 (Heparin-binding protein HBp15)	Red	Red	Red	Blue	Red	Green
PREDICTED: similar to 60S ribosomal protein L29 (Cell surface heparin-binding protein HIP)	Red	Blue	Blue	Red	Red	Green
PREDICTED: similar to Protein SET (Phosphatase 2A inhibitor I2PP2A)	Red	Blue	Blue	Red	Red	Red
PREDICTED: similar to Splicing factor, arginine/serine-rich, 46kD	Red	Red	Blue	Red	Red	Red
PREDICTED: similar to ubiquitin and ribosomal protein S27a precursor	Red	Red	Red	Blue	Red	Red
protease, serine, 1 preproprotein	Red	Red	Blue	Blue	Blue	Green
ras-related nuclear protein	Green	Blue	Blue	Red	Blue	Blue
ribosomal protein S3	Red	Red	Red	Green	Red	Red
ribosomal protein S7	Red	Red	Red	Blue	Green	Red
SERPINE1 mRNA binding protein 1 isoform 3	Blue	Red	Red	Blue	Red	Red
SMT3 suppressor of mif two 3 homolog 4	Green	Blue	Red	Red	Blue	Blue
SET translocation (myeloid leukemia-associated)	Red	Red	Green	Red	Red	Red
stress-induced-phosphoprotein 1 (Hsp70/Hsp90-organizing protein)	Red	Red	Red	Blue	Red	Red
tropomyosin 3 isoform 1	Red	Red	Red	Red	Blue	Red
valosin-containing protein	Green	Blue	Red	Red	Green	Red
vitronectin precursor	Red	Red	Red	Red	Green	Red
acidic (leucine-rich) nuclear phosphoprotein 32 family, member A	Red	Red	Red	Red	Blue	Blue
acidic (leucine-rich) nuclear phosphoprotein 32 family, member B	Red	Red	Red	Blue	Green	Blue
albumin precursor	Red	Red	Blue	Blue	Blue	Blue
myosin, heavy polypeptide 9, non-muscle	Red	Red	Red	Red	Red	Blue
PREDICTED: similar to ADP-ribosylation factor 1 like	Red	Red	Red	Red	Red	Blue
tropomyosin 3 isoform 2	Red	Red	Blue	Blue	Green	Blue

Appendix F Proteome Results for Methotrexate Treatment

Protein Identification	C	1	2	3	4	5
actinin, alpha 1	Green	Red	Blue	Blue	Red	Red
annexin A3	Blue	Red	Red	Red	Red	Red
annexin IV	Green	Blue	Green	Blue	Green	Red
basic transcription factor 3 isoform B	Blue	Blue	Red	Red	Red	Red
chaperonin containing TCP1, subunit 2	Green	Green	Green	Blue	Green	Red
coronin, actin binding protein, 1B	Blue	Red	Red	Red	Red	Red
filamin A, alpha	Blue	Green	Red	Red	Red	Red
GDP dissociation inhibitor 1	Blue	Blue	Green	Green	Green	Red
gelsolin isoform b	Blue	Blue	Green	Red	Red	Red
glycogen phosphorylase, liver	Blue	Red	Red	Red	Red	Red
H4 histone family, member B	Blue	Blue	Red	Red	Red	Red
heme binding protein 2	Blue	Blue	Red	Red	Red	Red
heterogeneous nuclear ribonucleoprotein A3	Green	Green	Green	Green	Green	Red
high mobility group AT-hook 1 isoform a	Green	Green	Green	Blue	Blue	Red
high-mobility group box1	Blue	Blue	Blue	Red	Red	Red
high-mobility group box2	Green	Blue	Blue	Red	Red	Red
hydroxypyruvate isomerase homolog	Blue	Red	Red	Red	Red	Red
interferon regulatory factor 6	Green	Red	Red	Red	Red	Red
keratin 1	Blue	Red	Red	Red	Red	Red
keratin 13 isoform a	Blue	Red	Red	Red	Red	Red
lamin A/C isoform 3	Blue	Red	Red	Red	Red	Red
moesin	Blue	Blue	Green	Blue	Blue	Red
non-POU domain containing, octamer-binding	Blue	Blue	Blue	Blue	Blue	Red
p47 protein isoform c	Green	Green	Green	Green	Green	Red
phosphoglycerate dehydrogenase	Green	Green	Blue	Green	Green	Red
PYD and CARD domain containing isoform c	Blue	Blue	Red	Red	Red	Red
ribosomal protein L5	Green	Green	Green	Green	Blue	Red
ribosomal protein L9	Blue	Blue	Blue	Blue	Green	Red
ribosomal protein S20	Green	Green	Green	Green	Blue	Red
ribosomal protein S4, X-linked X isoform	Blue	Blue	Green	Green	Red	Red
ribosomal protein S5	Blue	Green	Green	Blue	Blue	Red
septin 11	Blue	Red	Red	Red	Red	Red
SET translocation (myeloid leukemia-associated)	Blue	Red	Red	Red	Red	Red
sorbitol dehydrogenase	Blue	Blue	Blue	Red	Red	Red
TIP120 protein	Blue	Red	Red	Red	Red	Red
Treacher Collins-Franceschetti syndrome 1 isoform b	Blue	Red	Red	Red	Red	Red
tripartite motif-containing 25	Blue	Red	Red	Red	Red	Red
actin, gamma 1 propeptide	Green	Green	Green	Green	Green	Red
actinin, alpha 4	Green	Green	Green	Green	Green	Red
adenylyl cyclase-associated protein	Green	Green	Green	Green	Green	Blue
adipose specific 2	Green	Green	Green	Green	Green	Red
AHNAK nucleoprotein isoform 1	Green	Green	Green	Green	Green	Red
albumin precursor	Green	Green	Green	Green	Green	Red
aldo-keto reductase family 1, member A1	Green	Green	Green	Green	Green	Red
aldolase A	Green	Green	Green	Green	Green	Red
alpha 2 actin	Green	Green	Green	Green	Green	Red
annexin 5	Green	Green	Green	Green	Green	Red
annexin A11	Blue	Green	Green	Green	Green	Red
annexin A2 isoform 2	Green	Green	Green	Green	Green	Red
annexin A8-like 1	Green	Green	Green	Green	Green	Blue
annexin I	Green	Green	Green	Green	Green	Red
APEX nuclease	Green	Green	Green	Blue	Green	Blue
argininosuccinate synthetase 1	Green	Green	Green	Green	Green	Red
arginyl aminopeptidase (aminopeptidase B)	Green	Green	Green	Green	Green	Blue
ARP3 actin-related protein 3 homolog	Green	Green	Green	Green	Green	Blue
aspartyl-tRNA synthetase	Green	Green	Green	Green	Green	Blue
ATP-dependent DNA helicase II, 70 kDa subunit	Green	Green	Green	Green	Green	Red
calmodulin 2	Green	Green	Green	Green	Green	Red
calpain, small subunit 1	Green	Green	Green	Green	Green	Red
cofilin 1 (non-muscle)	Green	Green	Green	Green	Green	Red
cold shock domain protein A	Blue	Green	Blue	Blue	Blue	Blue
cortactin isoform a	Green	Green	Green	Green	Green	Red
cytosolic malate dehydrogenase	Green	Green	Green	Green	Green	Red
enolase 1	Green	Green	Green	Green	Green	Red
enolase 2	Green	Green	Green	Green	Green	Red
enolase 3	Green	Green	Green	Green	Green	Red

eukaryotic translation elongation factor 1 alpha 1						
eukaryotic translation elongation factor 1 alpha 2						
eukaryotic translation elongation factor 1 beta 2						
eukaryotic translation elongation factor 2						
eukaryotic translation initiation factor 2, subunit 1 alpha, 35kDa						
eukaryotic translation initiation factor 4A isoform 1						
eukaryotic translation initiation factor 4A2						
fatty acid synthase						
fructose-1,6-bisphosphatase 1						
fructose-bisphosphate aldolase C						
GDP dissociation inhibitor 2						
glucose phosphate isomerase						
glutathione transferase						
glyceraldehyde-3-phosphate dehydrogenase						
GTP-binding protein PTD004 isoform 1						
H2B histone family, member C						
heat shock 27kDa protein 1						
heat shock 70kDa protein 1A						
heat shock 70kDa protein 1-like						
heat shock 70kDa protein 4 isoform a						
heat shock 70kDa protein 8 isoform 2						
heat shock 90kDa protein 1, beta						
heat shock protein 90kDa alpha (cytosolic), class A member 1 isoform 2						
hepatoma-derived growth factor (high-mobility group protein 1-like)						
heterogeneous nuclear ribonucleoprotein A1 isoform a						
heterogeneous nuclear ribonucleoprotein A2/B1 isoform A2						
heterogeneous nuclear ribonucleoprotein F						
heterogeneous nuclear ribonucleoprotein H2						
heterogeneous nuclear ribonucleoprotein K isoform a						
involucrin						
IQ motif containing GTPase activating protein 1						
isocitrate dehydrogenase 1 (NADP+), soluble						
KH-type splicing regulatory protein (FUSE binding protein 2)						
lactate dehydrogenase A						
lactate dehydrogenase A-like 6B						
lactate dehydrogenase B						
LIM and SH3 protein 1						
myosin, heavy polypeptide 9, non-muscle						
myristoylated alanine-rich protein kinase C substrate						
nascent-polypeptide-associated complex alpha polypeptide						
non-metastatic cells 2, protein (NM23B) expressed in						
nuclease sensitive element binding protein 1						
nucleolin						
nucleophosmin 1 isoform 1						
PDZ and LIM domain 1 (elfin)						
peroxiredoxin 1						
peroxiredoxin 2 isoform a						
peroxiredoxin 5 precursor, isoform b						
peroxiredoxin 6						
PEST-containing nuclear protein						
phosphofructokinase, platelet						
phosphogluconate dehydrogenase						
phosphoglycerate kinase 1						
phosphoglycerate kinase 2						
plastin 3						
poly(rC) binding protein 3						
PREDICTED: similar to 40S ribosomal protein SA (p40)						
PREDICTED: similar to 60S ribosomal protein L12						
PREDICTED: similar to 60S ribosomal protein L32						
PREDICTED: similar to 60S ribosomal protein L32						
PREDICTED: similar to actin-like protein						
PREDICTED: similar to chromobox homolog 3						
PREDICTED: similar to cytoplasmic beta-actin						
PREDICTED: similar to Elongation factor 1-gamma (EF-1-gamma) (eEF-1B gamma)						
PREDICTED: similar to Heterogeneous nuclear ribonucleoprotein A1 (Helix-destabilizing protein)						
PREDICTED: similar to peptidylprolyl isomerase A isoform 1						

PREDICTED: similar to Phosphoglycerate mutase 1 (Phosphoglycerate mutase isozyme B)						
PREDICTED: similar to Protein SET (Phosphatase 2A inhibitor I2PP2A)						
profilin 1						
proteasome activator subunit 2						
pyrophosphatase 1						
pyruvate kinase 3 isoform 1						
pyruvate kinase 3 isoform 2						
Rho GDP dissociation inhibitor (GDI) beta						
ribosomal protein L17						
ribosomal protein L19						
ribosomal protein L3 isoform a						
ribosomal protein L8						
ribosomal protein P0						
S100 calcium binding protein A11						
S100 calcium binding protein A14						
S-adenosylhomocysteine hydrolase						
serine (or cysteine) proteinase inhibitor, clade B (ovalbumin), member 13						
serine (or cysteine) proteinase inhibitor, clade B (ovalbumin), member 5						
SERPINE1 mRNA binding protein 1 isoform 3						
small acidic protein						
splicing factor proline/glutamine rich (polypyrimidine tract binding protein associated)						
stratifin						
thioredoxin						
transgelin 2						
transketolase						
triosephosphate isomerase 1						
tropomyosin 3 isoform 2						
tubulin, alpha 1a						
tubulin, alpha, ubiquitous						
tubulin, beta 2B						
tubulin, beta 4						
tubulin, beta polypeptide						
tubulin, beta, 4						
tyrosine 3/tryptophan 5-monooxygenase activation protein, epsilon						
tyrosine 3/tryptophan 5-monooxygenase activation protein, theta						
tyrosine 3/tryptophan 5-monooxygenase activation protein, zeta						
tyrosine 3-monooxygenase/tryptophan 5-monooxygenase activation protein, beta						
tyrosine 3-monooxygenase/tryptophan 5-monooxygenase activation protein, gamma						
UV excision repair protein RAD23 homolog B						
valosin-containing protein						
villin 2						
vinculin isoform meta-VCL						
acidic (leucine-rich) nuclear phosphoprotein 32 family, member A						
ADP-ribosylation factor 5						
annexin VII isoform 2						
aspartate aminotransferase 1						
ATP-dependent DNA helicase II						
brain glycogen phosphorylase						
calpastatin isoform g						
catenin, alpha 1						
chaperonin containing TCP1, subunit 7 isoform b						
chloride intracellular channel 1						
chloride intracellular channel 6						
clathrin heavy chain 1						
CNDP dipeptidase 2 (metallopeptidase M20 family)						
cytokine induced protein 29 kDa						
DJ-1 protein						
eIF-5A2 protein						
erythrocyte membrane protein band 4.1-like 1 isoform a						
eukaryotic translation elongation factor 1 gamma						
eukaryotic translation initiation factor 3, subunit 12						
eukaryotic translation initiation factor 3, subunit 6 48kDa						
eukaryotic translation initiation factor 5A						
exportin 1						
filamin B, beta (actin binding protein 278)						
FK506-binding protein 4						

flap structure-specific endonuclease 1						
gelsolin-like capping protein						
heterogeneous nuclear ribonucleoprotein D isoform c						
histone H2a						
HLA-B associated transcript 1						
hypothetical protein LOC401019						
inosine triphosphatase isoform a						
keratin 15						
keratin 19						
keratin 1B						
lactate dehydrogenase C						
leucine rich repeat (in FLII) interacting protein 1						
LUC7-like 2						
myosin, light chain 6, alkali, smooth muscle and non-muscle isoform 1						
N-acetylneuraminic acid phosphate synthase						
N-myc downstream regulated gene 1						
opioid growth factor receptor						
peroxiredoxin 5 precursor, isoform a						
plastin 1						
poly (ADP-ribose) polymerase family, member 1						
PREDICTED: similar to 60S ribosomal protein L7a isoform 3						
PREDICTED: similar to aminopeptidase puromycin sensitive						
PREDICTED: similar to High mobility group protein B1						
PREDICTED: similar to nascent polypeptide-associated complex alpha polypeptide						
PREDICTED: similar to peptidylprolyl isomerase A (cyclophilin A)-like 4						
PREDICTED: similar to peptidylprolyl isomerase A isoform 1						
PREDICTED: similar to peptidylprolyl isomerase A isoform 1						
prosaposin isoform c preproprotein						
proteasome activator subunit 1 isoform 2						
protein phosphatase 1, catalytic subunit, beta isoform 1						
protein phosphatase 1, regulatory subunit 7						
ras-related nuclear protein						
RCC1-like						
ribosomal protein L23						
ribosomal protein L6						
ribosomal protein P2						
ribosomal protein S24 isoform c						
ribosomal protein S8						
small nuclear ribonucleoprotein D1 polypeptide 16kDa						
smooth muscle myosin heavy chain 11 isoform SM1A						
splicing factor 3b, subunit 1 isoform 1						
stress-induced-phosphoprotein 1 (Hsp70/Hsp90-organizing protein)						
T-complex protein 1 isoform a						
thioredoxin						
thioredoxin-like 5						
TNF receptor-associated protein 1						
tropomyosin 4						
tumor-associated calcium signal transducer 2 precursor						
ubiquitin and ribosomal protein L40 precursor						
vacuolar protein sorting 35						
visfatin precursor						
actinin, alpha 2						
ADP-ribosylation factor 1						
apolipoprotein A-I preproprotein						
apoptosis inhibitor 5						
apoptotic chromatin condensation inducer 1						
ATP-binding cassette, sub-family F, member 1 isoform a						
ATP citrate lyase isoform 1						
autoantigen La						
carbonic anhydrase II						
cathepsin D preproprotein						
CD1A antigen precursor						
CD9 antigen						
cellular retinoic acid binding protein 2						
chromatin modifying protein 4B						
core-binding factor, beta subunit isoform 2						

CSE1 chromosome segregation 1-like protein						
cytochrome P450, family 24 precursor						
eukaryotic translation initiation factor 3, subunit 4 delta, 44kDa						
eukaryotic translation initiation factor 4A, isoform 3						
F-actin capping protein alpha-1 subunit						
far upstream element-binding protein						
fascin 1						
fatty acid desaturase 1						
G protein-coupled receptor associated sorting protein 2						
glucose-6-phosphate dehydrogenase isoform a						
glycogen synthase kinase 3 beta						
glyoxalase I						
heat shock 105kD						
high-mobility group (nonhistone chromosomal) protein 1-like 1						
hypothetical protein LOC23277						
hypothetical protein LOC51493						
hypothetical protein LOC79017						
immunoglobulin binding protein 1						
liver phosphofructokinase isoform b						
major vault protein						
myosin, heavy chain 14 isoform 1						
myosin, heavy polypeptide 10, non-muscle						
myotrophin						
nucleosome assembly protein 1-like 1						
poly(A) binding protein, cytoplasmic 1						
polypyrimidine tract-binding protein 1 isoform c						
PREDICTED: hypothetical protein						
PREDICTED: similar to 60S ribosomal protein L29						
PREDICTED: similar to myosin regulatory light chain-like						
PREDICTED: similar to ribosomal protein L5 isoform 1						
PREDICTED: similar to ribosomal protein S12						
PREDICTED: similar to ribosomal protein S3a isoform 2						
PREDICTED: similar to tubulin, beta 6						
protein phosphatase 2, catalytic subunit, beta isoform						
purine nucleoside phosphorylase						
Rho GDP dissociation inhibitor (GDI) alpha						
ribosomal protein L10a						
ribosomal protein L12						
ribosomal protein S13						
ribosomal protein S3						
ribosomal protein S7						
RuvB-like 1						
septin 9						
signal transducer and activator of transcription 3 isoform 2						
small nuclear ribonucleoprotein polypeptide F						
solute carrier family 3 (activators of dibasic and neutral amino acid transport)						
splicing factor, arginine/serine-rich 3						
transaldolase 1						
tubulin, beta, 2						
tumor protein, translationally-controlled 1						
ubiquitin-activating enzyme E1						
ubiquitin-conjugating enzyme E2I						
v-crksarcoma virus CT10 oncogene homolog isoform b						
zinc finger, CCHC domain containing 11 isoform a						
ADP-ribosylation factor-like 1						
alanyl-tRNA synthetase						
alpha isoform of regulatory subunit A, protein phosphatase 2						
chaperonin containing TCP1, subunit 2						
coactosin-like 1						
coatamer protein complex, subunit gamma 1						
diazepam binding inhibitor isoform 3						
hypothetical protein LOC345651						
nascent-polypeptide-associated complex alpha polypeptide-like						
otubain 1						
PREDICTED: similar to 60S ribosomal protein L7 isoform 1						
PREDICTED: similar to Actin-related protein 2/3 complex subunit 1B						
PREDICTED: similar to eukaryotic translation initiation factor 3,						
PREDICTED: similar to eukaryotic translation initiation factor 3						
PREDICTED: similar to Heat shock protein HSP 90-beta						
PREDICTED: similar to Protein SET (Phosphatase 2A inhibitor I2PP2A)						
serine (or cysteine) proteinase inhibitor, clade B (ovalbumin), member 1						
Tax1 (human T-cell leukemia virus type I) binding protein 3						

Appendix G Proteome Results for Ciclosporin Treatment

Protein Identification	C	0.5	1	1.5	2	2.5
alanyl-tRNA synthetase	Blue	Red	Red	Red	Red	Red
chaperonin containing TCP1, subunit 8 (theta)	Blue	Red	Red	Red	Red	Red
diazepam binding inhibitor isoform 3	Blue	Green	Red	Red	Red	Red
dUTP pyrophosphatase isoform 1 precursor	Blue	Blue	Red	Red	Red	Red
high-mobility group (nonhistone chromosomal) protein 1-like 1	Blue	Blue	Blue	Red	Red	Red
histone H2a	Green	Blue	Blue	Green	Green	Red
keratin 20	Blue	Red	Red	Red	Red	Red
myotrophin	Blue	Red	Red	Red	Red	Red
myristoylated alanine-rich protein kinase C substrate	Green	Red	Red	Red	Red	Red
non-POU domain containing, octamer-binding	Blue	Red	Blue	Blue	Red	Red
p47 protein isoform b	Blue	Red	Red	Red	Red	Red
phosphofructokinase, platelet	Blue	Blue	Green	Green	Blue	Red
PREDICTED: similar to eukaryotic translation initiation factor 3	Blue	Red	Blue	Red	Red	Red
PREDICTED: similar to eukaryotic translation initiation factor 3	Blue	Red	Red	Red	Red	Red
PREDICTED: similar to Heat shock protein HSP 90-beta (HSP 84) (TSTA)	Blue	Red	Red	Red	Red	Red
PREDICTED: similar to High mobility group protein B1	Blue	Blue	Red	Red	Red	Red
PREDICTED: similar to ribosomal protein L5 isoform 1	Blue	Green	Red	Red	Red	Red
ribosomal protein S2	Blue	Red	Red	Red	Red	Red
tumor protein, translationally-controlled 1	Green	Blue	Red	Red	Red	Red
actin, gamma 1 propeptide	Green	Green	Green	Green	Green	Green
actinin, alpha 1	Green	Green	Green	Green	Green	Green
actinin, alpha 4	Green	Blue	Green	Green	Green	Green
adenylyl cyclase-associated protein	Green	Green	Green	Green	Green	Green
adipose specific 2	Green	Green	Green	Green	Green	Green
AHNAK nucleoprotein isoform 1	Green	Blue	Green	Green	Green	Green
albumin precursor	Green	Green	Green	Green	Green	Green
aldo-keto reductase family 1, member A1	Green	Green	Green	Green	Green	Green
aldolase A	Green	Green	Green	Green	Green	Green
alpha 2 actin	Green	Green	Green	Green	Green	Green
annexin 5	Green	Green	Green	Green	Green	Green
annexin A11	Green	Green	Green	Green	Green	Green
annexin A2 isoform 2	Green	Green	Green	Green	Green	Green
annexin A8-like 1	Green	Green	Green	Green	Green	Green
annexin I	Green	Green	Green	Green	Green	Green
apolipoprotein A-I preproprotein	Green	Green	Blue	Green	Green	Green
argininosuccinate synthetase 1	Green	Green	Green	Green	Green	Green
arginyl aminopeptidase (aminopeptidase B)	Green	Blue	Green	Green	Blue	Green
ARP3 actin-related protein 3 homolog	Green	Green	Green	Green	Green	Green
aspartyl-tRNA synthetase	Green	Green	Green	Green	Green	Green
ATP-dependent DNA helicase II, 70 kDa subunit	Green	Green	Blue	Green	Green	Green
calmodulin 2	Green	Green	Green	Green	Green	Green
calpain, small subunit 1	Green	Green	Green	Green	Green	Green
chaperonin containing TCP1, subunit 2	Blue	Blue	Green	Green	Green	Green
chloride intracellular channel 1	Green	Green	Green	Green	Green	Green
clathrin heavy chain 1	Green	Green	Green	Blue	Green	Green
cofilin 1 (non-muscle)	Green	Green	Green	Green	Green	Green
cold shock domain protein A	Green	Blue	Green	Green	Green	Blue
cortactin isoform a	Green	Green	Green	Green	Green	Green
cytosolic malate dehydrogenase	Green	Green	Green	Green	Green	Green
DJ-1 protein	Blue	Green	Blue	Blue	Green	Blue
eIF-5A2 protein	Blue	Green	Blue	Blue	Blue	Blue
enolase 1	Green	Green	Green	Green	Green	Green
enolase 2	Green	Green	Green	Green	Green	Green
enolase 3	Green	Green	Green	Green	Green	Green
eukaryotic translation elongation factor 1 alpha 1	Green	Green	Green	Green	Green	Green
eukaryotic translation elongation factor 1 alpha 2	Green	Green	Green	Green	Green	Green
eukaryotic translation elongation factor 1 beta 2	Green	Green	Green	Blue	Green	Green
eukaryotic translation elongation factor 2	Green	Green	Green	Green	Green	Green
eukaryotic translation initiation factor 4A isoform 1	Green	Green	Green	Green	Green	Green
eukaryotic translation initiation factor 4A2	Green	Green	Green	Green	Blue	Blue
fascin 1	Green	Green	Green	Blue	Blue	Blue
fatty acid synthase	Green	Green	Green	Green	Green	Green
filamin A, alpha	Green	Green	Green	Green	Green	Blue
fructose-1,6-bisphosphatase 1	Blue	Green	Green	Green	Green	Green
fructose-bisphosphate aldolase C	Green	Green	Green	Green	Green	Green
GDP dissociation inhibitor 1	Blue	Blue	Blue	Green	Blue	Blue

GDP dissociation inhibitor 2									
glucose phosphate isomerase									
glutathione transferase									
glyceraldehyde-3-phosphate dehydrogenase									
GTP-binding protein PTD004 isoform 1									
H2B histone family, member C									
heat shock 105kD									
heat shock 27kDa protein 1									
heat shock 70kDa protein 1A									
heat shock 70kDa protein 1-like									
heat shock 70kDa protein 4 isoform a									
heat shock 70kDa protein 8 isoform 2									
heat shock 90kDa protein 1, beta									
heat shock protein 90kDa alpha (cytosolic), class A member 1 isoform 2									
hepatoma-derived growth factor (high-mobility group protein 1-like)									
heterogeneous nuclear ribonucleoprotein A1 isoform a									
heterogeneous nuclear ribonucleoprotein A2/B1 isoform A2									
heterogeneous nuclear ribonucleoprotein F									
heterogeneous nuclear ribonucleoprotein H2									
heterogeneous nuclear ribonucleoprotein K isoform a									
high mobility group AT-hook 1 isoform a									
hypothetical protein LOC345651									
IQ motif containing GTPase activating protein 1									
isocitrate dehydrogenase 1 (NADP+), soluble									
KH-type splicing regulatory protein (FUSE binding protein 2)									
lactate dehydrogenase A									
lactate dehydrogenase A-like 6B									
lactate dehydrogenase B									
leucine rich repeat (in FLII) interacting protein 1									
LIM and SH3 protein 1									
moesin									
myosin, heavy polypeptide 9, non-muscle									
myosin, light chain 6, alkali, smooth muscle and non-muscle isoform 1									
nascent-polypeptide-associated complex alpha polypeptide									
nascent-polypeptide-associated complex alpha polypeptide-like									
non-metastatic cells 2, protein (NM23B) expressed in									
nuclease sensitive element binding protein 1									
nucleolin									
nucleophosmin 1 isoform 1									
nucleosome assembly protein 1-like 1									
p47 protein isoform c									
PDZ and LIM domain 1 (elfin)									
peroxiredoxin 1									
peroxiredoxin 2 isoform a									
peroxiredoxin 6									
PEST-containing nuclear protein									
phosphogluconate dehydrogenase									
phosphoglycerate dehydrogenase									
phosphoglycerate kinase 1									
phosphoglycerate kinase 2									
plastin 3									
poly(rC) binding protein 3									
PREDICTED: similar to 40S ribosomal protein SA (p40) binding protein)									
PREDICTED: similar to 60S ribosomal protein L12									
PREDICTED: similar to 60S ribosomal protein L32									
PREDICTED: similar to 60S ribosomal protein L32									
PREDICTED: similar to 60S ribosomal protein L7a isoform 3									
PREDICTED: similar to actin-like protein									
PREDICTED: similar to chromobox homolog 3									
PREDICTED: similar to cytoplasmic beta-actin									
PREDICTED: similar to Elongation factor 1-gamma (EF-1-gamma)									
PREDICTED: similar to Heterogeneous nuclear ribonucleoprotein A1									
PREDICTED: similar to peptidylprolyl isomerase A (cyclophilin A)-like 4									
PREDICTED: similar to peptidylprolyl isomerase A isoform 1									
PREDICTED: similar to Phosphoglycerate mutase 1 (Phosphoglycerate mutase isozyme B)									
PREDICTED: similar to Protein SET (Phosphatase 2A inhibitor I2PP2A)									
profilin 1									

proteasome activator subunit 1 isoform 2						
proteasome activator subunit 2						
protein phosphatase 1, catalytic subunit, beta isoform 1						
pyrophosphatase 1						
pyruvate kinase 3 isoform 1						
pyruvate kinase 3 isoform 2						
ras-related nuclear protein						
Rho GDP dissociation inhibitor (GDI) beta						
ribosomal protein L17						
ribosomal protein L19						
ribosomal protein L3 isoform a						
ribosomal protein L5						
ribosomal protein L8						
ribosomal protein P0						
ribosomal protein S20						
ribosomal protein S24 isoform c						
ribosomal protein S5						
S100 calcium binding protein A11						
S-adenosylhomocysteine hydrolase						
serine (or cysteine) proteinase inhibitor, clade B (ovalbumin), member 5						
SERPINE1 mRNA binding protein 1 isoform 3						
small nuclear ribonucleoprotein D1 polypeptide 16kDa						
stratifin						
thioredoxin						
TNF receptor-associated protein 1						
transgelin 2						
transketolase						
triosephosphate isomerase 1						
tropomyosin 3 isoform 2						
tropomyosin 4						
tubulin, alpha 1a						
tubulin, alpha, ubiquitous						
tubulin, beta 2B						
tubulin, beta 4						
tubulin, beta polypeptide						
tubulin, beta, 4						
tyrosine 3/tryptophan 5-monooxygenase activation protein, epsilon						
tyrosine 3/tryptophan 5-monooxygenase activation protein, theta						
tyrosine 3/tryptophan 5-monooxygenase activation protein, zeta						
tyrosine 3-monooxygenase/tryptophan 5-monooxygenase activation protein, beta						
tyrosine 3-monooxygenase/tryptophan 5-monooxygenase activation protein, gamma						
ubiquitin and ribosomal protein L40 precursor						
vacuolar protein sorting 35						
villin 2						
vinculin isoform meta-VCL						
visfatin precursor						
acidic (leucine-rich) nuclear phosphoprotein 32 family, member A						
adenylate kinase 1						
ADP-ribosylation factor-like 1						
aldehyde dehydrogenase 1A3						
alpha isoform of regulatory subunit A, protein phosphatase 2						
annexin A3						
annexin IV						
annexin VII isoform 2						
APEX nuclease						
aryl hydrocarbon receptor interacting protein						
ATP-dependent DNA helicase II						
basic transcription factor 3 isoform B						
brain glycogen phosphorylase						
calpastatin isoform g						
calreticulin precursor						
cathepsin D preproprotein						
CD1A antigen precursor						
CDV3 homolog						
cell division cycle 37 protein						
cellular retinoic acid binding protein 2						
chaperonin containing TCP1, subunit 3 isoform a						

chaperonin containing TCP1, subunit 3 isoform c						
chaperonin containing TCP1, subunit 7 isoform b						
chloride intracellular channel 6						
chromatin modifying protein 4B						
CNDP dipeptidase 2 (metallopeptidase M20 family)						
coatmer protein complex, subunit gamma 1						
cytidylate kinase						
cytokine induced protein 29 kDa						
cytosolic malic enzyme 1						
DEAD (Asp-Glu-Ala-Asp) box polypeptide 39						
erythrocyte membrane protein band 4.1-like 2						
eukaryotic translation elongation factor 1 gamma						
eukaryotic translation elongation factor 1 delta isoform 1						
eukaryotic translation initiation factor 2, subunit 1 alpha, 35kDa						
eukaryotic translation initiation factor 3, subunit 12						
eukaryotic translation initiation factor 5A						
exportin 1						
far upstream element-binding protein						
fatty acid desaturase 1						
filamin B, beta (actin binding protein 278)						
FK506-binding protein 1A						
FK506-binding protein 4						
flap structure-specific endonuclease 1						
G protein-coupled receptor associated sorting protein 2						
germ cell specific Y-box binding protein						
glucose-6-phosphate dehydrogenase isoform a						
glyoxalase I						
H4 histone family, member B						
heterogeneous nuclear ribonucleoprotein A3						
heterogeneous nuclear ribonucleoprotein D isoform c						
high-mobility group box1						
high-mobility group box2						
HLA-B associated transcript 1						
hydroxypyruvate isomerase homolog						
hypothetical protein LOC401019						
hypothetical protein LOC79017						
immunoglobulin binding protein 1						
integrin beta 4 binding protein isoform a						
interferon regulatory factor 6						
involucrin						
keratin 1						
keratin 10						
keratin 13 isoform a						
keratin 15						
keratin 19						
keratin 1B						
keratin 7						
keratin 9						
lactate dehydrogenase C						
liver phosphofructokinase isoform b						
major histocompatibility complex class I HLA-A29.1						
minichromosome maintenance deficient 6						
myosin regulatory light chain 9 isoform b						
myosin, heavy polypeptide 10, non-muscle						
N-acetylneuraminic acid phosphate synthase						
N-myc downstream regulated gene 1						
opioid growth factor receptor						
peroxiredoxin 5 precursor, isoform b						
phosphoserine aminotransferase isoform 1						
plastin 1						
PREDICTED: hypothetical protein						
PREDICTED: similar to 40S ribosomal protein SA (p40)						
PREDICTED: similar to 60S ribosomal protein L29						
PREDICTED: similar to Actin-related protein 2/3 complex subunit 1B						
PREDICTED: similar to myosin regulatory light chain-like						
PREDICTED: similar to peptidylprolyl isomerase A isoform 1						
PREDICTED: similar to peptidylprolyl isomerase A isoform 1						

PREDICTED: similar to Protein C6orf115						
PREDICTED: similar to tubulin, beta 6						
prefoldin subunit 5 isoform alpha						
programmed cell death 6 interacting protein						
proliferating cell nuclear antigen						
prosaposin isoform c preproprotein						
proteasome beta 7 subunit proprotein						
protein phosphatase 1, regulatory subunit 7						
protein phosphatase 2, catalytic subunit, beta isoform						
purine nucleoside phosphorylase						
Ras-GTPase-activating protein SH3-domain-binding protein						
RCC1-like						
Rho GDP dissociation inhibitor (GDI) alpha						
ribonuclease/angiogenin inhibitor						
ribosomal protein L23						
ribosomal protein L6						
ribosomal protein L9						
ribosomal protein P2						
ribosomal protein S13						
ribosomal protein S3						
ribosomal protein S4, X-linked X isoform						
ribosomal protein S8						
RuvB-like 1						
S100 calcium binding protein A14						
septin 9						
SET translocation (myeloid leukemia-associated)						
small acidic protein						
smooth muscle myosin heavy chain 11 isoform SM1A						
small nuclear ribonucleoprotein polypeptide F						
smooth muscle myosin heavy chain 11 isoform SM1A						
splicing factor proline/glutamine rich (polypyrimidine tract binding protein)						
staphylococcal nuclease domain containing 1						
superoxide dismutase 1, soluble						
T-complex protein 1 isoform b						
thioredoxin-like 5						
TIP120 protein						
transaldolase 1						
tubulin, alpha 4a						
tumor protein D52-like 2 isoform e						
tumor rejection antigen (gp96) 1						
ubiquitin-activating enzyme E1						
ubiquitin carboxyl-terminal esterase L3						
ubiquitin-conjugating enzyme E2L 3 isoform 1						
UV excision repair protein RAD23 homolog B						
valosin-containing protein						
v-crk sarcoma virus CT10 oncogene homolog isoform b						
zinc finger, CCHC domain containing 11 isoform a						
actinin, alpha 2						
alpha isoform of regulatory subunit A, protein phosphatase 2						
APEX nuclease						
aspartate aminotransferase 1						
chaperonin containing TCP1, subunit 5 (epsilon)						
chaperonin containing TCP1, subunit 7 isoform a						
CSE1 chromosome segregation 1-like protein						
eukaryotic translation initiation factor 3, subunit 2 beta, 36kDa						
gelsolin-like capping protein						
histone acetyltransferase 1 isoform b						
hypothetical protein LOC51493						
inosine triphosphatase isoform a						
karyopherin beta 1						
membrane-type 1 matrix metalloproteinase cytoplasmic tail binding protein-1						
myristoylated alanine-rich protein kinase C substrate						
poly (ADP-ribose) polymerase family, member 1						
polypyrimidine tract-binding protein 1 isoform c						
PREDICTED: similar to aminopeptidase puromycin sensitive						
PREDICTED: similar to Protein SET (Phosphatase 2A inhibitor I2PP2A(PHAPII))						
ribosomal protein L11						

ribosomal protein L12						
ribosomal protein S17						
Sec23 homolog B						
sorbitol dehydrogenase						
stress-induced-phosphoprotein 1 (Hsp70/Hsp90-organizing protein)						
T-complexprotein 1 isoform a						
tubulin, beta, 2						
tumor protein, translationally-controlled 1						